EJA

European Journal of Anatomy

Volume 27 - Number 6 November 2023

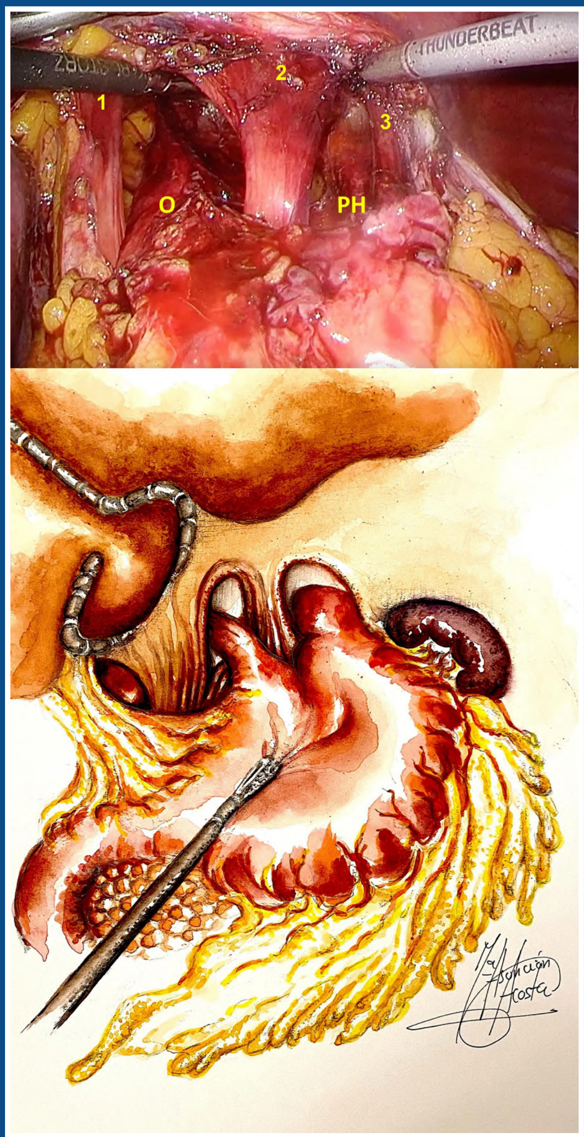

Indexed in:

CLARIVATE
- JCR:2020
- Q4 (21/23)
- I.F. J.C.I.: 0.19

DIALNET
EMBASE / Excerpta Medica

SCOPUS
- SJCR: 2020
- Q4 (31/39)
- I.F.: 0.162

Emerging Sources Citation Index
LATINDEX. Catálogo v1.0 (2002-2017)

Official Journal of the Spanish Society of Anatomy

Published by: **LOKI & DIMAS**

www.eurjanat.com

European Journal of Anatomy

Volume 27 - Number 6 November 2023

The role of thymus graft on the onset of puberty in juvenile male rats

Satya Prasad V.

Department of Anatomy, Dr. B.C. Roy Multi-Specialty Medical Research Centre, IIT Kharagpur, Kharagpur -721302, West Bengal, India

SUMMARY

There exists a bidirectional relation between the thymus gland and the hypothalamo- hypophysial-gonadal axis. The thymus secretes various hormones, some of which can regulate the reproductive axis. So, it is worth to explore the possible role of an additional thymus on the onset of puberty in male albino rats.

Two groups of male rats aged 5 and 10 days were used for the study. Each subgroup consisted of 4 pups each in control and experimental group. Thymus glands for graft were obtained from newborn male rat pups. Depending on the age group, 5 day or 10-day-old male rat pup were anaesthetized, 2-3 mm incision was made, and a thymus gland was grafted to the axilla. Sham operations were performed to the control pups. Without handling, animals were observed daily for the onset of puberty. On the day of descent of testes, body weight of the animal was noted, blood was collected and used for radio immunoassay. All morphometric measurements were done using an occular micrometer. Volume fraction of seminiferous tubules, intertubular connective tissue of testes, cortex and medulla of the thymus were estimated by point count method.

In both the age groups thymus graft advanced the age of descent of testes, and increased body weight and organ weight. It also increased the serum hormone levels.

In conclusion, this study indicates that an additional thymus gland has a positive effect on the male reproductive system towards pro-gonadal action, and this effect is more pronounced in older-age groups of rats.

Key words: Descent of testes – Hormones – Onset of puberty – Thymus graft

INTRODUCTION

The relation between the thymus gland and the hypothalamo-hypophysial-gonadal axis is bidirectional. Several soluble factors produced by the thymus gland and the cells it regulates can modulate the immune system through reproductive neuroendocrine circuits indirectly.

Many studies have been conducted to evaluate the effects of partially purified thymic extracts in treating various reproductive disorders, as well as changes in gonadal tissue weights. Also, studies have focused on the chemical nature of the factors responsible for regulating reproductive function. The thymus secretes various hormones, some of which can regulate the reproductive axis. The hypothalamic-pituitary function is affected by the

Corresponding author:
Dr. Satya Prasad V. Faculty in Anatomy, Dr. B.C. Roy Multi-Specialty Medical Research Centre, IIT Kharagpur, Kharagpur – 721302, West Bengal, India. Phone: 91 – 9949248348. E-mail: satyaprasad33@yahoo.co.in

Submitted: February 19, 2023. **Accepted:** April 23, 2023

https://doi.org/10.52083/SURU3839

peptides derived from the thymus. In programming the hypothalamic-pituitary axis in the prepubertal period in rodents, the thymic hormones may play a vital role (Strich et al., 1985).

Thymosin beta 4, one of the thymosin hormones secreted by the tymus is a potent inducer of Luteinizing hormone-releasing hormone (LHRH) release, which in turn stimulates pituitary Luteinizing hormone (LH) release. Other factors like interleukin-1 (IL-1) have been found to inhibit the release of luteinizing hormone-releasing hormone and luteinizing hormone (LH). Further, it has been also found that IL-1 alters the expression of rat granulosa cells LH receptors. Also, the estrogen and progesterone release are suppressed by certain interferons (Hall et al., 1992). Despite of the many studies on the various aspects of interrelationship between the thymus gland and the reproductive axis, there is a lacuna on the role of an additional thymus gland in the reproductive system.

With the abovementioned facts in mind, the present study is designed to evaluate the role of allogeneic thymus gland graft on the onset of puberty in male juvenile rats.

MATERIALS AND METHODS

Inbred strains of Albino rats bred under controlled lighting using 12 hours of light and 12 hours of dark (12L: 12D) cycle were used as per ethical guidelines.

Animal groups

Two groups of male rats aged 5 and 10 days were used for the study. Each subgroup consisted of 4 pups in the control group and 4 corresponding pups in the experimental group. Newborn male pups were used as donors for allogeneic thymus graft.

Allogeneic thymus graft

Thymus glands for graft were obtained from new-born male rat pups. These pups were anaesthetized by ether, thoracic cavity was opened from sternum, intact thymus gland was removed carefully by dissecting, and then transferred immediately into Tyrode's solution. The entire procedure was carried out under sterile conditions.

Depending on the age group, 5-day-old or 10-day-old male rat pups were anaesthetized: 2-3 mm incision was made in the region of the axilla after sterilizing the region with absolute alcohol. The thymus gland from the Tyrode's solution was blotted on filter paper and grafted to the axilla of the recipient rat pup. The incision was closed by approximating and smearing with solution containing persplex dissolved in chloroform. Animals were monitored carefully and post-operative care was taken during their recovery period from anesthesia. They were placed in separate cages for 1-2 hours to avoid cannibalism, and finally transferred back to the cage with their mother.

Sham operations were performed to the control pups, except for the placement of the thymus gland: the entire procedure was carried out in the same way as with the experimental pups.

Observation on Descent of Testes and Blood collection

Without handling, animals were observed daily for the onset of puberty in male rats which is judged by descent of testes and is a conventionally accepted sign for the event (Relkin, 1971; Satya Prasad, 2019). On the day of the descent of testes, the body weight of the animal was noted andanaesthetized with ether; then blood was collected, and serum was separated and used for radio immunoassay.

Evaluation of graft acceptance

The acceptance of the graft was confirmed by the presence of neovascular network in and around the area of the grafted site in the experimental animals.

Collection of tissues

After collecting the blood, animals were sacrificed as per the international ethical guidelines (for animals); the organs, testes, epididymides and thymus were dissected and weighed. The testes and thymus were fixed in Bouin's fluid for histological studies. Tissues were processed and paraffin blocks were prepared. Sections of 5mm thickness were cut as described by Drury et al. (1967). For every 20 serial sections, only 5 were

Table 1. Effect of thymus graft on descent of testes and body, testes, epididymis, thymus weight and tail length in 5-day-old and 10-day-old rats. Cont, Control; Expt, Experimental; *P<0.05, **P<0.01

	5-day-old		10-day-old	
	Cont	Expt	Cont	Expt
Age on Descent of testes (Day)	30.75±0.48	26.25*±0.48	29.25±0.85	26.50*±0.87
Body weight (g)	43.75±1.03	44.75±1.84	40.00±0.83	44.00*±1.01
Testes weight (mg)	117.00±3.88	136.50*±8.19	129.10±0.77	146.90*±5.57
Epidydimides weight (mg)	19.38±0.38	20.13±0.43	15.75±0.78	19.50*±1.06
Thymus gland weight (mg)	139.00±4.73	146.75±4.73	123.75±5.21	142.75*±3.31
Tail length (cm)	7.88±0.09	8.45**±0.13	7.60±0.07	8.30**±0.12

selected and the remaining was discarded. The sections were later stained with Ehrlich's Haematoxylin and Eosin (Drury et al., 1967).

Histological parameters

For morphometric analysis, the cross section of the tubules that showed clear and well demarcated boundaries was selected. All morphometric measurements were done using an ocular micrometer. The volume fraction of seminiferous tubules, the intertubular connective tissue of testes, the cortex and medulla of the thymus were estimated by point count method (Karapetrovic 1995) using the eyepiece graticule. Further, cortico-medullary volume fraction ratio was calculated.

Radioimmune assay

Radioimmune assay for Luteinizing Hormone (LH) and testosterone was done using the kits procured from the Diagnostic Systems Laboratories, Inc., Texas, USA, while growth hormone (GH) was estimated by using the kit from ICN pharmaceuticals, inc., Costamesa CA 92626.

Statistical analysis

All data were entered, and Student's unpaired t-test was applied to assess the significant differences between the mean of the experimental and of the control group animals for each characteristic under study.

RESULTS

Gross parameters

Thymus graft (TG) advanced the age of descent of testes, which was statistically significant. Body weight in 10-day-old rats showed significant increase in TG compared to control group. TG increased the testes' weight in 5-day-old and 10-day-old rats, and it was statistically significant in both age groups. TG produced an increase in epididymides' weight, which was statistically significant in 10-day-old rats. TG increased the weight of in-situ thymus in both 5 and 10-day-old rats, and it was statistically significant in 10-day-old rats. TG significantly increased the tail length in both age rats (Table 1).

Histological parameters

Testis

TG increased the tubule diameter in both age groups, which was statistically significant. TG resulted in significant increase in tubule volume and significant decrease in intertubular connective tissue volume in both age groups (Table 2) (Fig. 1).

Thymus Gland

The in-situ thymus gland exhibited well-developed cortex and medulla. The in-situ thymus gland's cortical volume in the experimental groups was significantly higher when compared to the control group of rats. Similarly, TG resulted in significant reduction in medulla volume in all the experimental groups. Cortico-medullary volume ratio was significantly higher in all the experimental groups of rats (Table 3) (Fig. 2).

Radioimmune assay

TG had increased higher serum LH levels; it was statistically significant in both age groups (Fig. 3). TG resulted in significant increase in the levels

Table 2. Effect of thymus graft on histomorphometry of testes in 5-day-old and 10-day-old rats. Cont, Control; Expt, Experiment; *P<0.05, **P<0.01, ***P<0.001

	5-day-old		10-day-old	
	Cont	Expt	Cont	Expt
Seminiferous tubule diameter (µm)	130.60±4.33	151.90**±1.58	136.0±1.03	146.40**±1.72
Seminiferous tubule volume fraction (mm^3/ mm^3)	0.81±0.01	0.87***±0.01	0.80±0.01	0.86**±0.01
Intertubular connective tissue volume fraction (mm^3/ mm^3)	0.19±0.01	0.13***±0.01	0.20±0.01	0.14*±0.01

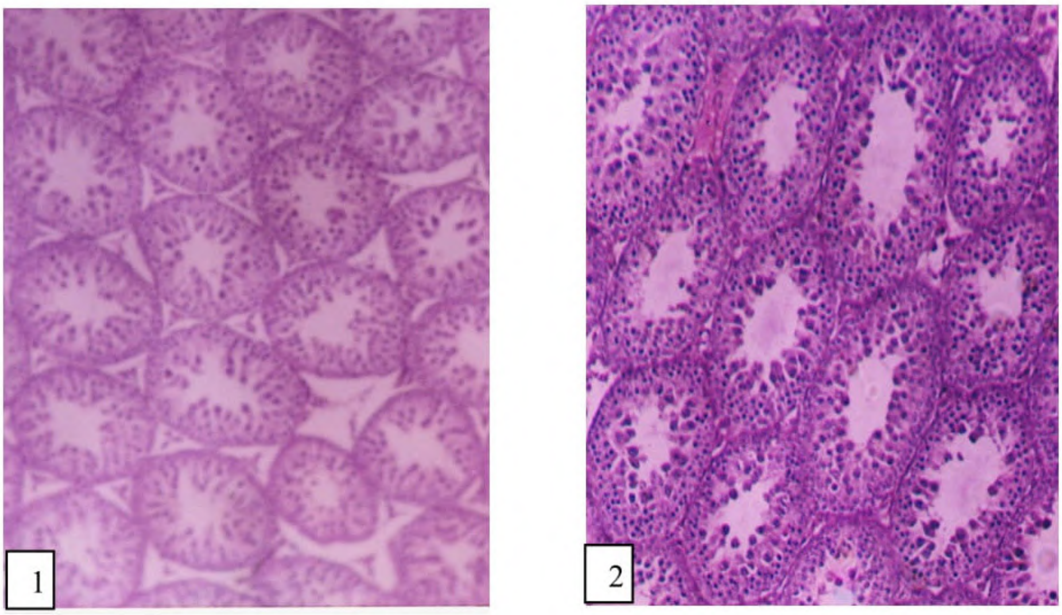

Fig. 1.- (1) Control rat testis showing normal tubule diameter, less compactness of tubules and normal interstitial connective tissue (H&E stain, X 100). **(2)** Experimental rat testis showing increased tubular diameter, compactness of tubules and reduced interstitial connective tissue (H&E stain, X 100).

Table 3. Effect of thymus graft on histomorphometry of in-situ thymus gland in 5-day-old and 10-day-old rats. Cont, Control; Expt, Experiment; *P<0.05

	5-day-old		10-day-old	
	Cont	Expt	Cont	Expt
Cortex volume fraction (mm^3/ mm^3)	0.77±0.01	0.85*±0.03	0.79±0.01	0.88*±0.03
Medulla volume fraction (mm^3/ mm^3)	0.23±0.01	0.15*±0.03	0.21±0.01	0.12*±0.02
Cortico-medullary volume fraction ratio (mm^3/ mm^3)	3.31±0.09	6.55*±0.53	3.68±0.20	8.98*±0.41

of testosterone in both age groups (Fig. 4). TG increased serum GH concentration that was found to be statistically significant in 10-day-old rats (Fig. 5).

DISCUSSION

Descent of testes normally occurs around 40 days of postnatal life in male rats (Bergh et al., 1978). The event is considered as the signal for the onset of puberty. The gain in tbody weight of the rat also directs for earlier sexual maturity. The result of the present study indicates that TG was able to advance the onset of puberty in experimental animals. The classical studies of Kennedy and Mitra established that the weight and composition of the body is well associated with the timing of sexual maturation (Kennedy et al., 1963).

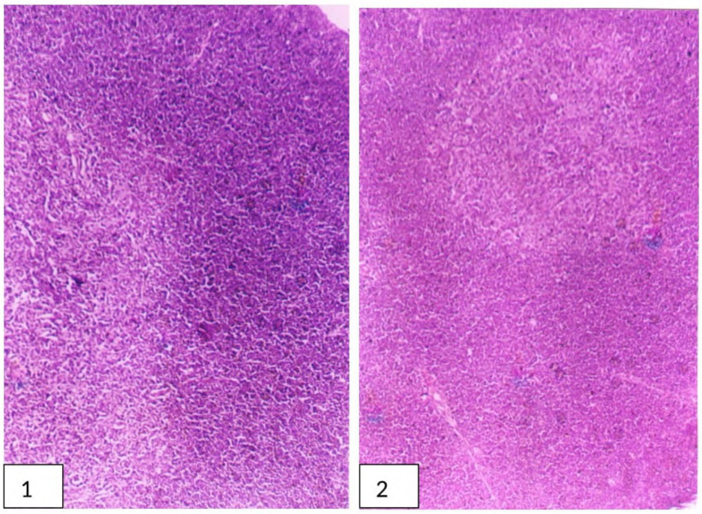

Fig. 2.- (1) In situ thymus gland of control rats (H&E stain, X 125) showing normal central medulla and peripheral cortex. **(2)** In situ thymus gland of experimental rats showing increased, dense, wider cortex and lesser medulla (H&E stain, X 125).

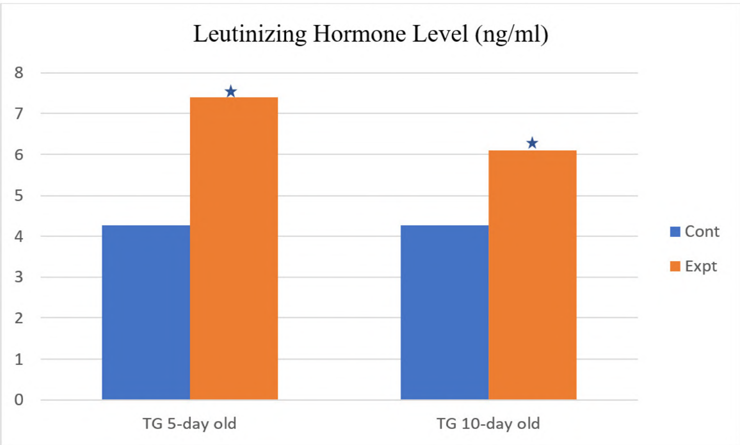

Fig. 3.- Effect of thymus graft on luteinizing hormone in 5-day-old rats and 10-day-old rats. P < 0.05 - *

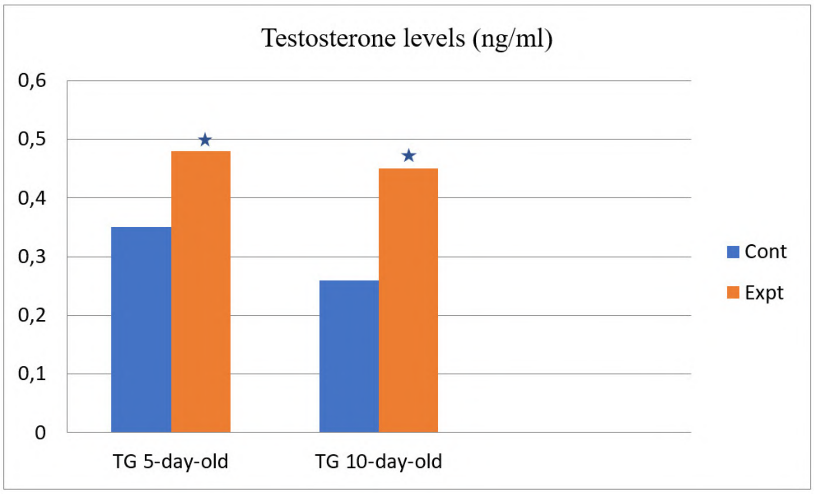

Fig. 4.- Effect of thymus graft on testosterone in 5-day-old rats and 10-day-old rats. P < 0.05 - *

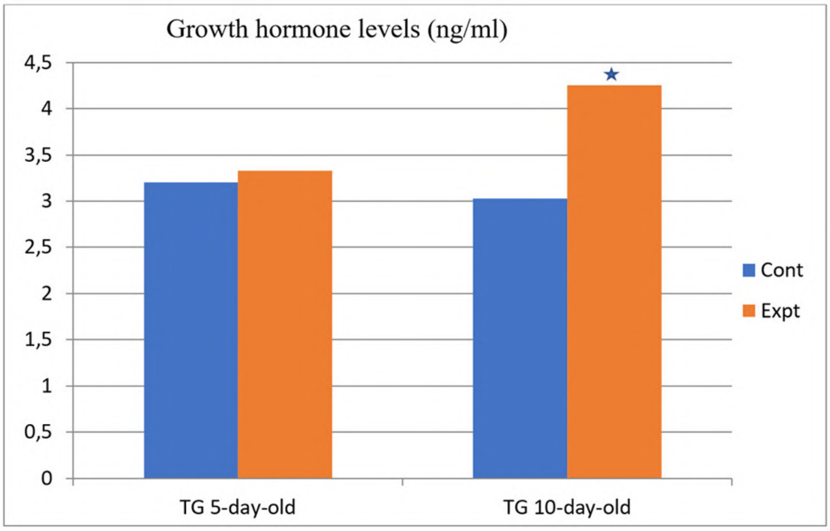

Fig. 5.- Effect of thymus graft on growth hormone in 5-day-old rats and 10-day-old rats. $P < 0.05$ - *

In the present study, TG increased body weight. Increase in body weight is more evident when the age of descent is taken into consideration, which is earlier compared to the control group. Also, it was found that TG increased tail length significantly, indicating the positive effect and supporting the studies of Kennedy and Mitra (1963). Interestingly, TG increased the testes' weight significantly, thus revealing that TG may be capable of exerting pro-gonadal effect, but the action may be local. TG also increased epidydimes' weight, which was statistically significant in 10-day-old rats, indicating the probable pro-gonadal effect at the individual organ level. TG increased in-situ thymus gland weight; the increased thymus may further exert a stimulatory effect on the hypothalamus and have results in the pro-gonadal effect. But, in the present study, the increase was significant in 10-day-old rats, substantiating the fact that TG was able to advance the onset of puberty by acting individually at the different organ levels, especially more effective in older-age groups.

Histological Parameters

TG resulted in significant increase in tubule diameter in both age groups, which corresponded with the weight of the testes. This may be due to the stimulatory action of TG. The increased tubule diameter of the testes in the experimental rats is indicative of the action of TG on higher centers, especially on the pituitary gland, which through its secretions brings about the changes in the histomorphometric aspects of the testes, which further accounts for the gross changes. The action at the organ level cannot be ruled out with the fact that testicular morphometry depends on the local secretions too. Increased seminiferous tubule volume and decreased intertubular connective tissue volume in corresponding groups supported the increased testes' weight in experimental groups.

The volume fraction of in-situ thymus gland cortex was significantly increased, and medullary volume fraction was decreased in experimental rats when compared to control rats. These changes possibly reflect the increased weight of in-situ thymus. The increased cortical volume fraction observed in the present study may account for the increased activity of the cortical cells, thereby increasing the secretions of the same, which may be responsible for bringing about the pro-gonadal action by acting at the higher centers as well as at the organ level. The results of cortico-medullary volume fraction ratio account for the increased thymus weight in the respective experimental groups. The thymus secretes various hormones, some of which can regulate the reproductive axis. The hypothalamic-pituitary function is affected by the peptides derived from the thymus. In programming the hypothalamic-pituitary axis in the prepubertal period in rodents, the thymic hormones may play a vital role (Strich et al., 1985). Also, there is an influence of age on the release of the active fraction of the thymus. During the neonatal period the inhibitory effect is high, and it is declined as the onset of puberty approaches (Reyes-Esparza et al., 1989). This is substantiated by the results of the present study, which indicate the higher pro-gonadal action in the older-age group of rats.

Radioimmuno Assay

Stimulatory action of TG on LH release goes well with the report of Hall *et al*., who stated that the thymus secretes thymosin beta-4, a potent inducer of LHRH release from the hypothalamus, thus stimulating the pituitary for LH release (Hall et al., 1992). TG had influenced LH levels significantly, which may be due to additional thymosin beta-4 secretion. Correspondingly TG was able to alter the testosterone concentration significantly, which resulted in the advancement of cytoarchitecture of testis, and was probably responsible for the pro-gonadal action when compared with control rats.

TG increased GH levels. The GH concentrations may probably result in the increased secretion of IGF-1. This is hypothesized with the background of the report stating that the deficiency of GH results in a low state of IGF-1, thereby affecting translational efficiency and secretory responses of both the hormones (Jevdjovic et al., 2005). The increase in GH levels seen in the present study may be connected to the increase in body weight and other histological parameters of reproductive organs concerned partially, which was stated to be associated with the sexual maturity as described by Kennedy and Mitra (1963), accounting for the pro-gonadal form of action. It can be concluded from the present study that an additional thymus gland has a positive effect on the male reproductive system towards the advancement of the onset of puberty, indicating probable pro-gonadal effect; and this was more pronounced in older groups of rats.

ACKNOWLEDGEMENTS

The author expresses gratitude to the JIPMER, Pondicherry for the facilities to carry out this work.

REFERENCES

BERGH A, HELANDER HF, WAHLQVIST (1978) Studies on factors governing testicular descent in the rat – particularly the role of gubernaculum testis. *Int J Androl,* 1(1-6): 342-356.

DRURY R, WALLINGTON EA (1967) Carleton's Histological technique, 4th edn. Oxford University Press, New York/Toronto, pp 279-280.

HALL NR, O'GRADY MP, MENZIES RA (1992) Thymic regulation of the hypothalamic-pituitary-gonadal axis. *Int J Immunopharmacol,* 14(3): 353-359.

JEVDJOVIC T, MAAKE C, ZWIMPFER C, KREY G, EPPLER E, ZAPF J, REINECKE M (2005) The effect of hypophysectomy on pancreatic islet hormone and insulin-like growth factor 1 content and mRNA expression in rat. *Histochem Cell Biol*, 123(2): 179-188.

KARAPETROVIC B, MICIC M, LEPSAVIC G (1995) Stereological analysis of the sexually mature rat thymus after orchidectomy. *Ind J Med Res,* 102: 42-48.

KENNEDY GC, MITRA J (1963) Body weight and food intake as initiating factors for puberty in the rats. *J Physiol,* 166: 408-418.

RELKIN R (1971) Absence of alteration in pubertal onset in male rats following amygdaloid lesioning. *Endocrinology*, 88(5): 1272-1274.

REYES-ESPARZA JA, ROMANO MC (1989) An age-dependent thymic secretion modulates testicular function. *J Steroid Biochem,* 34(1-6): 541-545.

SATYA PRASAD V (2019) Effect of melatonin on the onset of puberty in male juvenile rats. *Anat Cell Biol*, 52(3): 286-295.

STRICH G, PETZE JE, SILVA DE SA MF, REBAR RW (1985) The effects of thus-derived peptides on hypothalamic LRF and pituitary gonadotropin content in prepubertal congenitally athymic nude mice and their normal heterozygous littermates. *J Reprod Immunol,* 7(4): 351-359.

ORIGINAL ARTICLE Eur J Anat, 27 (6): 663-668 (2023)

Cephalometric radiograph-based approach for sex determination using maxillary sinus index in Surabaya, Indonesia

Arofi Kurniawan[1], Salma A. Athalia[1], Beshlina F.W.R. Prakoeswa[1], Beta N. Rizky[1], An'nisaa Chusida[1], Martinus Yudha[1], Karine Wijaya[1], Mieke S. Margaretha[1], Aspalilah Alias[2,1], Anand Marya[3]

[1] *Department of Forensic Odontology, Faculty of Dental Medicine, Universitas Airlangga, Surabaya, Indonesia*
[2] *Department of Basic Sciences and Oral Biology, Faculty of Dentistry, Universiti Sains Islam Malaysia, Kuala Lumpur, Malaysia*
[3] *Department of Orthodontics, Faculty of Dentistry, University of Puthisastra, Chennai, Cambodia*

SUMMARY

Accurate sex determination is a critical aspect of individual identification in various fields, including anthropology, forensic science, and archaeology. Various parameters from the skull, mandible, pelvis, and long bones are commonly utilized for this purpose. Recently, the potential of the maxillary sinus as a sex-discriminatory parameter has been studied by Khaitan et al. through the analysis of lateral cephalometric radiography. This study aimed to evaluate the feasibility of implementing the sex determination formula devised by Khaitan et al. for the adult population of Surabaya, Indonesia. For this purpose, 130 digital cephalometric radiographs of outpatients in the DHDC Dental Office in Surabaya, Indonesia, were assessed. The maxillary sinus height and width were measured to derive the maxillary sinus index (MSI) and calculate the discriminant score (D) for sex identification. This study revealed that the maxillary sinus's average height in males was 37.111±5.13 mm, while in females, it was 34.538±4.36 mm. Males had an average maxillary sinus width of 44.152±4.11 mm, while in females it was of 38.849±3.33 mm. The MSI values for males (1.204±0.14) were higher than for females (1.135±0.10). The discriminant scores showed notable variations between males and females, with an 86% success rate for females and 27.8% for males. The present study provides evidence that the Khaitan formula can serve as a valuable complementary approach for sex determination in females. Sex determination based on the MSI is thought to be a population-dependent parameter in forensic sciences and requires careful interpretation in its application.

Key words: Forensic identification – Legal identity – Maxillary sinus index – Sex determination

INTRODUCTION

Sex estimation is a critical aspect of forensic sciences, anthropology, and archaeology, involving assessing a set of physical features and characteristics to identify a specific individual. Forensic medicine uses medical sciences to support criminal investigations, while forensic dentistry

Corresponding author:
Arofi Kurniawan, DDS., Ph.D. Department of Forensic Odontology, Faculty of Dental Medicine, Universitas Airlangga, Surabaya 60132, Indonesia. E-mail: arofi.kurniawan@fkg.unair.ac.id

Submitted: March 23, 2023. **Accepted:** April 23, 2023

https://doi.org/10.52083/DHPM3206

involves examining dental evidence and providing accurate dental findings (Marini et al., 2020). Among the various factors involved in human identification, sex determination is essential, with bones such as the pelvis and skull proving to be valuable sources of information in cases where the body is skeletonized or burnt (Steyn and İşcan, 1998; Kurniawan et al., 2023). A range of indices can be examined for sex determination, including skull circumference, mandibular bone, palate shape and height, mastoid process, tooth size, dental pulp, and sinuses (e.g., frontal and maxillary sinuses). The maxillary sinus, the most prominent paranasal sinus, starts developing during the 10th week of fetal life and is the first to develop after birth (Lorkiewicz-Muszyńska et al., 2015). Available reports and research indicate that the maxillary sinus remains mostly unaffected after severe injuries or burns. The maxillary sinuses are two cavities in the maxillary bone, with their apex extending to the zygomatic process and their floor reaching the alveolar bone (Sidhu et al., 2014).

A radiographic image of the sinus is a valuable tool for forensic anthropology, facilitating the identification of skeletal remains and sex determination. Several imaging modalities are available, including conventional techniques such as water's view and lateral cephalogram, as well as advanced technologies such as computed tomography (CT) and cone beam computed tomography (CBCT). Among these, the lateral cephalogram is highly regarded for its ability to provide detailed architectural and morphological information about the skull, enabling supplementary characteristics and multiple points of comparison to be identified. Moreover, this radiograph is cost-effective, easily accessible, and reliable for medical diagnoses, treatment planning, and forensic and anthropology studies (Devang Divakar et al., 2016; Abasi et al., 2019).

Khaitan et al. (2017) introduced a novel discriminant function formula for sex determination using the maxillary sinus index (MSI) based on lateral cephalometric radiographs. The study involved 50 healthy subjects (25 males and 25 females) aged 25-55 from the Indian population (Khaitan et al., 2017). However, there are limitations to the established method, as it is not always reliable, and other factors such as age and ethnicity must be taken into account (Tambawala et al., 2016). Therefore, further validation studies are required in different populations, such as the Indonesian population, with a high-risk disaster potential. This study aimed to assess the feasibility of the sex determination formula by Khaitan et al. for the adult population in Surabaya, Indonesia.

MATERIALS AND METHODS

One hundred and thirty (36 males and 94 females, aged 20-40) digital lateral cephalometric radiographs were retrospectively collected from the database of the DHDC Dental Office in Surabaya, Indonesia, between 2019 and 2022. This study involves good quality lateral cephalometric radiograph without abnormalities (such as congenital development and fractures) appearing on the radiograph. Ethical clearance approval of the present study was obtained from the Health Research Ethical Clearance Commission at the Faculty of Dental Medicine, Universitas Airlangga (number: 365/HRECC.FODM/VI/2022).

The lateral cephalometric data, including subject sex and age, were compiled in Microsoft Excel. Maxillary sinus height and width were measured using the SIDEXIS neXT Generation software, and the MSI was calculated based on the width-to-height ratio. The maxillary sinus height is defined as the distance between the highest and lowest points of the sinus, while the maxillary sinus width is the distance between the most anterior and posterior points (Fig. 1). The measurement of maxillary sinus height and width was conducted twice by a single observer, with a two-week time span between measurements to assess intra-observer reliability. Sex determination for each subject was predicted using the formula developed by Khaitan et al.: $D=11.509 - (8.871*MSI)$. A subject was predicted as male if the D score was negative and predicted as female if the D score was positive.

The resulting data were tabulated in Microsoft Excel and analyzed using SPSS version 23.0 software. Descriptive analyses of maxillary sinus width, height, and MSI were performed, and the significance of the difference between males and females was analyzed using an independent *t*-test. The correct sex prediction based on the D score was calculated in percentages for males and females.

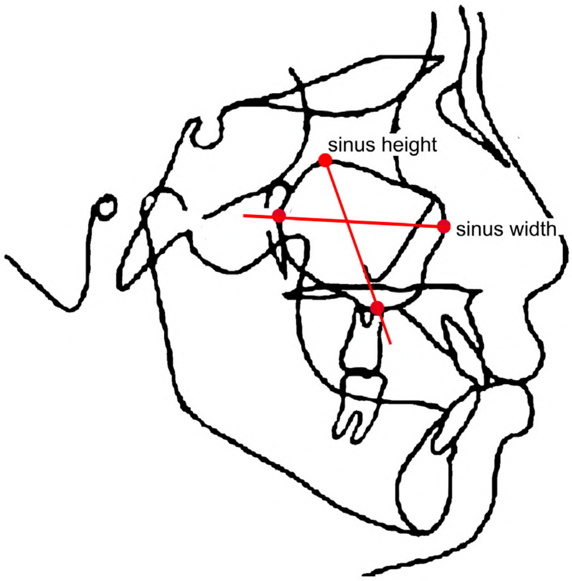

Fig. 1- Illustration of the maxillary sinus height and width on a lateral cephalometric radiograph.

RESULTS

This retrospective study analyzed 130 lateral cephalometric radiographs of patients aged from 20 to 40. The measurements of each parameter were found to have good reliability, with a Cronbach's Alpha value of 0.994 (>0.06). The study found that the parameters measured were significantly greater in males than in females. Table 1 presents the descriptive analysis and independent t-test results for maxillary sinus height, width, and MSI.

Maxillary Sinus Height

The maximum maxillary sinus height for males was 48.86 mm, while the minimum was 29.42 mm, with a mean of 37.112 ± 5.135 mm. On the other hand, the maximum sinus height for females was 49.27 mm, and the minimum was 23.91 mm, with a mean of 34.539 ± 4.362 mm. Our findings indicate that males have a significantly greater maxillary sinus height than females *($p < 0.05$)*.

Maxillary Sinus Width

The maxillary sinus width in males ranged from 37.06 mm to 52.67 mm, with a mean value of 44.153±4.114 mm. In females, the maximum maxillary sinus width was 46.83 mm, and the minimum width was 31.63 mm, with a mean of 38.849±3.335 mm. The independent *t*-test revealed a statistically significant difference in maxillary sinus width between males and females, with $p<0.05$.

Maxillary Sinus Index (MSI)

The MSI is calculated using the width-to-height ratio. The highest MSI value observed in males was 1.45, while the lowest was 0.91. Females had the highest MSI value of 1.49, and the lowest was 0.84. This study found a statistically significant difference in MSI values between males and females, with $p<0.05$. Furthermore, this study conducted the Pearson correlation test to analyze the correlation between the maxillary sinus index and sex determination. The results revealed a significant correlation between MSI and sex, with a coefficient of -0.256.

Table 1. Descriptive analysis and independent t-test of the maxillary sinus height, width, and MSI.

Parameters	Male			Female			Mean difference	*p-value*
	Mean	SD	SE	Mean	SD	SE		
Sinus height	37.112	5.135	0.856	34.539	4.362	0.452	2.573	0.005*
Sinus width	44.153	4.114	0.686	38.849	3.335	0.346	5.304	<0.001*
MSI	1.204	0.142	0.024	1.135	0.108	0.011	0.069	0.003*

MSI: Maxillary sinus index; SD: standards deviation; SE: standards error
*Indicates a significant difference between males and females; measurement unit for sinus height and width: mm

Discriminant Value for Sex Determination

In this study, the discriminant function formula developed by Khaitan et al. was utilized to predict the sex of the cephalometric radiographs based on the MSI value as follows: D= 11.509 – (8.871*MSI). Results showed that the Khaitan et al. formula accurately predicted the sex of 99 of 130 subjects (76.15%). Notably, the formula performed better in females, with a correct prediction rate of 94.68%, compared to males at 27.78% (Table 2).

Table 2. The performance of the sex determination formula by Khaitan for the Indonesian adult population.

Sex	N	Correct		Incorrect	
		N	%	N	%
Male	36	10	27.78%	26	72.22%
Female	94	89	94.68%	5	5.32%
Overall	130	99	76.15%	31	23.85%

DISCUSSION

Sex identification is crucial in establishing an individual identity for the living and the deceased. Previous studies have reported a 100% accuracy rate of sexual dimorphism in the complete skeleton. When utilizing a combination of the pelvis and cranium, the accuracy rate was 98%, followed by a combination of the pelvis and long bones (95%) (Teke et al., 2007; Tambawala et al., 2016). The pelvis and cranium are considered the most reliable anatomical sites for determining sex due to their accessibility and distinct sexual dimorphism. However, the reliability of sex determination from the skull appears to be lower before puberty. Several methodologies have been studied for sex determination, including DNA, morphological, and morphometric analyses (Sidhu et al., 2014; Prakoeswa et al., 2022).

Paranasal sinuses are essential in establishing an individual's identity (Leao de Queiroz et al., 2016). Among these sinuses, the maxillary sinus is the largest and the first to develop at approximately ten weeks of gestation. Subsequently, it continues to pneumatize until the eruption of the third molars (around 20 years of age) and eventually reaches a distance of 5 mm inferior to the nasal floor. After the maximum growth period, the volume of the maxillary sinus decreases due to mineral loss in the bone matrix. The maxillary sinus dimension tends to stabilize after the second decade of human life (Sahlstrand-Johnson et al., 2011; Gupta et al., 2014). Therefore, only subjects aged 20 years and above were considered in this study to ensure accurate measurements.

The present study revealed a significant difference between males and females in the average height and width of the maxillary sinus, with $p<0.05$. This finding is consistent with previous studies by Teke et al. (2007) and Queiroz et al. (2016), which also reported a greater mean height of the maxillary sinus in males than in females (Teke et al., 2007; Leao de Queiroz et al., 2016). Mathew et al. (2020) found significantly higher maxillary sinus dimensions in males than females, except for intermaxillary distance (Mathew and Jacob, 2020). A study by Uthman et al. (2011) and Tambawala et al. (2016) reported that maxillary sinus height was the best-discriminating parameter for studying sexual dimorphism, with an overall accuracy of 71.6% (Uthman et al., 2011; Tambawala et al., 2016).

In a study by Sharma et al. (2014), the measurement of maxillary sinus volume and dimension was analyzed using CT scans. The study yielded noteworthy findings, particularly concerning sexual dimorphism. Specifically, significant differences in maxillary sinus length and volume were observed between male and female subjects. Of the parameters analyzed, maxillary sinus length proved to be the most effective discriminator, with an accuracy rate of 69.81% (Sharma et al., 2014). The present study's findings are consistent with previous research, which suggests that the differences in observed parameters are more pronounced in the anteroposterior dimension of the maxillary sinus, with $p<0.001$.

A study conducted on 33 CT images of the maxillary sinus in a Korean population classified the maxillary sinuses into six categories based on their lateral aspects and the shapes of their inferior walls. The study found that all measurements, including the anteroposterior length, height, width, and volume of the sinuses, were more significant in males than in females, consistent with our findings (Kim et al., 2002).

Fernandes (2004) elucidated the role of the maxillary sinus in ethnic classification through their investigation. Their findings revealed that European crania had significantly larger antral volumes than Zulu. Moreover, males exhibited larger volumes compared to females. In contrast, Zulu male sinuses were narrower than Zulu female sinuses. The study showed that population group was a significant factor, with European sinuses being wider than Zulu sinuses (Fernandes, 2004).

The variations observed in the results of maxillary air sinus dimensions across various studies can be attributed to various factors. These include differences in ethnicity and population group, affecting body stature, skeletal size, height, and physique. Genetic and environmental factors may also play a role, as can anatomical variations of the sinus. Additionally, alterations in osteoclastic and osteoblastic activity, as well as the pneumatization process of the sinus, may contribute to these variations. These factors highlight the need to carefully consider the various influences on maxillary air sinus dimensions in research and clinical practice (Abu El-Dahab and Dakhli, 2023).

While the dimensions of the maxillary sinus can help support sex determination, there are limitations to this method. The maxillary sinus exhibits anatomical variability between the sexes, but there is also an overlap in measurements between males and females. Additionally, factors such as tooth loss, age, and ethnicity can affect the dimension of the maxillary sinus, which may impact its usefulness in sex determination (Tambawala et al., 2016; Leao de Queiroz et al., 2016; Velasco-Torres et al., 2017; Mathew and Jacob, 2020). Other factors affecting the maxillary sinus dimensions include cephalometric parameters and certain medical conditions such as chronic rhinosinusitis (Akay et al., 2020; Pérez Sayáns et al., 2020; Abate et al., 2023).

This study's limitations include a small sample size due to the strict inclusion and exclusion criteria. This study highlights the importance of conducting similar analyses on a more extensive and diverse population. Additionally, measuring the maxillary sinus on lateral cephalograms has limitations related to the two-dimensional view of the sinus, which can result in inaccurate measurements (Abate et al., 2023). Nonetheless, some studies have demonstrated that maxillary sinus measurements on lateral cephalograms are reliable and can assess the relationships between different skeletal classes (Dhiman et al., 2015).

CONCLUSIONS

The findings of this study provide evidence that the Khaitan formula can be a valuable supplementary method for sex determination in females. It is important to note that sex determination based on the MSI is a parameter influenced by the population in forensic science studies and requires careful interpretation during application.

REFERENCES

ABASI P, GHODOUSI A, GHAFARI R, ABBASI S (2019) Comparison of accuracy of the maxillary sinus area and dimensions for sex estimation lateral cephalograms of Iranian samples. *J Forensic Radiol Imaging,* 17: 18-22.

ABATE A, CAVAGNETTO D, LANTERI V, MASPERO C (2023) Three-dimensional evaluation of the maxillary sinus in patients with different skeletal classes and cranio-maxillary relationships assessed with cone beam computed tomography. *Sci Rep,* 13(1): 2098.

ABU EL-DAHAB O, DAKHLI I (2023) The role of cone beam computed tomography in sex identification of a sample of Egyptian population using maxillary sinus predictors. *Oral Surg Oral Med Oral Pathol Oral Radiol,* 6(1): 4-9.

AKAY G, YAMAN D, KARADAĞ Ö, GÜNGÖR K (2020) Evaluation of the relationship of dimensions of maxillary sinus drainage system with anatomical variations and sinusopathy: cone-beam computed tomography findings. *Med Princ Pract,* 29(4): 354-363.

DEVANG DIVAKAR D, JOHN J, AL KHERAIF A, MAVINAPALLA S, RAMAKRISHNAIAH R, VELLAPPALLY S, HASHEM M, DALATI M, DURGESH B, SAFADI R, ANIL S (2016) Sex determination using discriminant function analysis in Indigenous (Kurubas) children and adolescents of Coorg, Karnataka, India: A lateral cephalometric study. *Saudi J Biol Sci,* 23(6): 782-788.

DHIMAN I, SINGLA A, MAHAJAN V, JAJ HS, SETH V, NEGI P (2015) Reliability of frontal sinus with that of maxillary sinus in assessment of different types of skeletal malocclusions. *J Indian Orthod Soc,* 49(2): 96-103.

FERNANDES C (2004) Forensic ethnic identification of crania : the role of the maxillary sinus - a new approach. *Am J Forensic Med Pathol,* 25(4): 302-313.

GUPTA C, KUMAR S, D'SOUZA A, KIRUBA L (2014) A study of morphometric evaluation of the maxillary sinuses in normal subjects using computer tomography images. *Arch Med Health Sci,* 2(1): 12.

KHAITAN T, KABIRAJ A, GINJUPALLY U, JAIN R (2017) Cephalometric analysis for gender determination using maxillary sinus index: a novel dimension in personal identification. *Int J Dent,* 2017: 7026796.

KIM H, YOON H, KIM K, KANG M, KWAK H, PARK H, HAN S, PARK C (2002) Personal-computer-based three-dimensional reconstruction and simulation of maxillary sinus. *Surg Radiol Anat,* 24(6): 392-398.

KURNIAWAN A, CHUSIDA A, UTOMO H, MARINI MI, RIZKY BN, PRAKOESWA BFW, HAMDANI J, SALAZAR-GAMARRA R, DIB LL, ALIAS A, YUSOF MOHDYPM, MARYA A (2023) 3D Bitemark analysis in forensic odontology utilizing a smartphone camera and open-source monoscopic photogrammetry surface scanning. *Pesqui Bras Odontopediatria Clin Integr,* 23: e220087.

LEAO DE QUEIROZ C, TERADA ASSD, DEZEM TU, GOMES DE ARAÚJO L, GALO R, OLIVEIRA-SANTOS C, ALVES DA SILVA RH (2016) Sex determination of adult human maxillary sinuses on panoramic radiographs. *Acta Stomatol Croat,* 50(3): 215-221.

LORKIEWICZ-MUSZYŃSKA D, KOCIEMBA W, REWEKANT A, SROKA A, JOŃCZYK-POTOCZNA K, PATELSKA-BANASZEWSKA M, PRZYSTAŃSKA A (2015) Development of the maxillary sinus from birth to age 18. Postnatal growth pattern. *Int J Pediatr Otorhinolaryngol,* 79(9): 1393-1400.

MARINI MI, ANGROSIDY H, KURNIAWAN A, MARGARETHA MS (2020) The anthropological analysis of the nasal morphology of Dayak Kenyah population in Indonesia as a basic data for forensic identification. *Transl Res Anat,* 19: 100064.

MATHEW A, JACOB L (2020) 3D evaluation of maxillary sinus in gender determination: A cone beam computed tomography study. *J Indian Acad Oral Med Rad,* 32(4): 384.

PÉREZ SAYÁNS M, SUÁREZ QUINTANILLA J, CHAMORRO PETRONACCI C, SUÁREZ PEÑARANDA J, LÓPEZ JORNET P, GÓMEZ GARCÍA F, GUERRERO SÁNCHEZ Y (2020) Volumetric study of the maxillary sinus in patients with sinus pathology. *PLoS One,* 15(6): e0234915.

PRAKOESWA BFWR, CHUSIDA A, KURNIAWAN A, MARINI MI, RIZKY BN, AULIA A, ALIAS A (2022) Analysis of gonial angle related to age in Surabaya population, Indonesia. *Bull Int Assoc Paleodont,* 16(1): 17-21.

SAHLSTRAND-JOHNSON P, JANNERT M, STRÖMBECK A, ABUL-KASIM K (2011) Computed tomography measurements of different dimensions of maxillary and frontal sinuses. *BMC Med Imaging,* 11(1): 8.

SHARMA SK, JEHAN M, KUMAR A (2014) Measurements of maxillary sinus volume and dimensions by computed tomography scan for gender determination. *J Anat Soc India,* 63(1): 36-42.

SIDHU R, CHANDRA S, DEVI P, TANEJA N, SAH K, KAUR N (2014) Forensic importance of maxillary sinus in gender determination: A morphometric analysis from Western Uttar Pradesh, India. *Eur J Gen Dent,* 3(1): 53-56.

STEYN M, İŞCAN MY (1998) Sexual dimorphism in the crania and mandibles of South African whites. *Forensic Sci Int,* 98(1): 9-16.

TAMBAWALA S, KARJODKAR F, SANSARE K, PRAKASH N (2016) Sexual dimorphism of maxillary sinus using cone beam computed tomography. *Egypt J Forensic Sci,* 6(2): 120-125.

TEKE H, DURAN S, CANTURK N, CANTURK G (2007) Determination of gender by measuring the size of the maxillary sinuses in computerized tomography scans. *Surg Radiol Anat,* 29(1): 9-13.

UTHMAN A, AL-RAWI N, AL-NAAIMI A, AL-TIMIMI J (2011) Evaluation of maxillary sinus dimensions in gender determination using helical CT scanning. *J Forensic Sci,* 56(2): 403-408.

VELASCO-TORRES M, PADIAL-MOLINA M, AVILA-ORTIZ G, GARCÍA-DELGADO R, O'VALLE F, CATENA A, GALINDO-MORENO P (2017) Maxillary sinus dimensions decrease as age and tooth loss increase. *Implant Dent,* 26(2): 288-295.

Assessment of reproductive toxicity of Cyfluthrin and Pestban either individually or combined in adult male albino rats

Heba El-Sayed Mostafa[1,2], Eman A. Alaa El-Din[2], Eman M. Kamel[3], Shimaa A. Fareed[3]

[1] Al-Rayan National College of Medicine, Al Medina, Saudi Arabia

[2] Department of Forensic Medicine & Clinical Toxicology, Faculty of Medicine, Zagazig University, Egypt

[3] Department of Anatomy & Embryology, Faculty of Medicine, Suez Canal University, Ismailia, Egypt

SUMMARY

Many studies on individual pesticide risk assessments are available, but the toxicity of combined usage is still to estimate. So, the current study investigated reproductive toxicity induced by exposure to cyfluthrin (CYF) and pestban (PES) and their mixture in adult male albino rats. Forty adult male albino rats were randomized into four groups. All treatments were given daily by oral gavage for 60 days. Group I (control group): this group included 16 rats, divided into two equal subgroups: subgroup Ia (negative control) and subgroup Ib (a vehicle control), in which each rat received 2 ml of corn oil. Group II: CYF group (15.6 mg/kg). Group III; PES group (7.45 mg/kg). Group IV: CYF + PES. Individual CYF and PES exposure significantly decreased testicular weight, serum testosterone level, and epididymal sperm count when compared to the control group. These biochemical changes were confirmed by histological and ultra-structural disarray and reduced immunoreactions of Melan-A (also known as MART-1, Melanoma Antigen Recognized by T-cells), but mutual exposure to both pesticides resulted in a highly significant difference compared to other treated groups. Co-administration of CYF and PES aggravated testicular toxicity, exhausting the endogenous antioxidant status, and down-regulating the immune expression of Melan-A. So, mixing both components can intensify the damaging effects of each compound on testes.

Keywords: Cyfluthrin – Pestban – Testicular toxicity – Rats

INTRODUCTION

Nowadays, farming activities are highly contingent on pesticide use. The pesticide's use play has brought considerable benefits in increasing the availability and food quality by playing an essential role in the expansion of agriculture by decreasing the loss of crops and promoting yield, in addition to enhancing public health in general. Nevertheless, either overuse or misuse of pesticides leads to a great range of negative consequences to species diversity, the environment, and the health of both animals and humans, as is well reported in numerous toxicological studies (Silva et al., 2022).

Corresponding author:
Shimaa Antar Fareed. Department of Anatomy & Embryology, Faculty of Medicine, Suez Canal University, Ismailia, Egypt. E-mail: Shimaa.anter.79@gmail.com - ORCID ID: https://orcid.org/0000-0002-7780-3317

Submitted: February 26, 2023. **Accepted:** May 26, 2023

https://doi.org/10.52083/MMCK6104

The improper application of these pesticides can produce health problems, neurodegenerative diseases, reproductive toxicity, carcinogenicity, and perturbation of the endocrine system (Mohammadi et al., 2021). The widespread resistance and toxicological influence of hazardous pesticides pose unreceptive results on different environmental species and humans, straightforwardly by bioaccumulation or indirectly through the food chain.

Pesticide residues constantly present above permissible legal levels in diversified forms, so much attention has happened likely to regulate their usage without maleficence or negatively affecting the environment (Parra-Arroyo et al., 2022).

Following the World Health Organization reports, the intoxication of pesticides presents a foremost community and public health question; about 3 million cases of pesticide toxicity happen yearly, killing almost 250-370,000 individuals (Kamande et al., 2022).

β-Cyfluthrin (CYF), a class II Pyrethroid (PYR), is an insecticide used worldwide in farming, gardening, and household applications. Repeatedly it is used in veterinary medicine, farming against various pests, and residential and industrial settings. Studies explaining mechanisms of reproductive toxicity regarding this insecticide are limited (Wang et al., 2022).

Pestban (PES) is an organophosphorus (OP) insecticide containing 48% chlorpyrifos (CPF). It is used widely in many agricultural practices; against plants and pests to control animal ectoparasites, although CPF is known as a neurotoxicant through cholinesterase inhibition. Inclusive data assessing pestban effects on gestational length, reproduction, and fertility parameters of males and females are still not clear enough and limited (Morgan and El-Aty, 2008).

The marketing of PYR and OP mixes propagates widely in developing countries and has increased toxicity predominance**.** Trials to prophesy toxicity related to mixtures depending on individual chemicals' acquaintance commonly led to false and deficient conclusions. The interaction due to mixing two or more pesticides is not always expected, because this combination may have summative, potentiating collusive, or inhibitory effects (Alaa El-Din et al., 2022). Therefore, this study assessed testicular toxicity caused by individual and mutual exposure to cyfluthrin and pestban in adult albino rats.

MATERIALS AND METHODS

Chemicals

β-*Cyfluthrin*: it was manufactured by Sigma-Aldrich Company, Louis St., USA, and bought from Sigma Egypt.

Pestban: it was obtained from Indora (Italian company).

Corn oil: it was bought from Sekem Co. in Cairo, Egypt, (a vehicle for both insecticides)

Animals

This study was acted upon at the animal house of the Faculty of Medicine, Suez Canal University, Egypt. Forty adult male albino rats aged two months and ranging in weight from 150 to 170 grams, were used in the present study. The rats were purchased from the Faculty of Veterinary Medicine Animal House, Suez Canal University, Egypt. Rat food and water were freely available to the rodents in the breeding facility. The rats were kept in filter-top plastic cages in a room with artificial lighting and temperature control (23 ±1 °C). The procedure of the experiment was done according to the National Institute of Health Guidelines for the Care and Use of Laboratory Animals (NIH Publications No. 8023, revised 1978). The protocol of the study was confirmed by the Suez Canal University Faculty of Medicine's Research Ethics Committee. (Egypt) (Research Number: 5072#) on Oct 18, 2022.

Experimental design

The total male rats were randomly divided into four groups. The experiment lasted sixty days, and all groups received supplements by oral gavage each day.

Group I (control group): This group included 16 rats, and was divided into two equal subgroups:

Subgroup Ia (negative control): Each rat in this group received a regular diet and water for 60 days. These groups were used as reference comparable values.

Subgroup Ib (positive control): Each rat received 2 ml of corn oil (vehicle of CYF and PES).

Group II (β-Cyfluthrin group) (eight rats): Each rat was treated with CYF at a daily dose of 15.6 mg/kg b.w./day (1/20 of oral LD50) (LD 50 = 380 mg/kg b.w./day) according to Mohafrash et al. (2017)**.**

Group III (Pestban group) (eight rats): Each rat received PES at a daily dose of 7.45 mg/kg b.w./day (1/20 of the oral LD50) (Morgan and El-Aty, 2008), (Abd-Elhakim et al., 2021).

Group IV (Cyfluthrin + Pestban) (eight rats): Each rat received CYF+PES for 60 days (using the same previously mentioned doses and same exposure time).

After exposure to CYF and PES for 60 days, an intraperitoneal injection of thiopental (50 mg/kg) was used to anaesthetize the rats of all groups (Nagaya et al., 2004). In accordance with Nemzek et al. (2001), samples of blood were taken from the retroorbital venous plexus; then scarification of rats was performed. In order to preserve blood samples for hormonal examination, they were kept at -80 °C. Physiological saline was used to swiftly remove the testes, remove any adhering tissue, wash them, and dry them.

Body and testis weight measuring

A digital balance was used to weigh the rats before they were anaesthetized and sacrificed. Testes were removed and weighed, and organ/somatic index were calculated. The relative testes weight = Absolute testes weight/ Whole body weight ×100 (Hamoud, 2019)**.**

Hormonal study

Solid phase radioimmunoassay method was used to measure serum testosterone levels (Kim et al., 2012), while enzyme-linked immunosorbent assay (ELISA) was used to measure serum rat luteinizing hormone (LH) and follicular stimulating hormone (FSH) levels (Chen et al., 2015).

Measurement of blood levels of oxidative stress biomarkers:

Total antioxidant capacity (TAC) was evaluated by using the colorimetric technique following the method described by (Koracevic, 2001). Glutathione peroxidase (GPx), reduced glutathione (GSH), and malondialdehyde (MDA) were measured according to the methods described by Zhang et al. (2018), Ensafi et al. (2008) and Aini et al. (2022), respectively.

Epididymal spermatozoan examination:

Spermatozoa were collected according to Mostafa et al. (2016), epididymal content of every rat was obtained immediately by cutting the tail of the epididymis and squeezing it gently to gain the sparkling of freshly undiluted semen in a clean Petri dish and incubated at 37 °C for half of an hour for liquefaction then we started to proceed the following examinations; sperm count, motility of sperms, and epididymal sperm viability were studied and estimated according to the method reported by Adamkovicova et al. (2016). Then, the percentage of epididymal sperm abnormalities (abnormal forms) was calculated following Vasan (2011)**,** and the sperm abnormal forms were described according to Mori's classification, who classified abnormal sperms into deformed heads and tails (tailless and deformed) (Mori et al., 1991)**.**

Histopathological examination

Testes were preserved in 10% formalin solution, then dehydrated, cleared in xylene, fixed, and blocked-in paraffin using an automatic tissue processor. Five micrometers thick sections were cut by a rotary microtome and stained by the hematoxylin & eosin (H&E) and PAS stains (Hsu, 2015).

Ultrastructural study

Specimens from the testes for electron microscopy examination were promptly fixed in 2.5% phosphate-buffered glutaraldehyde (pH 7.4), post-fixed in 1% osmium tetroxide in the same buffer at 4°C, dehydrated and fixed in epoxy resin. Leica Ultracut UCT was used to create ultrathin slices that were then stained with uranyl acetate, and lead citrate (Van der Horst et al., 2019), seen using a JEOL JEM 1010 electron microscope and captured on camera (Jeol Ltd, Tokyo, Japan) in the Histology and Cell Biology Department, Faculty of Medicine, Al-Azhar University (Egypt).

Immunohistochemical examination

The sections of testis were stained with monoclonal antibodies targeting Melan-A by the avidin-biotin-peroxidase complex (ABC) kit. The sections were then deparaffinized, rehydrated, trypsinized (1 mg pronase/mL Tris-buffered saline), treated with 3% H_2O_2 for 30 minutes at room temperature, and then washed three times. After then, the slices were exposed to primary antibodies for an additional hour. ABC was incubated for 30 minutes following the second antibody infusion. Complete cleaning with Tris-buffered saline (pH: 7.4) was performed on the sections (Shojaeepour et al., 2021).

Statistical analysis

The mean and standard deviation of the data for all groups were displayed (X ± SD). The collected data were handled and analyzed using the SPSS program (SPSS Inc., 2007). One-way analysis of variance was used to find statistically significant differences (ANOVA), followed by the LSD test for multiple comparisons between the different groups. The percentage was assessed by the chi-square test. The test results were considered significant when p value <0.05. P-value <0.01, and <0.001 were considered highly significant.

RESULTS

Effects on body weight and testis weight

The present study showed that mean values of the final body weight and testicular weight (absolute and relative) in CYF (II) and PES (III) treated groups had significantly decreased compared to the control group, but they showed high significant decreases (p-value <0.01) in combined (CYF+PES) treated group (group IV) compared to other studied groups (Table 1).

Hormonal study

Table 2 showed that serum testosterone was significantly reduced in rats individually exposed to CYF and PES, and highly significantly reduced in combined CYF+PES-treated group (group IV). Serum levels of both LH &FSH were significantly decreased in CYF and PES groups; p-value <0.05, where more decrease was noticed in the combined group IV; p-value <0.01 compared with control groups.

Blood levels of oxidative stress biomarkers

Total antioxidant capacity (TAC), glutathione peroxidase (GPx), and reduced glutathione (GSH) were reduced in group-II and group-III treated rats, and were highly significantly reduced in combined treated groups. While Malondialdehyde (MDA) was significantly increased in rats individually exposed to CYF, PES was highly significantly increased in the mutually treated group (Table 3).

Table 1. Initial body weight, final body weight, absolute testis weight and relative testis weight in the study groups.

	Control groups		CYF	PES	CYF + PES
	Ia	Ib			
Initial body weight (g)	189.17± 6.61	188.67± 5.23	189.53± 3.71	190.75 ±8.27	190.23± 6.81
Final body weight (g)	217.83± 5.11	217.59± 7.44	184.83± 4.34*	183.96± 5.62*	160.17± 4.83**#
Absolute testis weight (g/100 g final body weight)	1.77± 0.06	1.76± 0.076	0.95 ±0.052*	0.89± 0.065*	0.660± 0.032**#
Relative testis weight (g)	0.721± 0.03	0.730± 0.05	0.524 ±0.07*	0.500± 0.09*	0.314± 0.08**#

The relative testis weight of each animal is calculated according to the formula:
Relative testis weight = Absolute weight (g) * 100
Final body weight
* p < 0.05 vs control groups
** p < 0.01 vs control groups
# p < 0.05 vs groups II & III

Table 2. Serum testosterone (ng/ml), FSH (ng/ml), and LH (mIU) of adult albino rats among the studied groups.

	Control groups		CYF	PES	CYF + PES
	Ia	Ib			
Testosterone (ng/ml)	1.67 ± 0.49	1.69 ± 0.35	0.86 ± 0.35*	0.90 ± 0.37*	0.25 ± 0.04**#
FSH (ng/ml)	5.96 ± 1.99	6.12 ± 0.32	3.76 ± 2.32*	4.12 ± 1.01*	3.00 ± 0.23**#
LH (mIU)	9.42 ± 1.79	9.37 ± 1.43	6.001 ± 1.62*	5.98 ± 1.39*	3.11 ± 0.89**#

* $p < 0.05$ vs control groups
** $p < 0.01$ vs control groups
\# $p < 0.05$ vs groups II & III

Table 3. Oxidative stress and apoptosis biomarkers in the testis homogenates of the study groups: Total antioxidant capacity (TAC), Glutathione peroxidase (GPx), Reduced glutathione (GSH) and Malondialdehyde (MDA).

	Control group		CYF	PES	CYF + PES
	Ia	Ib			
TAC (mmol/g protein)	0.99 ± 0.005	0.97 ± 0.005	0.68 ± 0.003*	0.65 ± 0.012*	0.38 ± 0.016**
GPx (ng/mg protein)	144.17 ± 4.37	144.06 ± 5.46	130.23 ± 3.09*	131.21 ± 2.07*	115.23 ± 3.09**#
GSH (mmol/ g protein)	3.89 ± 0.01	3.99 ± 0.04	2.39 ± 0.02*	2.46 ± 0.03*	1.77 ± 0.01**#
MDA (nmol/g protein)	11.31 ± 0.04	10.99 ± 0.07	14.1 ± 0.21*	15.3 ± 0.45*	18.4 ± 0.57**#

* $p < 0.05$ vs control groups
** $p < 0.01$ vs control groups
\# $p < 0.05$ vs groups II & III

Epididymal spermatozoa

Normal sperm morphology by Giemsa staining showed a normal head, normal mid-piece, and normal straight tail (Fig. 1a). Sperms of Cyfluthrin treated group showed abnormally polygonal heads, a missing middle piece with a very thin tail (Fig. 1b), while sperms of the Pestban treated group showed different shapes of heads either small oval, bent shape heads or absences of heads, with a detached tail (Fig. 1c). Sperms of combined Cyfluthrin & Pestban treated group showed absent heads, eroded midpiece, and irregular tail (Fig. 1d). Abnormal morphology of sperms in the study groups were described in Chart 1.

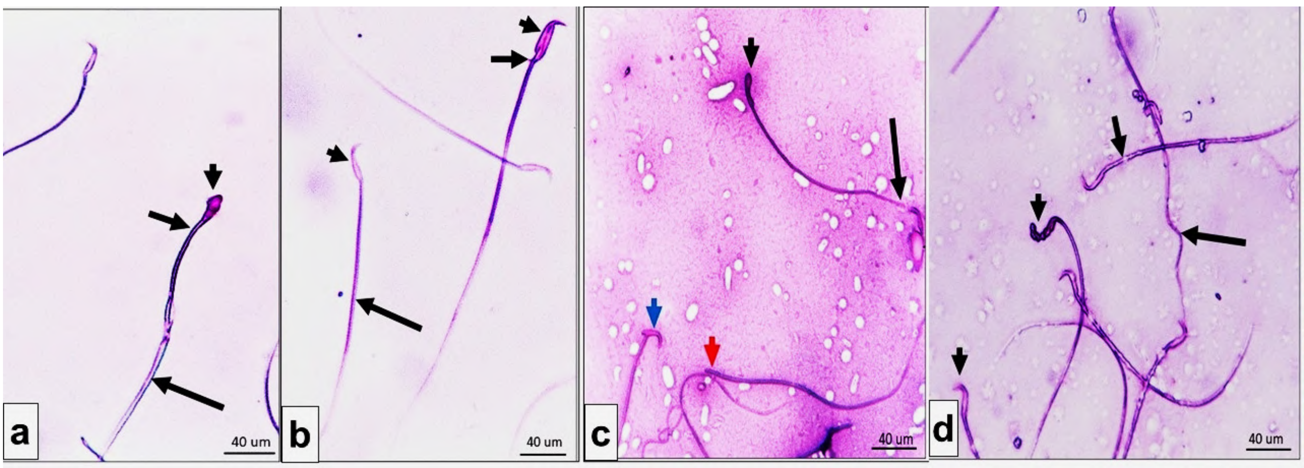

Fig. 1.- Sperm morphology in Giemsa staining **(a):** Normal sperm with normal head (arrowhead), normal midpiece (short head), and normal straight tail (long arrow). **(b):** Sperms of Cyfluthrin-treated group show abnormally polygonal heads (arrowheads), missing middle piece (short arrow) with very thin tail (long arrow). **(c):** Sperms of Pestban-treated group show different shapes of heads either small oval (black arrowhead), bent shape head (blue arrowhead), or absences of the head (red arrow head), with a detached tail (long arrow). **(d):** Sperms of combined Cyfluthrin-and-Pestba- treated group show absent heads (arrowheads), eroded midpiece (short arrow), and irregular tail (long arrow). Giemsa ×400. Scale bars = 40 µm.

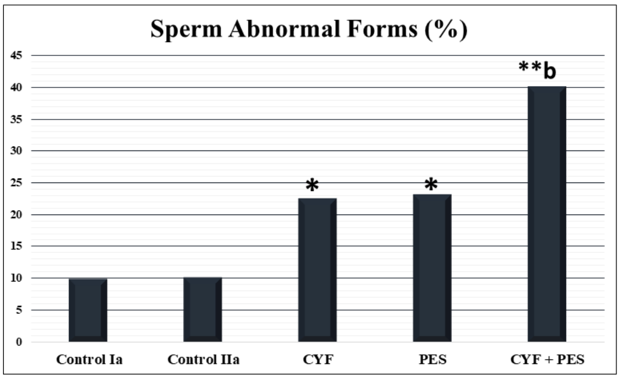

Chart -1 showing; the percent of sperm abnormal forms of the study groups. * p < 0.01 vs control groups. ** p < 0.001 vs control groups. **b** p < 0.001 vs groups II & III

The mean value of sperm motility, viability, and count of the CYF group (II), PES group (III), and combined treated group (IV) showed a highly significant reduction when compared to those in the control group. Additionally, rats treated with pesticides (groups II and III) substantially (p 0.05) had higher mean values of sperm head abnormalities than rats in the control group. While rats in the CYF + PES group (IV) showed the highest significant difference ($p < 0.01$) when compared to those of control and individual CYF- and PES-treated groups (II and III). All data were expressed in (Table 4) and (Chart 2).

Histopathological results

H&E staining

The testicular tissue of the control group showed normal-shaped seminiferous tubules, some with patent lumina, but others showed aggregation of sperms. They were separated by narrow interstitial cells containing Leydig cells and blood vessels (Fig. 2a). Myoid cells and all spermatogenic cell phases were present in the majority of the seminiferous tubules (Fig. 2b).

The testicular parenchyma of the Cyfluthrin-treated group (II) showed irregularly shaped seminiferous tubules, mostly showing a separation of germinal epithelium, irregularly arranged germinal cells, or empty seminiferous tubules. Thickened & edematous interstitial tissues with very dilated and congested blood vessels were noted (Fig. 3a). The primary spermatocytes were either destructed or collected near the center. The secondary spermatocytes were found near the center, and some spermatids were noticed near the basement membrane or irregularly distributed (Fig. 3b).

Table 4. Sperm count, motility, viability, and abnormal forms.

	Control		CYF	PES	CYF + PES
	Ia	IIa			
Sperm count (/ml)	92.55 ±3.55	91.73± 4.57	53.02 ± 7.4*	55.00 ± 6.1*	40.66± 11.83**a
Sperm motility %	73.65 ± 22.4	73.46 ± 51.1	57.74 ± 13.3#	56.99 ± 27.2#	32.42 ± 14.9*a
Sperm viability %	79.12 ± 23.4	78.32 ± 22.5	47.77 ± 12.1#	47.54 ± 23.5#	30.56 ± 15.4**a
Sperm abnormal forms (%)	9.98 ± 1.79	10.15 ± 2.33	22.50 ± 2.15*	23.21 ± 1.33*	40.10 ± 4.21** b

* p < 0.01 vs control groups
** p < 0.001 vs control groups
# p < 0.05 vs control groups
a p < 0.05 vs groups II & III
b p < 0.001 vs groups II & III

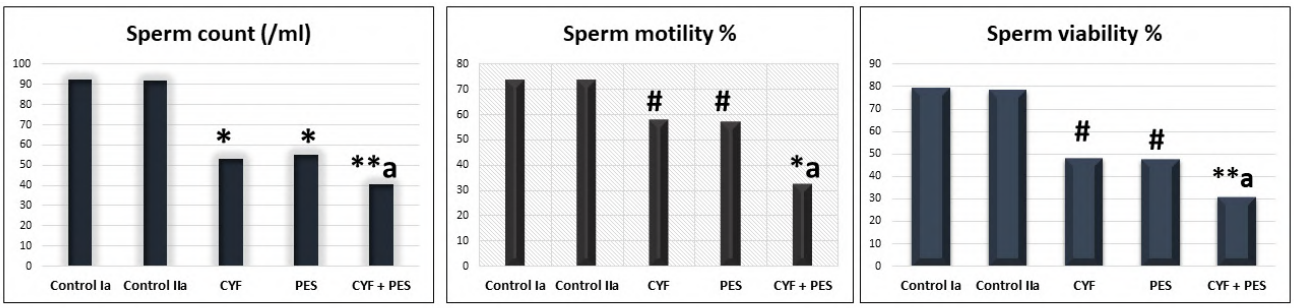

Chart-2 showing; the mean sperm count, percent of motility and viability.
* p < 0.01 vs control groups. ** p < 0.001 vs control groups. # p < 0.05 vs control groups. **a** p < 0.05 vs groups II & III

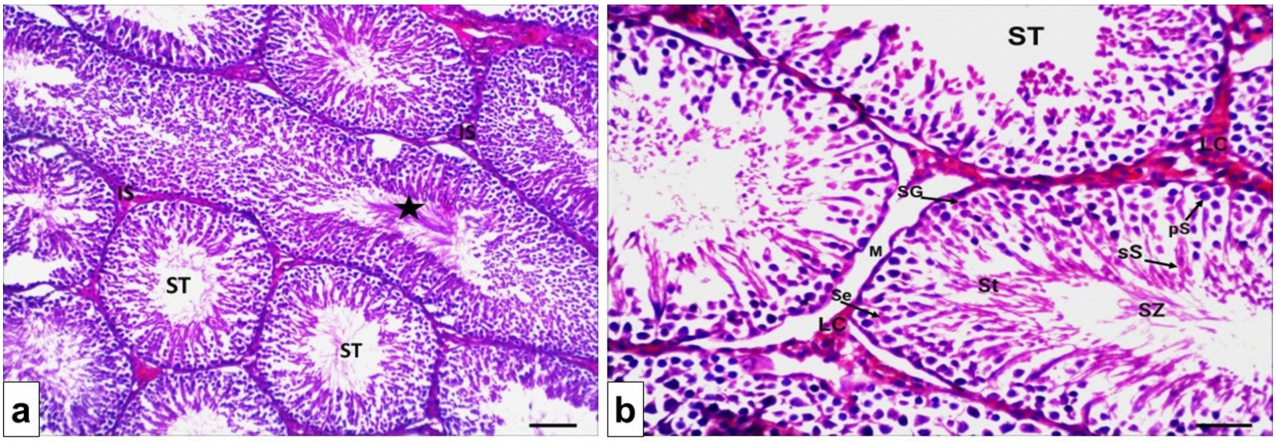

Fig. 2.- Testicular tissue of a rat from the control group showing **(a):** The testicular parenchyma contains seminiferous tubules (ST), some of their lumina were patent, but some showed aggregation of sperms (star). Seminiferous tubules are separated by narrow interstitial cells (IS). **(b):** Each seminiferous tubule contains the myoid cells (M), spermatogonia (SG), Sertoli cells (Se), primary spermatocytes (pS), secondary spermatocyte (sS), and elongated spermatids (St) and spermatozoa (SZ). Leydig cells in the interstitial tissues (LC). H&E staining. Scale bars: a = 40 µm (x200) and b = 20 µm (x400).

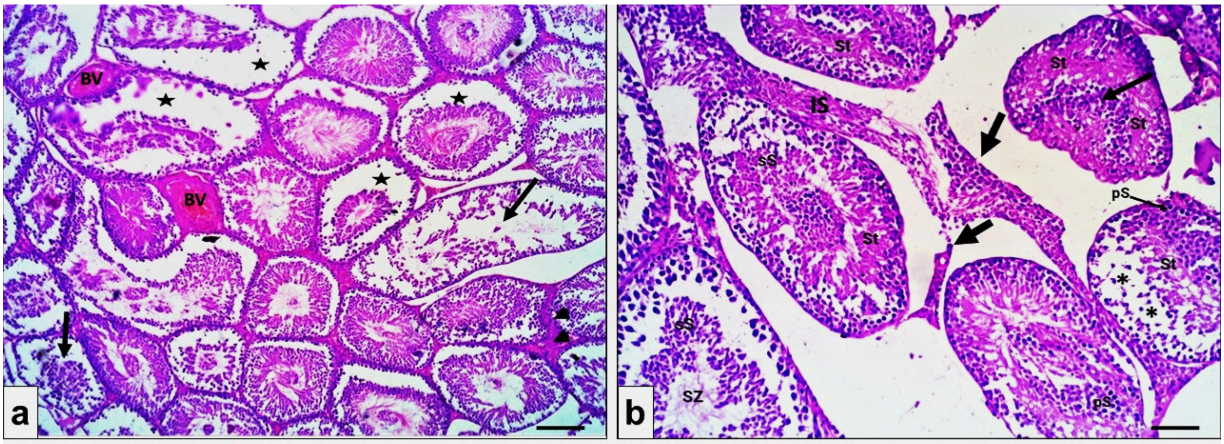

Fig. 3.- Testicular tissue of a rat from the Cyfluthrin-treated group showing **(a):** The testicular parenchyma contains irregularly shaped seminiferous tubules, mostly showing the separation of germinal epithelium (star) or irregularly arranged germinal cells (arrow). Thickened and congested interstitial tissues (arrowheads) with very dilated and congested blood vessels (BV). **(b):** The seminiferous tubules show great irregularity in the arrangement of germinal cells. The primary spermatocytes either destructed (arrow) or (pS) near the center, the secondary spermatocytes (Ss) near the center, and some spermatids (St) lie near the basement membrane or are irregularly distributed. Some tubules show normal spermatozoa (Sz) in their lumen. Others show empty spaces (*). Notice dilated interstitial tissues (IS) or destructed (short arrows). H&E staining. Scale bars: a = 40 µm (x200) and b = 20 µm (x400).

The testicular parenchyma of Pestban-treated group (III) showed a loss of interstitial spaces. Various components of seminiferous tubules were either normal, irregularly distributed tissues or destructed with linear germinal cells inning the basement membrane (Fig. 4a). Some tubules showed separation of germinal cells and were lined by thick capsule with subscapular separation of tissues and very dilated subscapular blood vessels. Some seminiferous tubules showed a collection of germinal cells at the center and spermatids near the center. The interstitial tissues showed infiltration and exudation (Fig. 4b).

The testicular parenchyma of the combined Pestban- and Cyfluthrin-treated group (IV) were lined by a very thick capsule with subscapular separation, exudation, and congested blood vessels. The interstitial tissues showed exudation and congested and dilated blood vessels (Fig. 5a). The seminiferous tubules showed separation of germinal cells from the basement membrane with a central collection of different germ cells (Fig. 5b). Some tubules showed intralaminar hemorrhages and necrotic areas (Fig. 5c). The Spermatogonia were condensed and enlarged. The primary spermatocytes were enlarged with pericellular space and few in number. Secondary spermatocytes were irregular in shape, linearly arranged, or collected in rows. Most of the spermatids were small (Fig. 5d).

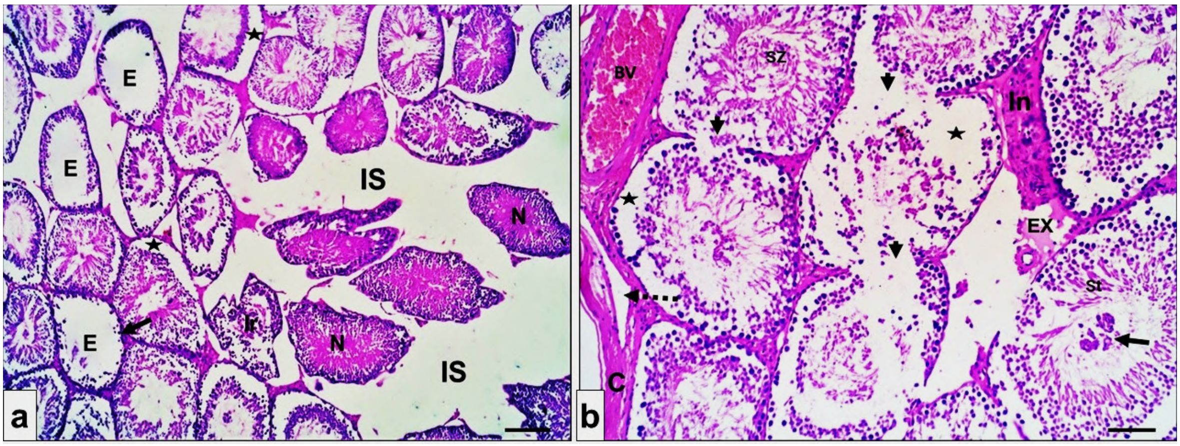

Fig. 4.- Testicular tissue of a rat from the Pestban-treated group showing **(a):** The testicular parenchyma shows loss of interstitial spaces (IS). Varied components of seminiferous tubules; either normal (N), irregularly distributed tissues (Ir), or empty (E) with linear germinal cells inning the basement membrane (short arrow). Some show the separation of germinal cells (star). **(b):** The testicular parenchyma is lined by a thick capsule (C), subscapular separation (detached arrow), and very dilated subscapular blood vessels (BV). The seminiferous tubules show destruction of their basement membranes (arrowheads), empty space (star), collected germinal cells at the center (short arrow), and spermatids near the center (St). notice infiltration (In) and exudation (EX) in the interstitial tissues. H&E staining. Scale bars: a = 40 µm (x200) and b = 20 µm (x400).

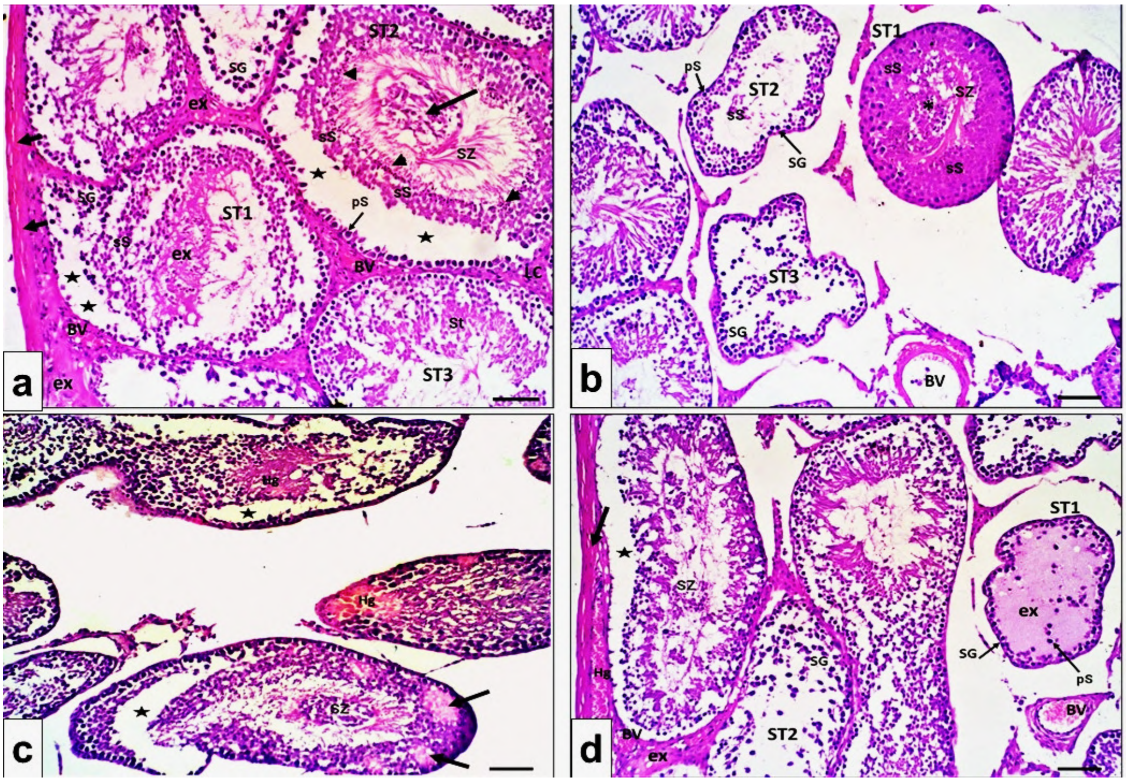

Fig. 5.- Testicular tissue of a rat from the combined Pestban-and-Cyfluthrin-treated group showing **(a):** The testicular parenchyma lined by a very thick capsule (short arrows), subscapular separation (detached arrow) with exudation(ex) and congested blood vessels (BV) of subcapsular area. The interstitial tissues showed exudation (ex), congested and dilated blood vessels (BV) with Leydig cells (LC). The seminiferous tubules show the separation of the germinal cell (star). The seminiferous tubule (ST1) shows condensed spermatogonia (SG), irregular secondary spermatocytes (sS), and exudation(ex). (ST2) shows enlarged primary spermatocytes (Ps) with pericellular space (arrow), linear arranged secondary spermatocytes (sS), small spermatid (arrowheads), spermatozoa (sz) with a central collection of different germ cells (long arrow). (ST3) appears normal. **(b):** Varied seminiferous tubules. (ST1) shows condensed rows of secondary spermatocytes (sS), linear & little spermatozoa (sz) with centrally located germinal cells (*). (ST2) shows enlarged spermatogonia (SG) and primary spermatocytes (pS) with little secondary spermatocytes (sS). (ST3) shows enlarged spermatogonia (SG). Notice enlarged blood vessels (BV). **(c):** The seminiferous tubules show intralaminar hemorrhages (Hg), separation of germinal cells away from the basement membrane (star), and necrotic areas (arrows). **(d):** the section shows thickened capsule (arrow) with subscapular hemorrhage (Hg), dilated blood vessels (BV) and exudation of interstitial tissues. The subscapular seminiferous tubule shows a separation of the germinal cell (star) with condensed spermatozoa in the center (SZ). The seminiferous tubule (ST1) shows intraluminal exudation (ex), and enlarged spermatogonia (SG) with few and enlarged primary spermatocytes (pS). (ST2) shows enlarged & widespread spermatogonia (SG). H&E staining. Scale bars = 20 µm (x400).

PAS staining

The control-group rats showed normal testicular morphology with PAS-positive germ cells and basement membranes of all seminiferous tubules (Fig. 6a). The CYF-treated group showed dense PAS stain of interstitial tissues with destructed basement membrane and separated germ cells (Fig. 6b). The PES-treated group showed mild positive PAS stain in the basement membrane of tubules, and some parts showed destruction (Fig. 6c). The combined PES- and CYF-treated groups showed a very light PAS stain and loss of greater parts of the basement membrane of seminiferous tubules, with few and irregularly distributed germinal cells (Fig. 6d).

Immunohistochemical results

The control groups showed strong positive cytoplasmic brown stains with Melan-A mainly in the interstitial cells of Leydig and in some myoid cells (Fig. 7a). The Cyfluthrin-treated group showed moderate brown stain in some intact interstitial cells of Leydig, but abnormally collected cells Leydig cells showed a negative stain (Fig. 7b). The Pestban-treated group showed a faint brown stain in the interstitial cells of Leydig, in the Sertoli cells and in the myoid cells (Fig. 7c). The combined Pestban-and-Cyfluthrin-treated group showed faint and linear brown staining in the damaged Leydig cells (Fig. 7d). The significant differences between the study groups were presented in Chart 3.

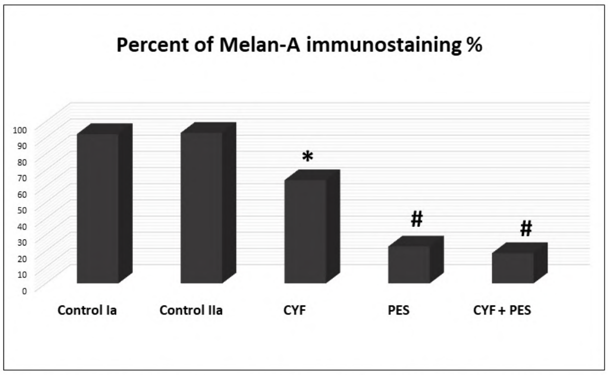

Chart-3 showing; the percent of Melan-A immunostaining in the study groups. * $p < 0.005$ vs control groups. # $p < 0.001$ vs other groups

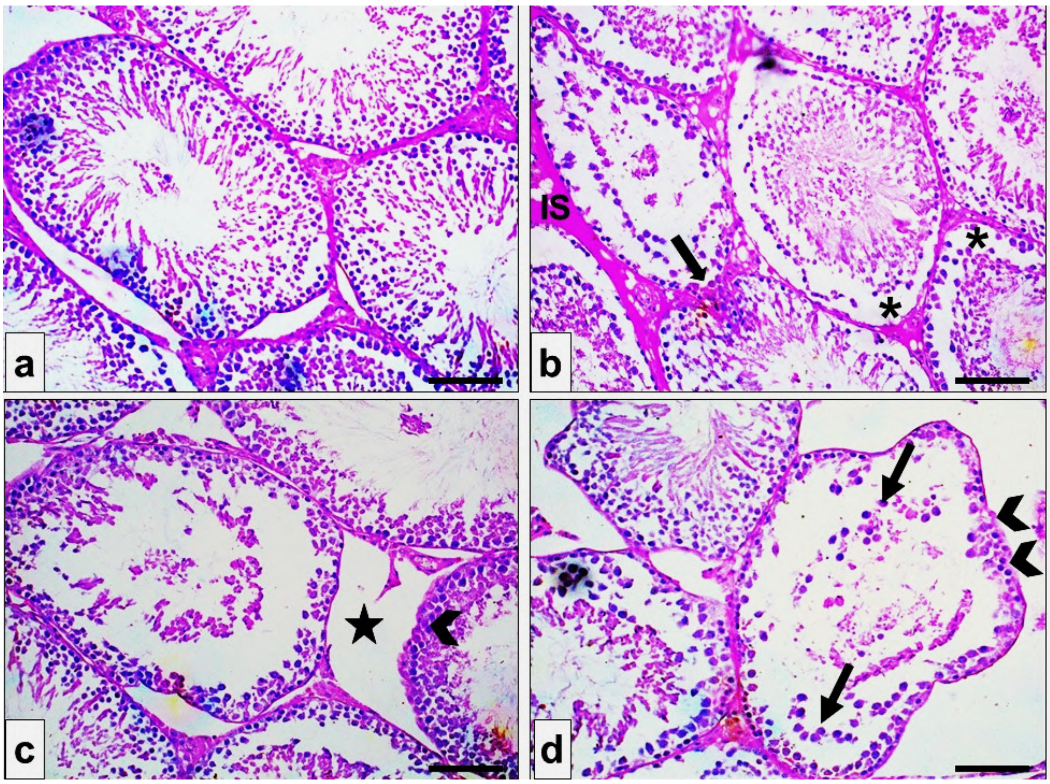

Fig.6. Light microscopy of testicular tissue in different groups stained with periodic acid-Schiff (PAS). (a) Control rat, showing normal testicular morphology with PAS-positive of germ cells and basement membranes of all seminiferous tubules. (b) Cyfluthrin-treated group shows dense PAS stain of interstitial tissues (IS), destructed basement membrane (thick arrow) with separated germ cells (*). (c) Pestban treated group shows mild positive PAS stain of the basement membrane of tubules and some parts showed destruction (arrowhead). (d) combined Pestban-and-Cyfluthrin-treated group shows very light PAS stain with loss of greater parts of the basement membrane of seminiferous tubules (arrowheads) with little and irregularly distributed germinal cells (arrows). PAS staining. Scale bars = 20 μm (x400).

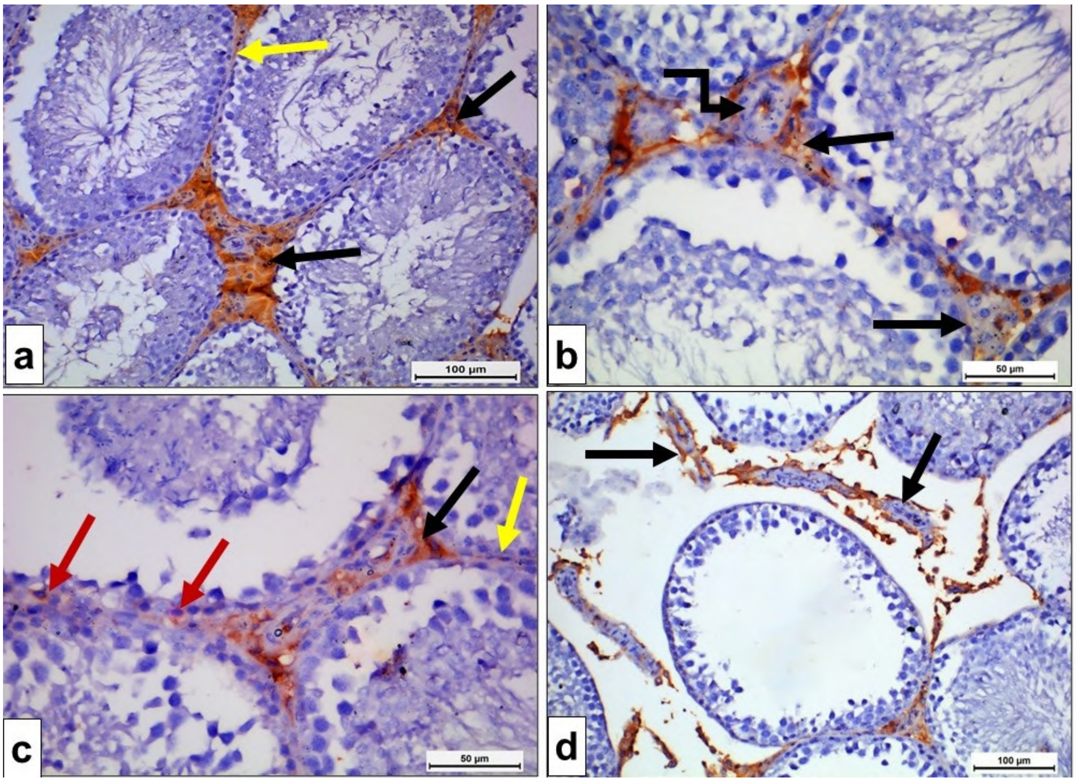

Fig. 7.- Rat testicular tissue of different groups, immuno-histochemical stained with anti-Melan-A. **(a):** The control group shows strong positive cytoplasmic brown stain mainly in the interstitial cell of Leydig (black arrows) and in some myoid cells (yellow arrow). **(b):** Cyfluthrin treated group shows moderate brown stain in some intact interstitial cells of Leydig (arrow), but abnormally collected cells (elbow arrow) showed negative stain. **(c):** Pestban treated group shows a faint brown stain in the interstitial cell of Leydig (black arrow), in the Sertoli cells (red arrows), and in myoid cells (yellow arrow). **(d):** combined Pestban- and-Cyfluthrin-treated group shows faint and linear brown staining in the damaged Leydig cells. (Immunohistochemical staining of anti-Melan-A). Scale bars: a,d = 100 µm; b,c = 50 µm.

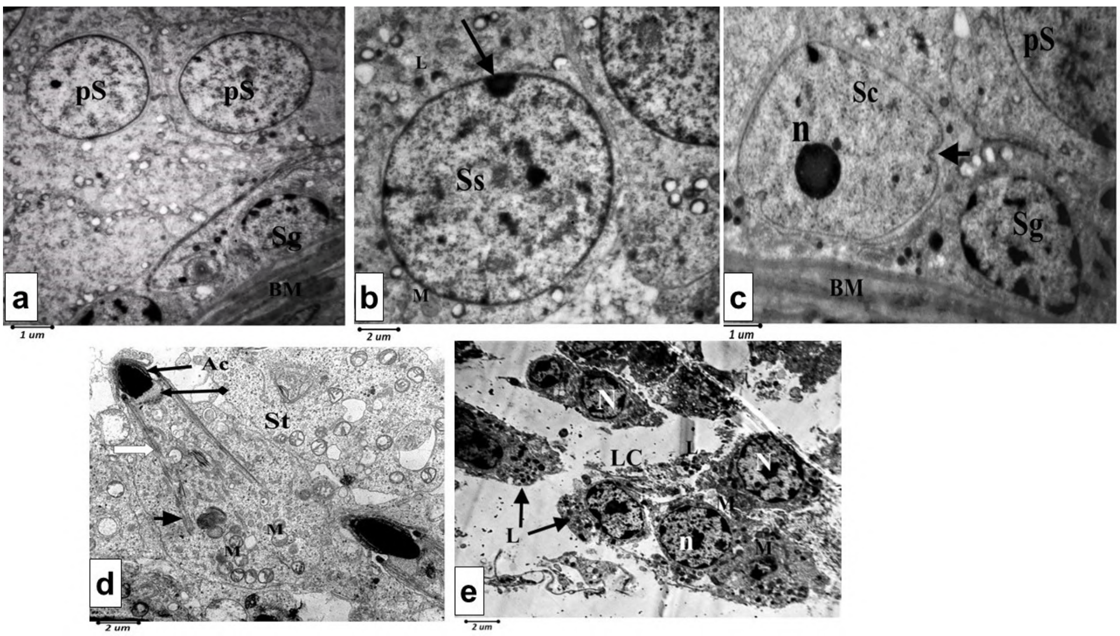

Fig. 8.- Electron micrographs of the control group rat's testis. **(a):** Spermatogonia (Sg) contains a rounded nucleus with peripheral heterochromatin clumps resting on a regular basement membrane (BM), Primary spermatocytes (Ps) with rounded nuclei. **(b):** Secondary spermatocyte (Ss) with large rounded nuclei with heterochromatin clump at one pole (arrow). It is surrounded by mitochondria (M) and lysosomes (L). **(c):** Sertoli cell (Sc) has a pale euchromatic nucleus with prominent nucleolus (n) and shows small nuclear enfolding (arrowhead). Notice spermatogonia (Sg) resting on the basement membrane (BM), with part of primary spermatocytes (Ps). **(d):** Spermatid (St) is composed of a head with an acrosomal cap (AC), middle piece (pointed arrow), cytoplasmic vacuoles (white arrow), annulus (arrowhead), and excess mitochondria (M). **(e):** Leydig cells (LC) showing euchromatic nuclei (N) with peripheral heterochromatin with euchromatic nucleolus (n). Their cytoplasm contains mitochondria (M) and lipid droplets (L). Scale bars: a,c = 1 µm; b,d,e = 2 µm.

Electron microscopic results

Electro micrographs of the control rat's testis showed spermatogonia with rounded nuclei and peripheral heterochromatin clumps resting on a regular basement membrane. The Primary spermatocytes had rounded nuclei (Fig. 8a), while the secondary spermatocyte showed large rounded nuclei with heterochromatin clump at one pole (Fig. 8b). The Sertoli cell showed a pale euchromatic nucleus and prominent nucleolus with small nuclear enfolding (Fig. 8c). The Spermatid was composed of a head with an acrosomal cap, middle piece, annulus, and excess mitochondria (Fig. 8d). Leydig cells showed euchromatic nuclei with peripheral heterochromatin and euchromatic nucleolus; their cytoplasm contained mitochondria and lipid droplets (Fig. 8e).

The Cyfluthrin-treated group (II) showed that the Sertoli cell had a pale euchromatic nucleus with very small nucleolus, and showed large nuclear enfolding lying nearer the thick basement membrane (Fig. 9a). The spermatogonia was elongated, had dark peripheral heterochromatin, and rested on a thick basement membrane; its cytoplasm contained enlarged mitochondria (Fig. 9b). The secondary spermatocyte nucleus showed irregular dense chromatin and an electron-dense body at its periphery, and its cytoplasm contained enlarged rough endoplasmic reticulum (Fig. 9c). The spermatid was composed of an enlarged irregular nucleus and a thin elongated acrosomal cap with residual filaments in front of it. Its cytoplasm contained enlarged mitochondria. Part of the sperm flagellum was surrounded by a huge cytoplasm (Fig. 9d). Differently shaped Leydig cells were noticed, either with oval nuclei, elongated with a small nucleus, or irregularly showing peripheral euchromatin with distributed chromatin. Their cytoplasm contained few lipid droplets (Fig. 9e).

The Pestban-treated group (III) showed pale and irregular Sertoli cells with a euchromatic nucleus, small nucleolus, and too large nuclear enfolding (Fig. 10a). The primary spermatocyte was enlarged, oval, and surrounded by polar perinuclear space. Its cytoplasm contained shrunken mitochondria. The spermatogonia had an enlarged oval-shaped nucleus with a linear collection of

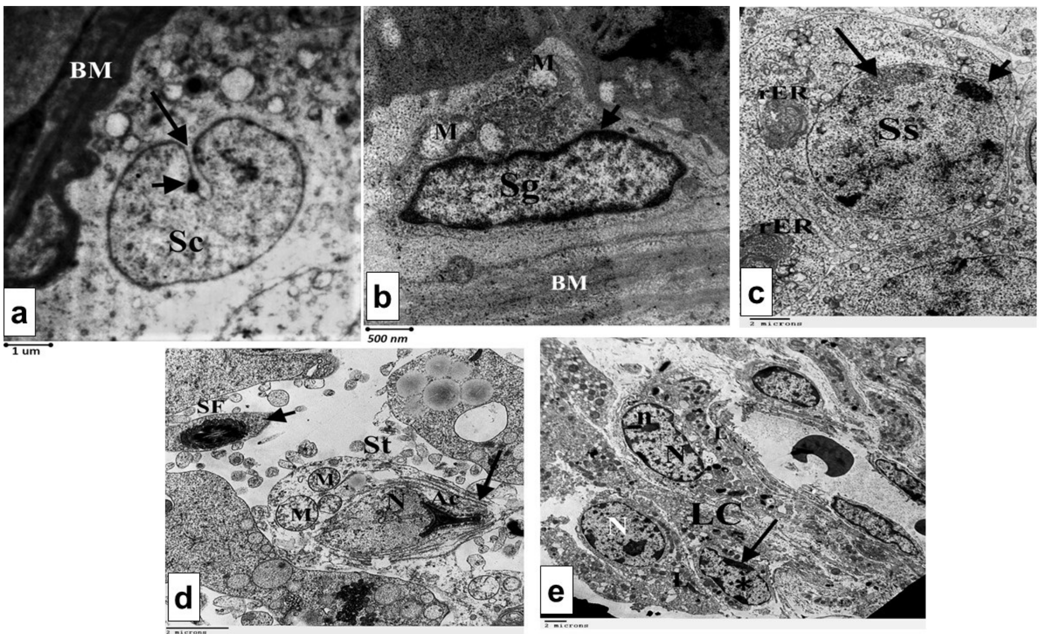

Fig. 9.- Electron micrographs of the testis of Cyfluthrin-treated group. **(a):** Sertoli cell (Sc) has a pale euchromatic nucleus with very small nucleolus (arrowhead) and shows large nuclear enfolding (arrow) and lies nearer to a thick basement membrane (BM). **(b):** elongated Spermatogonia (Sg) with dark peripheral heterochromatin (arrowhead) and resting on thick basement membrane (BM). Its cytoplasm contains enlarged mitochondria (M). **(c):** Secondary spermatocyte (Ss) containing irregular dense chromatin (arrow) and electron-dense body at the periphery of the nucleus (arrowhead). Its cytoplasm contains enlarged rough endoplasmic reticulum (rER). **(d):** Round spermatid (St) composed of enlarged & irregular nucleus (N), thin & elongated acrosomal cap (AC) with residual filaments in front it (arrow). Its cytoplasm contains enlarged mitochondria (M). Part of sperm flagellum (SF) surrounded by huge cytoplasm (arrowhead) **(e):** Different shaped Leydig cells (LC) either oval nucleus (white N), elongated (black N) with small nucleus (n) or irregular showing peripheral euchromatin (arrow) with distributed chromatin (*). Their cytoplasm contains few lipid droplets (L). Scale bars: a = 1 µm; b = 500 nm; c,d,e = 2 µm.

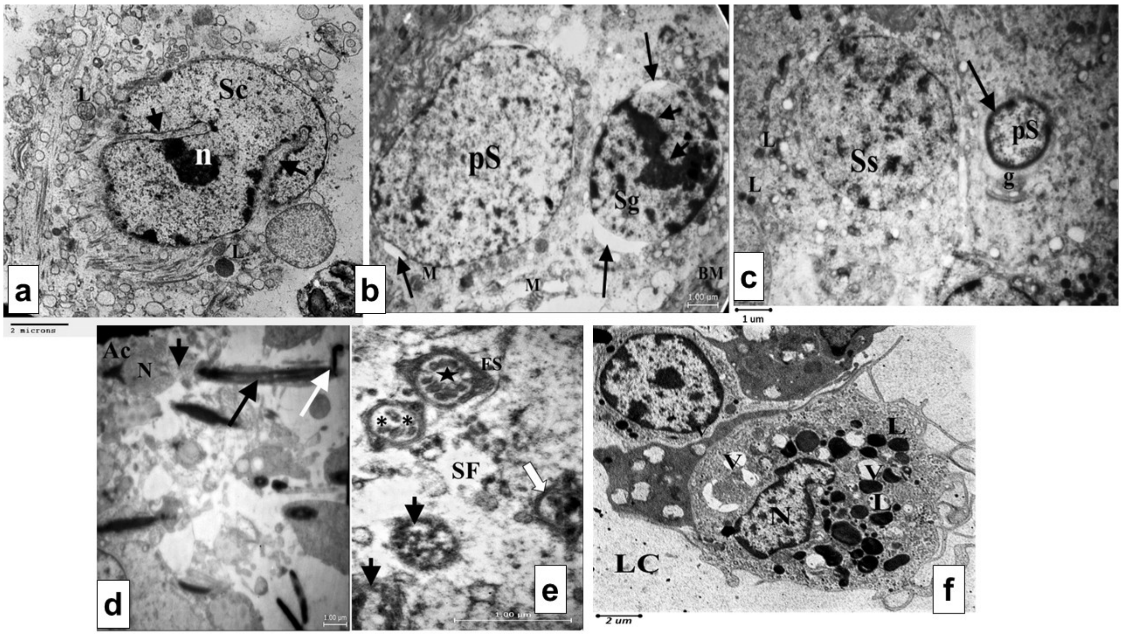

Fig. 10.- Electron micrographs of the testis of Pestban-treated group. **(a):** Sertoli cell (Sc) has a pale, irregular, and euchromatic nucleus with small nucleolus (n) and shows two large nuclear enfoldings (arrowheads). **(b):** Primary spermatocyte (pS) appears enlarged, oval in shape, and surrounded by polar perinuclear space (arrow). Its cytoplasm contains shrunken mitochondria (M). Spermatogonia (Sg) with enlarged and oval-shaped nucleus and resting on basement membrane (BM). It shows a linear collection of dense chromatins (arrowheads), also surrounded by polar perinuclear space (arrow). **(c):** Shrunken primary spermatocyte (pS) nucleus with a dark euchromatic edge (arrow) and surrounded by enlarged Golgi apparatus (g). Secondary spermatocyte (Ss); that's its cytoplasm contains excess lysosomes (L). **(d):** Long spermatid composed of a head with a small nucleus (N), acrosomal cap (Ac), degenerated middle piece (arrowhead), and very thick flagellum (black arrow) with the turned end (white arrow). **(e):** sperm flagellum with wide central vacuole (star) and thick polar fibrous sheath (FS), or with multiple internal vacuoles (*). Notice completely necrosed flagellum (arrowheads) or with thick rim with loss of internal structures (white arrow). **(f):** Leydig cell (LC) with irregular nucleus (N). its cytoplasm contains few lipid droplets (white L), excess (lysosomes (black L), and many vacuoles (V). Scale bars: a,f = 2 µm; b,c,d,e = 1 µm.

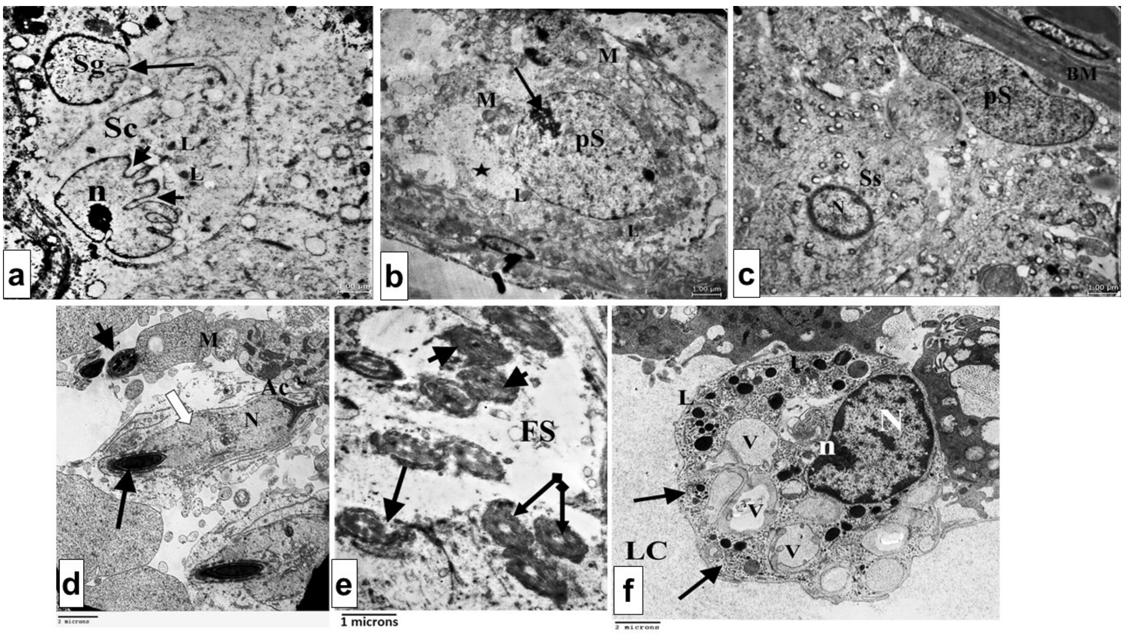

Fig. 11.- Electron micrographs of the testis of the combined Pestban-and-Cyfluthrin-treated group. **(a):** spermatogonia (Sg) which show dark euchromatic rim at one pole and nuclear infoldings at another pole (arrow). Sertoli cell (Sc) has an irregular nucleus with a small nucleolus (n) and shows many nuclear infoldings (arrowheads). Its cytoplasm contains a lot of lysosomes (L). **(b):** Primary spermatocyte (pS) with chromatin clumps at the periphery of the nucleus (arrow). Its cytoplasm shrunken mitochondria (M), lysosomes (L), and empty space (star). **(c):** Primary spermatocyte (pS) with long and euchromatic nucleus. Secondary spermatocyte (Ss); with shrunken nucleus (N). **(d):** abnormal spermatid with enlarged nucleus (N), huge middle piece (white arrow), and thick flagellum (arrow). **(e):** different sperms flagellum (SF) either completely fibrosed fibrous sheath (arrowheads)) or very thick with a small central hole (pointed arrow) or with destructed rim (arrow). **(f):** Leydig cell (LC) with nearly oval nucleus (N) and small polar nucleolus (n). Its cytoplasm contains lipid droplets (L), excess vacuoles (V), and deposited dense particles (arrows). Scale bars: a,b,c,e = 1 µm; d,f = 2 µm.

dense chromatins, also surrounded by polar perinuclear space (Fig. 10b), shrunken primary spermatocyte nucleus with dark euchromatic edge and surrounded by enlarged Golgi apparatus. The cytoplasm of the secondary spermatocyte contained excess lysozymes (Fig. 10c). The spermatid was composed of the head with a small nucleus, acrosomal cap, degenerated middle piece, and very thick flagellum with a turned end (Fig. 10d). The sperm flagellum showed a wide central vacuole and a thick polar fibrous sheath, sometimes completely necrosed (Fig. 10e). The Leydig cells showed an irregular nucleus, and their cytoplasm contained few lipid droplets, excess lysosomes, and many vacuoles (Fig. 10f).

The testicular tissues of the combined Pestban-and-Cyfluthrin-treated group (IV) showed the spermatogonia with a dark euchromatic rim at one pole and nuclear infoldings at another pole. The Sertoli cell owned numerous nuclear infoldings, small, irregular nuclei, and a large number of lysosomes in its cytoplasm (Fig. 11a). The nucleus of the primary spermatocyte displayed chromatin aggregates at its perimeter, and its cytoplasm displayed vacuolations, lysosomes, and reduced mitochondria (Fig. 11b). The nucleus of the secondary spermatocyte was small (Fig. 11c). All of the spermatids in this group had abnormally thick flagella with a variety of defects, including either a totally thickened fibrous sheath or a very thick flagellum with a small central hole (or with a destroyed rim) (Fig. 11d, e). The Leydig cells displayed a tiny polar nucleolus and an oval nucleus. Lipid droplets, extra vacuoles, and deposited dense particles were noticed in their cytoplasm (Fig. 11f).

DISCUSSION

Reproductive health is gradually deteriorating due to multiple endogenous and exogenous factors, such as environmental pollutants and endocrine disruptors, including pesticides (Singh et al., 2014). Over the previous decades, male infertility has obtained pronounced interest worldwide. The diminished sperm concentration is an exceptional problem which has appeared in the European and African populations in the last 50 years (Zhang et al., 2021).

Pesticide toxicity is occasionally constrained to single chemical exposure. However, people are usually subjected to different chemicals in their daily activities. This blended and mixed exposure can result in deteriorating health effects (Rani et al., 2021). In the present study, we tried to investigate reproductive toxicity triggered by single and mutual exposure to CYF and PES. Oral dosing of CYF, PES, and their combination for 60 days in our study triggered a significant decrease in the body weight and testis weight when compared to the control group, which agreed with previous research that studied mixtures of different pesticides (Wang et al., 2009; Sf et al., 2011; Abdel-Rahim et al., 2014).

Authors have suggested that the decreased body weight gain might be due to anorexia and associated lowering of food intake. Also, Iyyadurai et al. (2014) and Rajawat et al. (2014) reported a significant reduction in body weight of CYF-treated rats, due to its cytotoxic effect on somatic cells with direct cytotoxic action of PYR insecticide on the testicular tissues.

This theory was supported by others (Ghorbani-Taherdehi et al., 2020). They explained that OP and PYR exposure resulted in regressive and necrotic testicular changes, in addition to decreasing the germ cell numbers and spermatozoa. Alaa-Eldin et al. (2017) reported that a decrease in testicular weight might be directly related to reduced serum testosterone, FSH, and LH levels, as observed in the current study.

In the present study, the mean values of serum testosterone, follicle-stimulating hormone (FSH), and luteinizing hormone (LH) levels in CYF group and PES group decreased significantly. Rats in combined treated group displayed highly significant declines.

The results of the current study coincided with Zidan (2008), who reported that OP exposure at different doses could reduce testosterone levels. Kang et al. (2004) discussed that decreased testosterone level was associated with defects in gonads and suppression of LH and FSH levels. Kitamura et al. (2003) explained that PES could act as androgen receptor antagonists or suppress genes related to hypothalamic gonadotropin synthesis

(LH and FSH) or steroidogenesis. Sharma et al. (2005) reported similar results after exposure to PYR. Joshi et al. (2003) explained that lowering reproductive hormones in male rats suggests extra-testicular targets of PYR. CYF may influence the hypothalamus-pituitary axis. LH stimulates Leydig cells to produce testosterone; hence, a decrease in LH may be also a contributing factor to the low level of testosterone. PYR pesticides pose anti-gonadal action or deprived levels of androgens that resulted in decreased levels of male gonadal hormones, mitochondrial membranes alteration and damage in Leydig cells, down-regulating expression of gene signaling for essential proteins, and decreased sperm health.

In the present study, oxidative stress load (MDA) in individually CYF- and PES-treated rats showed a significant increase compared with the control group, while they significantly increased in CYF+PES-treated group showed highly significant increases compared to other groups. Various studies regarding OP including PES-induced oxidative stress in diverse tissues bolstered the results of current studies (Nurulain et al., 2013).

Exposure to broad OP pesticides from different sources builds indices of oxidative stress in cells, animals, and humans. These pesticides raise the production of ROS and stimulate alterations in endogenous antioxidant enzymes leading to free radical-mediated lipid peroxidation. In addition to declined antioxidant capacity, free radical-mediated DNA damage, and lipid peroxidation (Pearson and Patel, 2016).

During PYR metabolism, reactive oxygen species (ROS) are produced, leading to oxidative stress. Excess production could have damaging effects on cell membranes in the testes (Stewart et al., 2016). Our results were similar to Martínez et al. (2019), who reported that CYF induced a significant ROS generation, and lipid peroxides presented as malondialdehyde.

The results of the present study for sperm analysis revealed that single pesticide treatments significantly reduced sperm motility, viability, and count, whereas sperm head abnormalities increased significantly. Also, rats in the combined group showed the highest significant difference when compared with those of other groups. These results agreed with Farag et al. (2010), who reported that CPF oral gavage showed marked decrease in sperm count, motility, and an increased percentage of abnormal forms. Sperm count reduction observed in the present study may be directly related to decreased serum testosterone level leading to gradual inhibition of the spermatogenesis process or due to low FSH and LH levels (Sharma et al., 2005)**.** Moreover, reduced sperm motility could be attributed to distressed mitochondrial and intracellular ATP activity, altered fructose synthesis, and attrition of spermatozoan microtubule structure in pesticide-treated rats (Heikal et al., 2014). In accordance with our results, Prakash et al. (2010) explained that Cypermethrin administration led to enzymatic alterations in testes as well as disruption of testosterone synthesis. These changes may cause abnormal sperms leading to complete male sterility.

Yousef et al. (2003) suggested that PYR-induced male reproductive toxicity through a hormone-disrupting mechanism and a neuro-endocrine-mediated phenomenon. PYR interacts competitively with androgen receptors and sex hormone-binding globulin disrupting the endocrine system by mimicking the effect of the female hormone estrogen, leading to low sperm counts. Also, PYR exposure could evoke reactive oxygen species production and subsequently DNA damage, which adversely affects sperm motility and viability, and increases abnormal forms (Bian, 2004)**.** Oxidative damages associated with PYR could mainly affect both Sertoli and Leydig cells. Sertoli cells are accountable for supporting developing germ cells. So, sperm motility would be expected to decline following a decrease in serum testosterone concentration (Stewart et al., 2016).

According to the results of the present study, histological damage was observed in individually treated groups (II) and (III), but it was pronounced in mutual treatment in the combined group.

These results agreed with Rajawat et al. (2014), who stated that CYF caused varied testicular histopathological damage. For example, the germinal epithelium showed shrunken and broken areas, seminiferous tubules were displaced, and the luminal diameter became narrower with widening the interstitial spaces. Also, our results matched with Dohlman et al. (2016), pointing to cellular damage following CYF exposure due to oxidative stress.

Our findings coincided with Kalender et al. (2012)**,** who reported degeneration, necrosis, and decreased spermatogenic cells in some seminiferous tubules of CPF-treated rats (main constitutes of PES). Mosbah et al.(2016) observed a total loss of germinal cells (all the stages) with severe degeneration of seminiferous tubules.

The testicular changes in the current study following PES exposure could be referred to its ability to generate oxidative stress in different tissues and organs, leading to oxidative damage and deleterious pathological changes in the testis (Farag et al., 2010). It has been documented that OP compounds can cross the blood-testis barrier and directly degenerate the spermatogenic and Leydig cells (Uzun et al., 2009)**.**

The histopathological observations in the CYF group were near the results by Elbetieha et al. (2001), who studied the toxic effects of some synthetic PYR (cypermethrin). They found a significant reduction in seminiferous tubule cell layers, with excessive histopathological changes. Ahmad et al. (2012) noted spermatogenesis inhibition with giant cell formation related to disturbed steroidogenesis induced by cypermethrin exposure.

Our electron microscopic results revealed obvious damage in the cytoplasmic organelles in most cells of the seminiferous tubules in the rats individually and co-treated with CYF and PES, which point to functional changes of these cells. According to Joshi et al. (2011), mitochondria are the vital organelles representing cellular damage, and pesticide-derived mitochondrial pathologies are well known.

Spermatid organelles abnormalities found in the combined CYF-and-PES-treated group in our results were similar to those reported by Iwan and Golec, (2020)**,** who observed a significant reduction in intraluminal sperm concentrations following PYR treatment.

El-Gerbed (2013) stated that pesticides were classified as the foremost toxic chemicals that target Sertoli cells. It was assumed that the Sertoli cells facilitate all metabolic exchange with the systemic compartment. The present ultrastructural study revealed marked damage to the Sertoli cell components in the combined group.

Our immunohistochemical results using Melan-A were in accordant with Zhang et al. (2017) who focused on the role of oxidative stress on the viability and functions of the Leydig cells. Similarly, Shojaeepour et al. (2021) used Melan-A to investigate the possible role of Sertoli cells in processing the routes of Cadmium-induced testicular injury. Sertoli cells gathered and produced multinucleated giant cells in the seminiferous tubules throughout the atrophic process, which could be dependent upon Sertoli cells viability and function.

Sertoli cells play supportive and nourishing roles for germ cells in seminiferous tubules. So, they are involved in testis formation and spermatogenesis. Melan-A is considered one of the important markers more expressed by Sertoli cells (Meroni et al., 2019).

In conclusion, when considering the results for different PYR, including CYF studies, researchers found that all PYR types damaged the reproductive system of adult males. All the following parameters are inversely affected by PYR exposure: testis weight, sperm count, sperm morphology, sperm motility, and serum testosterone level, all are inversely affected (Zhang et al., 2018). OP and PYR co-exposure led to an excess reduction in reproductive organs' weight and a lower level of sex hormones (testosterone, FSH, and LH) than each pesticide alone, which was confirmed by histological and ultrastructural disorganization of the testis. Organophosphate pesticides can cross the blood–testicular barrier and cause degeneration of the spermatogenic epithelium and Leydig cells (Moreira et al., 2021).

Abd-Elhakim et al. (2021) recorded a synergistic outcome between two pesticides' (OP and PYR) co-exposure in almost all estimated parameters. Synergism and potentiation observed in the current study could be associated with ROS excess generation inducing more suppression of an essential silent information regulator type-1/ telomerase reverse transcriptase (TERT), and peroxisome proliferator-activated receptor gamma coactivator 1-alpha (PGC-1α) pathway to give rise to this synergistic effect. In this condition, Ma et al. (2019) stated that mixing or co-administration of pesticides that have androgenic antagonistic prosperities could act mutually, especially at the receptor level.

CONCLUSION

The present study indicated that single and mixed exposure to Cyfluthrin and Pestban had deleterious effects on the male reproductive system that could induce infertility. They impaired reproductive functions through abnormal reproductive parameters such as sperm count and viability. The testicular structural and ultra-structural outcomes confirmed the severely impaired and apoptotic germ cells. These findings were more prominent in co-exposure.

REFERENCES

ABD-ELHAKIM YM, EL SHARKAWY NI, EL BOHY KM, HASSAN MA, GHARIB HSA, EL-METWALLY AE, ARISHA AH, IMAM TS (2021) Iprodione and/or chlorpyrifos exposure induced testicular toxicity in adult rats by suppression of steroidogenic genes and SIRT1/TERT/PGC-1α pathway. *Environ Sci Pollut Res*, 28: 56491-56506.

ABDEL-RAHIM EA, ABDEL-MOBDY YE, ALI RF, MAHMOUD HA (2014) Hepatoprotective effects of solanum nigrum linn fruits against cadmium chloride toxicity in albino rats. biol. *Trace Elem Res*,160: 400-408.

ADAMKOVICOVA M, TOMAN R, MARTINIAKOVA M, OMELKA R, BABOSOVA R, KRAJCOVICOVA V, GROSSKOPF B, MASSANYI P (2016) Sperm motility and morphology changes in rats exposed to cadmium and diazinon. *Reprod Biol Endocrinol*, 14: 42.

AHMAD L, KHAN A, KHAN MZ (2012) Pyrethroid induced reproductive toxico-pathology in non-target species. *Pak Vet J Pak*, 32: 1-9.

AINI N, SUSTRIAWAN B, WAHYUNINGSIH N, MELA E (2022) Blood sugar, haemoglobin and malondialdehyde levels in diabetic white rats fed a diet of corn flour cookies. *Foods*, 11: 1819.

ALAA-EL-DIN EA, EL-SHAFEI DA, ABOUHASHEM NS (2017) Individual and combined effect of chlorpyrifos and cypermethrin on reproductive system of adult male albino rats. *Environ Sci Pollut Res*, 24: 1532-1543.

ALAA EL-DIN E, ABDALLAH AA, ABDALLAH EL-SHAFEI D, ABOUHASHEM N, MOSTAFA H (2022) Individual and mixture effect of Deltamethrin and Dimethoate on liver: A biochemical, histopathological, immuno-histochemical, and genotoxic study. *Egypt J Forensic Sci Appl Toxicol*, 22: 23-38.

BIAN Q (2004) Study on the relation between occupational fenvalerate exposure and spermatozoa DNA damage of pesticide factory workers. *Occup Environ Med*, 61: 999-1005.

CHEN L, WANG R, WANG W, LU W, XIAO Y, WANG D, DONG Z (2015) Hormone inhibition during mini-puberty and testicular function in male rats. *Int J Endocrinol Metab*, 13(4): e25465.

DOHLMAN TM, PHILLIPS PE, MADSON DM, CLARK CA, GUNN PJ (2016) Effects of label-dose permethrin administration in yearling beef cattle: I. Bull reproductive function and testicular histopathology. *Theriogenology*, 85: 1534-1539.

ELBETIEHA A, DA'AS SI, KHAMAS W, DARMANI H (2001) Evaluation of the toxic potentials of cypermethrin pesticide on some reproductive and fertility parameters in the male rats. *Arch Environ Contam Toxicol*, 41: 522-528.

EL-GERBED MS (2013) Histopathological and ultrastructural effects of methyl parathion on rat testis and protection by selenium. *J Appl Pharm Sci*, 3: S53-S63.

ENSAFI AA, KHAYAMIAN T, HASANPOUR F (2008) Determination of glutathione in hemolysed erythrocyte by flow injection analysis with chemiluminescence detection. *J Pharm Biomed Anal*, 48: 140-144.

FARAG AT, RADWAN A H, SOROUR F, EL OKAZY A, EL-AGAMY E, EL-SEBAE AE (2010) Chlorpyrifos induced reproductive toxicity in male mice. *Reprod Toxicol*, 29: 80-85.

GHORBANI-TAHERDEHI F, NIKRAVESH MR, JALALI M, FAZE A, GORJI VALOKOLA M (2020) Evaluation of the anti-oxidant effect of ascorbic acid on apoptosis and proliferation of germinal epithelium cells of rat testis following malathion-induced toxicity. *Iran J Basic Med Sci*, 23: 569-575.

HAMOUD A (2019) Possible role of selenium nanoparticles on gentamicin-induced toxicity in rat testis: Morphological and morphometric study. *Egypt J Histol*, 42: 861-873.

HEIKAL TMH, MOSSA AT, IBRAHIM AW, ABDEL-HAMI HF (2014) Oxidative damage and reproductive toxicity associated with cyromazine and chlorpyrifos in male rats: the protective effects of green tea extract. *Res J Environ Toxicol*, 8: 53-67.

HOŁYŃSKA-IWAN I, SZEWCZYK-GOLEC K (2020) Pyrethroids: how they affect human and animal health? *Medicina (Mex.)*, 56: 582.

HSU YC (2015) Theory and practice of lineage tracing. *Stem Cells*, 33: 3197-3204.

IYYADURAI R, PETER JV, IMMANUEL S, BEGUM A, ZACHARIAH A, JASMINE S, ABHILASH KP (2014) Organophosphate-pyrethroid combination pesticides may be associated with increased toxicity in human poisoning compared to either pesticide alone. *Clin Toxicol*, 52: 538-541.

JOSHI SC, MATHUR R, GAJRAJ A, SHARMA T (2003) Influence of methyl parathion on reproductive parameters in male rats. *Environ Toxicol Pharmacol*, 14: 91-98.

JOSHI SC, BANSAL B, JASUJA, ND (2011) Evaluation of reproductive and developmental toxicity of cypermethrin in male albino rats. *Toxicol Environ Chem*, 93: 593-602.

KALENDER Y, KAYA S, DURAK D, UZUN FG, DEMIR F (2012) Protective effects of catechin and quercetin on antioxidant status, lipid peroxidation and testis-histoarchitecture induced by chlorpyrifos in male rats. *Environ Toxicol Pharmacol*, 33: 141-148.

KAMANDE DS, ODUFUWA OG., MBUBA E, HOFER L, MOORE SJ (2022) Modified World Health Organization (WHO) tunnel test for higher throughput evaluation of insecticide-treated nets (ITNs) considering the effect of alternative hosts, exposure time, and mosquito density. *Insects*, 13: 562.

KANG HG, JEONG SH, CHO JH, KIM DG, PARK JM, CHO MH (2004) Chlropyrifos-methyl shows anti-androgenic activity without estrogenic activity in rats. *Toxicology*, 199(2-3): 219-230.

KIM S, KWON H, PARK JH, CHO B, KIM D, OH SW, LEE CM, CHOI HC (2012) A low level of serum total testosterone is independently associated with nonalcoholic fatty liver disease. *BMC Gastroenterol*, 12: 69.

KITAMURA S, SUZUKI T, OHTA S, FUJIMOTO N (2003) Antiandrogenic activity and metabolism of the organophosphorus pesticide fenthion and related compounds. *Environ Health Perspect*, 111: 503-508.

KORACEVIC D (2001) Method for the measurement of antioxidant activity in human fluids. *J Clin Pathol*, 54: 356-361.

MA M, CHEN C, YANG G, WANG Y, WANG T, LI Y, QIAN Y (2019) Combined anti-androgenic effects of mixtures of agricultural pesticides using in vitro and in silico methods. *Ecotoxicol Environ Saf*, 186: 109652.

MARTÍNEZ MA, RODRÍGUEZ JL, LOPEZ-TORRES B, MARTÍNEZ M, MARTÍNEZ-LARRAÑAGA MR, ANADÓN A, ARES I (2019) Oxidative stress and related gene expression effects of cyfluthrin in human neuroblastoma SH-SY5Y cells: Protective effect of melatonin. *Environ Res*, 177: 108579.

MERONI SB, GALARDO MN, RINDONE G, GORGA A, RIERA MF, CIGORRAGA SB (2019) Molecular mechanisms and signaling pathways involved in Sertoli cell proliferation. *Front Endocrinol*, 10: 224.

MOHAFRASH SMM, ABDEL-HAMID HF, MOSSA ATH (2017) Adverse effects of sixty days sub-chronic exposure to β-cyfluthrin on male rats. *J Environ Sci Technol*, 10: 1-12.

MOHAMMADI M, SHADNOUSH M, SOHRABVANDI S, YOUSEFI M, KHORSHIDIAN N, MORTAZAVIAN AM (2021) Probiotics as potential detoxification tools for mitigation of pesticides: a mini review. *Int J Food Sci Technol*, 56: 2078-2087.

MOREIRA S, PEREIRA SC, SECO-ROVIRA V, OLIVEIRA PF, ALVES MG, PEREIRA M DE L (2021) Pesticides and male fertility: a dangerous crosstalk. *Metabolites*, 11: 799.

MORGAN AM, EL-ATY AMA (2008) Reproductive toxicity evaluation of pestban insecticide exposure in male and female rats. *Toxicol Res*, 24: 137-150.

MORI K, KAIDO M, FUJISHIRO K, INOUE N, KOIDE O, HORI H, TANAKA I (1991) Dose dependent effects of inhaled ethylene oxide on spermatogenesis in rats. *Occup Environ Med*, 48: 270-274.

MOSBAH R, YOUSEF MI, MARANGHI F, MANTOVANI A (2016) Protective role of Nigella sativa oil against reproductive toxicity, hormonal alterations, and oxidative damage induced by chlorpyrifos in male rats. *Toxicol Ind Health*, 32: 1266-1277.

MOSTAFA HES, ABD EL-BASET SA, KATTAIA AAA, ZIDAN RA, AL SADEK MMA (2016) Efficacy of naringenin against permethrin-induced testicular toxicity in rats. *Int J Exp Pathol*, 97: 37-49.

NAGAYA N, FUJII T, IWASE T, OHGUSHI H, ITOH T, UEMATSU M, YAMAGISHI M, MORI H, KANGAWA K, KITAMURA S (2004) Intravenous administration of mesenchymal stem cells improves cardiac function in rats with acute myocardial infarction through angiogenesis and myogenesis. *Am J Physiol Heart Circ Physiol*, 287: H2670-H2676.

NEMZEK JA, BOLGOS GL, WILLIAMS BA, REMICK DG (2001) Differences in normal values for murine white blood cell counts and other hematological parameters based on sampling site. *Inflamm Res*, 50: 523-527.

NURULAIN S, SZEGI P, TEKES K, NAQVI S (2013) Antioxidants in organophosphorus compounds poisoning. *Arch Ind Hyg Toxicol*, 64: 169-177.

PARRA-ARROYO L, GONZÁLEZ-GONZÁLEZ RB, CASTILLO-ZACARÍAS C, MELCHOR MARTÍNEZ EM, SOSA-HERNÁNDEZ JE, BILAL M, IQBAL, HMN, BARCELÓ D, PARRA-SALDÍVAR R (2022) Highly hazardous pesticides and related pollutants: Toxicological, regulatory, and analytical aspects. *Sci Total Environ*, 807: 151879.

PEARSON JN, PATEL M (2016) The role of oxidative stress in organophosphate and nerve agent toxicity: Redox and organophosphates. *Ann NY Acad Sci*, 1378: 17-24.

PRAKASH N, KUMAR V, SUNILCHANDRA U, PAVITHRA B, PAWAR A (2010) Evaluation of testicular toxicity following short-term exposure to cypermethrin in albino mice. *Toxicol Int*, 17: 18.

RAJAWAT N, SONI I, MATHUR P, GUPTA D (2014) Cyfluthrin-induced toxicity on testes of Swiss albino mice. *Int J Curr Microbiol App Sci*, 3: 334-343.

RANI L, THAPA K, KANOJIA N, SHARMA N, SINGH S, GREWAL AS, SRIVASTAV AL, KAUSHAL J (2021) An extensive review on the consequences of chemical pesticides on human health and environment. *J Clean Prod*, 283: 124657.

SF AMA, AO A, MU K (2011) Protective effect of vitamin C on biochemical alterations induced by subchronic co-administration of chlorpyrifos and lead in Wistar rats. *J Environ Anal Toxicol*, 1: 108.

SHARMA Y, BASHIR S, IRSHAD M, NAG TC, DOGRA TD (2005) Dimethoate-induced effects on antioxidant status of liver and brain of rats following subchronic exposure. *Toxicology*, 215: 173-181.

SHOJAEEPOUR S, DABIRI S, DABIRI B, IMANI M, FEKRI SOOFI ABADI M, HASHEMI F (2021) Histopathological findings of testicular tissue following cadmium toxicity in rats. *Iran J Pathol*, 16: 348-353.

SILVA AM, MARTINS-GOMES C, SILVA TL, COUTINHO TE, SOUTO EB, ANDREANI T (2022) In vitro assessment of pesticides toxicity and data correlation with pesticides physicochemical properties for prediction of toxicity in gastrointestinal and skin contact exposure. *Toxics*, 10: 378.

SINGH R, SHARMA P, HUQ A (2014) Cypermethrin-induced reproductive toxicity in the rat is prevented by resveratrol. *J Hum Reprod Sci*, 7: 99.

STEWART J, SHIPLEY C, IRELAND F, JARRELL V, TIMLIN C, SHIKE D, FELIX T (2016) Long-term effects of pyrethrin and cyfluthrin, a type II synthetic pyrethroid, insecticide applications on bull reproductive parameters. *Reprod Domest Anim*, 51: 680-687.

UZUN FG, KALENDER S, DURAK D, DEMIR F, KALENDER Y (2009) Malathion-induced testicular toxicity in male rats and the protective effect of vitamins C and E. *Food Chem Toxicol*, 47: 1903-1908.

VAN DER HORST G, KOTZÉ SH, O'RIAIN MJ, MAREE L (2019) Testicular structure and spermatogenesis in the naked mole-rat is unique (degenerate) and atypical compared to other mammals. *Front Cell Dev Biol*, 7: 234.

VASAN S (2011) Semen analysis and sperm function tests: How much to test? *Indian J Urol*, 27: 41.

WANG C, CHEN F, ZHANG Q, FANG Z (2009) Chronic toxicity and cytotoxicity of synthetic pyrethroid insecticide cis-bifenthrin. *J Environ Sci*, 21: 1710-1715.

WANG Z, LIU RAN, ZHANG L, YU S, NIE Y, DENG Y, LIU RUI, ZHU W, ZHOU Z, DIAO J (2022) Thermoregulation of Eremias argus alters temperature-dependent toxicity of beta-cyfluthrin: Ecotoxicological effects considering ectotherm behavior traits. *Environ Pollut*, 293: 118461.

YOUSEF MI, EL‐DEMERDASH FM, AL‐SALHEN KS (2003) Protective role of isoflavones against the toxic effect of cypermethrin on semen quality and testosterone levels of rabbits. *J Environ Sci Health Part B*, 38: 463-478.

ZHANG X, ZHANG T, REN X, CHEN X, WANG S, QIN C (2021) Pyrethroids toxicity to male reproductive system and offspring as a function of oxidative stress induction: Rodent studies. *Front Endocrinol*, 12: 656106.

ZHANG YF, YANG JY, LI YK, ZHOU W (2017) Toxicity and oxidative stress induced by T-2 toxin in cultured mouse Leydig cells. *Toxicol Mech Meth*, 27: 100-106.

ZHANG Z, WU Y, YUAN S, ZHANG P, ZHANG J, LI H, LI X, SHEN H, WANG Z, CHEN G (2018) Glutathione peroxidase 4 participates in secondary brain injury through mediating ferroptosis in a rat model of intracerebral hemorrhage. *Brain Res*, 1701: 112-125.

ZIDAN NEH (2008) Evaluation of the reproductive toxicity of chlorpyrifos methyl, diazinon and profenofos pesticides in male rats. *Int J Pharmacol*, 5: 51-57.

The behavior of adrenal progenitor stem cells in response to chronic stress and recovery

Nermeen H.A. Lashine, Amany Shams, Shaima M. Almasry, Huda El-Tahry, Marwa Abd El-kader

Department of Anatomy and Embryology, Faculty of Medicine, Mansoura University, Egypt

SUMMARY

Stressors affect the differentiation of stem cells in the hypothalamic-pituitary-adrenal axis (HPA). This study was designed to ensure the presence of progenitor cells in the adult adrenal gland and to evaluate their behavior under chronic stress and after recovery. Also, to assess their ability to recruit new glial and chromaffin cells. Three groups of adult male rats (6 rats each): control, chronic-stress (rats were placed individually in stainless restrainers 2h/day for six days), recovered (rats were housed in an enriched circumference for seven days after the same stress modality). Both chronic-stress and recovered groups showed increased adrenal glands weight and cortisol levels with vacuolation, hemorrhage, and edema in the cortex and medulla. The chronic-stress group illustrated a significant increase in the chromaffin reaction, which was reduced in the recovered group. Evaluation of the immunohistochemical results revealed a significant decrease in the Nestin and GFAP (glial fibrillary acidic protein) reactions, but an increase in the chromogranin-A reaction in the chronic-stress group. The recovered group demonstrated a significant increase in the Nestin and GFAP and a reduction in the chromogranin-A immunohistochemical reactions. These results indicate the differentiation of the progenitor (Nestin expressing) stem cells into chromaffin (chromogranin-A expressing) cells under stress conditions for stress adaptation. Conversely, under normal conditions, the differentiation moved toward the glial cells.

Key words: Stem cell – Suprarenal gland – Nestin – GFAP – Chromogranin-A – Stress

ABBREVIATIONS

ACTH: Adrenocorticotropic hormone
ANOVA: analysis of variance
CN: control group
CRH: corticotropin-releasing hormone
CS: chronic stress
GFAP: glial fibrillary acidic protein
HPA: hypothalamic-pituitary-adrenal axis
Hx&E: Hematoxylin and eosin
IRP: Intuitional Research Board
MERC: Medical Experimental Research Center of Mansoura University
NIH: National Institutes of Health
REC: recovery after chronic stress
RIA: radioimmunoassay
SD: standard deviation
SPSS: Statistical package for social sciences
ZF: zona fasciculata
ZG: zona glomerulosa
ZR: zona reticularis

Corresponding author:
Marwa Abd El-kader. Department of Anatomy and Embryology, Faculty of Medicine, Mansoura University Post Office, Mansoura 35516, Egypt. Phone: 002-050-2247358, Mobile: +201004955661. E-mail: dr.marwa5566@yahoo.com / marwa5566@msns.edu.eg - ORCID: 0000-0002-3975-8586

Submitted: May 16, 2023. **Accepted:** June 7, 2023

https://doi.org/10.52083/IMOV9344

INTRODUCTION

Generally, the term "stress" describes our difficulty in dealing with the challenges of life. It is linked to our perceptions of unexpected mental or physical efforts or any work burden we are exposed to (Stalder et al., 2017). Chronic stress results from repetitive, frequent, and intermittent stressors. It can initiate several responses: sensitization, desensitization, and habituation. Sustained activation of the HPA axis results in pulsatile and repetitive glucocorticoid secretion (Holinger et al., 2018).

In times of stress, the CRH (corticotropin-releasing hormone) is released from the hypothalamus and this motivates the pituitary gland to secrete adrenocorticotropic hormone (ACTH). ACTH motivates the release of glucocorticoid from the inner adrenal cortex and the aldosterone from the outer cortex. CRH also impacts the, locus coeruleus, which triggers the sympathetic nervous system to secrete norepinephrine which stimulates the adrenal medulla to generate catecholamines (Berends et al., 2019). Despite the different origins and the nature of the hormones produced, the connection between the cortex and medulla is vital to the appropriate function of the adrenal gland and its adaptation to stress (Dutt et al., 2022).

From the first day of our life, internal and external stressors affect the process of stem and progenitor cell differentiation in the HPA to achieve a fully efficient endocrine stress system (Flak et al., 2012). Previously, the chromaffin stem cells were isolated and differentiated from the murine, bovine, and human adrenal medulla (Rizzoti et al., 2013; Vukicevic et al., 2015).

Various neural crest derivatives preserve in their tissues multipotent neural crest cells (Crane and Trainor, 2006), or even cells that have pluripotent characteristics (Sieber-Blum and Hu, 2008). Nestin is a class VI intermediate filament protein existent in proliferative cells in different fetal and embryonic tissues. Nestin expression is linked to the stem or progenitor cell with multipotent or regenerative properties (Yin et al., 2016). Regarding its distinctive expression pattern, Nestin is considered a marker of stem or progenitor cells (Obara et al., 2019; Bornstein et al., 2020).

A definite pool of Nestin-expressing glial-like progenitor cells was identified. These multipotent cells can differentiate into both neurons and chromaffin cells either in vitro or in vivo (Rubin de Celis et al., 2015). Moreover, Nestin-expressing progenitors are not only found in the adrenal medulla but also in the cortex. So, mature steroid-producing cells could be induced from this pool in response to any physical or metabolic stressors (Steenblock et al., 2017). However, it is uncertain if the multipotent neural stem cells still exist in the medulla of the adult adrenal gland and can participate in its adaptation to stress.

This study was designed to evaluate the adrenal histopathological changes induced by chronic stress and recovery. Also, to assess the existence of stem cells and their response to stress state and recovery by assessment of Nestin immunohistochemical expression. Lastly, to evaluate the capacity of those progenitor stem cells to recruit new glial and chromaffin cells by studying their specific markers (chromogranin-A and GFAP respectively).

MATERIALS AND METHODS

Animals used

Adult male Sprague Dawley rats (total number: 18, weight 220-250 g) were purchased from MERC (Mansoura University Medical Experimental Research Center). Two weeks before the experiment, the rats were housed six per cage under a comfortable environment (temperature: 22 °C, humidity: 55 ± 3%, reversed light/dark cycle: 12/12h) with *ad libitum* access to water and food for acclimatization. The current study was approved by the local ethical committee on animal experimentation, Intuitional Research Board (IRB) (code number: MD.18.03.17-2018/03/14), Faculty of Medicine, Mansoura University. It followed the NIH guidelines for animal care.

Experimental groups

The rats were divided into three experimental groups, six rats each. CN (Control**):** the rats were housed in ordinary stainless cages (60× 35×20 cm) under comfortable conditions during the experiment (El-Desouki et al., 2012). CS (Chronic-stress): each rat in this group was retained individually in stainless-steel wire restrainers (12×7×5 cm to restrict the movement of the animals) (Soliman, 2006), daily for six days (2 h/day: 9 AM to 11 AM) without water or food (Rubin de Celis et al., 2015), then sacrificed on the 7th day. REC (Recovered): after exposure to the same stress design, the rats were returned to an enriched environment for seven days and then sacrificed on the 14th day.

Sacrifice of rats, specimen collection, and assessment of the adrenal gland weight

The body weight was determined at the beginning of the experiment and before sacrifice. After isoflurane anesthesia, the rats were decapitated, abdominal incisions were made, adrenal glands were carefully dissected, immediately weighed, and fixed in buffered formalin (10%) and used for paraffin sections. Other slices from the adrenal glands were fixed in a mixture of potassium chromate and potassium dichromate and then processed for the chromaffin reaction. Samples of blood were collected directly from the left ventricle and for plasma cortisone assessment.

Plasma glucocorticoid hormone

The blood was collected in an EDTA-treated glass tube and centrifuged (1800 rcf, 20 min, 4°C). The plasma was collected and stored at −80°C until used. The plasma glucocorticoid levels were determined by radioimmunoassay (RIA) using a Corticosterone Double Antibody RIA kit (#07–120102, MP Biomedicals, Santa Ana, California) (Bekhbat et al., 2018).

Histology and Immunohistochemistry

The fixed gland tissues were dehydrated using ascending graded concentrations of alcohol, cleared in xylene, and embedded in soft and then hard paraffin wax. Sections were cut (5 µm) and stained with Hematoxylin and eosin (Hx&E) (Bancroft and Gamble, 2002) for Histopathological evaluation. For immunohistochemical staining, sections of the adrenal gland were treated with hydrogen peroxide (3%) to block the activity of endogenous peroxidases, then were rinsed in phosphate buffered saline (pH 7.4). For antigen retrieval, the slides were incubated in sodium citrate buffer (0.01 M - pH 6.0) in a water bath (95°C – 30 minutes). After reaching room temperature, the slides were incubated (1 hr) with bovine serum albumin (1%), then with the primary antibodies (overnight - 4°C): Rabbit polyclonal anti-nestin antibody (N5413, Sigma Chemicals Co., St. Louis, MO, USA – dilution: 1/100) (Bellafiore et al., 2006; Klein et al., 2014), Rabbit polyclonal Anti-chromogranin-A antibody (A0430, Abcam chemicals, Kemet, Egypt – dilution: 1/1500) (Zhang et al., 2018), and Anti- GFAP antibody (ab7260, Abcam chemicals, Kemet, Egypt – dilution: 1/1000) (Nedzvetskii et al., 2016). The sections were treated with HRP-conjugated secondary antibodies (30 minutes - 37°C). The labeled streptavidin-biotin was then applied (30 minutes). The reactions were remarked with DAB (diaminobenzidine) and counterstained with Hx.

For the chromaffin reaction (which demonstrates catecholamine granules in chromaffin cells), the freshly excised tissues were immersed for 16 hours in a solution containing 10 volumes of 5% potassium dichromate and one volume of 5% potassium chromate. They were then washed in three changes of distilled water for a total of 60 minutes, trimmed properly, and embedded in gelatin at 37°C for one hour. Frozen sections were cut at 15 microns, and the slides dried for 2 hours at room temperature to ensure adherence. They were later mounted in glycerol jelly. Adrenaline secreting cells stain lightly (yellow or yellowish-brown), while noradrenaline secreting cells usually stain dark brown (Hillarp and Hokfelt, 1955).

Morphometric study

The thickness of the zona fasciculata (ZF) and medulla were measured in Hx&E-stained sections at 100X magnification. The value was the mean of three measurements of the maximum, medium, and minimum thickness (Gannouni et al., 2014). The optical density (OD) of chromaffin and immunohistochemical (Nestin, chromogranin-A, and GFAP) stained sections were evaluated in five non-overlapping randomized fields. The fields were photographed using a digital camera (Olympus® SC100) installed on a light microscope

(Olympus® CX41). The morphometric analysis was done using the NIH (National Institutes of Health, Bethesda, MD, USA) Image J program, observing the program instructions.

Statistical analysis

The data were analyzed by the statistical package for social science program (SPSS version 22) for descriptive statistics represented as mean±standard deviation (SD) and analytical statistics for comparison between the different groups. The significance of difference was tested either by using analysis of variance (ANOVA) to compare between more than two groups of parametric data followed by post-hoc Tukey test, or Kruskal–Wallis test to compare between more than two groups of non-parametric data followed by Mann- Whitney test for multiple comparisons. *P*-value <0.05 was considered statistically significant.

RESULTS

Assessment of rat's body weight

Assessment of the body weight revealed a significant decrease (*P<0.011*) in CS group (184.2±10.034) as compared to CN group (200.8 ±10.848). Regards REC group (205.2±7.295), there was a significant increase (*P<0.002*) in body weight when compared to CS group and non-significant increases (*P<0.464*) in comparison to CN group (Fig. 1).

Assessment of the adrenal gland weight

The weight of the adrenal gland significantly increased (*P<0.0001*) in CS group (35.25±1.279) as compared to CN group (30.176±1.854). Although, the adrenal gland weight of REC group (35.11±1.279) demonstrated a non-significant (*P<0.867*) difference from CS group, it significantly increased (*P<0.0001*) when compared to CN group (Fig. 2).

Assessment of the plasma cortisol level

The plasma cortisol level significantly increased (*P<0.0001*) in CS group (10.156±0.769) as compared to CN group (5.554±0.252). The elevated cortisol level significantly reduced (*P<0.0001*) in REC group (8.482±0.82) as compared to CS group. However, it is still significantly elevated (*P<0.0001*) than CN group (Fig. 3).

Assessment of the histopathological results

Hematoxylin and eosin-stained sections

Sections of CN group revealed apparent normal histological structure. The adrenal gland was formed of an inner pale central medulla and outer dark cortex surrounded by a connective tis-

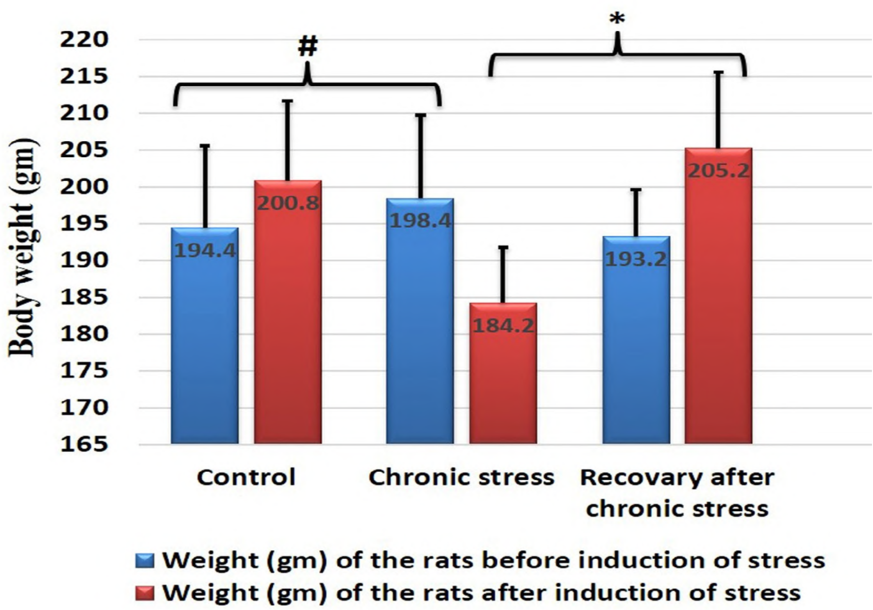

Fig. 1.- Histogram illustrating a significant decrease in the bodyweight of the CS group comparing to the CN group, and a significant increase in the REC group comparing to the CS group. #p<0.05, *p<0.01.

sue capsule. The cortex was formed of zona glomerulosa (ZG), zona fasciculata (ZF), and zona reticularis (ZR) (Fig. 4A). The cells of ZG were columnar with deeply stained, rounded nuclei, and arranged in small nests (Fig. 4B). The cells of ZF were large and polyhedral, containing central rounded vesicular nuclei; they were arranged in parallel cords, disjoined by blood sinusoids (Fig. 4C). The cells of ZR appeared small, rounded, and dark, with hyperchromatic nuclei, and characteristic brown wear and tear lipofuscin pigment; they were arranged in anastomosing cords separated by blood sinusoids (Fig. 4D). The adrenal medulla consisted of follicles of chromaffin cells that contain basophilic catecholamines granules and vesicular nuclei. Connective tissue trabeculae were seen extending between the medullary follicles. Blood sinusoids, medullary venules, and clusters of ganglion cells were seen in the interfollicular space (Fig. 4E).

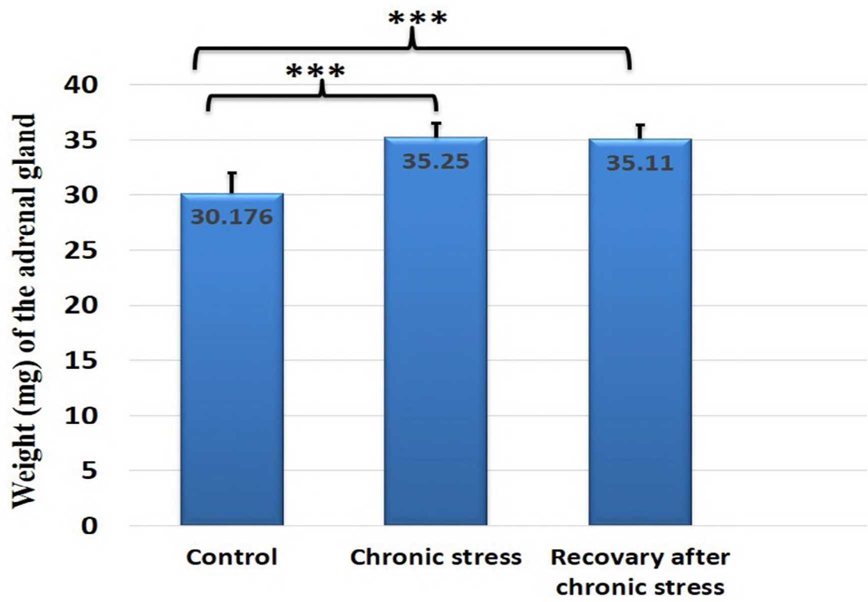

Fig. 2.- Histogram illustrating a significant increase in the adrenal gland weight of both CS and REC groups comparing to the CN group. ***p<0.0001.

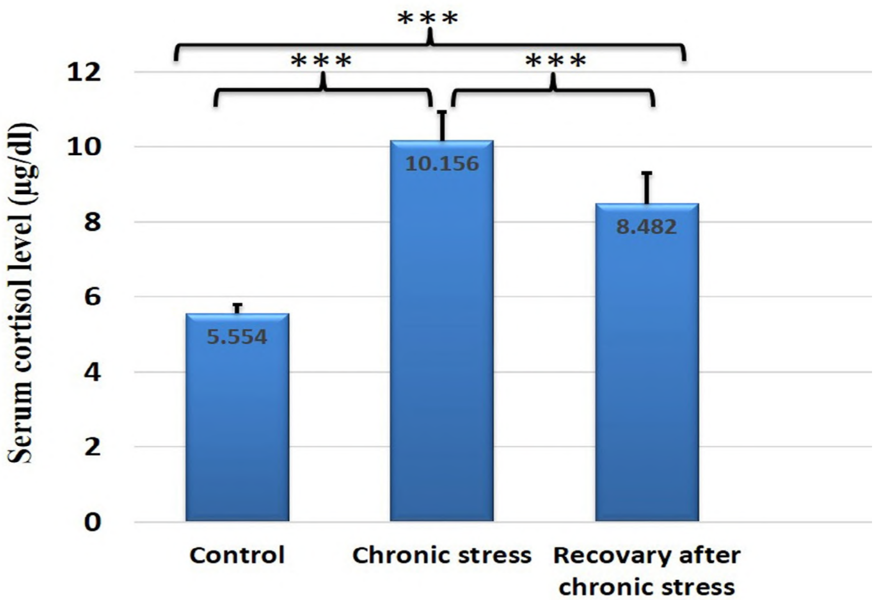

Fig. 3.- Histogram illustrating a significant increase in the serum cortisol level in both CS and REC groups comparing to the CN group. However, it shows a significant decrease in the REC group comparing to the CS group. ***p<0.0001.

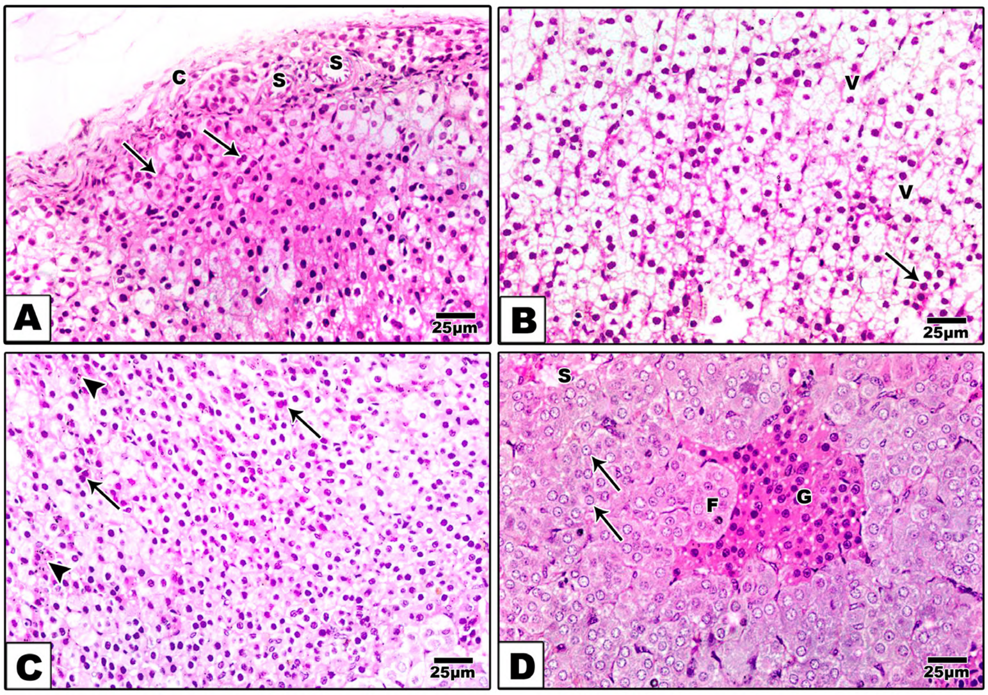

Fig. 4.- Photomicrographs of Hx&E-stained adrenal gland of a CN rat showing **A):** Capsular and subcapsular regions of rat suprarenal gland. The capsule (C) has blood sinusoids (S) between its cells and surrounds the peripheral subcapsular thin zona glomerulosa which consists of small nests of cells (arrows) with dark cytoplasm. **B):** The cells of the zona fasciculata are arranged in parallel cords of cells (arrow). The cells appear large and polyhedral containing large rounded nuclei. Their cytoplasm has tiny cytoplasmic vacuoles (V) and is stained faintly acidophilic. **C):** The zona reticularis cells are rounded dark cells arranged in anastomosing cords and have hyperchromatic nuclei and dense cytoplasm (arrows). A brown pigment (arrow heads) is seen between the cords. **D):** The medulla is formed of basophilic chromaffin cells with vesicular nuclei (arrows) which are arranged in follicles (F) surrounding blood sinusoids (S). A cluster of ganglion cells (G) is seen in the interfollicular space. Scale bars = 25 µm.

The adrenal gland of CS group revealed atrophy of ZG, congested blood sinusoids, and vacuolations (Fig. 5A). In ZF, many vacuoles were detected in between swollen cells, indicating edema. Some cells with pyknotic nuclei and hemorrhage were observed (Fig. 5B). The ZR showed blood engorgement, dilated sinusoids, and vacuolations (Fig. 5C). The adrenal medulla showed packed chromaffin cells with constriction of the follicular lumen and reduction of the space between the follicles. Extracellular eosinophilic material and degenerated chromaffin cells were detected. There was also an increasing number and congestion in medullary blood sinusoids as well as hemorrhage between the follicles (Figs. 5E, 5D).

The ZG of REC group showed hemorrhage, dilated congested blood sinusoids, and vacuolations (Fig. 6A). In ZF, swollen cells were still observed due to edema. Cellular mitotic figures, vacuoles, and hemorrhage are present between the cells (Fig. 6B). The ZR cells still showed vacuolations and hemorrhage (Fig. 6C). The medulla still showed vacuoles inside the follicular cells, as well as reduction in the follicular lumen and the interfollicular space. Extracellular eosinophilic material was detected. There was congestion in medullary blood sinusoids, as well as hemorrhage in between the follicles (Fig. 6D).

Zona fasciculata thickness: There was a significant increase (*P<0.025*) in ZF thickness in CS group (668±94.98) (Fig. 7B) compared to CN one (533.4±25.24) (Fig. 7A). The ZF thickness in REC group (579.8±37.16) (Fig. 7C) was little lower than CS group (*P<0.129*) and higher than CN group (*P< 0.415*) (Fig. 8).

Chromaffin-stained sections

The chromaffin reaction in CN group revealed a positively stained central brown medulla and a negatively stained peripheral yellowish cortex (Fig. 9A). The catecholamine granules in the adrenaline secreting cells are stained yellowish-brown, while those in the noradrenaline secreting cells are stained dark brown (Fig. 9B).

CS group (Figs. 9C, D) showed a non-significant increase (*P<0.663*) in OD of adrenaline cell

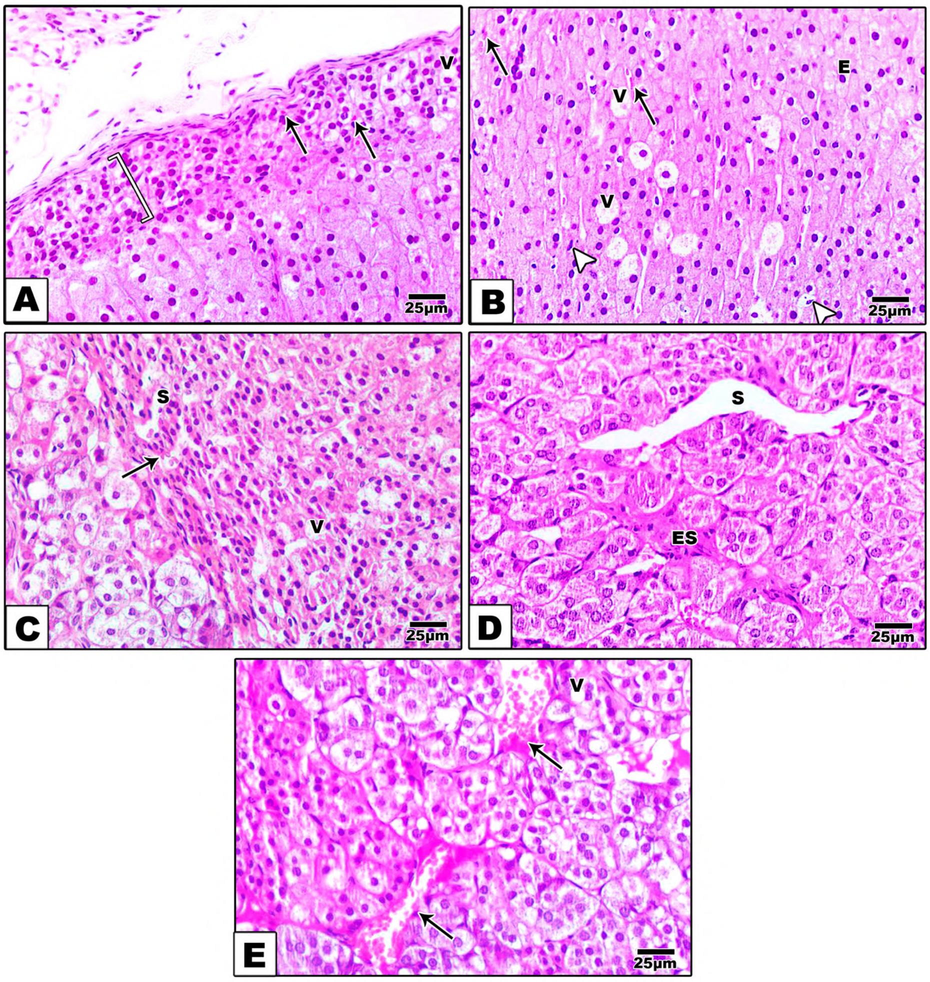

Fig. 5.- Photomicrographs of Hx&E-stained adrenal gland of a CS rat showing **A):** decreasing the zona glomerulosa thickness, vacuolation (V), and hemorrhage (arrows). **B):** The zona fasciculata represents, vacuolation (V), hemorrhage (arrows), and pyknotic nuclei (arrow heads). **C):** The zona reticularis represents dilated sinusoid (S), vacuolation (V), and hemorrhage (arrow). **D, E):** The medulla showing dilated blood sinusoids (S), hemorrhage in between chromaffin follicles (arrows), vacuolation (V), and eosinophilic material (ES). There is crowding and swelling of chromaffin cells with obliteration of many follicular lumens. Scale bars = 25 µm.

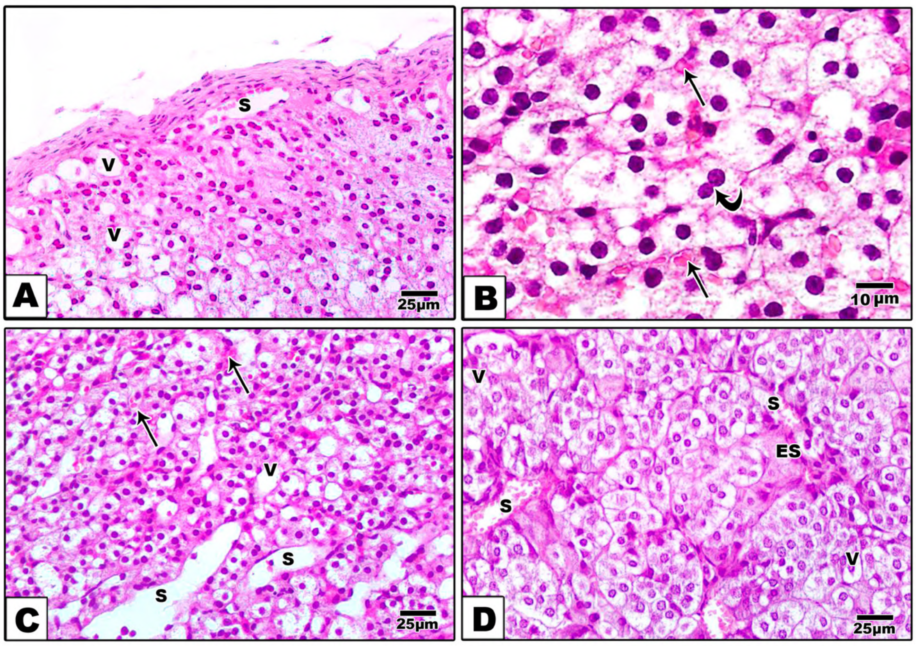

Fig. 6.- Photomicrographs of Hx&E-stained adrenal gland of a REC rat after chronic stress showing **A):** vacuolation (V) and dilatation in blood sinusoids (S) of zona glomerulosa. **B).** The zona fasciculata illustrates hemorrhage (arrows) between its cells. The curved arrow points to the mitotic nucleus. **C):** The zona reticularis represents vacuolation (V), hemorrhage (arrows), and dilated blood sinusoids (S). **D)**: The medulla showing dilated blood sinusoids (S), vacuolation (V), and extracellular eosinophilic material (ES). Scale bars = 25 µm.

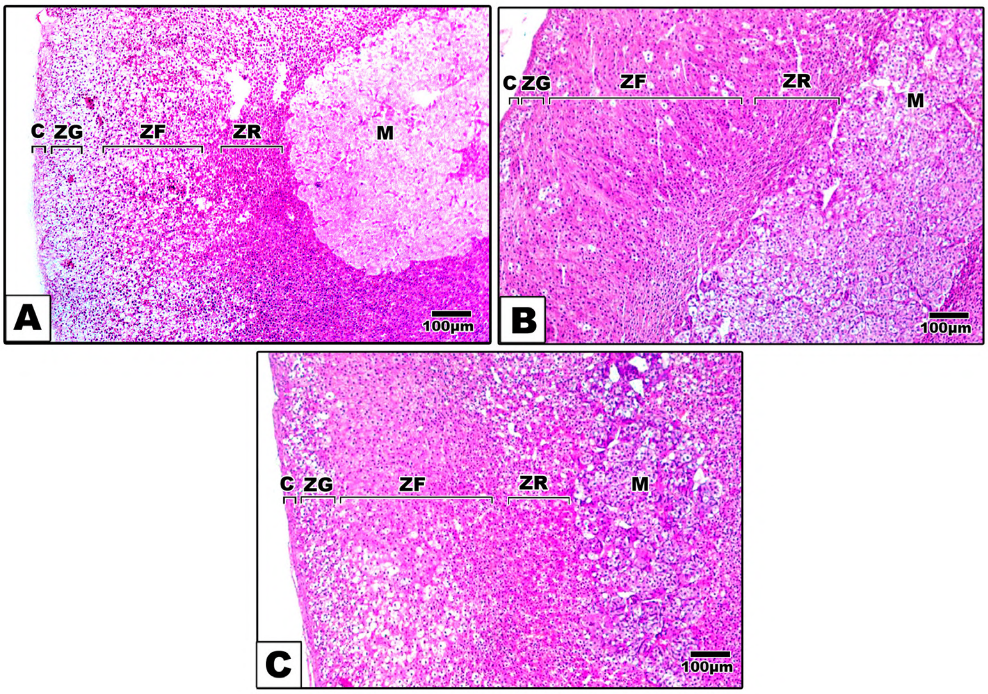

Fig. 7.- Panoramic of rat adrenal glands of **A):** CN, **B):** CS, and **D):** REC rats showing the capsule (C), the three cortical layers; zona glomerulosa (ZG), zona fasciculate (ZF), zona reticularis (ZR), and medulla (M). Scale bars = 100 µm.

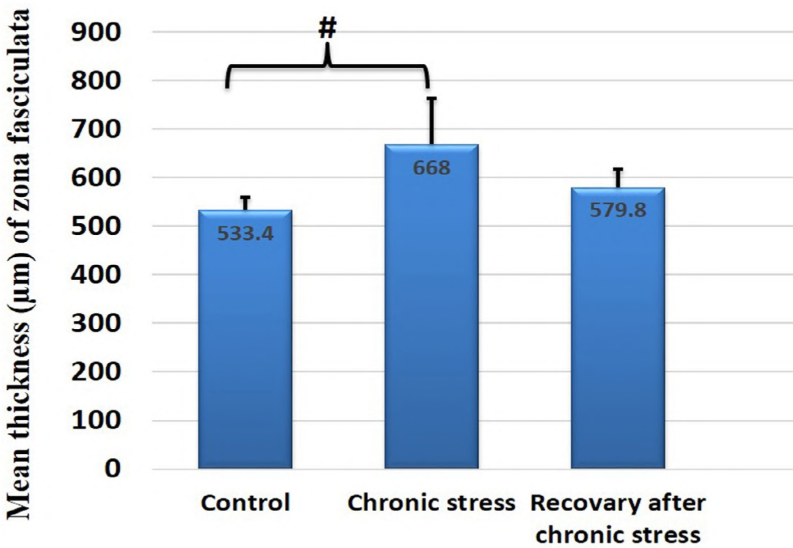

Fig. 8.- Histogram showing significant increase in the ZF thickness in the CS group. #p<0.05.

(0.171±0.023), and a significant increase (*P<0.01*) in the nor-adrenaline cells (0.277±0.066). Regarding REC group (Figs. 9E, F), although it illustrated a non-significant difference (*P<0.992, P< 0.655*) in the OD of adrenaline cell (0.171±0.036) compared to CS and CN groups, and in OD of nor-adrenaline cells (0.21±0.034) compared to CN group (*P<0.102*), it had a significant decrease effect (*P<0.034*) on OD of nor-adrenaline cells compared to CS group (Fig. 10).

Assessment of the immunohistochemical results

Immunohistochemistry for Nestin

The Nestin immunohistochemical reaction in CN group was represented as diffuse and dotted in the cytoplasm of ZG cells (Fig. 11A). The immune stain was scattered in cells of ZF (Fig. 11B) and ZR (Fig. 11C). The medulla showed a strong positive reaction (Fig. 11D).

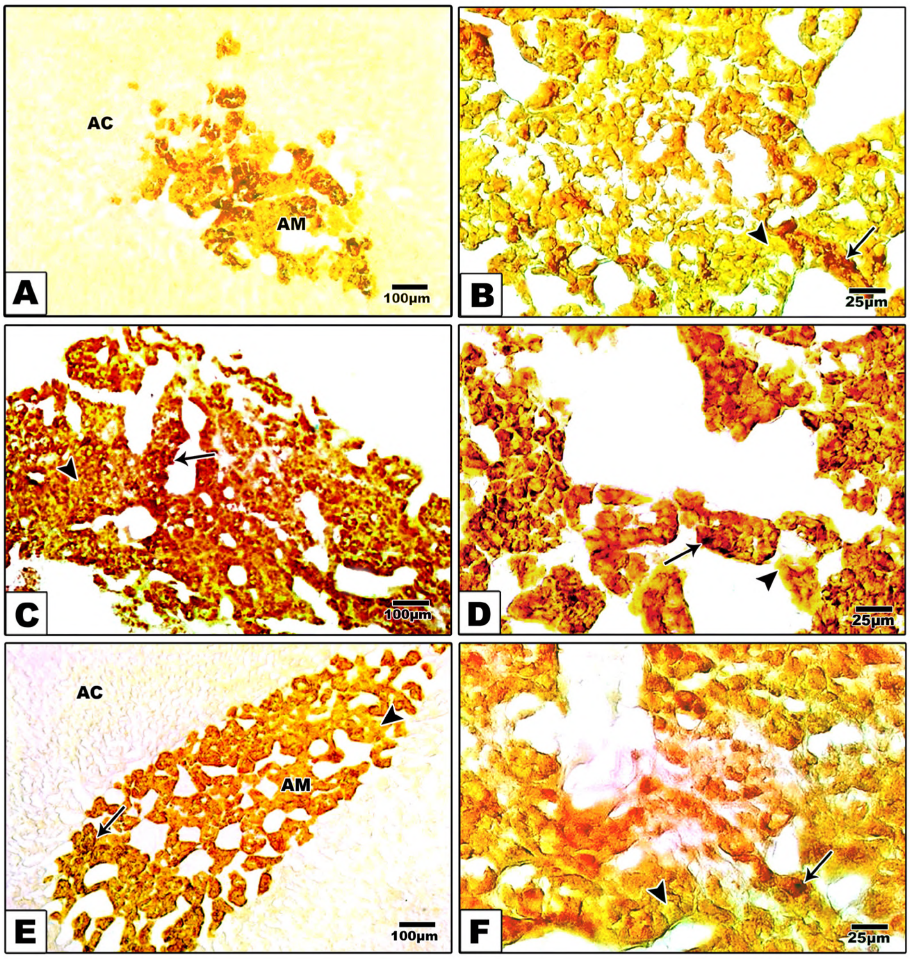

Fig. 9.- Chromaffin reaction in the adrenal glands of **A, B):** CN rat showing positively stained central brown medulla (M) and a negatively stained peripheral yellowish cortex (C). The catecholamine granules in adrenaline secreting cells (blue arrow) are stained yellowish-brown while those in noradrenaline secreting cells are stained dark brown (black arrow). **C, D):** CS rat. Showing the catecholamine granules in adrenaline secreting cells (blue arrow) were moderately stained yellowish-brown while those in noradrenaline secreting cells are strongly stained dark brown (black arrow). **E, F):** The REC rat after chronic stress showing the catecholamine granules in adrenaline secreting cells (blue arrow) were moderately stained yellowish-brown and those of noradrenaline secreting cells were moderately stained dark brown (black arrow). Scale bars A, C,E = 100 µm; B,D,F = 25 µm.

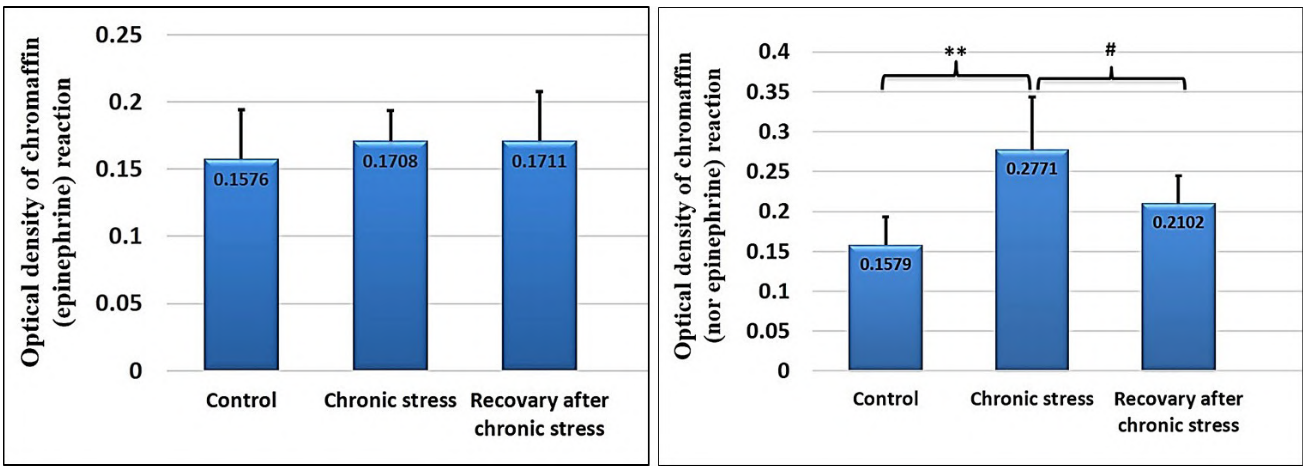

Fig. 10.- Histograms illustrate the statistical differences in the OD of the chromaffin reaction (epinephrine and nor-epinephrine respectively) between the studied groups. The epinephrine reaction represents a non-significant difference between the studied groups. The nor-epinephrine reaction represents a significant increase in the CS group comparing both CN and REC groups. #p<0.05, **p<0.001.

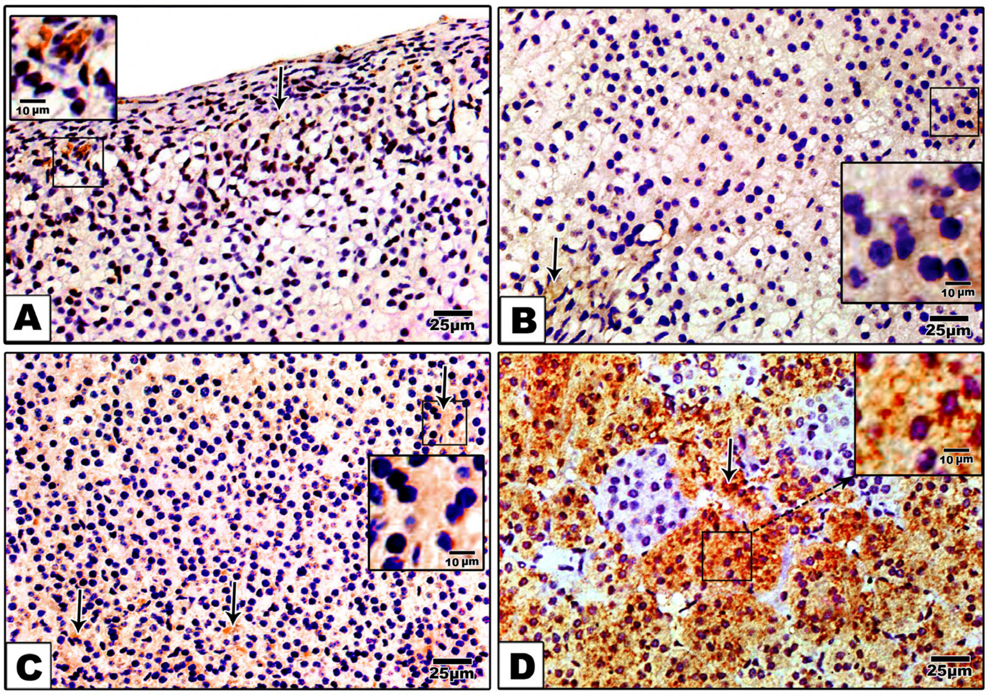

Fig. 11.- Nestin immunostained suprarenal gland sections of the CN rat showing **A):** diffuse and dotted (magnified square) faint immunohistochemical reaction (arrow) in the cytoplasm of the capsular and subcapsular region (zona glomerulosa)**. B):** scattered immunostaining (arrow) is in the cells of zona fasciculate (magnified square)**. C):** dispersed immunoreaction (arrows) in the zona reticularis. **D):** There is a strong positive immune reaction (arrow) in the medulla**.** (Nestin immunohistochemical stain with Hx&E counterstain). Scale bars = 25 µm.

The CS group showed weak Nestin immunostaining in the cytoplasm of capsular and subcapsular (ZG) regions (Fig. 12A), ZF (Fig. 12B), ZR (Fig. 12C), and medulla (Fig. 12D), with a highly significant decrease (*P<0.0001*) in OD of the total adrenal Nestin-stained cells (0.097±0.023) as compared to CN group (0.160±0.029). The REC group showed a mild Nestin immunohistochemical reaction in ZG

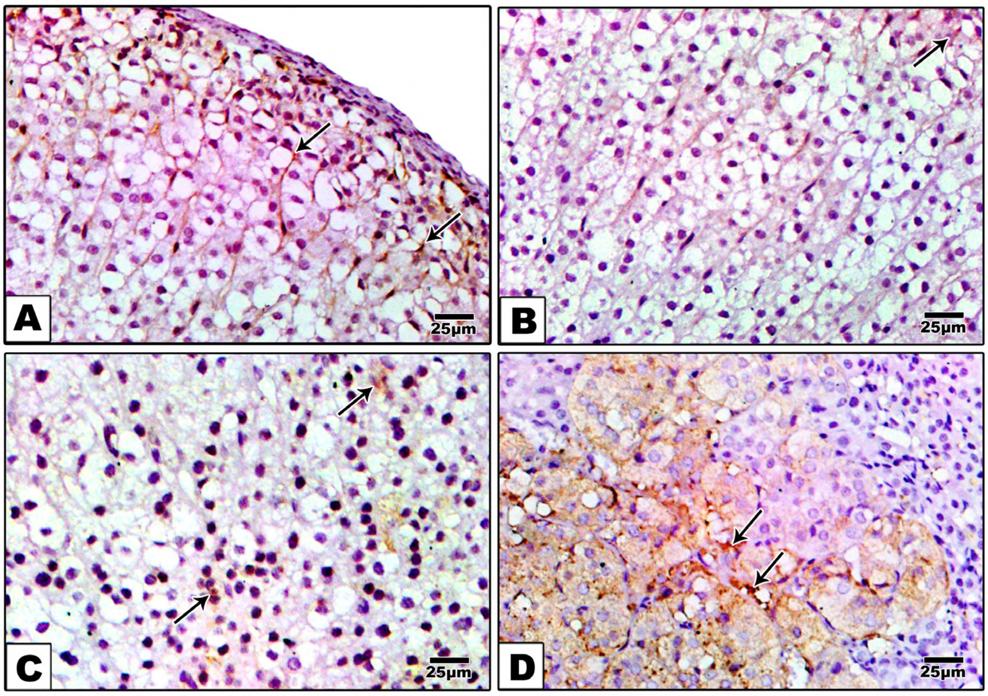

Fig. 12: Nestin immunostained suprarenal gland sections of the CS rat showing **A):** moderate weak positive immunoreaction (arrows) in the cytoplasm of capsular and subcapsular region (zona glomerulosa)**. B):** faint immunoreaction (arrows) in zona fasciculata**. C):** Cells of the zona reticularis weakly express the immune stain (arrows). **D):** There is decreased positive immune reaction in the medulla (arrow)**.** (Nestin immunohistochemical stain with Hx&E counterstain). Scale bars = 25 µm.

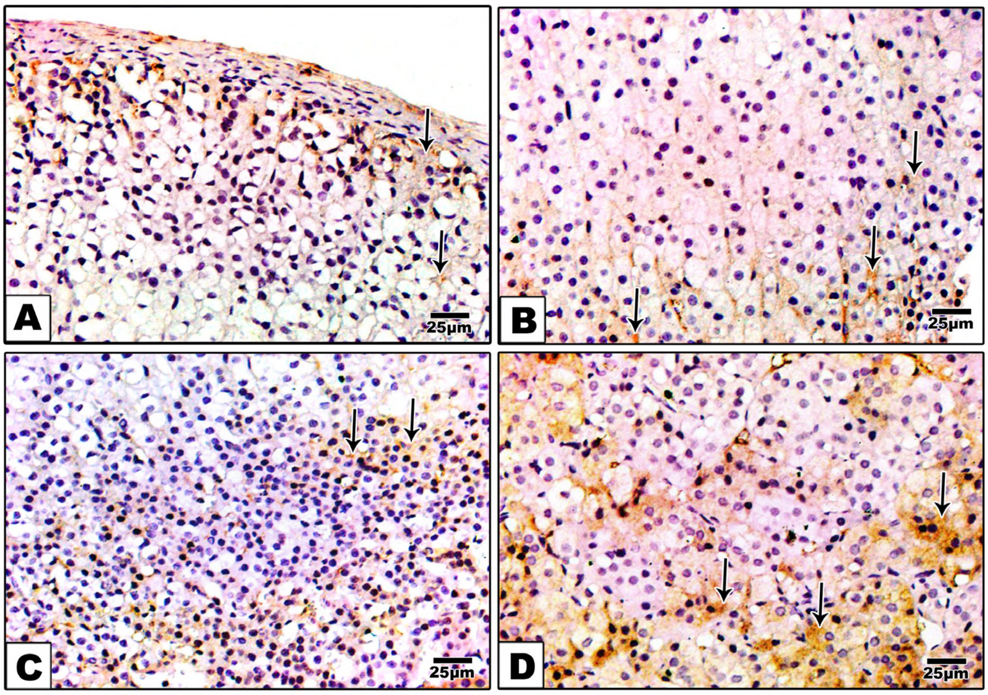

Fig. 13.- Nestin immunostained suprarenal gland sections of the REC rat after chronic-stress showing **A):** weak positive immunoreaction (arrow) in the cytoplasm of the capsular and subcapsular region (zona glomerulosa layer)**. B):** weak immunoreaction (arrows) in zona fasciculata**. C):** faint immunoreaction (arrows) in the zona reticularis. **D):** There is moderate positive immunoreaction (arrow) in the medulla**.** (Nestin immunohistochemical stain with Hx&E counterstain). Scale bars = 25 µm.

(Fig. 13A). Cells of ZF (Fig. 13B) and ZR (Fig. 13C) showed weak expression of the immune stain. There is a moderate immunohistochemical reaction in the medulla (Fig. 13D). The REC group showed a significant increase (*P<0.012*) in OD of total adrenal Nestin-stained cells (0.137±0.033) as compared to CS group, and a non-significant decrease (*P<0.155*) with CN group (Fig. 14).

Immunohistochemistry for Chromogranin-A

The chromogranin-A immunohistochemical reaction in CN group represented as diffuse and dotted cytoplasmic reaction in the cells of adrenal medulla (Fig. 15A). The CS group revealed a strong cytoplasmic reaction (Fig. 15B) with a significant increase (*P1=0.0001*) in OD (0.130±0.002)

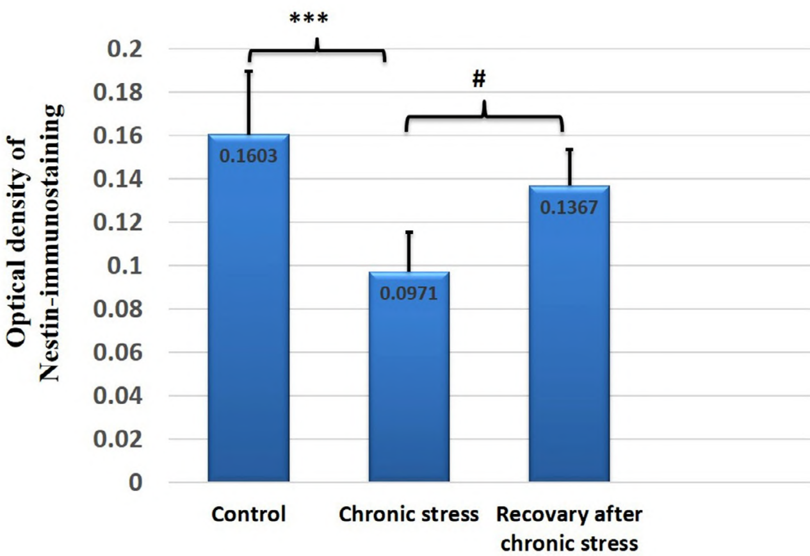

Fig. 14.- Histogram illustrating the statistical difference in the OD of Nestin immunohistochemical staining between the studied groups. It represents a significant decrease in the CS group comparing to both CN and REC groups. #p<0.05, ***p<0.0001.

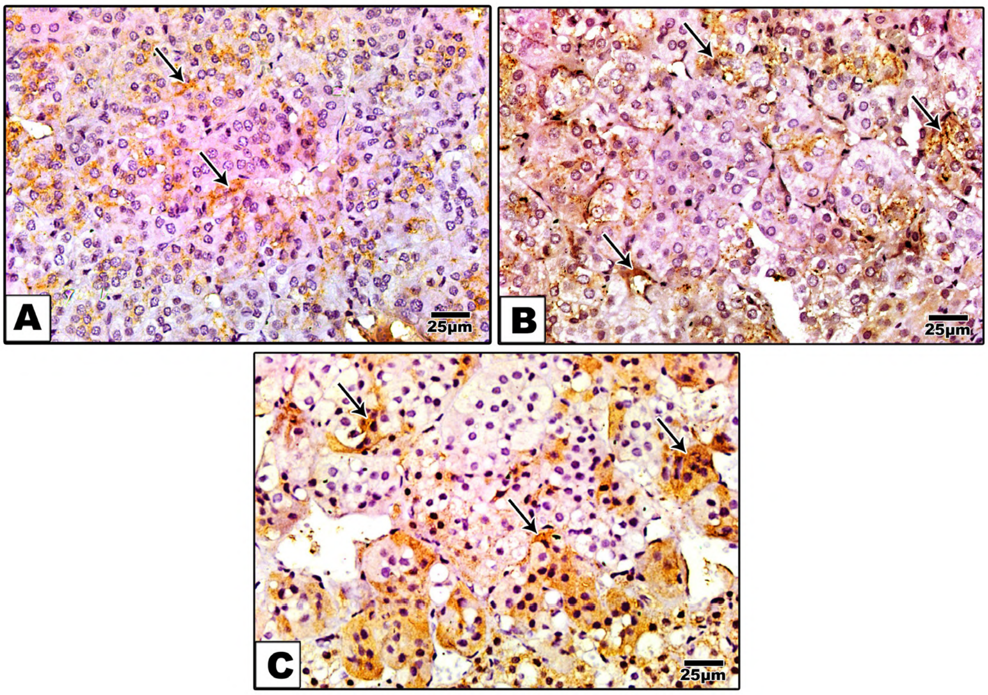

Fig. 15.- Chromogranine-A immunostained suprarenal gland sections of A) CN rat showing strong diffuse and dotted immunoreaction (arrow) in the adrenal medulla. **B):** CS rat showing stronger medullary immunohistochemical reaction (arrows). **C):** REC rat after chronic stress showing moderate medullary immunohistochemical reaction (arrows). (Chromogranine-A immunohistochemical stain with Hx&E counterstain). Scale bars = 25 µm.

as compared to CN group (0.130±0.002). The REC group showed a moderate immunohistochemical reaction (Fig. 15C) with a significant reduction (*P<0.004*) in OD of chromogranin-A positive cells (0.276±0.013) as compared to CS group, and significant elevation (*P< 0.0001*) as compared to CN group (Fig. 16).

Immunohistochemistry for GFAP

The positive GFAP immunoreaction in the CN group appeared diffuse cytoplasm staining in the cortical and medullary cells. The capsule showed strong positive immunoreaction (Fig. 17A). The ZG (Fig. 17A), ZF (Fig. 17B), and ZR (Fig. 17C) showed moderate positive reactions. The medulla showed a strong positive reaction (Fig. 17D).

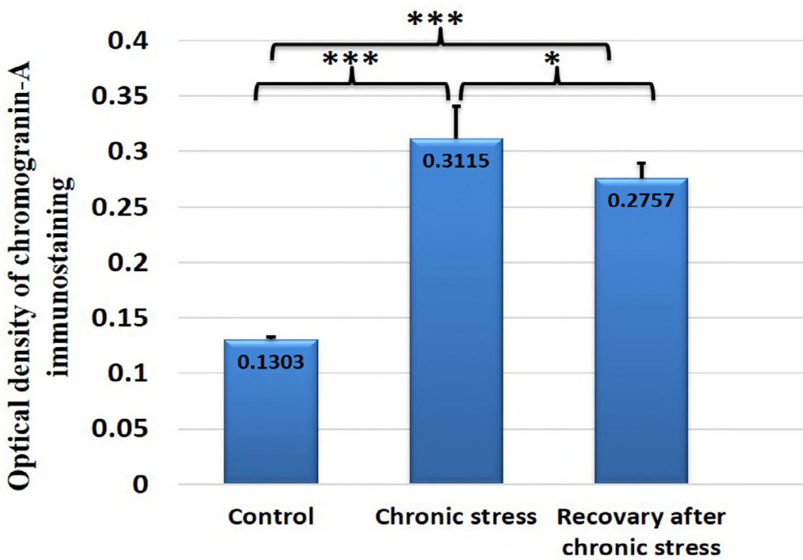

Fig. 16.- Histogram illustrates the statistical difference in the OD of the chromogranin-A immunohistochemical staining between the studied groups. It represents a significant increase in both CS and REC groups comparing to the CN group. *p<0.01, ***p<0.0001.

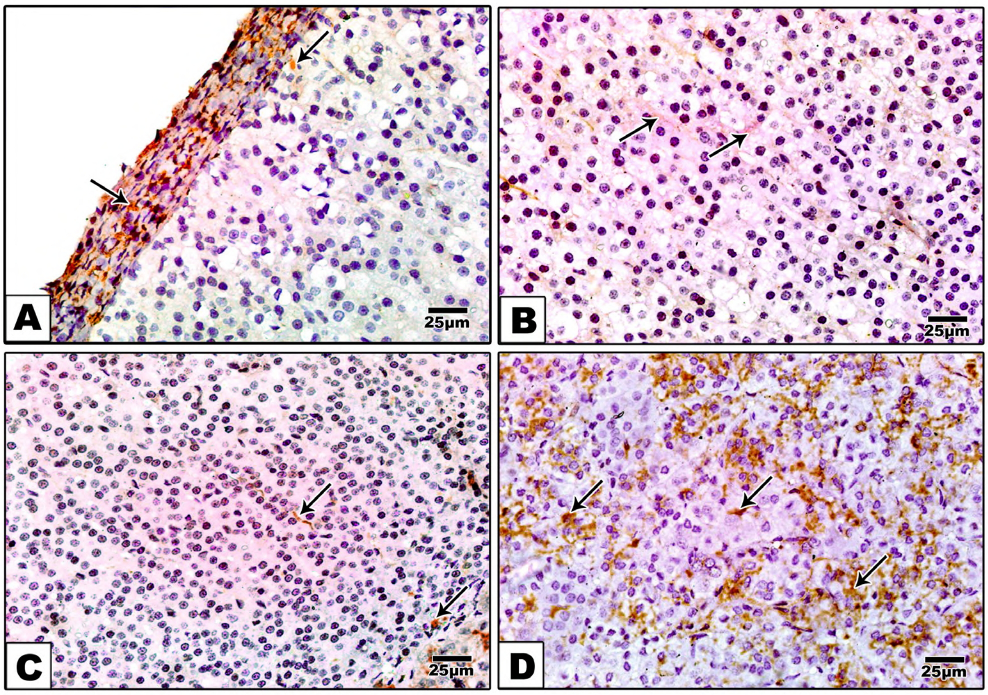

Fig. 17.- GFAP immunohistochemical stained suprarenal gland sections of CN rat showing **A):** diffuse strong immunoreaction (arrows) in the cytoplasm of the capsular and subcapsular region (zona glomerulosa)**. B):** moderate immunostaining (arrows) is in the cells of zona fasciculate**. C):** moderate immunoreaction (arrows) in the zona reticularis. **D):** There is a strong immunoreaction (arrow) in the medulla (magnified square)**.** (GFAP immunohistochemical stain with Hx&E counterstain). Scale bars = 25 µm.

The CS group revealed a strong cytoplasmic reaction in the capsular and ZG cells (Fig. 18A). Cells of ZF (Fig. 18B) and ZR (Fig. 18C) showed weak GFAP immune expression. There was a weak positive immune reaction in the medulla (Fig. 18D). This CS group illustrated a significant decrease (*P<0.01*) in OD of total adrenal GFAP positive cells (0.086±0.020) as compared to the CN group

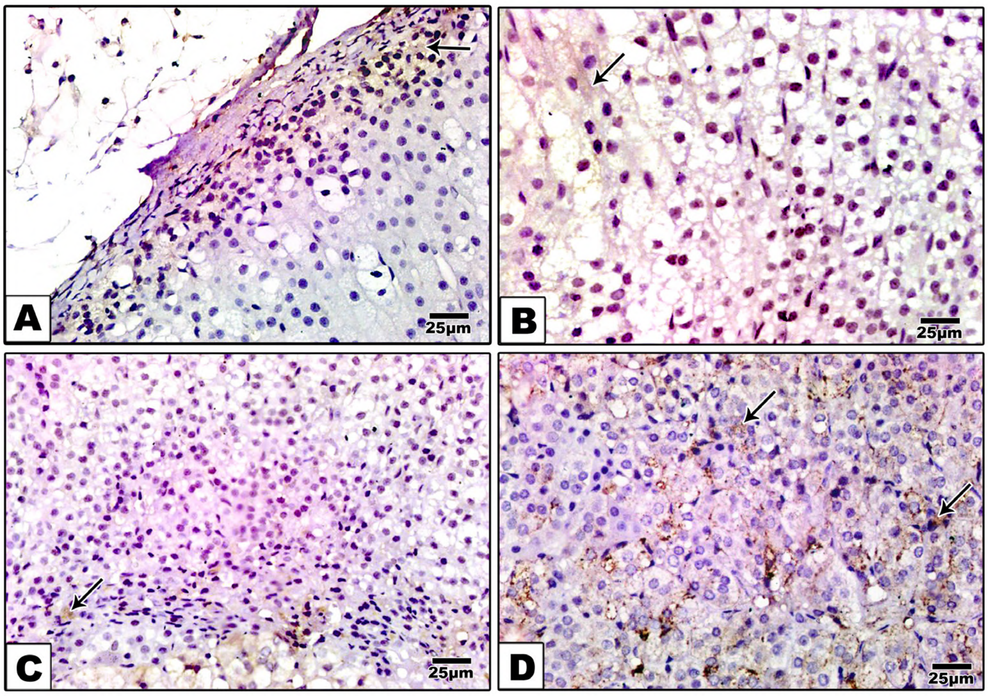

Fig. 18.- GFAP immunohistochemical stained suprarenal gland sections of CS rat showing **A):** strong cytoplasmic reaction (arrows) in the capsular and subcapsular region (zona glomerulosa)**. B):** weak immunoreaction (arrow) in zona fasciculata**. C):** Cells of the zona reticularis faintly express the immune stain (arrows). **D):** There is a weak positive immune reaction in the medulla (arrows)**.** (GFAP immunohistochemical stain with Hx&E counterstain). Scale bars = 25 µm.

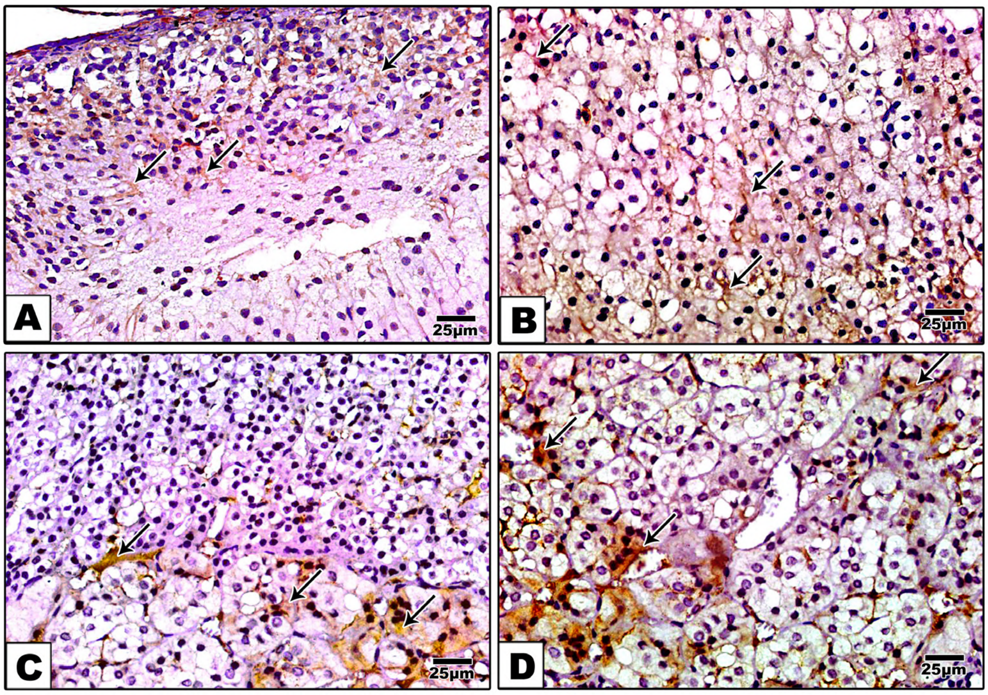

Fig. 19.- GFAP immunostained suprarenal gland sections of the REC rat after chronic stress showing **A):** moderate positive immunoreaction (arrow) in the cytoplasm of capsular and subcapsular region (zona glomerulosa layer)**. B):** weak immunoreaction (arrows) in zona fasciculata**. C):** weak immunoreaction (arrows) in the zona reticularis. **D):** There is a strong positive immunoreaction (arrow) in the medulla**.** (GFAP immunohistochemical stain with Hx&E counterstain). Scale bars = 25 µm.

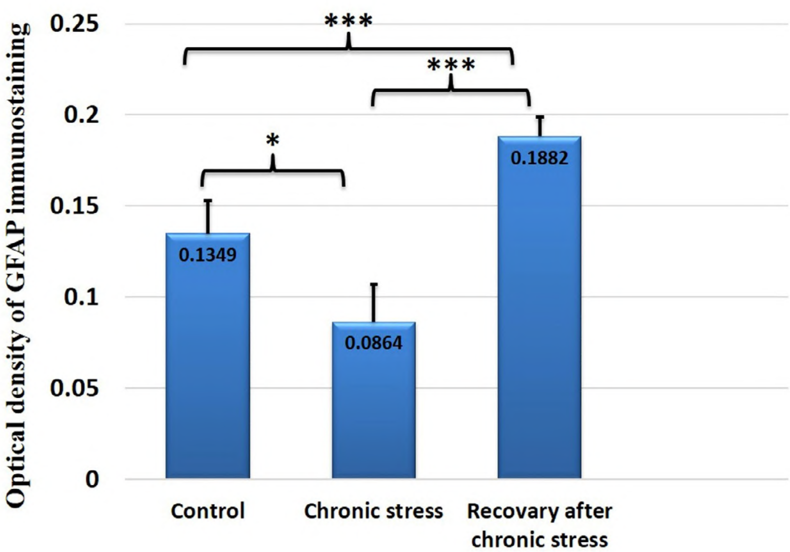

Fig. 20.- Histogram showing the statistical differences in the OD of GFAP immunohistochemical staining between the studied groups. It represents a significant decrease in the CS group comparing both CN and REC groups. The REC group illustrates a significant increase comparing to the CN group. *p<0.01, ***p<0.0001.

(0.135±0.018). The REC group showed a moderate immunoreaction in the cytoplasm of the capsular and ZG cells (Fig. 19A). The ZF (Fig. 19B) and ZR (Fig. 19C) faintly express the immune stain. There is a strong immunoreaction in the medulla (Fig. 19D). The REC group represented a highly significant elevation (*P<0.0001*) in OD of total adrenal GFAP positive cells (0.188±0.0108) as compared to CS and CN groups (Fig. 20).

DISCUSSION

The outcomes of this experiment are of interest from two points of view: first, they extend our knowledge about the impact of the chronic stressor on the function and structure of the adrenal gland; and second, they assess the existence of adrenal gland progenitor cells, with their possibility of transformation into new chromaffin and glial cells. The present study showed that there were a decreased number of progenitor cells after exposure to stress due to its transformation into chromaffin and glial cells.

In the present work, chronic stress was achieved by restricting the movement of each rat in a mesh restrainer two hours per day for six days. Restraint stress is the most widely used stressor in rodents. The effects of restraint stress are evidenced with impairments in the immune, neuroendocrine, and cognitive functions (Mo et al., 2019).

Our study showed a decrease in the body weight of CS group compared with CN group, while, when the rats were allowed to recover for seven days, they regained their body weight. These findings were in agreement with previous studies (Bhatnagar et al., 2006; Rubin de Celli et al., 2015). The reduction in body weight of CS rats can be explained by the affection of appetite. Stress decreases body weight by reduction of food and water intake (Ranjbaran et al., 2013) and anorexia induction (Halataei et al., 2011) due to the central release of CRH during stress that suppresses food ingestion (Grill et al., 2000; Heinrichs et al., 2001). Also, this effect is linked to the involvement of either the amygdala or the ventral tegmental area (Nasihatkon et al., 2014; Sadeghi et al., 2015).

The present study showed that CS had a significant increase in the adrenal gland weight versus CN. The REC group showed a non-significant effect on the adrenal gland weight versus the CS group, and a significant increase versus the CN group. Our findings were in agreement with Rostamkhani et al. (2012), who stated that chronic stress causes a significant increase in the weight of adrenal glands. Also, Rubin de Celli et al. (2015) found that the adrenals of chronically strained rats are increased in size by approximately 22%. The increase in the adrenal weight could be explained by the increased corticosterone demand and the capacity of the gland to produce higher amounts of corticosterone.

The present study showed a marked elevation in the cortisol level of CS group. The REC group showed a highly significant reduction versus CS group, but still significantly higher than CN group. Similar results were documented by several studies (Kiank et al., 2010; Cho et al., 2011; Zhang et al., 2011; Jameel et al., 2014). The endocrine system responds to stress by the interaction between the HPA and the adrenomedullary neuroendocrine system, accompanied by the release of adrenocortical glucocorticoids and adrenomedullary epinephrine (Demirci and Sahin, 2017).

In this study, the CS group showed several pathological changes in the adrenal cortices such as cellular edema, vacuolations, pyknosis, vascular congestion, and atrophy (decrease in its thickness) of ZG. Inconsistent with these results, Howard (2018) documented that vacuolar degeneration in ZG and ZR is a nonspecific pathology related to trauma, stress, or disease. In the medulla, the present study reported extracellular eosinophilic material, dilated congested blood sinusoid, and degenerated chromaffin cells. The extracellular eosinophilic material noted in the adrenal medulla is probably leaked serum from the arteries and veins.

Adrenal hemorrhage, congestion, and dilatation of blood sinusoids were associated with chronic stress in the present study. These changes were due to an increased ACTH level, which motivates the catecholamines release, thus increasing the adrenal blood flow and inducing vasoconstriction. This results in congestion with increased pressure in the capillaries (Simon and Palese, 2009). Moreover, Zidan and Elnegris (2013) reported that ACTH elevation enhances the prostaglandins formation, which is responsible for tissue congestion.

In the current study, the chromaffin reaction in the CS group illustrated a marked increase in the nor-epinephrine secreting cells which was significantly decreased to CN level after recovery. Sabban et al. (2012) found that the adrenal medulla increased the neurosecretory capacity with more efficient catecholamine storage in response to repeated exposure to stress. Tank and Lee Wong (2015) demonstrated that the body responds to stress by activating catecholaminergic neurons in the brain stem; then the spinal cord efferent stimulates the sympathetic nervous system and adrenal medulla to secrete epinephrine and nor-epinephrine.

In the current study, the evaluation of immunohistochemical data revealed that the positive immunoreaction reaction of Nestin is diffuse and dotted in the cytoplasm of ZG cells, and dispersed in ZF and ZR. The medulla showed a strong positive reaction. Inconsistent with our findings, Steenblock et al. (2018) demonstrated the highest prevalence of Nestin-stained cells is in the medulla and ZG directly beneath the capsule, while a few positive cells were scattered in ZF and ZG. Chang et al. (2013) and Finco et al. (2018) reported that distinct populations of adrenocortical progenitors located in the subcapsular region were responsible for the regeneration of the adrenal gland. Langton et al. (2018) have demonstrated the presence of Nestin-immunostained cells in the medulla adult adrenal gland.

Under basal conditions, these progenitors are displaced centripetally through the different zones of the adrenal cortex until they reach the corticomedullary boundary, where they become apoptotic (Chang et al., 2013; Steenblock et al., 2018). Nestin-positive cells traverse the whole adrenal, so that they connect the medulla with the capsule and make direct signaling. Moreover, the sub-capsular Nestin-positive cells are interconnected all around the capsule (Steenblock et al., 2018).

It was reported that Nestin levels reduced on cell differentiation, but elevated transiently after neuronal injury (Bott et al., 2019). The present study demonstrated a highly significant decrease in the total adrenal Nestin-immunoreaction in the CS group as compared to the CN group. However, the REC group showed a significant increase as compared to the CS group and a non-significant decrease with the CN group. In line with our results, Rubin de Celli et al. (2015) documented low proliferation rate of Nestin-positive cells at basal conditions, and increased proliferation after acute stress (one-day stress). When stress became chronic, the number of Nestin cells in the medullae was significantly decreased by 50%, indicating their participation in the gland adaptation. After the resting period, the number of Nestin-stained cells had returned to their basal levels.

Under basal conditions, Nestin-positive cells can differentiate into neuronal, glial, and chromaffin cells. However, under stress, they preferentially differentiate into chromaffin cells (Rubin de Celli et al., 2015). The chromogranin-A (Co-A) is the chief protein for the medullary chromaffin cells (Machado et al., 2010). There was no detected cellular co- staining for Nestin and chromogranin-A in the previous studies on the adult adrenal gland, suggesting that mature chromaffin cells never express Nestin protein (Taupenot et al., 2003).

This study detected positive chromogranin-A cytoplasmic immunoreaction in the medullary cells. This reaction increased significantly in CS group versus CN group. The recovery for seven days resulted in a significant decrease as compared to CS group but still significantly higher than CN group.

It has been shown that repeated immobilization stress resulted in increased the level of catecholamine. This was related to augmented catecholamines synthesis due to the increased expression of enzyme that converts norepinephrine to epinephrine (Kvetnansky et al., 2013). In addition to this molecular adaptation, the results in Rubin de Celli et al. (2015) illustrated cellular adaptation by recruiting new chromaffin cells from the stem cell pool located in the medulla of the adult adrenal gland.

Unlike the chromogranin-A, Rubin de Celli et al. (2015) showed that nearly 62% of the cells in the adrenal medulla which are stained with Nestin were co-stained for GFAP, specifying parallel features of with Nestin stem cells.

In this study, the adrenal GFAP immunohistochemical reaction illustrated a significant decrease in the CS group versus the CN group. The REC group had a highly significant increase versus the CS and CN groups. Our results were in agreement with Rubin de Celli et al. (2015),as who found that GFAP/Nestin-positive immune stained cells were significantly reduced in the stressed groups compared with the CN group. These results suggested that the Nestin-positive medullary stem cells behave as activated glial cells and they proliferate to increase this glia population.

In conclusion, under normal conditions, the differentiation of adrenal progenitor cells was towards the glial cell lineage. Conversely, with chronic stress, the differentiation significantly proceeded towards the chromaffin lineage resulting in overproduction of chromaffin cells for stress adaptation.

ACKNOWLEDGEMENTS

The authors would like to express their gratitude to the Human Anatomy and Embryology Department and the Medical Experimental Research Center, Mansoura University, Egypt, for providing administrative and technical support.

REFERENCES

BANCROFT JD, GAMBLE M (2002) Theory and practice of the histological techniques. In: Bancroft JD, Gamble M (eds). *The Haematoxylin and Eosin*, 5th edn. Chp. 8, Churchill Livingstone, London, pp 125-139.

BEKHBAT M, GLASPER ER, ROWSON SA, KELLY SD, NEIGH GN (2018) Measuring corticosterone concentrations over a physiological dynamic range in female rats. *Physiol Behav*, 194: 73-76.

BELLAFIORE M, SIVVERINI G, CAPPELLO F, DAVID S, PALMA A, FARINA F, ZUMMO G (2006) Research of cardiomyocyte precursors in adult rat heart. *Tissue Cell*, 38(6): 345-351.

BERENDS A, EISENHOFER G, FISHBEIN L, VAN DER HORST-SCHRIVERS AN, KEMA IP, LINKS TP, LENDERS JWM, KERSTENS MN (2019) Intricacies of the molecular machinery of catecholamine biosynthesis and secretion by chromaffin cells of the normal adrenal medulla and in pheochromocytoma and paraganglioma. *Cancers*, 11(8): 1121.

BHATNAGAR S, VINING C, IYER V, KINNI V (2006) Changes in hypothalamic-pituitary-adrenal function, body temperature, body weight and food intake with repeated social stress exposure in rats. *J Neuroendocrinol*, 18(1): 13-24.

BORNSTEIN SR, BERGER I, STEENBLOCK C (2020) Are Nestin-positive cells responsive to stress? *Stress*, 23(6): 662-666.

BOTT CJ, JOHNSON CG, YAP CC, DWYER ND, LITWA KA, WINCKLER B (2019) Nestin in immature embryonic neurons affects axon growth cone morphology and Semaphorin3a sensitivity. *Mol Biol Cell*, 30(10): 1214-1229.

CHANG SP, MORRISON HD, NILSSON F, KENYON CJ, WEST JD, MORLEY SD (2013) Cell proliferation, movement and differentiation during maintenance of the adult mouse adrenal cortex. *PloS One*, 8(12): e81865.

CHO YJ, KIM JH, YIM HE, LEE DM, IM SK, LEE KJ (2011) Role of corticotrophin-releasing factor in the stress-induced dilation of esophageal intercellular spaces. *J Korean Med Sci,* 26(2): 279-283.

CRANE JF, TRAINOR PA (2006) Neural crest stem and progenitor cells. *Annu Rev Cell Dev Biol,* 22: 267-286.

DEMIRCI T, SAHIN E (2017) Heart and stress: A morphometric and light microscopic study in a rat model. *Averroes Eur Med J,* 4(2): 9.

DUTT M, WEHRLE CJ, JIALAL I (2022) Physiology, Adrenal Gland. In: *StatPearls.* StatPearls Publishing, Treasure Island, Florida.

EL-DESOUKI NI, EL-REFAIY AI, AFIFI DF, ABDEL-KADER AA (2012) Histological, histochemical, and immunohistochemical studies of the cardiac muscle of the albino rat under immobilization stress and the curative role of diazepam. *Egypt J Exp Biol (Zool)*, 8(2): 273-285.

FINCO I, LERARIO AM, HAMMER GD (2018) Sonic hedgehog and WNT signaling promote adrenal gland regeneration in male mice. *Endocrinology*, 159(2): 579-596.

FLAK JN, SOLOMON MB, JANKORD R, KRAUSE EG, HERMAN JP (2012) Identification of chronic stress-activated regions reveals a potential recruited circuit in rat brain. *Eur J Neurosci,* 36(4): 2547-2555.

GANNOUNI N, MHAMDI A, EL MAY M, TEBOURBI O, RHOUMA KB (2014) Morphological changes of adrenal gland and heart tissue after varying duration of noise exposure in adult rat. *Noise Health*, 16(73): 416-421.

GRILL HJ, MARKISON S, GINSBERG A, KAPLAN JM (2000) Long-term effects on feeding and body weight after stimulation of forebrain or hindbrain CRH receptors with urocortin. *Brain Res*, 867(1-2): 19-28.

HALATAEI BAS, KHOSRAVI M, ARBABIAN S, SAHRAEI H, GOLMANESH L, ZARDOOZ H, JALILI C, GHOSHOONI H (2011) Saffron (Crocus sativus) aqueous extract and its constituent crocin reduces stress-induced anorexia in mice. *Phytother Res*, 25(12): 1833-1838.

HEINRICHS SC, LI DL, IYENGAR S (2001) Corticotropin-releasing factor (CRF) or CRF binding-protein ligand inhibitor administration suppresses food intake in mice and elevates body temperature in rats. *Brain Res*, 900(2): 177-185.

HILLARP NA, HOKFELT B (1955) Histochemical demonstration of noradrenaline and adrenaline in the adrenal medulla. *J Histochem Cytochem*, 3(1):1-5.

HOLINGER M, FRÜH B, STOLL P, GRAAGE R, WIRTH S, BRUCKMAIER R, PRUNIER A, KREUZER M, HILLMANN E (2018) Chronic intermittent stress exposure and access to grass silage interact differently in their effect on behaviour, gastric health and stress physiology of entire or castrated male growing-finishing pigs. *Physiol Behav*, 195: 58-68.

HOWARD EB (2018) Miscellaneous diseases. In: *Pathobiology of marine mammal diseases*. CRC Press, Boca Raton, Florida, pp 163-225.

JAMEEL MK, JOSHI AR, DAWANE J, PADWAL M, JOSHI AR, PANDIT VA, MELINKERI R (2014) Effect of various physical stress models on serum cortisol level in wistar rats. *J Clin Diagn Res,* 8(3): 181-183.

KIANK C, ZEDEN JP, DRUDE S, DOMANSKA G, FUSCH G, OTTEN W, SCHUETT C (2010) Psychological stress-induced, IDO1-dependent tryptophan catabolism: implications on immunosuppression in mice and humans. *PLoS One*, 5(7): e11825.

KLEIN D, MEISSNER N, KLEFF V, JASTROW H, YAMAGUCHI M, ERGÜN S, JENDROSSEK V (2014) Nestin (+) tissue-resident multipotent stem cells contribute to tumor progression by differentiating into pericytes and smooth muscle cells resulting in blood vessel remodeling. *Front Oncol, 4*: 169.

KVETNANSKY R, LU X, ZIEGLER MG (2013) Stress-triggered changes in peripheral catecholaminergic systems. *Adv Pharmacol*, 68: 359-397.

LANGTON K, GRUBER M, MASJKUR J, STEENBLOCK C, PEITZSCH M, MEINEL J, LENDERS J, BORNSTEIN S, EISENHOFER G (2018) Hypertensive crisis in pregnancy due to a metamorphosing pheochromocytoma with post-delivery Cushing's syndrome. *Gynecol Endocrinol*, 34(1): 20-24.

MACHADO JD, DÍAZ-VERA J, DOMÍNGUEZ N, ÁLVAREZ CM, PARDO MR, BORGES R (2010) Chromogranins A and B as regulators of vesicle cargo and exocytosis. *Cell Mol Neurobiol*, 30(8): 1181-1187.

MO C, RENOIR T, HANNAN AJ (2019) Stress and glucocorticoids as experience-dependent modulators of Huntington's disease. In: *Stress: Physiology, Biochemistry, and Pathology.* Academic Press, pp 163-225.

NASIHATKON ZS, KHOSRAVI M, BOURBOUR Z, SAHRAEI H, RANJBARAN M, HASSANTASH SM, BAGHLANI K (2014) Inhibitory effect of NMDA receptors in the ventral tegmental area on hormonal and eating behavior responses to stress in rats. *Behav Neurol,* 2014: 294149.

NEDZVETSKII VS, PRYSHCHEPA IV, TYKHOMYROV AA, BAYDAS G (2016) Inhibition of reactive gliosis in the retina of rats with streptozotocin-induced diabetes under the action of hydrated C60 fullerene. *Neurophysiol,* 48(2): 130-140.

OBARA K, TOHGI N, MII S, HAMADA Y, ARAKAWA N, AKI R, SINGH SR, HOFFMAN RM, AMOH Y (2019) Hair-follicle-associated pluripotent stem cells derived from cryopreserved intact human hair follicles sustain multilineage differentiation potential. *Sci Rep*, 9(1): 9326.

RANJBARAN M, MIRZAEI P, LOTFI F, BEHZADI S, SAHRAEI H (2013) Reduction of metabolic signs of acute stress in male mice by papaver Rhoaes hydro-alcoholic extract. *Pakistan J Biol Sci,* 16: 1016-1021.

RIZZOTI K, AKIYAMA H, LOVELL-BADGE R (2013) Mobilized adult pituitary stem cells contribute to endocrine regeneration in response to physiological demand. *Cell Stem Cell*, 13(4): 419-432.

ROSTAMKHANI F, ZARDOOZ H, ZAHEDIASL S, FARROKHI B (2012) Comparison of the effects of acute and chronic psychological stress on metabolic features in rats. *J Zhejiang Univ Sci* B, 13(11): 904-912.

RUBIN DE CELIS, MF, GARCIA-MARTIN R, WITTIG D, VALENCIA GD, ENIKOLOPOV G, FUNK RH, CHAVAKIS T, BORNSTEIN SR, ANDROUTSELLIS-THEOTOKIS A, EHRHART-BORNSTEIN M (2015) Multipotent glia-like stem cells mediate stress adaptation. *Stem Cells*, 33(6): 2037-2051.

SABBAN EL, TILLINGER A, NOSTRAMO R, SEROVA L (2012) Stress triggered changes in expression of genes for neurosecretory granules in adrenal medulla. *Cell Mol Neurobiol,* 32(5): 795-800.

SADEGHI B, SAHRAEI H, ZARDOOZ H, ALIBEIK H, SARAHIAN N (2015) Effects of intra-amygdala memantine infusion on metabolic symptoms induced by chronic stress in male NMRI mice. *Koomesh*, 16(3): 376-383.

SIEBER-BLUM M, HU Y (2008) Epidermal neural crest stem cells (EPI-NCSC) and pluripotency. *Stem Cell Rev,* 4: 256-260.

SIMON DR, PALESE MA (2009) Clinical update on the management of adrenal hemorrhage. *Curr Urol Rep,* 10(1): 78-83.

SOLIMAN AA (2006) Effect of stress on the mammary gland of lactating albino rat: a light and electron microscopic study. *Egypt J Histol*, 29(2): 259-268.

STALDER T, STEUDTE-SCHMIEDGEN S, ALEXANDER N, KLUCKEN T, VATER A, WICHMANN S, KIRSCHBAUM C, MILLER R (2017) Stress-related and basic determinants of hair cortisol in humans: A meta-analysis. *Psychoneuroendocrinology*, 77: 261-274.

STEENBLOCK C, DE CELIS MFR, ANDROUTSELLIS-THEOTOKIS A, SUE M, SILVA LFD, EISENHOFER G, BORNSTEIN SR (2017) Adrenal cortical and chromaffin stem cells: Is there a common progeny related to stress adaptation? *Mol Cell Endocrinol*, 441: 156-163.

TANK AW, LEE WONG D (2015) Peripheral and central effects of circulating catecholamines. *Comp Physiol,* 5(1): 1-15.

TAUPENOT L, HARPER KL, O'CONNOR DT (2003) The chromogranin–secretogranin family. *N Engl J Med*, 348(12): 1134-1149.

VUKICEVIC V, DE CELIS MFR, PELLEGATA NS, BORNSTEIN SR, ANDROUTSELLIS-THEOTOKIS A, EHRHART-BORNSTEIN M (2015) Adrenomedullary progenitor cells: Isolation and characterization of a multi-potent progenitor cell population. *Mol Cell Endocrinol*, 408: 178-184.

YIN Z, HU JJ, YANG L, ZHENG ZF, AN CR, WU BB, ZHANG C, SHEN WL, LIU HH, CHEN JL, HENG BC, GUO GJ, CHEN X, OUYANG HW (2016) Single-cell analysis reveals a nestin+ tendon stem/progenitor cell population with strong tenogenic potentiality. *Sci Adv*, 2(11): e1600874.

ZHANG D, XIE C, WANG R, YANG Q, CHEN H, LING S, WANG S, JIA K (2018) Effective preparation of a monoclonal antibody against human chromogranin A for immunohistochemical diagnosis. *BMC Biotechnol*, 18(1): 25.

ZHANG SY, WANG JZ, LI JJ, WEI DL, SUI HS, ZHANG ZH, ZHOU P, TAN JH (2011) Maternal restraint stress diminishes the developmental potential of oocytes. *Biol Reprod*, 84(4): 672-681.

ZIDAN RA, ELNEGRI HM (2013) A histological study on the effect of noise on the adrenal cortex of adult male guinea pigs and the possible role of combined vitamins (A, C, and E) supplementation. *Egypt J Histol,* 36(4): 857-868.

Comparative assessment of the morphology and antigenicity of human osteochondral units using formalin and coagulant fixatives

Ganesh Parasuraman[1], Elizabeth Vinod[1,2], Abel Livingston[3], Solomon Sathishkumar[2], Deepak Vinod Francis[4]

[1] Centre for Stem Cell Research, (A unit of InStem, Bengaluru), Christian Medical College, Vellore, India

[2] Department of Physiology, Christian Medical College, Vellore, India

[3] Department of Orthopaedics, Christian Medical College, Vellore, India

[4] Department of Anatomy, Christian Medical College, Vellore, India

SUMMARY

Fixation is crucial for preserving tissue integrity during processing, and the most commonly used cross-linking fixative in immunohistochemistry is neutral buffered formalin, which requires antigen retrieval as a crucial step. The successful use of newer coagulant fixatives like methacarn and EMA to preserve isotopes and eliminate the need for antigen retrieval has been reported recently, but their role in decalcified osteochondral unit samples remains unknown. Limited information on the use of coagulant fixatives as formalin substitutes makes it important to comparatively evaluate their effects on osteochondral samples and the impact of antigen retrieval on different days. Osteochondral units from a patient with osteoarthritis who underwent total knee-replacement surgery were fixed with three studied fixatives (Formalin, Methacarn, EMA) and divided into four portions, for different time periods (Day 1, 3, 7, 10). Sections were decalcified, stained with Safranin O, Alcian Blue, Toluidine Blue, PicroSirius Red, Hematoxylin and Eosin, and immunohistochemical analysis of Collagen type II and type X with and without antigen retrieval was conducted.

Formalin showed better hematoxylin uptake than coagulant-based fixatives, while all fixatives preserved tissue morphology without necrosis or cellular degeneration with comparable staining quality. Methacarn and EMA-fixed tissues showed higher uptake of collagen type II compared to formalin-fixed tissues, with collagen type II uptake occurring only in the cartilage region and collagen type X uptake occurring only in the bone region. The study highlights the effectiveness of methacarn and EMA as efficient alternatives to formalin, preserving tissue morphology and antigen specificity.

Keywords: Formalin – Methacarn – EMA fixative – Osteochondral unit – Antigen retrieval – Collagen type II

Corresponding author:
Dr. Elizabeth Vinod. Associate Professor/Adjunct Scientist. Department of Orthopaedics/ Centre for Stem Cell Research (A unit of inStem, Bangalore) Christian Medical College, Vellore. e-mail id: elsyclarence@cmcvellore.ac.in. Ph no: +91 9677651977. ORCID: 0000-0001-7340-8320

Submitted: April 28, 2023. **Accepted:** June 7, 2023

https://doi.org/10.52083/CVZF3774

INTRODUCTION

Fixation is a process that occurs through a combination of physical and chemical mechanisms, and it involves reactions where the fixative acts by slowly diffusing into the tissues (Dey, 2018). Fixation is crucial to maintain the cellular architecture and composition of biopsy tissue specimens during processing, thereby preserving tissue integrity for further study. Following fixation, the tissues can be embedded in paraffin wax and used for further analysis, including immunohistochemistry and molecular studies. Furthermore, fixation is vital in preserving the spatial relationships between carbohydrates, proteins and other intracellular bioactive molecules, which enables their examination and analysis. Neutral Buffered Formalin (NBF), Methacarn, and EMA (mixture of ethanol, methanol and acetic acid) are all fixatives commonly used in histology to preserve tissue samples (Howat and Wilson, 2014). Methacarn and EMA are both coagulative and alcohol fixatives.

NBF fixation is a widely used and optimized fixative that preserves tissue morphology, aids in examining cell architecture and identifying abnormalities (Thavarajah et al., 2012). However, it is known to cause tissue artifacts, tissue shrinkage and distortion, particularly in delicate tissues such as brain or lung tissue. Another disadvantage of NBF fixation is that it can affect the antigenicity of specific proteins, leading to false negative results in the immunohistochemical analysis, thereby leading to loss of time and money due to the standardization of any IHC test (Buesa, 2008). Despite these disadvantages, NBF remains the most commonly used fixative in histology due to its effectiveness, reliability, and ease of use.

Methacarn is an effective coagulant fixative for preserving specific tissues, like nervous and muscular tissues, with minimal shrinkage and distortion (Shibutani et al, 2000). It also preserves protein antigenicity for accurate immunohistochemical analysis. However, it requires longer fixation times and can be more expensive. EMA fixative is a non-formalin coagulant fixative commonly used for preserving tissue morphology and antigenicity. Unlike formalin, which crosslinks proteins, EMA fixative penetrates the tissue and denatures the proteins, thus preserving their native conformation and antigenicity. This makes EMA fixative particularly useful for immunohistochemical analysis, as it allows for more accurate detection of specific antigens. EMA fixative is also compatible with molecular analysis techniques, such as RNA and DNA extraction (Rahman et al., 2022). However, like other non-formalin fixatives, EMA fixative is more expensive and may require longer fixation times (Nietner et al., 2012). Despite these limitations, EMA fixative is a valuable tool in histology for preserving tissue morphology and antigenicity for further analysis.

Decalcification is an essential prerequisite for the immunohistochemical analysis of bone or tissue that contains bone (Alers et al., 1999). Bone's hydroxyapatite crystals, which provide strength, make it challenging to section and analyze (Dermience et al., 2015). Decalcification removes mineral salts, making it easier to section, but it can affect the organic components needed for histological analysis. Fixation before decalcification is necessary to preserve the tissue's cellular and fibrous components (Shields and Heinbockel, 2018). Decalcification and tissue fixation may result in poor antibody binding due to epitope masking or cross-link formation (D'Amico et al., 2009). Therefore, using an appropriate antigen retrieval technique is crucial for examining bone-containing tissue through immuno-histochemical analysis.

Since information about the use of coagulant fixatives as a substitute for formalin fixatives is significantly limited, and each fixative has its own set of benefits and drawbacks, the primary objective of this study was to comparatively evaluate the fixatives for their effect on morphology and antigenicity in osteochondral samples. Since coagulant fixatives have been suggested to be time-dependent and preserve antigenicity more effectively, the study also compared the impact of performing antigen retrieval versus not performing it on different days.

MATERIALS AND METHODS

Tissue sample procurement and processing

All methods used in the study were per the regulations set by the Institution's Review Board and Ethics Committee, as stated in the declaration of

Helsinki. After obtaining written informed consent from the patient, human osteochondral units (OCUs) were harvested from a patient undergoing total knee replacement as a part of the treatment for osteoarthritis (Radiological Kellgren Lawrence score of Grade 4). The osteochondral units were harvested using a Colibri hand drill equipped with a 12 mm Impact Bi-Metal Hole saw (Sutton Tools). The osteochondral units were harvested from a non-weight-bearing area of the joint that contained preserved cartilage.

The OCUs were divided using a microtome blade into three parts for different fixatives, with each piece further divided into four portions for the specified time points (Fig. S1). The three fixatives used were a) 10% neutral buffered formalin, b) Methacarn and c) EMA, ensuring that the volume of the fixative was 15 times the volume of the tissue. The fixation time points included the following days: 1, 3, 7, and 10. The OCUs were decalcified by immersing the joints in a solution of 10% EDTA (Qualigens, Cat.No. Q12635, pH 7.4). The joints were kept on a biological magnetic stirrer at 650 rpm, 25 ˚C, for a period of 35 days. The decalcified OCUs were processed by an automated tissue processor (Leica TO 10120), dehydrated by gradually increasing the ethanol concentration, and then infiltrated with wax and paraffin-embedded. 5 µm sections were placed on poly-L-lysine (SIGMA, P8920) coated slides using the semi-automated Leica microtome (RM-2245). To verify the accumulation of glycosaminoglycans (GAG), the sections were stained with Safranin O, Alcian blue and Toluidine blue. To assess for collagen and for total collagen, the OCUs were subjected to routine staining using PicroSirius red, immunohistochemical analysis for Collagen type II and type X, and Hematoxylin and Eosin staining.

Staining protocol

a) Hematoxylin and Eosin (HE) staining

HE staining was carried out following standard protocols. In summary, transverse sections were stained with hematoxylin solution for 8 minutes, then dipped twice in 1% acid alcohol, rinsed with tap water, and dipped in lithium carbonate. Subsequently, the sections were stained with eosin solution for 30 seconds. The sections were dehydrated using graded alcohol and cleared using xylene.

b) GAG stains: Safranin O, Alcian Blue and Toluidine blue

To perform Safranin O fast green (Fischer Scientific, Cat No:39962), staining, the sections were first treated with Weigert's Iron Hematoxylin, followed by 1% acid alcohol, 0.05% fast green solution, 1% acetic acid, and 0.1% Safranin O solution. Alcian blue staining (pH: 2.5, Cat No: J60122, Alfa Aesar, US) was done by incubating the slides with the dye for 5 minutes and counterstaining with neutral red. For Toluidine blue (Qualigens, C.I.52040) staining, the sections were incubated with 0.1% dye solution for 5 minutes.

c) Collagen stain: PicroSirius red, Collagen type II and type X

0.1% PicroSirius red (Qualigens, C.I.35782) dye was applied to assess the total collagen, followed by Hematoxylin counterstain. For the immunohistochemical analysis of Collagen type II, the tissue sections underwent sequential antigen retrieval using pronase (1 mg/ml, Roche CAS 9036-06-0) and hyaluronidase (2.5 mg/ml, Sigma, Cat No:H3506). While for Collagen Type X, the sections were retrieved using chondroitinase ABC (0.1 units/ml: 1 h, C3667, Sigma Aldrich) and pepsin (pH 2.2, 1 mg/ml:15 min, R2283, Sigma Aldrich). Subsequently, the slides were incubated overnight with mouse monoclonal anti-collagen type II antibodies (5 g/mL, DSHB, II-II6B3) or collagen type X (1 in 200 dilutions, ab49945, Abcam). Subsequently, staining with HRP-labelled goat anti-mouse immunoglobulin secondary antibody (31430, Pierce) at a concentration of 1:100, and 3,3-diaminobenzidine (DAB, Sigma Cat No: D5637) solution and counterstaining with Hematoxylin was performed. For immunohistochemical staining namely collagen type II and X, the sections were stained with and without antigen retrieval. Negative controls included parallel staining, albeit the primary antibody.

All slides were dehydrated, cleared with xylene, mounted with DPX (Merck, DD9DF69319) and scanned using an EVOS FL AUTO slide scanner.

RESULTS

Hematoxylin and Eosin (HE) staining

The comparative assessment showed that the NBF fixative resulted in better haematoxylin uptake compared to the alcohol-based fixatives, Methacarn and EMA (Fig. 1, Fig. S2, Fig. 9). None of the tested fixatives affected the visualization of tissue features on the slide, and no signs of necrosis or cellular degeneration were observed, indicating that all fixatives were effective in preserving tissue morphology. The cartilage lacuna contained chondrocytes with a bright eosinophilic cytoplasm, and the surrounding territorial matrix appeared more basophilic (Fig. 2). Conversely, the lacuna in bone samples was typically empty, and, if cellular, did not exhibit the staining property of the territorial matrix. Notably, lamella could be appreciated in the region of bone (Fig. 2). Finally, the staining of the cartilage gradually changed basophilic towards the bony side and abruptly stopped to give rise to an eosinophilic bony layer, giving rise to a wavefront-like appearance (Fig. 2). Overall, these findings suggest that NBF is a reliable fixative for preserving both the tissue morphology and staining properties in cartilage and bone samples.

GAG stains: Safranin O, Alcian Blue and Toluidine blue

Hyaline cartilage's extracellular matrix includes ground substance and collagen fibers, with the former composed of water, proteoglycans (PGs) and glycosaminoglycans. Safranin O stains PGs and GAGs, forming a red-to-orange complex that indicates high content. Fixative exposure duration did not affect staining quality, as all tested fixatives produced comparable results (Fig. 3). However, the cartilage in slides preserved with EMA and Methacarn fixatives showed less safranin O staining, possibly due to the tissue retaining the cytoplasmic stain (Fast green) better, requiring a more extended differentiation period or might be due to the poorer uptake of Safranin O, requiring a longer duration of exposure to the stain (Fig. 3, Fig. 9). The cellular features were preserved with no signs of necrosis or cellular degeneration. Notably, robust Safranin O uptake was observed in the cartilage, particularly in the territorial matrix.

Alcian blue stains the sulfated and carboxylated glycosaminoglycans in cartilage, giving rise to a blue or turquoise coloration, depending on the pH of the staining solution. Neutral red, conversely, selectively stains chondrocyte nuclei, producing

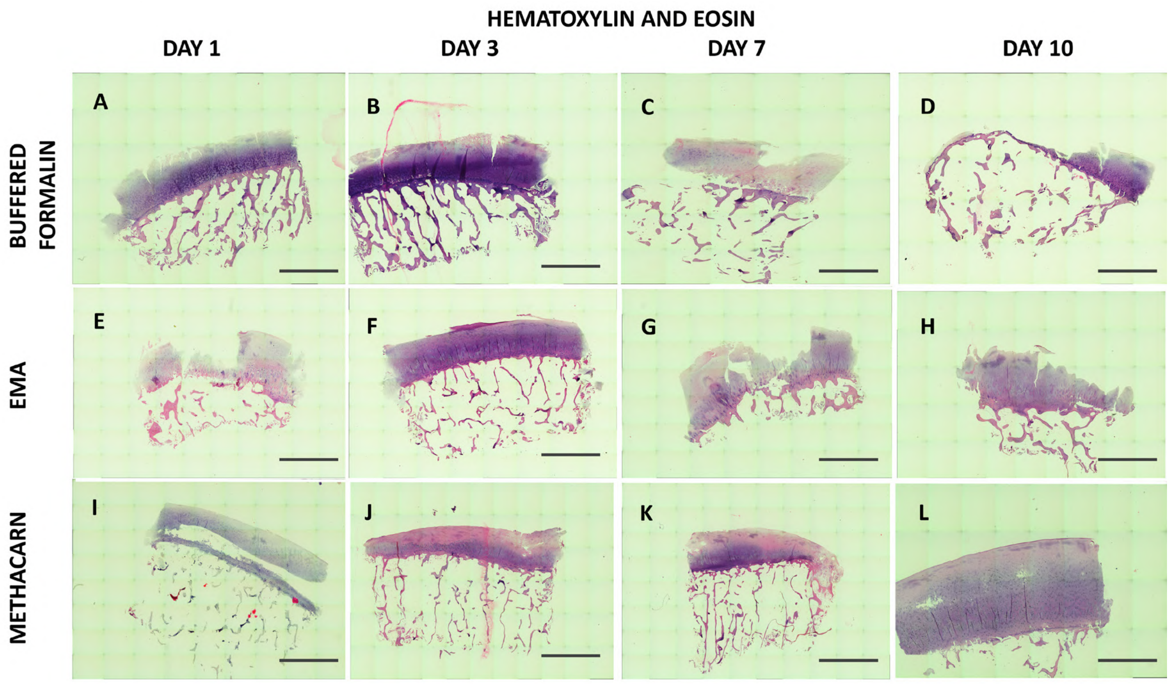

Fig. 1.- Hematoxylin and Eosin staining of the osteochondral unit sections following fixation by either NBF, Methacarn or EMA, and decalcification by 10% EDTA. Magnification 10X. NBF: 10% Neutral buffered formalin, EMA: Mixture of ethanol, methanol and acetic acid at 3:1:1 ratio. Scale bars = 100 µm.

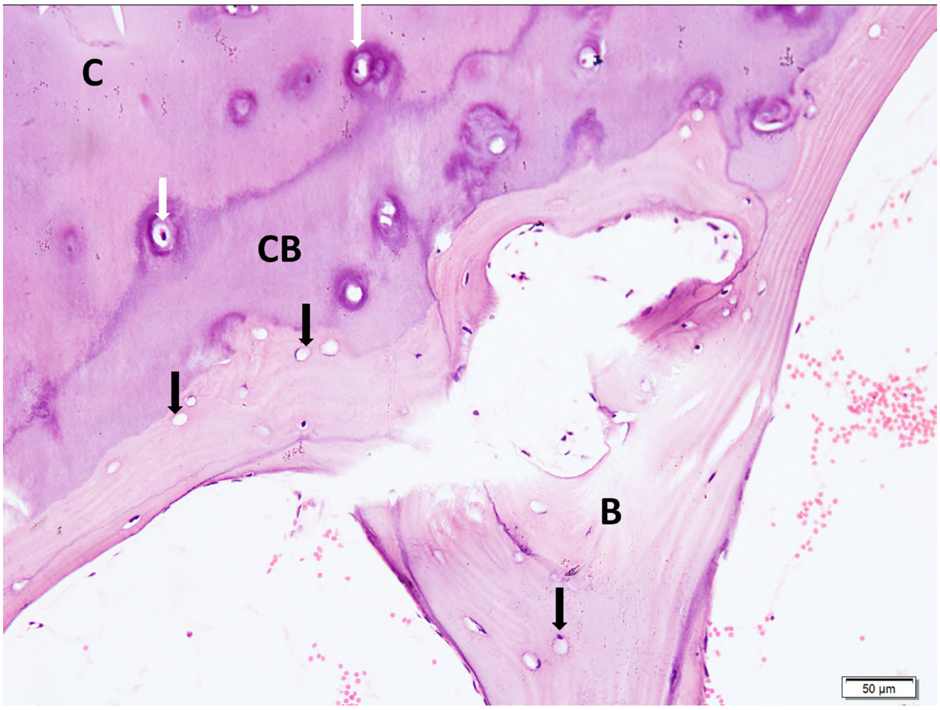

Fig. 2.- Cartilage bone junction fixed with NBF for 3 days taken with the objective set at 20X magnification. Chondrocytes seen as eosinophilic cells in the lacuna of the cartilage(C) with the territorial matrix surrounding them staining basophilic (white arrows). Bone (B) lacuna predominantly appear empty with no surrounding basophilia (black arrows). Lamella can be seen. There is a well-defined area in the junction (CB) which stains basophilic and resembles a wavefront. Scale bar = 50 µm.

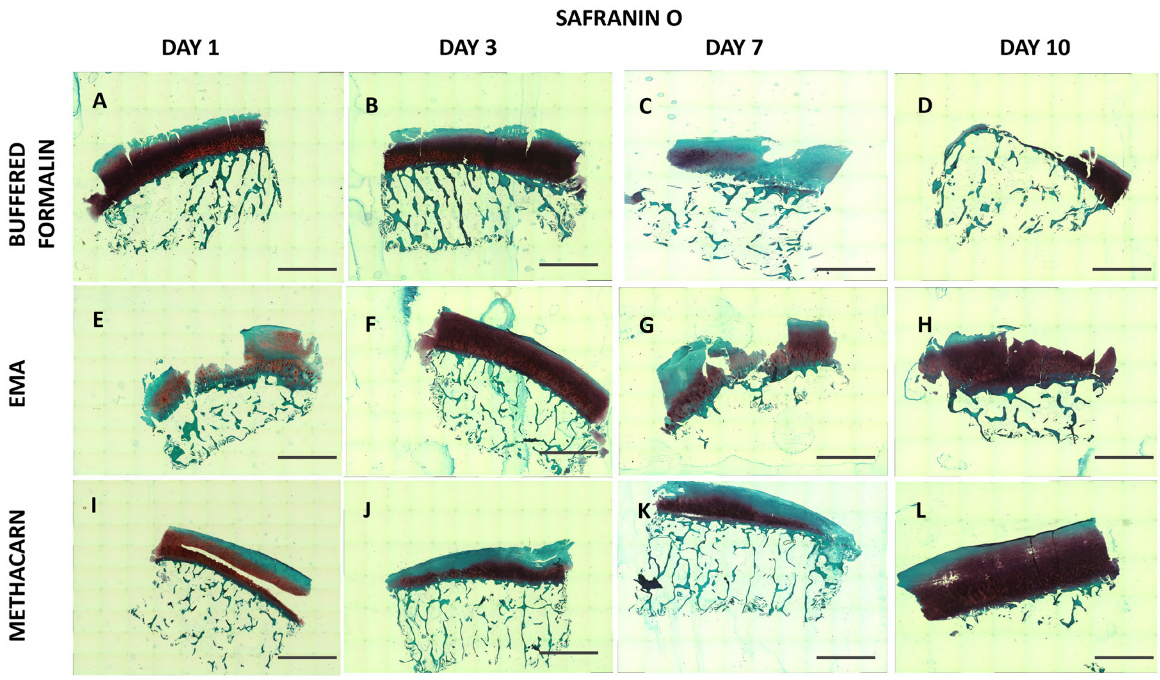

Fig. 3.- Safranin O staining of the osteochondral unit sections following fixation by either NBF, EMA and Methacarn, and decalcification by 10% EDTA. Magnification 10X. NBF: 10% Neutral buffered formalin, EMA: Mixture of ethanol, methanol and acetic acid at 3:1:1 ratio. Scale bars = 100 µm.

a red or pink coloration, which contrasts well with the blue coloration of the Alcian blue-stained matrix (Fig. 4, Fig. 9). Our examination revealed that both Methcarn and EMA exhibited poor uptake of the counterstain on the first day, although they produced similar results to the formalin fixative on the other days.

Toluidine blue is a basic metachromatic dye that can selectively stain cartilage proteoglycans, providing insight into cartilage tissue's extracellular

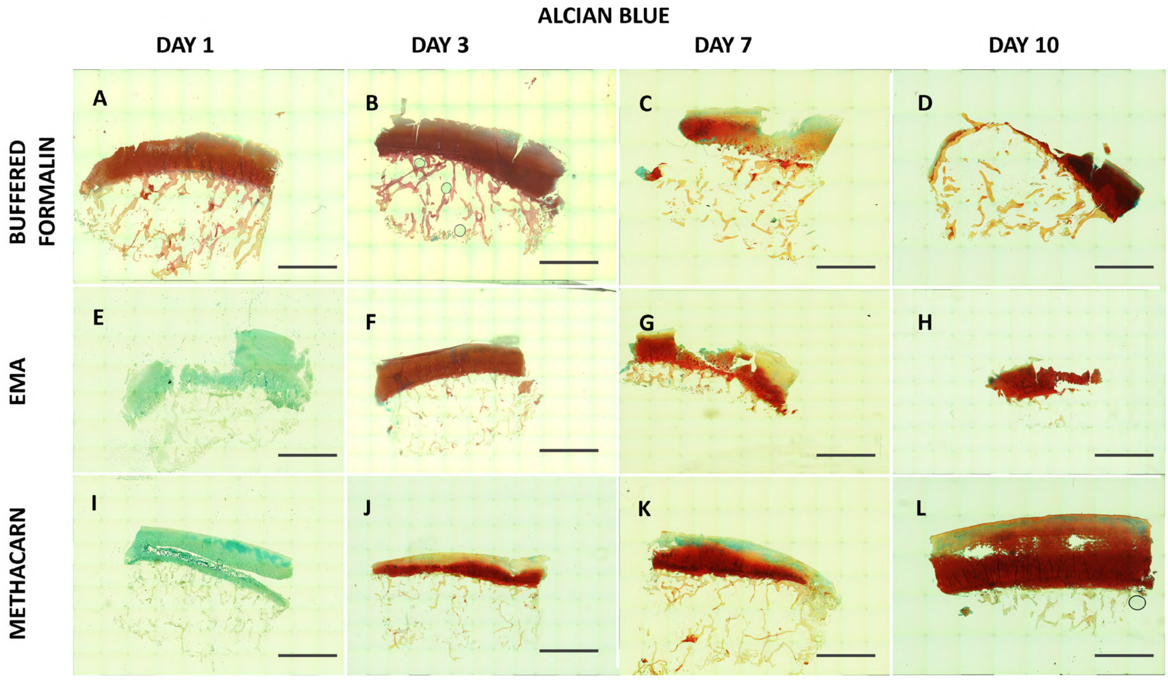

Fig. 4.- Alcian Blue staining of the osteochondral unit sections following fixation by either NBF, EMA and Methacarn, and decalcification by 10% EDTA. Magnification 10X. NBF: 10% Neutral buffered formalin, EMA: Mixture of ethanol, methanol and acetic acid at 3:1:1 ratio. Scale bars = 100 µm.

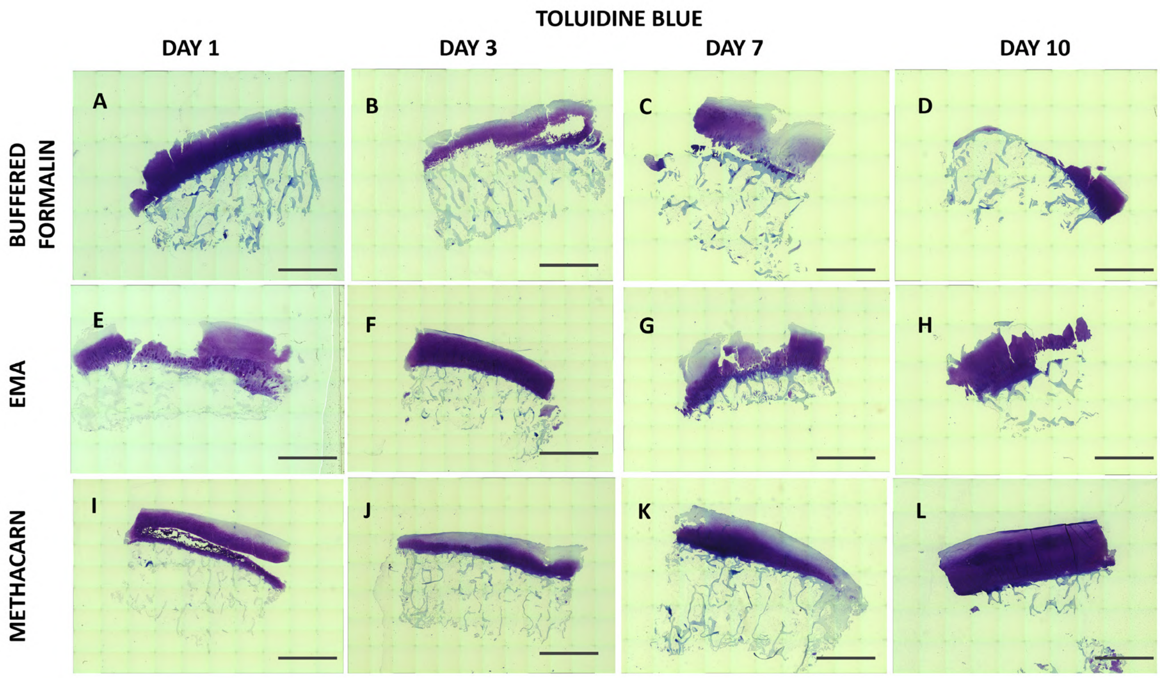

Fig. 5.- Toluidine Blue staining of the osteochondral unit sections following fixation by either NBF, EMA and Methacarn, and decalcification by 10% EDTA. Magnification 10X. NBF: 10% Neutral buffered formalin, EMA: Mixture of ethanol, methanol and acetic acid at 3:1:1 ratio. Scale bars = 100 µm.

matrix composition and structure. Comparative staining was observed between the three groups not affected by the fixation period (Fig. 5, Fig. 9).

Collagen stain: PicroSirius red, Collagen type II and X

PicroSirius red staining is a commonly used technique in histology that selectively stains collagen fibers, allowing for visualization and analysis of collagen distribution and density in various tissues. Analysis of the three groups showed that PicroSirius red stained the collagen network uniformly across the different fixative groups and periods (Fig. 6, Fig. 9).

Analysis of collagen type II uptake showed that negative control (Fig. S3) without primary antibody exposure and test slides without antigen retrieval demonstrated only mild DAB uptake, thus considered negative background staining. Conversely, all test slides with antigen retrieval exhibited strong uptake, with methacarn and EMA-fixed tissues showing higher uptake than formalin-fixed slides (Fig. 7, Table 1A). The observation was that uptake occurred solely in the cartilage region with a clear boundary between the cartilage area displaying strong uptake and the bone region with no uptake. The territorial matrix of the cartilage revealed robust uptake, confirming the specificity of the staining. Notably, the bone demonstrated negative uptake of DAB, which could thus serve as an internal negative control for future studies.

Concerning Collagen Type X, examining the negative control without the primary antibody showed a mild DAB uptake in the area just below the surface and the transition zone (Fig. S3). Similar results in test slides without antigen retrieval were also observed, thus considered negative background staining. However, all test slides with antigen retrieval demonstrated strong DAB uptake, with methacarn and EMA-fixed tissues exhibiting comparable uptake to NBF-fixed slides (Fig. 7, Table 1B). Importantly, we observed DAB uptake only in the bone region, with a clear boundary between the cartilage region, which had no uptake, and the bone area with robust uptake (Fig. 8). Intriguingly, the interlamellar planes of the bone exhibited particularly strong DAB uptake (Fig. 8). In contrast, the cartilage region displayed no DAB uptake, suggesting that it can be used as an internal negative control for future studies.

DISCUSSION

Standardizing staining of osteochondral units is crucial for ensuring accurate and reproducible assessment of tissue structure and composition, which can inform diagnoses and treatment decisions for joint-related diseases (Lepage et al., 2019). Fixation of osteochondral samples before staining is vital to preserve tissue structure and prevent artifacts that can distort the tissue's mor-

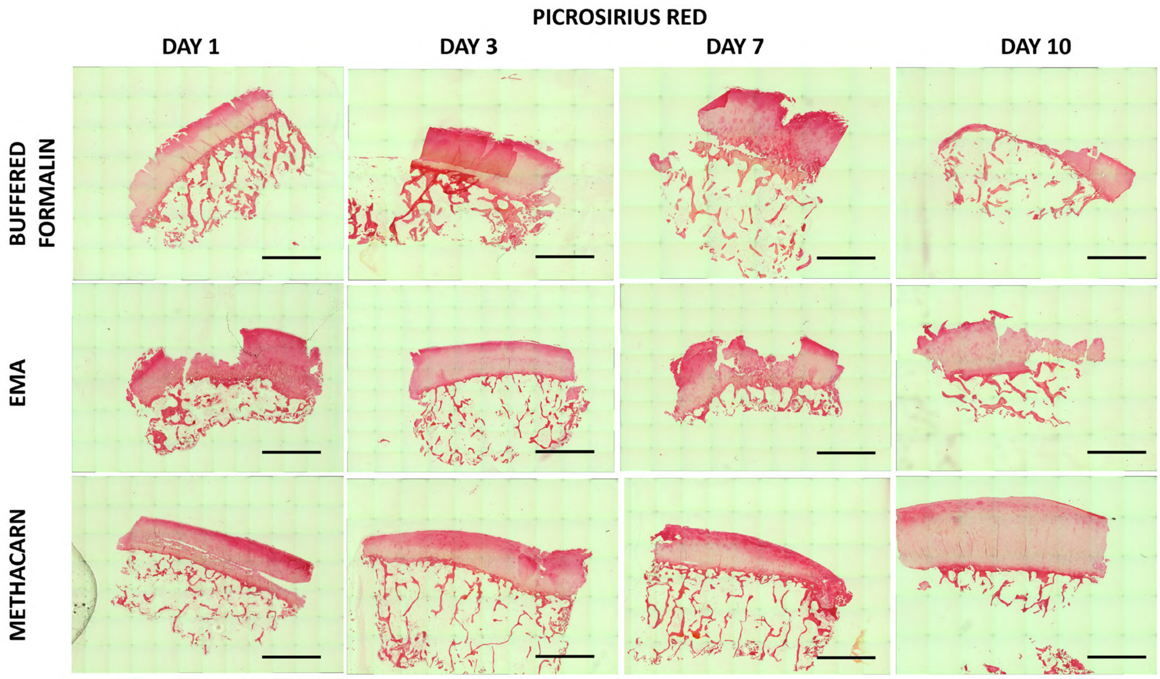

Fig. 6.- PicroSirius Red staining of the osteochondral sections following fixation by either NBF, EMA and Methacarn, and decalcification by 10% EDTA. Magnification 10X. NBF: 10% Neutral buffered formalin, EMA: Mixture of ethanol, methanol and acetic acid at 3:1:1 ratio. Scale bars = 100 µm.

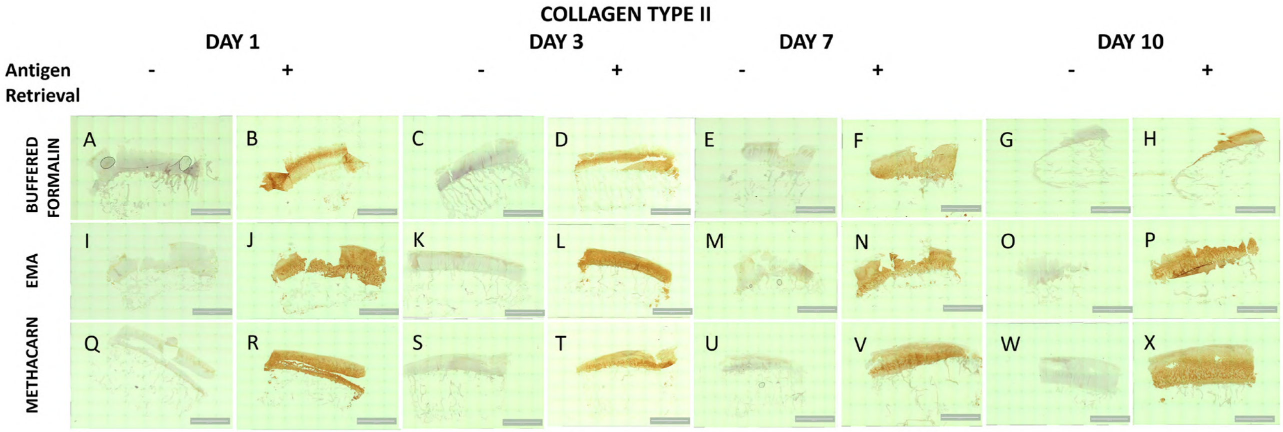

Fig. 7.- Immunohistochemical staining of the osteochondral unit sections for collagen type II following fixation by either NBF, EMA and Methacarn, and decalcification by 10% EDTA with and without antigen retrieval. The retrieval was performed using pronase and hyaluronidase. Magnification 10X. NBF: 10% Neutral buffered formalin, EMA: Mixture of ethanol, methanol and acetic acid at 3:1:1 ratio. Scale bars = 100 µm.

Table 1. A) Grading of Collagen type II and B) Collagen type X stain uptake by the osteochondral sections following fixation by either NBF, Methacarn and EMA, and decalcification with and without antigen retrieval.

A: Collagen Type II									
Days of Fixation		**Day 1**		**Day 3**		**Day 7**		**Day 10**	
Antigen Retrieval Pronase + Hyaluronidase		With	Without	With	Without	With	Without	With	Without
Fixative	NBF	+	-	+	-	+	-	+	-
	Methacarn	++	-	++	-	++	-	++	-
	EMA	++	-	++	-	++	-	++	-
B: Collagen Type X									
Days of Fixation		**Day 1**		**Day 3**		**Day 7**		**Day 10**	
Antigen Retrieval Chondroitinase ABC + Pepsin		With	Without	With	Without	With	Without	With	Without
Fixative	NBF	++	-	+	-	++	-	+	-
	Methacarn	+	-	++	-	++	-	+	-
	EMA	++	-	+++	-	++	-	+	-

Grading scale: no stain uptake (-), good stain uptake (+), very good stain uptake (++).

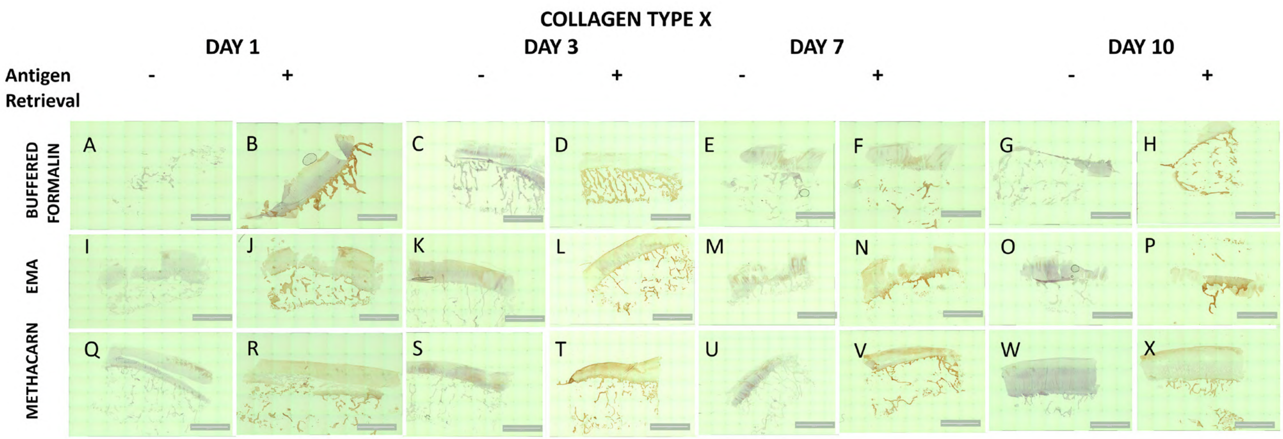

Fig. 8.- Immunohistochemical staining of the osteochondral unit sections for collagen type X following fixation by either NBF, EMA and Methacarn, and decalcification by 10% EDTA with and without antigen retrieval. The retrieval was performed using Chondroitinase ABC and pepsin. Magnification 10X. NBF: 10% Neutral buffered formalin, EMA: Mixture of ethanol, methanol and acetic acid at 3:1:1 ratio. Scale bars = 100 µm.

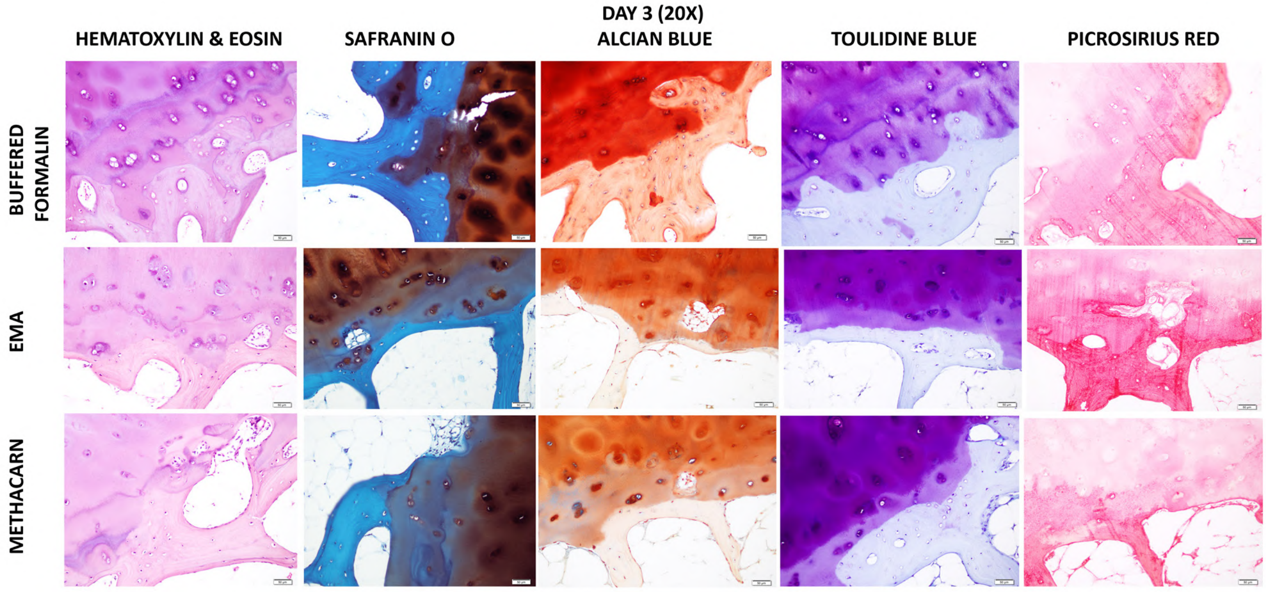

Fig. 9.- Cartilage bone junction fixed with either NBF, EMA and Methacarn for 3 days taken with the objective set at 20X magnification. Scale bars = 50 µm.

Figure S1: Study algorithm depicting the procedure for processing the osteochondral unit, derived from human adult OA knee joints using the three fixatives: NBF, Methacarn and EMA, the time period for fixation and staining used. NBF: 10% Neutral Buffered Formalin, EMA: Mixture of ethanol, methanol and acetic acid at 3:1:1 ratio.

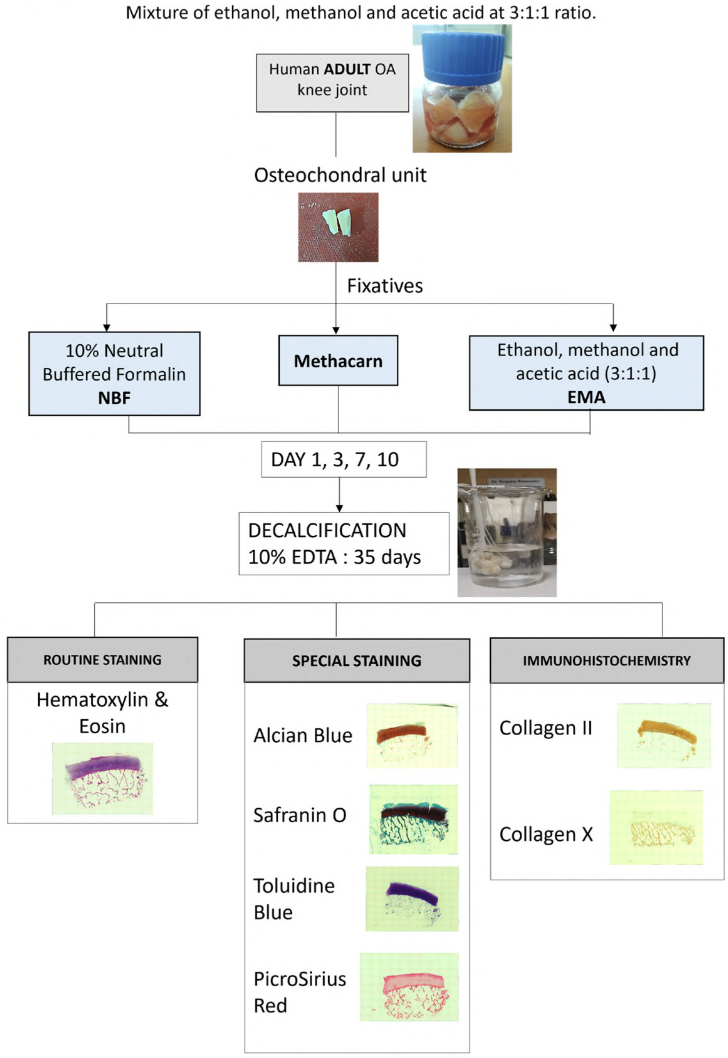

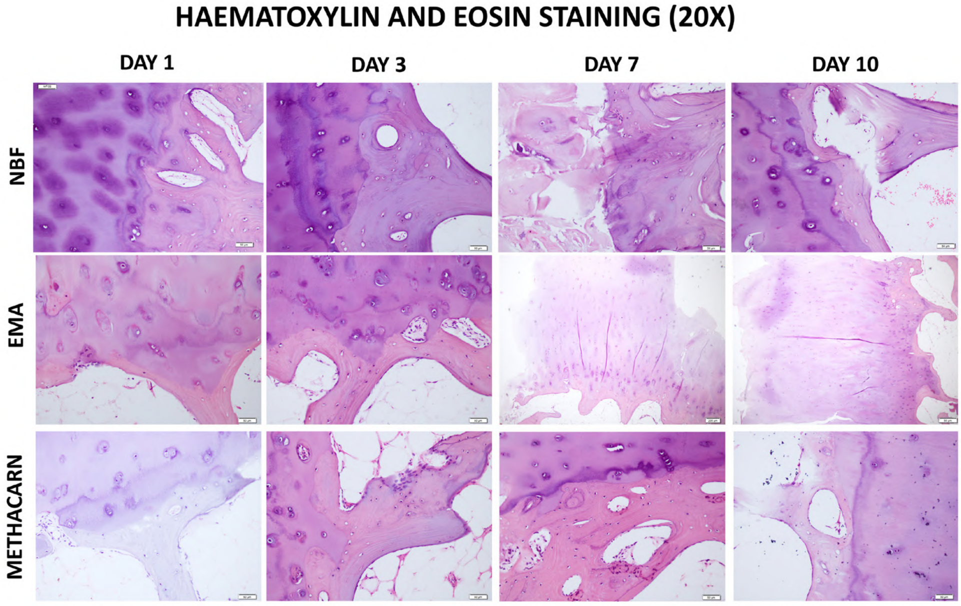

Figure S2: Hematoxylin and Eosin staining of the osteochondral sections for following fixation by either NBF, EMA and Methacarn, and decalcification by 10% EDTA. Magnification 20X.
NBF: 10% Neutral buffered formalin, EMA: Mixture of ethanol, methanol and acetic acid at 3:1:1 ratio.

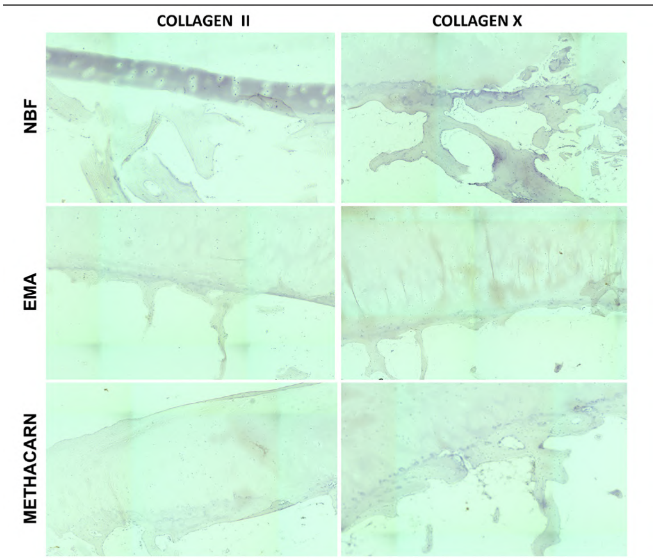

Figure S3: Negative controls: Immunohistochemical staining of the osteochondral sections for collagen type II and collagen following fixation by either NBF, EMA and Methacarn, and decalcification by 10% EDTA with antigen retrieval but without primary antibody incubation.

phology and composition, thereby ensuring reliable and consistent staining results for accurate histological analysis. Being a complex tissue that requires additional processing such as decalcification and antigen retrieval, the need to explore and optimize alternative strategies becomes paramount (Amirtham et al., 2019; Orth et al., 2015).

NBF, methacarn, and EMA are common coagulant fixatives used in histology. NBF provides good preservation of tissue structure but can result in tissue shrinkage (Thavarajah et al., 2012). Methacarn preserves lipids and yields less shrinkage but is time-consuming (Shibutani et al., 2000). EMA is a newer fixative that provides excellent tissue morphology and antigenicity preservation with minimal protein cross-linking (Rahman et al., 2022). The choice of fixative depends on the study's specific needs and the tissue being analyzed.

The present study evaluated the efficacy of these different fixatives in preserving tissue morphology and staining properties in cartilage and bone samples. Hematoxylin and eosin (HE) staining showed that NBF fixative resulted in better haematoxylin uptake compared to alcohol-based fixatives. All fixatives effectively preserved tissue morphology without necrosis or cellular degeneration. Safranin O staining showed that all tested fixatives produced comparable staining quality, with robust uptake especially observed in the territorial matrix of the stained cartilage. Alcian blue staining revealed poor uptake of the counterstain on the first day with coagulative fixatives like Methacarn and EMA fixatives, while Toluidine blue staining was not affected by the fixative or the fixation period. Picrosirius red staining was uniform across all fixative groups and periods.

The analysis of collagen type II and type X uptake showed that the negative control and test slides without antigen retrieval had mild DAB uptake and were considered negative background staining. However, all test slides processed with antigen retrieval exhibited strong DAB uptake, with methacarn and EMA-fixed tissues showing higher uptake of collagen type II than formalin-fixed tissues. The uptake occurred solely in the cartilage region for collagen type II and only in the bone region for collagen type X. The territorial matrix of the cartilage for collagen type II and the interlamellar planes of the bone for collagen type X exhibited particularly strong DAB uptake.

Our novel findings highlight the utility of different fixatives and their effects on routine, special and immunohistochemical staining in cartilage and bone tissue research. The coagulant fixatives displayed superiority to formalin with stronger collagen type II uptake. However, antigen retrieval was required with all fixatives unlike IHC studies performed without decalcification. A minimum period of 3 days is required for coagulant fixatives to provide staining consistent with formalin fixatives. Overall, methacarn and EMA serve to be good alternatives to formalin for the processing of cartilage or bone-containing tissues, with better preservation of its morphology and antigen specificity. Further studies using different tissue samples and a larger cohort would provide insights into the wider use of alternative fixatives based on the obtained immunohistochemical assays individually for specific antigen targets.

ACKNOWLEDGEMENTS

We would like to acknowledge Dr. Soosai Manickam Amirtham, Ms. Esther Rani and Mr. Ashok Kumar for technical support, and the Centre for Stem Cell Research (A unit of inStem Bengaluru), Christian Medical College, Vellore for infrastructural support. This project was supported by the Department of Biotechnology (BT/PR32777/MED/31/415/2019), Govt. of India and Fluid Research Grant (IRB Min No: 14299), Christian Medical College, Vellore.

REFERENCES

ALERS JC, KRIJTENBURG PJ, VISSERS KJ, VAN DEKKEN H (1999) Effect of bone decalcification procedures on DNA in situ hybridization and comparative genomic hybridization. EDTA is highly preferable to a routinely used acid decalcifier. *J Histochem Cytochem*, 47(5): 703-710.

AMIRTHAM SM, OZBEY O, KACHROO U, RAMASAMY B, VINOD E (2019) Optimization of immunohistochemical detection of collagen type II in osteochondral sections by comparing decalcification and antigen retrieval agent combinations. *Clin Anat*. 33(3):343-349.

BUESA RJ (2008) Histology without formalin? *Ann Diag Pathol*, 12(6): 387-396.

D'AMICO F, SKARMOUTSOU E, STIVALA F (2009) State of the art in antigen retrieval for immunohistochemistry. *J Immunol Meth*, 341(1): 1-18.

DERMIENCE M, LOGNAY G, MATHIEU F, GOYENS P (2015) Effects of thirty elements on bone metabolism. *J Trace Elem Med Biol*, 32*:* 86-106.

DEY P (2018) Fixation of histology samples: principles, methods and types of fixatives. In: Dey P (ed.). *Basic and Advanced Laboratory Techniques in Histopathology and Cytology*. Singapore: Springer, pp 3-17.

HOWAT WJ, WILSON BA (2014) Tissue fixation and the effect of molecular fixatives on downstream staining procedures. *Methods*, 70(1): 12-19.

LEPAGE SIM, ROBSON N, GILMORE H, DAVIS O, HOOPER A, ST. JOHN S, KAMESAN V, GELIS P, CARVAJAL D, HURTIG M, KOCH TG (2019) Beyond cartilage repair: the role of the osteochondral unit in joint health and disease. *Tissue Eng Part B Rev*, 25(2): 114-125.

NIETNER T, JARUTAT T, MERTENS A (2012) Systematic comparison of tissue fixation with alternative fixatives to conventional tissue fixation with buffered formalin in a xenograft-based model. *Virchows Archiv*, 461(3): 259-269.

Orth P, Peifer C, Goebel L, Cucchiarini M, Madry H (2015) Comprehensive analysis of translational osteochondral repair: Focus on the histological assessment. *Prog Histochem Cytochem*, 50(3): 19-36.

RAHMAN MA, SULTANA N, AYMAN U, BHAKTA S, AFROSE M, AFRIN M, HAQUE Z (2022) Alcoholic fixation over formalin fixation: A new, safer option for morphologic and molecular analysis of tissues. *Saudi J Biol Sci*, 29(1): 175-182.

SHIBUTANI M, UNEYAMA C, MIYAZAKI K, TOYODA K, HIROSE M (2000) Methacarn fixation: A novel tool for analysis of gene expressions in paraffin-embedded tissue specimens. *Lab Invest*, 80(2): 199-208.

SHIELDS VDC, HEINBOCKEL T (2018) Introductory Chapter: Histological Microtechniques. *Histology*. https://doi.org/10.5772/intechopen.82017

THAVARAJAH R, MUDIMBAIMANNAR VK, ELIZABETH J, RAO UK, RANGANATHAN K (2012) Chemical and physical basics of routine formaldehyde fixation. *J Oral Maxillofac Pathol,* 16(3): 400-405.

Prevalence of Morton's toe and assessment of the associated risk factors: a cross-sectional study

Bhagath K. Potu[1], Bader M.M. Saleem[2], Noor Al-Shenawi[2], Amer Almarabheh[3]

[1] Department of Anatomy, College of Medicine and Medical Sciences, Arabian Gulf University, Manama, Kingdom of Bahrain
[2] College of Medicine and Medical Sciences, Arabian Gulf University, Manama, Kingdom of Bahrain
[3] Department of Family and Community Medicine, College of Medicine and Medical Sciences, Arabian Gulf University, Manama, Kingdom of Bahrain

SUMMARY

Morton's toe results in an uneven distribution of pressure across the feet. Awareness about Morton's toe and its associated risk factors is clinically important. Although studies have reported the prevalence of Morton's toe, not many studies appear in literature discussing its impact on the associated risk factors such as hammertoe, bunion deformity, overpronation and plantar fasciitis, respectively. Hence, we have undertaken this study to analyze the prevalence of Morton's toe in the Gulf region to assess its impact on the foot. A cross-sectional descriptive epidemiological study was carried out between November 2021 and December 2022 on the feet of 100 individuals (male=50; female=50) with ages ranging from 17 to 75 years. The study included the Bahraini & non-Bahraini residents. Individuals with severe foot injuries and deformities resulting from surgery were excluded. A total of 56 Morton's toe cases (male=18; female=38) were noted in the study sample. The overall prevalence of Morton's toe was 28% and majority of the participants with Morton's toe were females (67.9%). Of 56 Morton's toe cases, the majority were seen in the age group from 30 to 40 years, particularly in females. Our findings clearly showed a significant association between Morton's toe and hammertoe (*p=0.044*), bunion and usage of high heels (*p<0.001*), respectively. However, the association between Morton's toe and other risk factors such as plantar fasciitis and overpronation of the foot were found to be statistically nonsignificant (*p>0.05*). Our study provides baseline data for the first time on the prevalence of Morton's toe and associated risk factors.

Key words: Prevalence – Morton's toe – Gulf region – Associated risk factors

INTRODUCTION

The human foot normally has five toes. Each toe has three phalanges, which are the proximal, middle, and distal, except the first toe. The first toe has only two phalanges, which are the proximal and distal (Agur and Dailey, 2006). The first toe is very important for maintaining the biome-

Corresponding author:
Bhagath Kumar Potu. Department of Anatomy, College of Medicine & Medical Sciences, Arabian Gulf University, Manama, Kingdom of Bahrain. E-mail: potubk@agu.edu.bh - ORCID ID: 0000-0002-7945-5037

Submitted: May 4, 2023. **Accepted:** June 10, 2023

https://doi.org/10.52083/ZOJG4094

chanics of the foot. Normally, in most cases, the first toe is longer than the second toe because the first metatarsal bone is longer than the second metatarsal bone. However, studies have reported that the first toe could be shorter than the second toe. When the second toe is longer and lower than the first toe, it is called Morton's toe. This structural anomaly was first described by American orthopedic surgeon Dudley Morton (Morton, 1927).

Morton's toe results in an uneven distribution of pressure across the feet. This uneven distribution of pressure causes inward curling of the first toe leading to the formation of hammertoe. Over time, this can lead to an overpronation (turning inward) of the foot along with other risk factors, such as bunion deformity and plantar fasciitis, respectively (Gutteck et al., 2019; Dang and Coughlin, 2020). Knowledge about Morton's toe and its associated risk factors is clinically important. Studies about the prevalence of Morton's toe in various populations are few, and no studies appear in the literature in a way in which we conducted our study, i.e., discussing its impact on the associated risk factors. Hence, we have undertaken this study to analyze the prevalence of Morton's toe in the Gulf region to assess its impact on the foot.

MATERIALS AND METHODS

Type of study

A cross-sectional descriptive epidemiological study was carried out between November 2021 and December 2022.

Sample size

This study was conducted on the feet of 100 individuals (male=50; female=50) with ages ranging from 17 to 75 years with mean age of 39.3±14.3. The study included the Bahraini & non-Bahraini residents. Any individuals with severe foot injuries and deformities resulting from surgeries were excluded. This study was approved by the Research and Ethics Committees of the College of Medicine and Medical Science (CMMS) at Arabian Gulf University (AGU) (approval number: (E24-PI-11-21). Informed consent was obtained from all the individuals who participated in this study.

Assessment of Morton's toe and associated risk factors

Each individual was asked to place his/her foot on a horizontal surface to examine the length of the 2nd toe. If the 2nd toe is longer than the first toe, it was considered a Morton's toe. The subjects who presented Morton's toe were also examined for their hammertoe, bunion deformity, overpronation of the foot and plantar fasciitis, respectively. The females that presented with Morton's toe in this study were also asked whether they use high-heeled footwear. This was done to assess the association of high-heel usage with Morton's toe.

Statistical analysis

The collected data were analyzed by using the Statistical Package for Social Sciences (SPSS), version 28 (Chicago, IL,USA). Categorical variables were represented as frequencies and percentages, whereas continuous variables were represented as the mean and standard deviation. A pie chart and clustered bar chart were used to present a categorical variable. The number and ratio of the presence of Morton's toe were calculated according to different risk factors. The chi-square test was used to measure the associations between outcome variable (Morton's toe) and some categorical variables. A *p-value* of less than 0.05 was considered statistically significant.

Power estimation

To determine the appropriate sample size for Chi-square of independence (Pearson Chi-square test), power analysis was conducted using G*power software based on several factors: target power (0.80); a significance level (alpha level) α=0.05; large effect size (0.6) for Cramer's phi. The power estimation suggested a minimum sample size of 76 participants.

RESULTS

Prevalence of Morton's toe

In our study of 100 individuals, 50% were males (n=50) and 50% were females (n=50). A total of 200 feet were assessed for Morton's toe. A total of 56 Morton's toe cases (male=18; female=38) were noted in the individuals aged between 17-75 years (Table 1). The overall prevalence of Morton's toe was 28%, and the majority of participants with Morton's toe were females (67.9%). Of 56 Morton's toe cases, the majority were seen in the age group from 30 to 40 years, particularly in females. The results revealed that there was a significant relationship between the outcome variable (Morton's toe) and each gender and age groups (*χ^2=9.921, df=1, p=0.002*; *χ^2=9.543, df=3, p=0.023*), respectively (Table 1, Fig. 1).

Morton's toe and associated risk factors

Morton's toe with associated risk factors is presented in Fig. 2. Our findings clearly showed that there was a statistically significant association between Morton's toe and hammertoe *(p=0.044)*, whereas the association between Morton's toe, bunion deformity (*χ^2=19.056, df=1, p<0.001*); and usage of high heels was highly significant statistically (*χ^2=11.360, df=1, p<0.001*). However, the association between Morton's toe and overpronation of foot (*χ^2=2.584, df=1, p=0.108*) and plantar fasciitis (*χ^2=1.644, df=1, p=0.200*) were not statistically significant (Table 2). All the associated risk factors except overpronation of the foot were noted significantly higher in females (Fig. 3).

DISCUSSION

Morton's toe, which is also referred to as Greek foot, Royal toe, Turkey toe, LaMay toe or Sheppard's toe, occurs due to congenital shortening of the first metatarsal bone. Studies have reported that the premature closure of the epiphysis in the

Table 1. The association between Morton's toe and socio-demographic variables.

Demographic Variables	Morton's toe		Chi-Square Value	P-value
	Present n (%)	Absent n (%)		
Gender				
Male (*n=100*)	18 (32.1)	82 (56.9)	9.921	*0.002*
Female (*n=100*)	38 (67.9)	62 (43.1)		
Age Group				
< 30 Years (*n=60*)	16 (28.6)	44 (30.6)	9.543	*0.023*
30-40 Years (*n=66*)	27 (48.2)	39 (27.1)		
41-50 Years (*n=32*)	6 (10.7)	26 (18.1)		
>50 Years (*n=42*)	7 (12.5)	35 (24.3)		

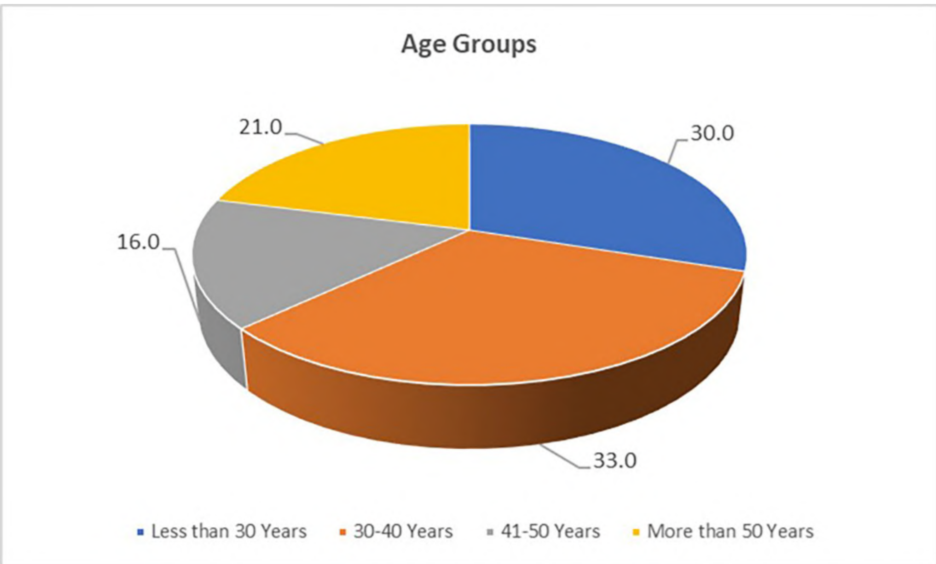

Fig. 1.- Age wise occurrence of Morton's toe.

Table 2. The association between Morton's toe and the risk factors.

Risk Factors	Morton's toe		Chi-Square Value	P-value
	No n (%)	Yes n (%)		
Hammer's toe				
No (*n=189*)	139 (96.5)	50 (89.3)	4.069	*0.044*
Yes (*n=11*)	5 (3.5)	6 (10.7)		
Bunion deformity				
No (*n=184*)	140 (97.2)	44 (78.6)	19.056	*< 0.001*
Yes (*n=16*)	4 (2.8)	12 (21.4)		
Overpronation of foot				
No (*n=199*)	144 (100)	55 (98.2)	2.584	*0.108*
Yes (*n=1*)	0 (0)	1 (1.8)		
Plantar fasciitis				
No (*n=155*)	115 (79.9)	40 (71.4)	1.644	*0.200*
Yes (*n=45*)	29 (20.1)	16 (28.6)		
Usage of high heels				
No (*n=150*)	117 (81.8)	33 (58.9)	11.360	*< 0.001*
Yes (*n=49*)	26 (18.2)	23 (41.1)		

Fig. 2.- Morton's toe observed in one of the cases (2A) and the Morton's toe with Hammertoe (2B) and bunion. * in 2A showing Morton's toe and * in 2B showing the hammertoe and the bunion.

first metatarsal bone could be a contributing factor for the occurrence of Morton's toe (Marinova et al., 2022). Data available in literature suggest that the prevalence of Morton's toe varies in populations between 0.5% - 50% (Ogawa and Hyakusoku, 2006; Vounotrypidis and Noutsou, 2015; Aigbogun et al., 2019; Marinova et al., 2022; Paul et al., 2023). Our data show a prevalence of 28%, with more cases of Morton's toe in the female gender and in the age group from 30 to 40 years. This

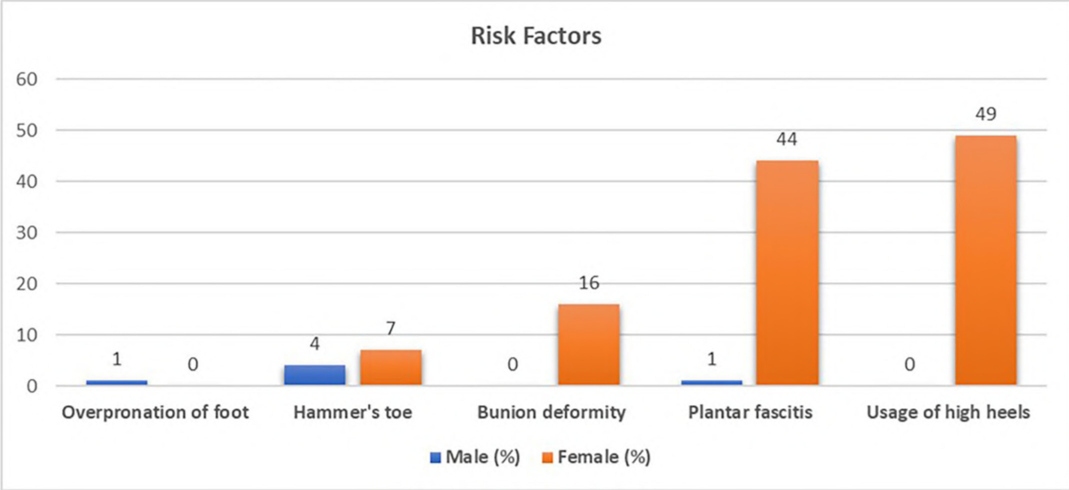

Fig. 3.- Percentage of associated risk factors of Morton's toe among male and female.

pattern was also observed in a recent study, but in males (Paul et al., 2023). Contrary to Morton's toe, few studies have reported that the first toe is the longest in 69% of the population studied, and this is termed as Egyptian foot (Ogawa and Hyakusoku, 2006). Similarly, a cross-sectional, descriptive study conducted on 331 participants from a Spanish population revealed that the most prevalent foot was Egyptian foot, followed by square foot and Greek foot, respectively (Perez Pico et al., 2018). Another study of a Nigerian population reported that these anomalies could be genetically inherited (Aigbogun et al., 2019). However, our study did not show any pattern of inheritance.

It has been postulated that the shortened first metatarsal bone puts more stress load on the longest second toe during the propulsive phase of the gait, and this could disturb the distribution of body weight during gait. Therefore, individuals with Morton's toe are at an increased risk of developing associated clinical risk such as metatarsalgia, hammertoe, plantar fasciitis, bunions, and Morton's neuroma, respectively. Our findings revealed a significant association between Morton's toe and hammertoe. The hammertoe deformity resulting from foot anomalies leads to painful callosities, difficulties in wearing shoes, and painful ambulation(Dang and Coughlin, 2020). Although we did not find a significant association between Morton's toe and plantar fasciitis in our study, it is very important to understand a hypothesis that the individuals with Morton's toe are more likely to overpronate their feet inwards when they run or walk, and this could increase the distance between the calcaneus and the toes. Furthermore, this is associated with greater tension on the plantar fascia leading to plantar fasciitis and myofascial pain syndrome (Gutteck et al., 2019). In cases of hammertoe, when inward curling of the first toe occurs, the pressure and frictional force are exerted on the skin and soft tissue of the first metatarsophalangeal joint. Over time, this might lead to callous formation. Although, it is thought to be secondary to hereditary and environmental factors, the higher incidence of bunion is seen in women compared to men is believed to be due to tightly fitting women's footwear (Ayub et al., 2005).

Studies reported that the Morton's neuroma resulting from anatomical variations such as Morton's toe could be seen more in females, particularly those wearing narrow and high-heeled footwear (Del Mar Ruiz-Herrera et al., 2022). This is evident from our study, besides the fact that all the associated risk factors were statistically significant in females including usage of high-heeled footwear and Morton's toe. Studies reported that the pain in Morton's neuroma cases is often exacerbated by walking, use of tight or heeled shoes, while the rest of cases or wearing the right footwear with appropriate insoles and orthotics ameliorated the pain (Mahadevan et al., 2015; Ganguly et al., 2018; Hartz and Biancalana, 2022). Furthermore, a recent study conducted on 214 patients revealed that the uneven distribution of the pressure on the foot with Morton's toe contributed to back pain, knee pain, hip pain and neck pain (Hartz and Biancalana, 2022).

In conclusion, our data confirmed a significant association between Morton's toe and the majority of the associated risk factors and provided a standard dataset on the prevalence of Morton's toe. With these findings, it is essential to raise awareness of Morton's toe in the region, and of taking preventive measures for mitigating associated risk factors.

AUTHORS' CONTRIBUTIONS

Conceptualization and study design: PBK. Data acquisition: BMMS, NA, PBK. Data analysis and interpretation: PBK, AA, BMMS. Drafting of the manuscript: PBK. Critical revision of the manuscript: PBK, AA.

ACKNOWLEDGEMENTS

All the authors sincerely thank the volunteers who participated in the study.

REFERENCES

AGUR AM, DAILEY AF (2006) Moore's essential anatomy. 3rd ed. Baltimore: Lippincott Williams & Wilkins.

AIGBOGUN EO, ALABI AS, DIDIA BC, ORDU KS (2019) Morton's Toe: Prevalence and inheritance pattern among Nigerians. *Int J Appl Basic Med Res*, 9(2): 89-94.

AYUB A, YALE SH, BIBBO C (2005) Common foot disorders. *Clin Med Res*, 3(2): 116-119.

DANG DY, COUGHLIN MJ (2020) Mallet toes, hammertoes, neuromas, and metatarsophalangeal joint instability: 40 years of development in forefoot surgery. *Indian J Orthop*, 54(1): 3-13.

DEL MAR RUIZ-HERRERA M, CRIADO-ÁLVAREZ JJ, SUAREZ-ORTIZ M, KONSCHAKE M, MORONI S, MARCOS-TEJEDOR F (2022) Study of the anatomical association between Morton's neuroma and the space inferior to the deep transverse metatarsal ligament using ultrasound. *Diagnostics*, 12(6): 1367.

GANGULY A, WARNER J, ANIQ H (2018) Central metatarsalgia and walking on pebbles: beyond Morton's neuroma. *Am J Roentgenol*, 210(4): 821-833.

GUTTECK N, SCHILDE S, DELANK KS (2019) Pain on the plantar surface of the foot. *Dtsch Arztebl Int*, 116(6): 83-88.

HARTZ R, BIANCALANA M (2022) Re-examining Morton's toe as a pain disorder. *Pract Pain Manag*, 22(2).

MAHADEVAN D, VENKATESAN M, BHATT R, BHATIA M (2015) Diagnostic accuracy of clinical tests for Morton's neuroma compared with ultrasonography. *J Foot Ankle Surg*, 54(4): 549-553.

MARINOVA D, ANGELOVA M, ZHEKOVA V (2022) Morton's toe frequency among the Bulgarian population and its association with high arched foot. *Acta Morphol Anthropol*, 29(1-2): 124-129.

MORTON DJ (1927) Metatarsus atavicus: the identification of a distinct type of foot disorder. *J Bone Joint Surg*, 9: 531-544.

OGAWA R, HYAKUSOKU H (2006) Does Egyptian foot present an increased risk of ingrown toenail? *Plast Reconst Surg*, 117(6): 2111-2112.

PAUL JN, OCHAI J, MADUME AK, DIDIA M, DIMKPA GC, EKOKODJE JW, AMADI H, OGBA AA, WOHA BJ, EDWA UF (2023) Prevalence of Morton's toe among the Idoma tribe, Benue state, Nigeria. *Sch J App Med Sci*, 11(3): 506-510.

PÉREZ-PICO AM, MARCOS TEJEDOR F, MARTINEZ QUINTANA R, IGLESIAS SANCHEZ MJ, MAYORDOMO R (2018) Digital formula is conditioned by deformities and footwear characteristics in older people. A comparison between general population and population with psychiatric disorders. *Eur J Anat*, 22(1): 51-58.

VOUNOTRYPIDIS P, NOUTSOU P (2015) Greek foot: is it a myth or reality? An epidemiological study in Greece and connections to past and modern global history. *Br J Rheumatol*, 54 (Suppl.1): i182-i183.

Is there a change in ischiofemoral space in lateral position in comparison to supine

H. Abdolmohammadpour Bonab[1], D. Treytak[1], C. Azzopardi[2], Karthikeyan. P. Iyengar[3], Rajesh Botchu[2]

[1] Aston Medical School, Aston, Birmingham, UK
[2] Department of Musculoskeletal Radiology, Royal Orthopedic Hospital, Birmingham, UK
[3] Department of Orthopedics, Southport and Ormskirk Hospital NHS Trust, Southport and Ormskirk Hospitals Mersey and West Lancashire Teaching NHS Trust , Southport, UK

SUMMARY

Ischiofemoral impingement (IFI) is caused due to impingement of soft tissues between the ischium and the lesser trochanter of the femur, resulting in pain and discomfort. IFI can be caused due to anatomical abnormality, previous trauma and surgery. The quadratus femoris muscle is usually affected in these cases, which can become oedematous and show fatty atrophy. Management of IFI include analgesics, physiotherapy, image-guided intervention and surgery. This study aims to provide an overview of IFI, evaluate the ischiofemoral space in a cohort of ten patients, and suggest the safest position for image-guided interventions in patients with IFI.

The ischiofemoral space and distance between the sciatic nerve and the medial part of the femoral neck were measured in supine and lateral positions on 10 consecutive patients by two fellowship-trained musculoskeletal radiologists on Computed Tomography (CT) axial sequence. There were 10 patients in the study (3 female and 7 males), with an average age of 29 years (11-70 years). A statistically significant increase in the ischiofemoral space and the distance between the sciatic nerve and the medial part of the femoral neck was found in the lateral position compared to the supine position. There was good intra- and inter-observer reliability, with a kappa value of 0.8. The increase in the ischiofemoral interval in the lateral position suggests that it is relatively safer to perform image-guided interventions and injections in the ischiofemoral interval in the lateral position with a potential reduction in the risk of incidental sciatic nerve injury.

Key words: Ischiofemoral impingement – Quadratus femoris – Ischiofemoral space – Ischiofemoral interval – Computed Tomography

INTRODUCTION

Ischiofemoral space is the area between the lateral cortex of ischial tuberosity and the medial cortex of the lesser trochanter. IFI is characterised by impingement of soft tissues between the ischium and the lesser trochanter of the femur, resulting in pain and discomfort (Johnson, 1977; Souto et al., 2009; Torriania et al., 2009; Taneja et al., 2013). IFI is an uncommon cause for hip and posterior thigh pain. This was first described by Johnson in 1977. IFI syndrome is associated with pre-existing trauma and hip surgery. IFI is caused by a narrowing of the space located between the

Corresponding author:
Dr Rajesh Botchu. Department of Musculoskeletal Radiology, The Royal Orthopedic Hospital, Bristol Road South, Northfield, Birmingham, UK. Phone: -00441216854000. E-mail: drbrajesh@yahoo.com

Submitted: April 14, 2023. **Accepted:** June 13, 2023

https://doi.org/10.52083/OAQD8529

lateral aspect of the os ischium and the lesser trochanter of the femur that entraps soft-tissue structures (Taneja et al., 2013). The quadratus femoris muscle is primarily affected, becoming irritated and manifesting with muscle-belly oedema or even fatty degeneration in chronic disease (Torriania et al., 2009) (Fig. 1).

A mechanical compression with, and oedema of, the soft tissues causes impingement of the surrounding tissues; the quadratus femoris muscle in particular is affected by this. This pathology is seen in symptomatic patients with IFI. The mean normal safe ischiofemoral distance (IFD) in a healthy female is approximately 18.6 +/- 68 mm, and 23 +/- 67 mm in a healthy male (Hujazi et al., 2016).

The presenting symptoms of IFI are posterior hip pain and may be misinterpreted with other deep gluteal and hamstring syndromes. It has been associated with different conditions such as congenital posteromedial femoral position, coxa valga, large lesser trochanter, osteochondromatosis of the hip and malunited extracapsular fractures of the proximal femur (Torriania et al., 2009; Hujazi et al., 2016).

IFI pain is usually localised to the posterior hip, but may radiate to the posterior thigh and knee due to irritation of the sciatic nerve (Gollwitzer et al., 2017). Clinically, pain can be elicited with passive hip extension, flexion, adduction, external and internal rotation.

The narrowing of the IFD, during repeated hip movements, may be the cause of the changes in the quadratus femoris muscle (Torriania et al., 2009). Concomitant pathologies such as post-surgical pathologies of gluteal tendons and hamstring, as well as coxa valga, are initially addressed when treating IFI. Management options of IFI includes rest, physiotherapy, anti-inflammatory medication, CT-guided injections with local anaesthetic, and steroid and rarely surgical intervention is necessary if conservative care is unsuccessful. Surgical management options for ischiofemoral impingement include lesser trochanteric osteotomy and release of the quadratus femoris tendon.

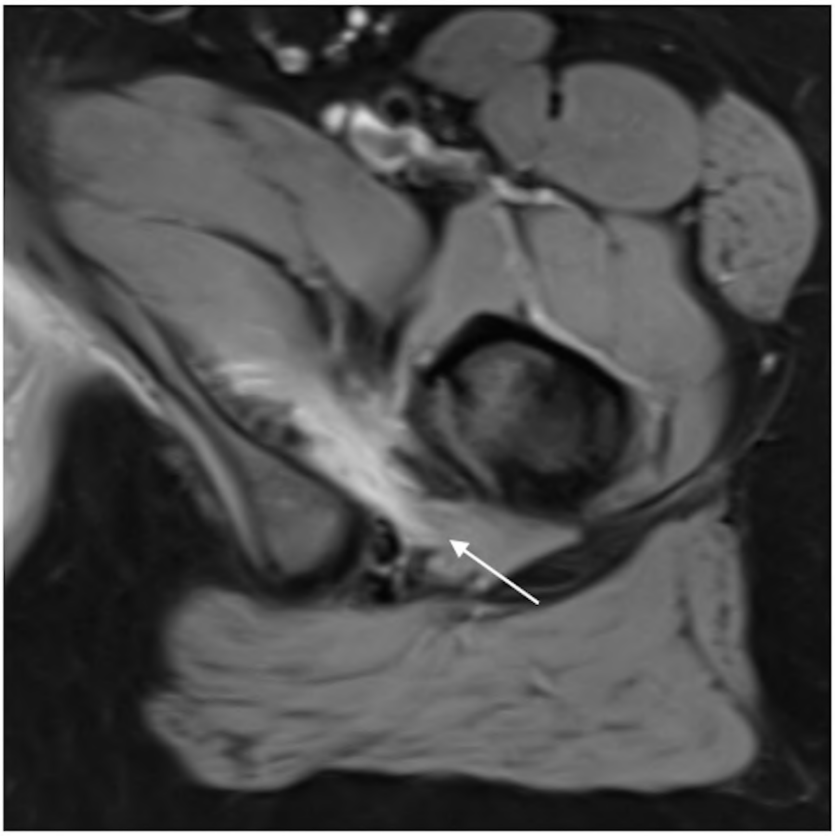

Fig. 1.- Axial PDFS (proton density fat suppressed) image of left hip showing moderate narrowing of ischiofemoral interval with marked oedema of quadratus femoris (arrow).

Image-guided interventions for IFI can be performed in prone or lateral position. We hypothesise that it is relatively safer to perform image-guided intervention in lateral position in comparison to prone position, and this pilot study explores the concept.

MATERIAL AND METHODS

Patients

A pilot study of 10 consecutive patients who had CT scans of the pelvis in supine and lateral position over a 2-year period were included in the study. Patients had imaging (supine and lateral) as part of the investigation for either hip pain or suspected malignancy at our centre. Supine imaging was performed for diagnostic purposes and CT in lateral was obtained as a part of planning for biopsy or CT-guided injection. All images were performed on Siemens Somatom AS (Erlangen, Germany).

Image analysis

The IFD (distance between the ischium and medial part of the femoral neck) and distance between the sciatic nerve and medial part of the femoral neck were measured in supine and lateral images (Figs. 2, 3). This was evaluated by a fellowship-trained musculoskeletal radiologist with over 10 years' experience and another fellowship-trained radiologist with over 5 years' experience. One reader repeated measurement after an interval of 4 weeks. The data that were collected included, age, sex, IFD and distance between the sciatic nerve and the medial part of the femoral neck.

Statistical analysis

Microsoft Excel data sheet was used for data collection. SPSS 24.0 software (SPSS Inc., Chicago, Illinois, USA) was used for statistical analysis. Descriptive statistics analysis was undertaken. Mean and standard deviation or median (range) were used to summarise the data for continuous variables and frequency/percentage for categorical variables. Comparison of frequencies of paired data was performed using the chi-square test, while means were compared using the Student's t-test. A p-value of <0.05 was considered significant. Kappa Test was used to evaluate for intra and inter observer reliability.

RESULTS

There were 10 patients in the study (3 female and 7 males) with an average age of 29 years (11-70 years). The average safe ischiofemoral distance (IFD) significantly increased in the lateral position compared to the supine position (3.8 cm vs 2.9 cm, *p-value* of 0.01). In addition, the distance between the sciatic nerve and femoral neck

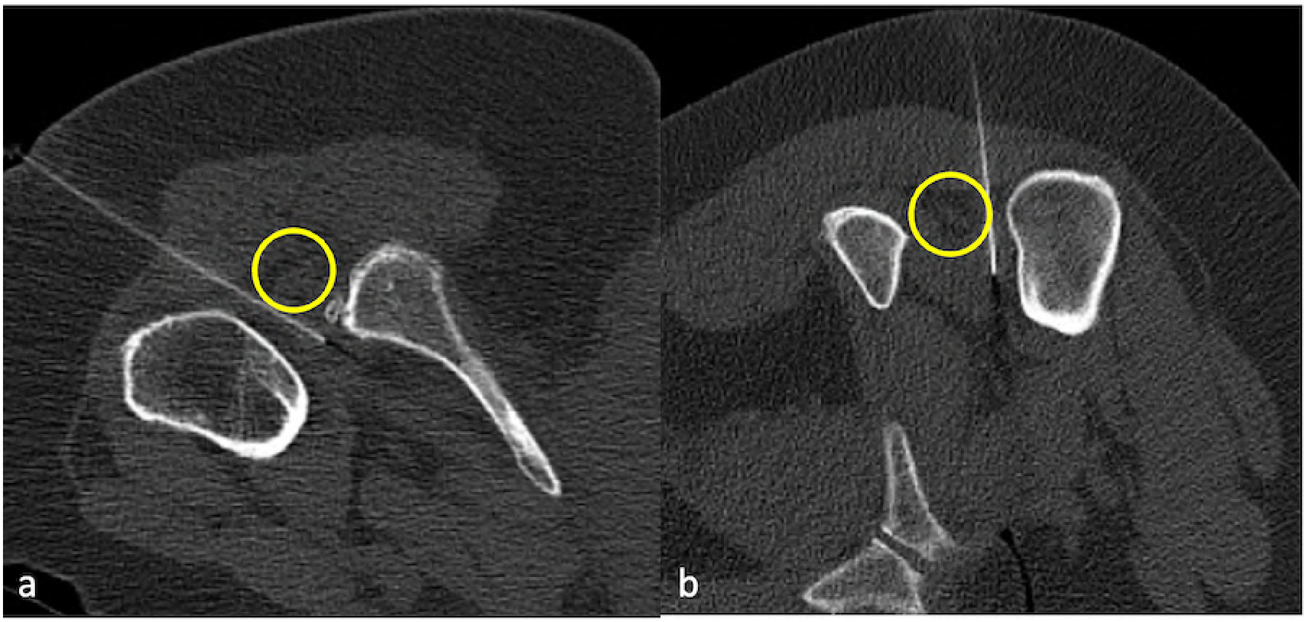

Fig. 2.- Axial CT showing needle in the ischiofemoral interval in prone (**a**) and lateral (**b**) position. Yellow circle shows the sciatic nerve.

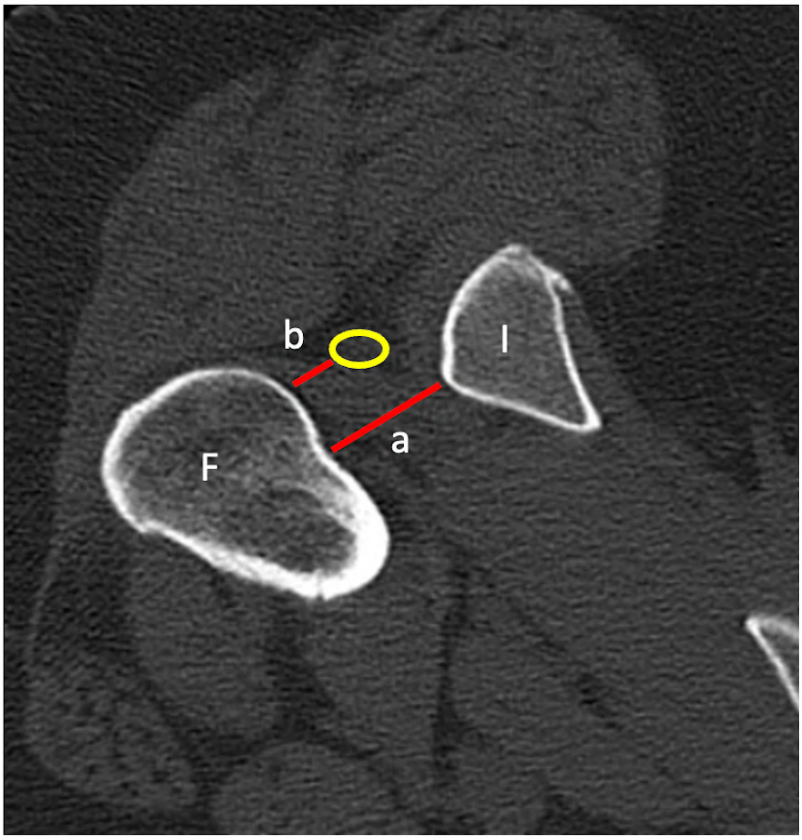

Fig. 3.- Axial CT showing ischiofemoral distance (a) between the medial part of the femoral neck (F) and ischium (I) and distance between the sciatic nerve (yellow ring) and medial part of the femoral neck (distance b).

increased in the lateral position (2.58 cm) compared to the supine position (1.96 cm, *p-value* of 0.03), indicating that it may be safer to perform an injection of the ischiofemoral interval in the lateral position, potentially reducing the incidence of sciatic nerve injury.

The study also revealed a 30-32% increase in the ischiofemoral interval in the lateral position. (Table 1: Summary of Results). A good intra and inter observer reliability was found with a kappa value of 0.8.

Table 1. IFD (ischiofemoral distance) and distance between the sciatic nerve and femoral neck in supine and lateral position. CI- confidence interval.

	IFD supine (cm)	IFD lateral (cm)	Sciatic nerve to femoral neck in supine (cm)	Sciatic nerve to femoral neck in lateral (cm)
Mean	2.920	3.8770	1.960	2.580
SD (Standard deviation)	0.888	0.6081	0.532	0.670
SEM (Standard error mean)	0.281	0.1923	0.168	0.212
90% CI	2.405 to 3.435	3.5245 to 4.2295	1.652 to 2.268	2.192 to 2.968
95% CI	2.285 to 3.555	3.4420 to 4.3120	1.580 to 2.340	2.101 to 3.059
99% CI	2.007 to 3.833	3.2521 to 4.5019	1.414 to 2.506	1.892 to 3.268
Minimum	0.9	3	0.8	1.3
Median	2.95	3.885	2	2.6
Maximum	4.2	4.7	2.9	3.3

DISCUSSION

Ischiofemoral impingement (IFI) is an increasingly recognised condition characterised by vague deep buttock pain with overlapping features of other common conditions in this region, such as hamstring pathologies, piriformis syndrome or spinal radiculopathy, and thus provide diagnostic challenges Jeyaraman et al., 2023).

CT-guided interventions such as steroid injections can be used to deliver medical therapy locally, and have been used to alleviate pain, discomfort and help with symptom management. CT-guided injections can be performed in prone or lateral position (Singer et al., 2015). The optimal position for administering these injections, however, has been a matter of debate. One of the risks of image-guided interventions is inadvertent nerve injury. The sciatic nerve is at particular risk in CT-guided interventions for IFI.

On a PubMed search there were no studies identified which compared the prone and lateral approaches. One study preferred prone position and had stated that going through hamstring tendons is easier and safer, since placing the needle in this direction reduces the risk of damage to the sciatic nerve, which is adjacent to quadratus femoris (Volokhina and Dand, 2013). A lateral approach has been suggested with the needle inserted lateral and deep to the sciatic nerve (Wilson and Keene, 2016). However, there were no studies conducted to compare both of the approaches and suggest the safest route.

Our results have demonstrated a significant increase in the safe ischiofemoral distance (IFD) and the distance between the sciatic nerve and the femoral neck when patients were in the lateral position as compared to the supine position. The increase in IFD in lateral position can be attributed to internal rotation of the femur. This subsequently increases the distance between the sciatic nerve and the medial part of the femoral neck. Planning the trajectory of the needle along the medial part of the femoral neck during imaging-guided injection ensures that the relative distance between the needle and the sciatic nerve is increased in lateral position. The clinical implication of this finding implies that the lateral position may be relatively safer for administering injections in the ischiofemoral space, thereby reducing the risk of sciatic nerve injury. Moreover, a good intra- and inter-observer reliability with a kappa of 0.8 supports the reproducibility of our measurements.

Limitations of the study

We acknowledge that our study has some limitations. First, the sample size is small, with only 10 patients included in this pilot study. This limits the generalizability of our findings and warrants further research with a larger sample size to confirm the results. However, with a good intra- and inter-observer reliability observed, it strengthens our proposition. Second, our study population included patients who had CT scans of the pelvis for various indications, such as hip pain or suspected malignancy, and hence may introduce potential confounding factors or selection bias. Furthermore, the study only compared supine and lateral positions, assuming that the supine position would be similar to the prone position. Further large prospective studies would help to confirm the results of our pilot study and a more accurate assessment of the safest position for image-guided injections.

CONCLUSION

Our pilot study suggests that the lateral position may be relatively safer than the prone position for administering image-guided injections in patients with ischiofemoral impingement, and provide a potential reduction in the risk of incidental sciatic nerve injury.

REFERENCES

GOLLWITZER H, BANKE IJ, SCHWAUWECKER J, GERDESMEYER L, SUREN C (2017) How to address ischiofemoral impingement? Treatment algorithm and review of the literature. *J Hip Preserv Surg*, 4(4): 289-298.

HUJAZI I, JONES T, JOHAL S, BEARCROFT P, MUNIZ-TERRA G, KHANDUJA V (2016) The normal ischiofemoral distance and its variations. *J Hip Preserv Surg,* 3(3): 197-202.

JEYARAMAN M, IYENGAR KP, BEALE D, BOTCHU R (2023) Ischiofemoral impingement caused by an intrapelvic lipoma of the sciatic nerve-A rare case presentation. *J Orthop Rep,* 2(3): 100165.

JOHNSON KA (1977) Impingement of the lesser trochanter on the ischial ramus after total hip arthroplasty. Report of three cases. *J Bone Joint Surg Am,* 59(2): 268-269.

SINGER AD, SUBHAWONG TK, JOSE J, TRESLEY J, CLIFFORD PD (2015) Ischiofemoral impingement syndrome: a meta-analysis. *Skeletal Radiol.* 44(6): 831-837.

SOUTO SC, THOMAS BJ, OUELLETTE H, BREDELLA MA (2009) Ischiofemoral impingement syndrome: an entity with hip pain and abnormalities of the quadratus femoris muscle. *Am J Roentgenol,* 193(1): 186-190.

TANEJA AK, BREDELLA MA, TORRIANI M (2013) Ischiofemoral impingement. *Magn Reson Imaging Clin N Am,* 21: 65-73.

TORRIANIA M, SOUTO SC, THOMAS BJ, OUELLETTE H, BREDELLA MA (2009) Ischiofemoral impingement syndrome: an entity with hip pain and abnormalities of the quadratus femoris muscle. *Am J Roentgenol,* 193(1):186-190.

VOLOKHINA Y, DAND D (2013) Using proximal hamstring tendons as a landmark for ultrasound- and CT-guided injections of ischiofemoral impingement. *Radiol Case Rep,* 8(1): 789.

WILSON MD, KEENE JS (2016) Treatment of ischiofemoral impingement: Results of diagnostic injections and arthroscopic resection of the lesser trochanter. *J Hip Preserv Surg*, 3(2): 146-153.

YANAGISHITA CM, FALOTICO GG, ROSARIOA DA, PUDINA GG, WEVER AA, TAKATA ET (2012) Ischiofemoral impingement – an etiology of hip pain: Case report. *Revista Brasil Ortopedia (English Edition*), 47(6): 780-783.

Morphometric analysis of cavitas glenoidalis with multidedector CT

Ali Keleş[1], Mehmet T. Yilmaz[2], Orhan Özbek[3], Duygu A. Saygin[2], Muzaffer Şeker[2]

[1] *Department of Anatomy, Faculty of Medicine, Karamanoglu Mehmetbey University, Karaman, Turkey*
[2] *Department of Anatomy, Meram Faculty of Medicine, Necmettin Erbakan University, Konya, Turkey*
[3] *Department of Radiology, Necmettin Erbakan University, Konya, Turkey*

SUMMARY

The glenoid cavity is a sliced egg-shaped joint surface located on the lateral margin of the scapula to form the shoulder joint. Recognition of variations in shape and dimensions of the glenoid cavity is important for a better comprehension of joint-associated diseases, especially in total shoulder arthroplasty procedures. The aim of this study was to perform morphometric measurements on the glenoid cavity. Glenoid cavities of 391 individuals (197 males [50.4%], 194 females [49.6%]) were reviewed by using Multi-detector Computed Tomography. The maximum length and maximum width of glenoid cavities, as well as the width, depth and circumference at the notch level were measured, and the index value was calculated. The glenoid cavity shapes were typed as pear, inverted comma and oval type. Furthermore, the metric values that provide the best differentiation between genders were identified through ROC analysis.

The pear glenoid cavity type was detected in 53.2%, inverted comma type was detected in 28.4%, and oval type was detected in 18.4% of cases. In all of our morphometric measurements, male values were higher than female values, and there was significant difference between them. Results of ROC analysis revealed significant measurements for the maximum length and maximum width measurements of the glenoid for gender determination. Morphometric information of the glenoid cavity can be useful in order to increase clinical success in case of Bankart lesion, rotator cuff disease, and osteochondral defect. Recognition of different shapes and dimensions of the glenoid cavity is essential for the design of the glenoid component, especially for total shoulder arthroplasty procedure. We believe that the data obtained in our study would be useful for prosthesis designers and orthopaedic surgeons.

Key words: Glenoid cavity – Morphometric – Computed tomography – Gender – Index – Variations

ABBREVIATIONS

GC: Glenoid cavity
MDCT: Multi-detector Computed Tomography
SI: Glenoid cavity length
AP1: Glenoid cavity width (Anterior-Posterior glenoid diameter-1)
AP2: Glenoid cavity width at notch level (Anterior-Posterior glenoid diameter-2)

Corresponding author:
Duygu Akin Saygin. Department of Anatomy, Meram Faculty of Medicine, Necmettin Erbakan University, Konya, Turkey. Phone: +90 (0332) 22373 28. E-mail: d.akin.42@hotmail.com

Submitted: January 12, 2023. **Accepted:** June 16, 2023

https://doi.org/10.52083/MRFP5453

DGC: Glenoid cavity depth
PGC: Glenoid cavity circumference
GCI: Glenoid cavity index
$R_{n:}$ Number of right side
$L_{n:}$ Number of left side
$M_{n:}$ Number of male
$F_{n:}$ Number of female

INTRODUCTION

The glenoid cavity (GC) is located on the concave surface of the shoulder joint on the lateral angle of the scapula (Halder et al., 2001). The joint surface is surrounded by a structure called the glenoid labrum without restriction of movement (Pagnani and Warren 1994; Halder et al., 2001). The glenoid labrum contributes to the stability of the glenohumeral joint, and increases the concavity of the GC (Lippitt et al., 1993).

Prescher and Klümpen (1997) stated that if the notch in the antero-superior part of the GC is prominent, the glenoid labrum is not fixed to the notch region and may predispose to the Bankart lesion. However, the presence of the glenoid notch may not always predispose to having anatomical variants in the labrum. Thomson et al. (2015) reported that the presence of the glenoid notch is not a useful tool to predict a normal variant of the anterior and superior labrum. Research suggests that individuals with a GC notch have a greater rate of recurrent shoulder dislocation, with a reported 61% occurrence rate (Lo et al., 2004). The shoulder joint is more stable since the glenoid labrum is attached along GC margins when the glenoid notch is absent (Coskun et al., 2006; Khan et al., 2020).

The shoulder joint is the most common dislocating joint. Glenoid fractures are common along with dislocations due to trauma. Prostheses and arthroplasty are needed several times for solution. The morphometry and variation of the GC is actually important in order to decide adequate size of the glenoid component in shoulder arthroplasty for traumatic or pathological conditions associated with shoulder area (Mamatha et al., 2011; Rajput et al., 2012; Singh et al., 2019).

Mamatha et al. (2011) stated that recognition of variation in normal anatomy of the GC is essential for evaluation of pathological conditions such as Bankart lesion and osteochondral defects.

Hassanein (2015) conducted a study to detect morphological types and diameters of the GC in scapula samples of adult Egyptians, and expressed that variations in the form and size of the GC should be well-known in order to understand the shoulder joint arthroplasty, and to minimize the failure rates that affect the glenoid component. There are other studies that analyse the morphometric parameters of the glenoid cavity on the dry scapula (Khan et al., 2020), cadaver (Mathews et al., 2017), or CT (Jia et al., 2020).

The aim of this study was to collect morphological data of GC, to reveal important measurements that are important for gender determination through the data obtained, and to evaluate these in comparison to the literature. Therefore, we believe that this study would provide anatomic parameters that would guide anatomists, orthopaedic surgeons, prosthesis designers, and anthropologists.

MATERIAL AND METHODS

In the present study, the scapulae of individuals were measured through Multi-detector Computed Tomography (MDCT) in the Radiology Department of Meram Faculty of Medicine within Necmettin Erbakan University. MDCT (Sensation 64, Siemens, Erlangen, Germany) parameters are as follows; KV: 120, Effective MaS: 50-170, MAS: 86, Pitch 1,4, Rotation speed: 0,5 sec, Detector area: 1,2 mm, Slice thickness: 1,5 mm. 3D and inspace programs (Leonardo, Siemens, Germany) were used in measuring parameters and GC typing.

In this study, all patients (443) whose scapulae were visible on comparative thoracic MDCT images between the 1st of January 2014 and the 30th of April 2016 were examined. A total of 52 individuals with fractures, defects, osteoporotic appearance, and pathological conditions in the measurement area were not included in the study. The measurements were carried out on a total of 391 (197 males and 194 females) individuals without any history of trauma or pathology of the shoulder joint. The age average of males was 60.28 ± 15.43 years with an age range of 9 to 94 years; the age average of females was 58.82 ± 16.38 years with an age range of 10 to 92 years**.** Approval of the local ethics committee was obtained by decision number of 2016/574 within Necmettin Erbakan University. Measurements were made once by a researcher who has been working in the field of radiology for 11 years.

The measurements analysed in the present study are as follows:

GC length (SI): Maximum length between lowest point of the GC and the most prominent point of supraglenoid tubercle (Fig. 1).

GC width (AP1): Maximum width of the joint space (Fig. 1).

GC width at notch level (AP2): The width of the joint space at the glenoid notch level (Fig. 1).

GC depth (DGC): The length of the line drawn between the top and lowest points on axial images, and the length of the line drawn 90 degrees vertically from the deepest point of the GC to this line (Fig. 1).

GC circumference (PGC): The GC measurement including all margins from supraglenoid tubercle, and ending in the start point (Fig. 1).

GC index (GCI): It was calculated as (AP1 ÷ SI) × 100 [12].

SI, AP1, AP2, DGC and PGC parameters were measured in mm and GCI was calculated in %.

There is a notch on the anterosuperior part of the GC. When the notch is present, the shape of the glenoid cavity can be described as pear-shaped or as inverted comma-shaped (when the notch is distinct, it is an inverted comma; when the notch is slight, it is pear-shaped). When it is absent, the cavity is oval-shaped (Prescher and Klümpen, 1997). In this study, GC was typed in three groups as pear (Fig. 2A), inverted comma (Fig. 2B), and oval shape (Fig. 2C).

Statistical analysis of the measurements was performed through IBM SPSS Statistics 21.0 program. The Paired-Samples T test was used in order to compare the measurements on the right and left sides. All measurements were also evaluated

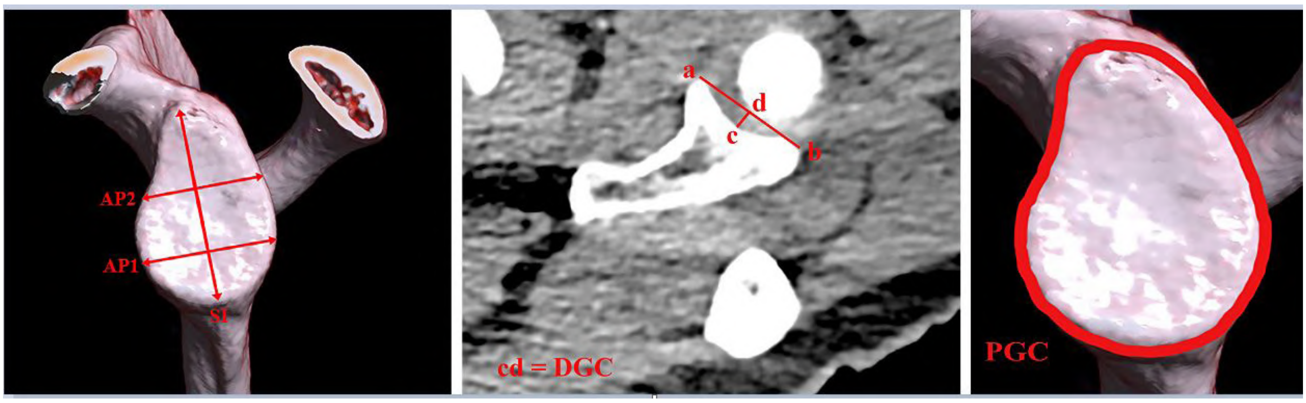

Fig. 1.- SI: Superior-inferior glenoid diamater, **AP1**: Anterior-Posterior glenoid diameter-1, **AP2**: Anterior-Posterior glenoid diameter-2, **DGC**: Depth of glenoid cavity (**ab length:** The length of the line drawn between the top and lowest points on axial images.**cd length:** The length of the line drawn 90 degrees vertically from the deepest point of the GC to this line, **PGC**: Perimeter of glenoid cavity.

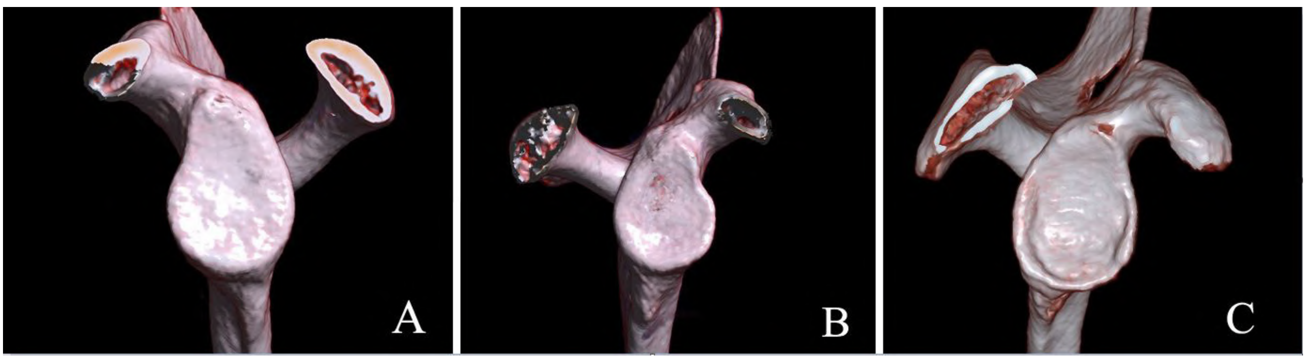

Fig. 2.- Different shapes of the glenoid cavity. **A:** Pear shape, **B:** Inverted comma shaped, **C:** Oval shaped.

according to genders through Independent-Samples T test. Furthermore, the cut-off point, sensitivity, specificity and the area under the curve were found for metric values that provide the best differentiation between genders by ROC analysis.

RESULTS

There was not any significant difference between right and left GC values in SI, AP1, PGC, and GCI parameters; however, a significant difference was detected between right and left GC values for AP2 and DGC. Furthermore, a significant difference was detected in all measurements between males and females; morphometric values of male GC measurements were detected greater (Table 1) ($p < 0.05$).

In the present study, 13.1% of the right-side samples appeared without notch (Fig. 3A), 81.3% of right-side samples appeared with a single notch (Fig. 3B) and 5.6% appeared with double notches (Fig. 3C); as far as the left-side samples are concerned, 12.5% appeared without notch, 83.1% appeared with a single notch, and 4.4% appeared with double notches. Moreover, 11% of males had no notch; 84% and 5% of males presented single and double notch, respectively; and 15% of females had no notch, whereas 80% and 5% of them had single and double notch, respectively. The ratio of the single notch is higher on both sides and in both genders. While the ratio of the notch was statistically significant between the right and left sides, the difference between the sexes was not significant (Table 2).

GC shape was found to have pear shape in genders. The pear GC type was detected in 53.2%, inverted comma type was detected in 28.4%, and oval type was detected in 18.4% of cases. The difference between the genders according to GC shape was not statistically significant ($p>0.05$) (Table 3).

According to the data obtained as a result of ROC analysis in our study, AP1, SI, PGC and AP2 parameters give the highest rate in estimation of gender, respectively. In addition, it was observed that left-sided parameters gave a higher rate in estimating gender than right-sided parameters (Table 4, Fig. 4).

Table 1. Glenoid cavity morphometry

n		**Glenoid cavity morphometry**					
		SI	**AP1**	***AP2**	**DGC**	**PGC**	**GCI**
Laterality	**Rn = 391** **Ln = 391**	39.20 ± 3.80 38.80 ± 3.70	26.60 ± 3.10 26.40 ± 2.90	19.20 ± 2.20 18.80 ± 2.10	4.20 ± 1.10 4.0 ± 1.10	112.9 ± 10.9 111.9 ± 11.6	67.91 ± 5.08 68.13 ± 5.56
	P-value	0.170	0.367	**0.022**	**0.012**	0.227	0.564
Gender	**Mn = 394**	41.60 ± 3.00	28.60 ± 2.30	20.20 ± 1.80	4.50 ± 1.20	119.3 ± 9.90	68.82 ± 5.77
	Fn = 388	36.40 ± 2.40	24.40 ± 2.0	17.80 ± 1.70	3.80 ± 0.90	105.5 ± 7.70	67.20 ± 4.70
	P- value	**0.000***	**0.000***	**0.000***	**0.000***	**0.000***	**0.000***

SI: Superior-inferior glenoid diamater, **AP1**: Anterior-Posterior glenoid diameter-1, **AP2**: Anterior-Posterior glenoid diameter-2, **DGC**: Depth of glenoid cavity, **PGC**: Perimeter of glenoid cavity. **R_n:** Right, **L_n:** Left, **M_n:** Male, **F_n:** Female.
(* For **AP2** Rn: 340, Ln: 340; Mn: 350, Fn: 330) (mm) (Mean ± SD) (SD: Standard deviation)

Table 2. Glenoid cavity notch numbers

n		**Glenoid cavity notch numbers**						
		Bilateral without glenoid notch		**One-sided glenoid notch**		**Bilateral glenoid notch**		**p**
		N	**%**	**N**	**%**	**N**	**%**	
Laterality	**R_n = 391**	51	13.1	318	81.3	22	5.6	**0.000***
	L_n = 391	49	12.5	325	83.1	17	4.4	**0.000***
Total	**n_T = 782**	100	12.8	643	82.2	39	5	
Gender	**M_n = 394**	43	11	331	84	20	5	0.498
	F_n = 388	57	15	312	80	19	5	0.505

N: Number, **R_n:** Right, **L_n:** Left, **M_n:** Male, **F_n:** Female, **n_T:** Total, * $p<0.05$

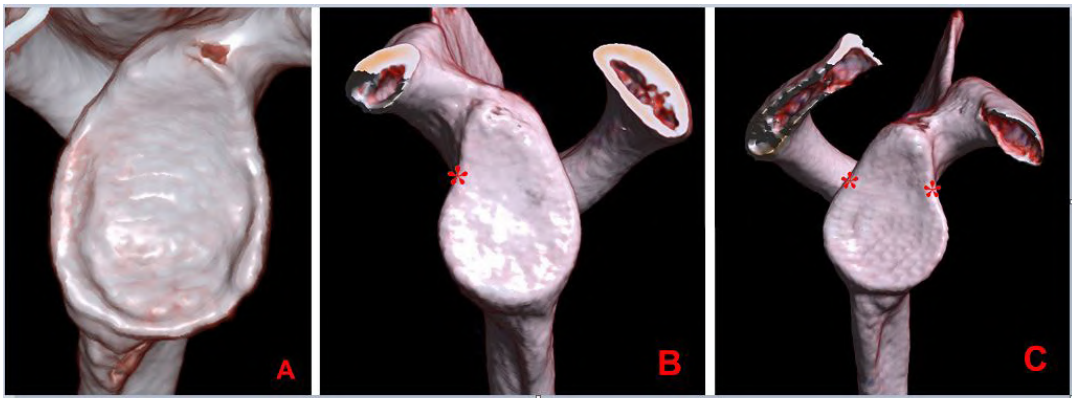

Fig. 3.- Glenoid cavity notch numbers. **A:** Bilateral without glenoid notch**, B:** One-sided glenoid notch**, C:** Bilateral glenoid notch, ***:** shows the glenoid notch.

Table 3. Different shapes of the glenoid cavity

Glenoid Shape	Incidence (%)			p
	Total	Male	Female	
Pear shape	53.2	52.2	54.1	0.724
Inverted comma shaped	28.4	28	28.9	
Oval shaped	18.4	19.8	17	
Total	100	100	100	

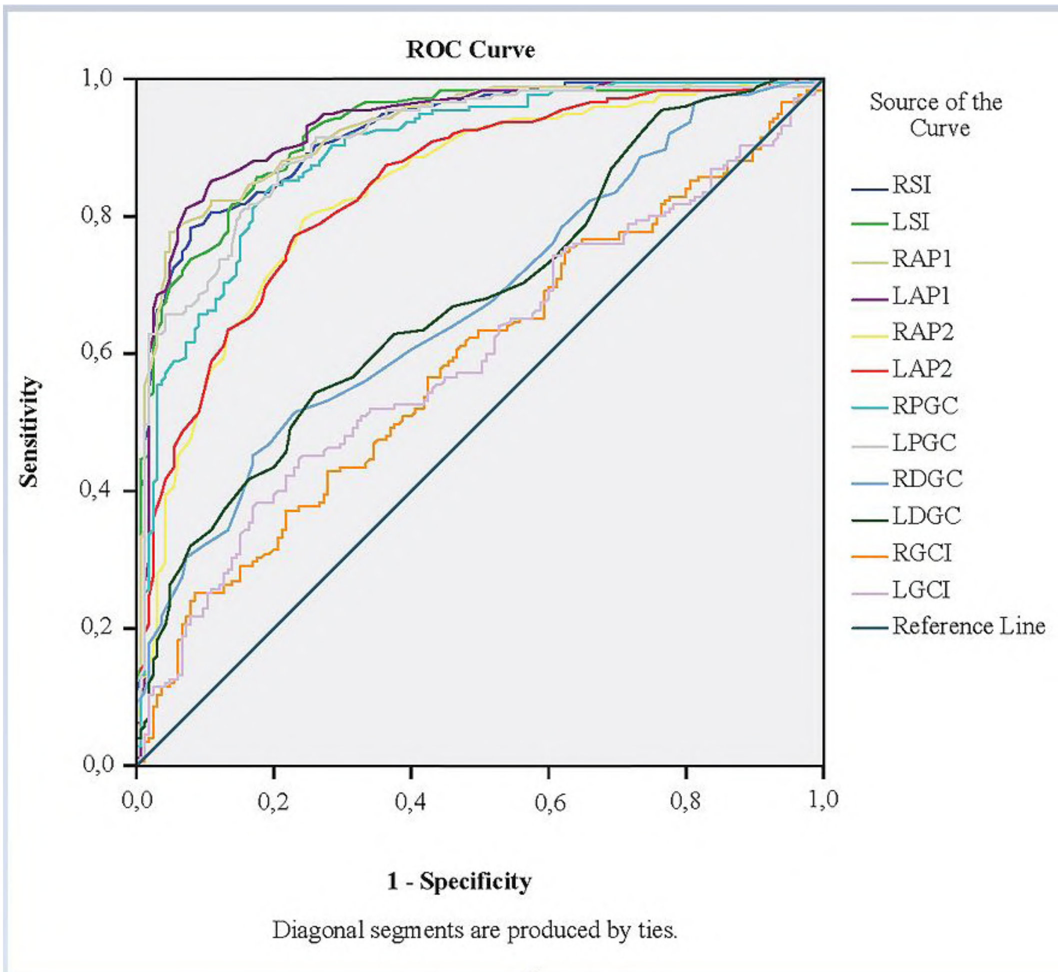

Fig. 4.- Roc curve.

Table 4. ROC's analysis

Parameters	AREA	p	Cutt off (mm)	Sensitivity (%)	Specifity (%)
RSI	0.921	0.000	39	83.4	82.4
LSI	0.922	0.000	38.6	83.4	83.6
RAP1	0.926	0.000	26.2	83.4	84.2
LAP1	0.931	0.000	26.1	86.9	84.8
RAP2	0.837	0.000	19.3	76	77
LAP2	0.843	0.000	18.7	77.1	77
RPGC	0.892	0.000	112.2	81.7	82.4
LPGC	0.908	0.000	112.4	81.7	82.4
RDGC	0.671	0.000	4.1	60.6	0.6
LDGC	0.678	0.000	3.9	62.9	62.4
RGCI	0.585	0.007	67.67	56.6	56.4
LGCI	0.595	0.002	67.54	56.6	55.2

GC: Glenoid cavity, **RSI:** Right-GC length, **LSI:** Left-GC length, **RAP1:** Right- GC width, **LAP1:** Left- GC width, **RAP2:** Right- GC width at notch level, **LAP2:** Left- GC width at notch level, **RPGC:** Right- GC circumference, **LPGC:** Left- GC circumference, **RDGC:** Right- GC depth, **LDGC:** Left- GC depth, RGCI: Right- GC index, **LGCI:** Left- GC index

DISCUSSION

Evaluation of the morphometry of the glenoid cavity plays a key role in different pathological conditions such as Bankart lesion, rotator cuff disease, osteochondral defect. Various researchers have performed the morphometric analysis of the glenoid cavity in different populations (Coskun et al., 2006; Mamatha et al., 2011; Hassanein, 2015; Akhtar, 2016; Singh et al., 2019; Khan et al., 2020). This study is a radiological study, and measurements were performed through multidetector CT. The data obtained was compared with the literature findings. We believe that our study may provide a great contribution to the literature since there are right and left side findings as well as gender data.

SI appears to be greater on the right side than left side; however, this finding does not have any statistical significance. Although our data are similar to results obtained by El-din and Ali (2015) Chhabra et al. (2015) and Vaishnani et al. (2018), these data are longer than results of other researchers. Furthermore, SI was greater in males when compared with females in our study. We believe that the possible cause is greater bone mass quantity of male individuals. Gender-dependent SI data is greater than the data obtained by all previous researchers. SI values on females detected in our study are similar to those obtained on female individuals by Polguj et al. (2013)

In this study, AP1 was found greater on the right side than on the left. The AP1 values on the right obtained by Merill et al. (2009) and Shi et al. (2013), and the left obtained by Aigbogun et al. (2017) were similar to our data; however, data obtained by El-din and Ali (2015) was greater than our data. AP1 values were detected 28.60 ± 2.30 mm in males, and 24.40 ± 2.0 mm in females in our study. Merill et al. (2009) detected similar AP1 values to our study in males. Von Schroeder et al. (2001) Mathews et al. (2017) and Jia et al. (2020) detected greater values whereas results of other researchers are lower (Table 5).

AP2 value measurements were found greater on the right side than the left side. Findings of Chhabra et al. (2015) are close to our results; however, findings of El-din and Ali (2015) are greater. The AP2 value (17.40 ± 2.60 mm) in women reported by Khan et al (2020) and the AP2 value (17.80 ± 1.70 mm) in women in our study were similar. Merill et al. (2009) and Shewales et al. (2017) detected lower gender-based findings than our data (Table 5).

Merill et al. (2009) reported DGC 4.54 ± 0.06 mm in males, and 3.78 ± 0.07 mm in females. In our study, it was found 4.50 ± 1.20 mm in males, and 3.80 ± 0.90 mm in females. Our results are consistent with results obtained by Merill et al. (2009). The difference between male and female DGC may be important for prosthesis designers. Furthermore, DGC was detected 4.20 ± 1.10 mm on the right, and 4.0 ± 1.10 mm on the left on all scapulae; believe that these data would contribute to further studies (Table 5).

Macaluso et al. (2011) measured PGC values as 103.04 ± 5.38 mm in men and 91.13 ± 4.73 mm in women in South Africa Shi et al. (2013) found it to be 97.31 ± 8.43 mm on the right and 97.12 ± 8.83 mm on the left in their study in China. In our study, PGC was found as 112.9 ± 10.9 mm in the right, 111.9 ± 11.6 mm in the left, 119.3 ± 9.90 mm in men and 105.5 ± 7.70 mm in women. Our data were found longer than Macaluso et al. (2011) and Shi et al. (2013) (Table 5). We think this is due to racial difference.

Table 5. Comparison of GC parameters with different researchers

Observers	Method	n	SI (MEAN ± SD)	AP1 (MEAN ± SD)	AP2 (MEAN ± SD)	DGC (MEAN ±SD)	PGC (MEAN ± SD)	GCI (MEAN ± SD)
Von Schroeder et al.(2001)	C	(Mn/Fn) (14/12)	38.0±3.30/33.60±1.70	30.90±3.10/25.80±0.90	-	-	-	-
		(Rn/Ln)	-	-	-	-	-	-
Ozer et al. (2006)	DS	(Mn/Fn) (94/92)	38.71±2.71/33.79±3.08	27.33±2.40/22.72±1.72	-	-	-	-
		(Rn/Ln)	-	-	-	-	-	-
Merrill et al. (2019)	DS	(Mn/Fn) (184/184)	37.01±0.18/33.83±0.18	28.56±0.17/23.67±0.17	17.58±0.16/15.85±0.17	4.54±0.06/3.78±0.07	-	-
		(Rn/Ln) (184/184)	35.21±0.12/35.63±0.12	25.94±0.11/26.29±0.11	-	-	-	-
Mamatha et al. (2011)	DS	(Mn/Fn)	-	-	-	-	-	-
		(Rn/Ln) (98/104)	33.67±2.82/33.92±2.87	23.35±2.04/23.05±2.30	-	-	-	-
Macaluso (2011)	DS	(Mn/Fn) (60/60)	38.21±1.90/33.87±1.92	27.02±1.82/23.59±1.45	-	-	103.04±5.38/91.13±4.73	-
		(Rn/Ln)	-	-	-	-	-	-
Rajput et al. (2012)	DS	(Mn/Fn)	-	-	-	-	-	-
		(Rn/Ln) (43/57)	34.76±3.0/34.43±3.21	23.30±3.0/22.92±2.80	15.10±2.54/13.83±2.45	-	-	-
Kavita and Singh (2013)	DS	(Mn/Fn)	-	-	-	-	-	-
		(Rn/Ln) (67/62)	35.20±3.0/34.70±2.80	25.07±2.70/24.90±2.0	16.80±1.8/16.30±2.0	-	-	-
Shi et al. (2013)	CT	(Mn/Fn)	-	-	-	-	-	-
		(Rn/Ln) (60/60)	34.74±3.21/34.90±3.26	27.08±2.65/26.97±2.58	-	-	97.31±8.43/97.12±8.83	-
Polguj et al. (2013)	DS	(Mn/Fn) (41/33)	40.04±2.97/36.09±2.20	29.14±2.14/25.65±1.98	-	-	-	71.88±5.77/72.98±5.34
		(Rn/Ln)	-	-	-	-	-	-
Dhindsa and Singh (2014)	DS	(Mn/Fn)	-	-	-	-	-	-
		(Rn/Ln) (41/39)	34.13±3.16/34.11±2.57	24.05± 2.86/23.36±2.22	-	-	-	70.37 ± 4.08/68.59 ± 4.36
Patil et al. (2014)	DS	(Mn/Fn)	-	-	-	-	-	-
		(Rn/Ln) (104/120)	33.68±4.32/32.09±4.11	23.29±2.34/24.90±2.95	-	-	-	-
El-Din and Ali (2015)	DS	(Mn/Fn)	-	-	-	-	-	-
		(Rn/Ln) (80/80)	38.88±2.63/39.01±2.49	28.31±2.38/27.99±2.55	21.33±2.49/21.69±2.06		-	-
Hassanein (2015)	DS	(Mn/Fn)	-	-	-	-	-	-
		(Rn/Ln) (38/30)	33.10±3.90/28.70±4.10	24.40±4.40/22.10±4.40	-	-	-	73.67±9.08/76.71±8.37

Gupta et al. (2015)	DS	(Mn/Fn)	-	-	-	-	-	-
		(Rn/Ln) (30/30)	34.90±4.40/33.0±3.30	23.10±3.10/20.60±3.0	-	-	-	-
Chhabra et al. [14]	DS	(Mn/Fn)	-	-	-	-	-	-
		(Rn/Ln) (55/71)	38.46±2.81/39.03±3.18	25.04±2.69/24.85±2.46	18.70±2.22/18.6± 2.07	-	-	65.11±5.11/63.67±3.76
Akhtar et al. (2016)	DS	(Mn/Fn)	-	-	-	-	-	-
		(Rn/Ln) (126/102)	36.03±3.15/35.52±3.12	23.67±2.53/23.59±2.47	16.30±2.16/16.0±2.34	-	-	66.13±8.67/66.73±7.47
Aigbogun et al. (2017)	DS	Mn/Fn)	-	-	-	-	-	-
		(Rn/Ln) (96/104)	37.71±4.24/36.22±3.58	26.20±3.30/24.35±3.64	-	-	-	69.59±5.529/67.11±6.031
Shewela et al. (2017)	DS	(Mn/Fn) (102/40)	35.95±2.30/31.0±2.50	24.60±1.96/20.30±2.25	17.46±2.52/14.8±1.91	-	-	-
		(Rn/Ln)	-	-	-	-	-	-
Mathews et al. (2017)	C	(Mn/Fn) (7/11)	39.50±3.50/34.80±2.20	30.30±3.30/26.20±1.60	-	-	-	-
		(Rn/Ln)	-	-	-	-	-	-
Pai et al. (2018)	DS	Mn/Fn)	-	-	-	-	-	-
		(Rn/Ln) (74/62)	34.81±2.46/33.37±2.96	24.07±2.58/22.75±2.45	15.27±1.92/15.19±2.31	-	-	-
Vaishnani et al. (2018)	DS	Mn/Fn)	-	-	-	-	-	-
		(Rn/Ln) (36/38)	38.49±3.17/38.06±3.34	24.76±2.49/24.23±2.14	18.83±2.19/17.97±2.08	-	-	-
Singh et al. (2019)	DS	Mn/Fn)	-	-	-	-	-	-
		(Rn/Ln) (56/44)	34.84±3.46/33.48±2.88	24.25±2.55/25.52±2.78	13.69±1.54/12.01±1.77	-	-	69.87±1.54/70.44±7.59
Jia et al. (2020)	CT	(Mn/Fn) (55/29)	-	29.09±2.27/25.52±1.72	-	-	-	-
		(Rn/Ln)	-	-	-	-	-	-
Khan et al. (2020)	DS	(Mn/Fn) (68/96)	35.30±3.10/34.60±2.80	24.20±2.70/23.70±2.80	18.20±3.30/17.40±2.60	-	-	-
		(Rn/Ln) (80/84)	35.20±3.10/34.90±3.0	24.50±2.90/23.60±20.60	18.40±3.30/17.50±2.90	-	-	-
Gnanasundaram et al. (2022)	DS (Acrylic mould)	(Mn/Fn)	-	-	-	-	-	-
		(Rn/Ln) (52/54)	31.65±2.32/31.78±2.56	22.91±2.86/22.99±2.48	16.10±2.11/15.69±1.62	-	-	-
Present study	CT	(Mn/Fn) (394/388)	41.60±3.00/36.40±2.40	28.60±2.30/24.40±2.0	20.20±1.80/17.80±1.70	4.50±1.20/3.80±0.90	119.3±9.90/105.5±7.70	68.82±5.77/67.20±4.70
		(Rn/Ln) (391/391)	39.20±3.80/38.80±3.70	26.60±3.10/26.40±2.90	19.20±2.20/18.80±2.10	4.20±1.10/4.0±1.10	112.9±10.9/111.9±11.6	67.91±5.08/68.13±5.56

C: Cadaver, **DS**: Dry Scapula, **CT**: Computer Tomography, **SD**: Standard deviation, (mm). $\mathbf{R_n}$**:** Right, $\mathbf{L_n}$**:** Left, $\mathbf{M_n}$**:** Male, $\mathbf{F_n}$**:** Female.

Table 6. Comparison of notch and non-notch GC values with different researchers

Observers	Population	n	Notch (%)	Non-notch (%)
Prescher ve Klümpen (1997)	Germany	n_T: 236	55	45
Mamatha et al. (2011)	India	Rn: 98	80	20
		Ln: 104	76	24
Rajput et al. (2012)	India	Rn: 43	84	16
		Ln: 57	85	15
Patil et al. (2014)	India	Rn: 104	81.74	18.27
		Ln: 120	77.5	22.5
Hassanein (2015)	Egypt	Rn: 38	76.32	23.68
		Ln: 30	76.67	23.33
Present study	Turkey	Rn: 391	87	13
		Ln: 391	87.5	12.5

R_n: Right, **L_n:** Left, **n_T:** Total.

Polguj et al. (2013) detected male and female GCI values (71.88 ± 5.77 and 72.98 ± 5.34, respectively) higher than our data. Right and left GCI values detected in our study are greater than Chhabra et al. (2015) and Akhtar et al. (2016) and lower than values found by Dhindsa and Singh (2014), Hassanein (2015) and Singh et al. (2019) (Table 5).

Since GC has a variable morphology, anatomy is important for surgeons and prosthesis designers. The notch on antero-superior part of the GC affects the morphology of the glenoid labrum. Anatomic variations of the GC is also important for different pathologies including the shoulder joint (Yang et al., 2018). Previous studies on the notch of the GC in the literature, and data obtained were provided in Table 6. In the study, notch was detected on the right side by 87%, no notch was detected on the right side by 13%; and notch was detected on the left side by 87.5%, and no notch was detected on the left side by 12.5%. We believe that higher values of our study than all other researches may be associated with race differences. The closest values to our findings are obtained by Rajput et al. (2012). Prescher and Klümpen (1997) stated about the cause of such difference as loose attachment of the glenoid labrum onto the GC at notch area. In the absence of the glenoid notch, the glenoid labrum is attached along GC margins; therefore, the shoulder joint is more stable (Coskun et al., 2006; Khan et al., 2020). We reviewed GCs with notch according to the notch count. We detected that GC had no notch by 12.8%, one notch by 82.2%, and two notches by 5% (Table 6). Number of the notches was also reviewed by Prescher and Klümpen (1997); rates of GC with no notch (35%) and two notches (30%) were higher than our findings; however, the rate of GC with one notch (35%) was lower.

The pear GC type was detected by 53.2%, inverted comma type was detected by 28.4%, and oval type was detected by 18.4%. Prescher and Klümpen (1997) detected the most common types as pear (55%) and inverted comma types in German population. Similar to our study, the most common GC type was found as the pear type by Kavita and Singh (2013) by 58%, by Akhtar et al. (2016) by 50.44%, by Singh et al. (2019) in Indian population, by Hassanein (2015) by 45.59% in Egyptian population. Among all studies conducted on this topic, El-Din and Ali (2015) found the most common type as the oval type (50.63%) in Egyptian population (Table 7).

The present study has some limitations. The first limitation is that interobserver variability was not used in the study. Measurements were performed by a single researcher. This disadvantage can be overcome by repeating the measurements by more than one investigator. Secondly, 391 samples could be included in the study because the study was conducted on a limited geography. Although we think that it is sufficient for this study, this number can be increased in future studies and it can be planned in a wider geography. Third,

Table 7. Comparison of glenoid cavity typing with different researchers

Observers	Populations	Method	Pear Shaped (%)	Inverted Comma Shaped (%)	Oval Shaped (%)
Prescher and Klümpen (1997)	Germany	DS	55		45
Kavita et al. (2013)	India	DS	58	11	30
El-Din and Ali (2015)	Egypt	DS	31.25	18.12	50.63
Gupta et al. (2015)	India	DS	42	38	20
Hassanein (2015)	Egypt	DS	45.59	30.88	23.53
Akhtar et al. (2016)	India	DS	50.44	35.96	13.60
Pai et al. (2018)	India	DS	62.5	15.4	22.1
Singh et al. (2019)	India	DS	44	22	34
Das et al. (2020)	India	DS	43.46	33.96	22.64
Presents study	Turkey	CT	53.2	28.4	18.4

DS: Dry Scapula, **CT**: Computer Tomography.

because the study was planned retrospectively, a specific age group could not be established among the obtained data. Prospective studies to be carried out may eliminate this limitation.

When metric values obtained are compared to the data obtained by other researchers, different results were obtained in studies conducted in different countries and populations. Results obtained in our study would be useful for prosthesis designers in glenoid component designing, and for orthopaedic surgeons for shoulder pathologies and shoulder arthroplasty. In conclusion, we think that taking these values into account can help design glenoid components for the Turkish population.

Handicaps like the gender uncertainty in dried bone studies, or the limited number of the cases in cadaver studies were not experienced in our study. Different from other studies, AP1 and SI values were detected as important measurements for gender determination (Table 4). Therefore, data obtained would contribute to the literature for gender and number. Since the method used in our study ensured reliable data evaluation visually, cases with abnormal anatomic structures that show osteophytes and surface roughness were easily detected and excluded from the study. However, such deformations constitute a limitation in studies conducted on dried bones; this was minimized in our study. Therefore, the data obtained would ensure reliable measurements for healthy individuals.

REFERENCES

AIGBOGUN EO, OLADIPO GS, OYAKHIREE MO, IBEACHU CP (2017) Morphometry of the glenoid cavity and its correlation with selected geometric measurements of the scapula. *Bangladesh J Med Sci,* 16 (4): 572-579.

AKHTAR MJ, KUMAR B, FATIMA N, KUMAR V (2016) Morphometric analysis of glenoid cavity of dry scapulae and its role in shoulder prosthesis. *Int J Res Med Sci,* 4(7): 2770-2776.

CHHABRA N, PRAKASH S, MISHRA B (2015) An anatomical study of glenoid cavity: its importance in shoulder prosthesis. *Int J Anat Res,* 3(3): 1419-1424.

COSKUN N, KARAALI K, CEVIKOL C, DEMIREL BM, SINDEL M (2006) Anatomical basics and variations of the scapula in Turkish adults. *Saudi Med J,* 27(9): 1320-1325.

DAS S, PAUL M, SETT TK (2020) A study of morphological and morphometric analysis of the glenoid fossa. *Int J Anat Res,* 8(2.2): 7476-7480.

DHINDSA GS, SINGH Z (2014) A study of morphology of the glenoid cavity. *J Evol Med Dental Sci,* 3(25): 7036-7044.

EL-DIN WA, ALI MH (2015) A morphometric study of the patterns and variations of the acromion and glenoid cavity of the scapulae in Egyptian Population. *J Clin Diagn Res,* 9(8): 8-11.

GNANASUNDARAM V, RAJILARAJENDRAN H, BALAJI T (2022) A study on the morphometric analysis of glenoid cavity of scapula using a polymerizing acrylic mould. *Eur J Anat,* 26(3): 295-301.

GUPTA S, MAGOTRA R, KOUR M (2015) Morphometric analysis of glenoid fossa of scapula. *J Evol Med Dental Sci*, 4(45): 7761-7767.

HALDER AM, KUHL SG, ZOBITZ ME, LARSON D, AN KN (2001) Effects of the glenoid labrum and glenohumeral abduction on stability of the shoulder joint through concavity-compression: an in vitro study. *J Bone Joint Surg,* 83(7): 1062-1069.

HASSANEIN GHE (2015) Morphometry of glenoid fossa in adult Egyptian scapulae. *Int J Anat Res,* 3(2): 1138-1142.

JIA Y, HE N, LIU J, ZHANG G, ZHOU J, WU D, WEI B, YUN X (2020) Morphometric analysis of the coracoid process and glenoid width: a 3D-CT study. *J Orthop Surg Res,* 15(1): 69.

KAVITA P, SINGH J (2013) Morphology of coracoid process and glenoid cavity in adult human scapulae. *Int J Analyt Pharmac Biomed Sci,* 2(2): 62-65.

KHAN R, SATYAPAL KS, LAZARUS L, NAIDOO N (2020) An anthropometric evaluation of the scapula, with emphasis on the coracoid process and glenoid fossa in a South African population. *Heliyon*, 6(1): 1-6.

LIPPITT SB, VANDERHOOFT JE, HARRIS SL, SIDLES JA, HARRYMAN DT II, MATSEN FA 3RD (1993) Glenohumeral stability from concavity-compression: a quantitative analysis. *J Shoulder Elbow Surg,* 2(1): 27-35.

LO IK, PARTEN PM, BURKHART SS (2004) The inverted pear glenoid: an indicator of significant glenoid bone loss. *Arthroscopy: J Arthrosc Rel Surg,* 20(2): 169-174.

MACALUSO PJ (2011) Sex discrimination from the glenoid cavity in black South Africans: morphometric analysis of digital photographs. *Int J Legal Med,* 125(6): 773-778.

MAMATHA T, PAI SR, MURLIMANJU BV, KALTHUR SG, PAI MM, KUMAR B (2011) Morphometry of glenoid cavity. *Online J Health Allied Sci,* 10(3): 1-4.

MATHEWS S, BURKHARD M, SERRANO N, LINK K, HÄUSLER M, FRATER N, FRANKE I, BISCHOFBERGER H, BUCK FM, GASCHO D, THALI M, SEROWY S, MÜLLER-GERBL M, HARPER G, QURESHI F, BÖNI T, BLOCH H-R, ULLRICH O, RÜHLI F-J, EPPLER E (2017) Glenoid morphology in light of anatomical and reverse total shoulder arthroplasty: a dissection-and 3D-CT-based study in male and female body donors. *BMC Musculoskelet Disord,* 18(1): 9.

MERRILL A, GUZMAN K, MILLER SL (2009) Gender differences in glenoid anatomy: an anatomic study. *Surg Radiol Anat,* 31(3): 183-189.

OZER I, KATAYAMA K, SAHGIR M, GÜLEÇ E (2006) Sex determination using the scapula in medieval skeletons from East Anatolia. *Collegium Antropolog,* 30(2): 415-419.

PAGNANI MJ, WARREN RF (1994) Stabilizers of the glenohumeral joint. *J Shoulder Elbow Surg*, 3(3): 173-190.

PAI DN, MARTIN L, CHAITRA D (2018) A morphometric study on glenoid-cavity of South Indian population. *CIBTech J Surg,* 7(3): 1-5.

PATIL GV, KOLAGI SI, RAMDURG U (2014) Morphometrical study of scapular glenoid cavities. *Global J Med Res: Orthoped Musculoskelet System*, 14(2): 5-10.

POLGUJ M, JĘDRZEJEWSKI KS, TOPOL M (2013) Sexual dimorphism of the suprascapular notch-morphometric study. *Archiv Med Sci,* 9(1): 177-183.

PRESCHER A, KLÜMPEN T (1997) The glenoid notch and its relation to the shape of the glenoid cavity of the scapula. *J Anat,* 190(3): 457-460.

RAJPUT HB, VYAS KK, SHROFF BD (2012) A study of morphological patterns of glenoid cavity of scapula. *Nat J Integr Res Med,* 2(4): 504-507.

SHEWALE SN, LAEEQUE M, SUKRE SB, PATIL SC (2017) Morphometric study of glenoid cavities of scapulae in Marathwada population. *Int J Anat Res,* 5(2.1): 3759-3765.

SHI L, GRIFFITH JF, HUANG J, WANG D (2013) Excellent side-to-side symmetry in glenoid size and shape. *Skeletal Radiol*, 42(12): 1711-1715.

SINGH A, SINGH A, AGARWAL P, GUPTA R (2019) A morphological and morphometric study of glenoid fossa of scapula and its implication in shoulder arthroplasty. *Int J Anat Radiol Surg,* 8(3): 6-9.

THOMPSON JM, CARRİNO JA, SKOLASKY RL, CHHABRA A, FAYAD LM, MACHADO A 2ND, SOLDATOS T, MORRİSON WB, MCFARLAND EG (2015) Glenoid notch MRI findings do not predict normal variants of the anterior and superior labrum. *Clin Radiol*, 70(8): e90-96.

VAISHNANI H, JETHVA K, RATHWA A, SHARMA P (2018) Morphometry and morphology of glenoid cavity of scapula. *Int J Anat Res,* 6(1.1): 4798-4802.

VON SCHROEDER HP, KUIPER SD, BOTTE MJ (2001) Osseous anatomy of the scapula. *Clin Orthop Rel Res,* 383: 131-139.

YANG Y, ZUO J, LIU T, SHAO P, WU H, GAO Z, XIAO J (2018) Glenoid morphology and the safe zone for protecting the suprascapular nerve during baseplate fixation in reverse shoulder arthroplasty. *Int Orthop,* 42(3): 587-593.

ORIGINAL ARTICLE

Eur J Anat, 27 (6): 741-758 (2023)

Logistic regression analysis of sex-related morphological and dimensional variations of maxillary bone: a cone-beam computed tomography-based retrospective study

Santiago Palacio-Gutiérrez[1], Sara Morales-Galeano[1], Jorge L. Obando-Castillo[2], Clara I. Saldarriaga-Naranjo[3], Sergio I. Tobón-Arroyave[1]

[1] Graduate Oral and Maxillofacial Surgery Program, Faculty of Dentistry, University of Antioquia. Medellín, Colombia

[2] Department of Radiology, Cooperative University of Colombia, San Juan de Pasto, Colombia

[3] Department of Radiology, CES University and RADEX 3D Specialized Radiology Center. Medellín, Colombia

SUMMARY

This study aimed to determine, using a retrospective cone beam computed tomography (CBCT) assessment and a logistic regression analysis, which variations of the maxillary structures of interest in surgical, forensic, and anthropological practices might be linked to the sex trait in a representative sample of Colombian adults with different age and alveolar process status categories. A total of 208 CBCT scans obtained from 83 males and 125 females were evaluated. The protocol included the assessment of 40 parameters, of which 25 were bilateral and 15 were unique. The strength of association between the study variables and the sex of the individuals was examined individually and adjusted for confounding using univariate and multivariate binary logistic regression models. Although the age and alveolar process status had a confounding influence on the results, posterior maxillary region-related variables including maxillary sinus, infraorbital foramen, and greater palatine canal dimensions, but also anterior maxilla/upper middle line-related variables comprising nasopalatine canal length, anterior buccal bone thickness, and incisive foramen diameter, revealed higher values in males and remained strongly and independently associated with the male sex after adjusting for confounders. It was concluded that the maxillary bone can present several morphological variations, as well as dimensional differences that may be strongly liaised to sex, but are independent of age, side, and the state of the alveolar process of the population observed. Even so, both aging and alveolar process status should be considered when applying the anatomical variation data to the needs of the particular case.

Key words: Anatomy – Cone beam computed tomography – Maxillary bone – Retrospective studies – Sex characteristics

Corresponding author:
Sergio Iván Tobón-Arroyave, Laboratory of Immunodetection and Bioanalysis, Faculty of Dentistry, University of Antioquia, Calle 70 N° 52-21, Medellín, Colombia. Phone: (604) 2196735. E-mail: stobonarroyave@gmail.com / sergio.tobon@udea.edu.co

Submitted: March 11, 2023. **Accepted:** June 16, 2023

https://doi.org/10.52083/WQSJ7197

INTRODUCTION

Accurate knowledge of the anatomical characteristics and their variants is important for the timely diagnosis and successful treatment of the alterations of the maxillofacial region, as it allows the preservation of the integrity of morphological features and the minimization of risk of complications such as neurosensitive disorders, disruption of the cortical bone, hemorrhagic accidents, as well as nasal/sinus perforations related with improper or unsafe procedures and/or misdiagnosis (Güncü et al., 2011). For this purpose, although two-dimensional imaging methods including intra- and extra-oral radiographs have been commonly used, problems such as the overlapping, radiographic noise, magnification, and geometric distortion might make them insufficient for the detection of anatomical variants (Hakbilen and Magat, 2018) when performing oral and maxillofacial surgical interventions, thus leading to a deficient assessment and a possible iatrogenic injury. In contrast, three-dimensional methods, such as cone beam computed tomography (CBCT), allow the detailed evaluation of the configuration and exact location of the anatomical structures in the maxillofacial region (Genç et al., 2018; Hakbilen and Magat, 2018).

Compelling evidence has addressed the ability of CBCT images to characterize the alveolar process morphology (Canger and Celenk, 2012; Hakbilen and Magat, 2018; Manzanera et al., 2018) and to determine the variations in the morphological and morphometric characteristics of the maxillary sinus (MS) and accompanying anatomical structures (Genç et al., 2018; Güncü et al., 2011; Kanthem et al., 2015; Khojastehpour et al., 2016; Sahlstrand-Johnson et al., 2011; Talo Yildirim et al., 2017), infraorbital foramen (IOF) and accessory infraorbital foramen (AIOF) (Ali et al., 2018; Bahşi et al., 2019a; Dagistan et al., 2017; Martins-Júnior et al., 2017; Nanayakkara et al., 2016; Polo et al., 2019), greater palatine canal (GPC) and greater palatine foramen (GPF) (Aoun et al., 2015; Bahşi et al., 2019b; Ikuta et al., 2013; Rapado- González et al., 2015), nasopalatine canal (NPC) (Bahşi et al., 2019c; Hakbilen and Magat, 2018; Jayasinghe et al., 2020; Khojastepour et al., 2017), midpalatal suture (MPS) (Angelieri et al., 2013; Angelieri et al., 2015; Angelieri et al., 2017; Reis et al., 2020), as well as to detect incidental findings (Lopes et al., 2017; Price et al., 2012) particularly important in the surgical planning process. In spite of the acknowledged advantages of CBCT in the evaluation of these structures, all the studies available so far have only examined the effect of individual variables on their anatomical characteristics, concluding that certain parameters, including age (Genç et al., 2018; Hakbilen and Magat, 2018; Khojastepour et al., 2017), sex (Aoun et al., 2015; Bahşi et al., 2019a; Ikuta et al., 2013; Kanthem et al., 2015; Rapado-González et al., 2015; Sahlstrand- Johnson et al., 2011), and alveolar process status (Canger and Celenk, 2012; Hakbilen and Magat, 2018; Rapado-González et al., 2015), may significantly modify the morphology and dimensions of mature maxilla. Notwithstanding, research data in this field have not only been inconsistent, but also have not provided information concerning those covariables that could influence the variations as potential confounders, so that it is not possible to draw firm conclusions.

Given that the dimensional and morphological characteristics of the maxillary bone are highly variable among populations and even within the same individual, this study aimed to comprehensively determine, through a CBCT analysis, which variations of the maxillary structures of interest in the surgical, forensic, and anthropological practices could be linked to the sexual trait in a representative sample of Colombian adults with different age and alveolar process status categories.

MATERIALS AND METHODS

Study design and setting

This cross-sectional observational study was approved by the Institutional Ethics Committee for Human Studies of the University of Antioquia (Concept Number 62-2020), and was conducted following the ethical guidelines of the Helsinki Declaration on CBCT scans of patients attending a private imaging specialized center (RADEX 3D Specialized Radiology Center) in Medellín, Colombia. The sample size was calculated on the basis of patientpopulation referred for radiological examination, with a range of indications such as dental implants, endodontic procedures, orthodontics, oral diseases, and oral or periodontal surgery between January 2020 and April of 2021. Considering a total of 358 referred patients for maxillary CBCT scans, the sample size calculation using a web-based program (Raosoft® Inc., Seattle, WA, USA) indicated a sample size requirement of at least 186 digital imaging and communications of medicine (DICOM) files to identify significant variations in the bivariate comparisons with a 95% confidence level and an alpha value of 5%. However, to improve the statistical power, the study sample was increased by 22 DICOM files, which resulted in the definite inclusion of 208 maxillary scans. The inclusion criteria were patients aged over or equal to 18 years and with absence of pathological changes or traumatic and congenital deformities in the maxillary bone. On the contrary, the exclusion criteria were the low quality of CBCT images, limited field of view hindering the visualization of the full maxillary anatomy, as well as evidence of ongoing orthodontic treatment or maxillofacial surgery. Appropriate informed consent was taken from the patients to use the images for research purposes before performing CBCT scans.

Image acquisition and evaluation

CBCT images were obtained with the i-CAT® 17-19 system (Imaging Sciences International, Inc., Hatfield, Pennsylvania, USA) operated at 120 kVp, 37.07 mA, 26.9 seconds of exposure time, 16 cm x 13 cm of field vision, and 0.25 mm voxel size. All of CBCT scans were acquired using the Frankfort horizontal and the midfacial planes as references in order to prevent measurement bias induced by head position during image recording. The images were simultaneously analyzed, using the i-CATVision 1.9® software (Imaging Sciences International), by two Oral and Maxillofacial Surgeons (S. P-G. and S. M-G.) standardized by two qualified Maxillofacial Radiologists (C.I. S-N. and J.L O-C). The standardization was conducted through written guidelines and illustrative images of the different morphological changes and morphometric parameters to be evaluated. When discrepant information was reported between the two examiners, new assessments were conducted and further disagreements were arbitrated by a third researcher. All evaluations were performed on a computer screen under ideal light conditions, using the magnification function of the software to enlarge the images and the maximum intensity projection mode to achieve superior image performance.

Evaluated parameters in the analysis

Patient-related demographic parameters gathered from the study sample included information about sex (i.e., *male vs female*), age at the time of CBCT imaging, maxillary segment (i.e., *right posterior*, *left posterior*, or *anterior maxilla*), and the alveolar process status (i.e., *non-atrophic*, fully dentate *vs atrophic/partially-atrophic,* with totally edentulous maxillary segments or at least one extracted tooth, except third molars) (Talo Yildirim et al., 2017). Using multiplanar reconstructions, maxillary anatomical structures were analyzed separately on both sides of the posterior maxillary region and on the anterior maxilla/upper middle line as described below:

- The assessment of MS and their related anatomical structures included the measurement of maximum craniocaudal (height), anteroposterior (depth), and transversal (width) dimensions (Fig. 1a-c) (Kanthem et al., 2015). The maximum MS height was measured on coronal views as the distance between the uppermost point of the roof and the lowermost point of the floor, whereas the depth and width were measured on axial views estimating the distances among the most anterior and posterior walls and among the outermost and medial point of the MS, respectively. Then, the minimum perpendicular distance from the sinus floor to the alveolar crest (AC) was determined (Figs. 1d and e) taking as landmark the deepest point of the sinus floor within the alveolar process as observed in the panoramic and coronal cuts.
- Other parameters included in the data set were the presence/absence of antral septa (Fig. 1f and g), identified as walls of cortical bone with a minimal expansion of 2 mm in any of the orthogonal views within the MS (Hungerbühler et al., 2019); and the detec-

tion of the posterior superior alveolar artery canal (PSAAC), its greater diameter, as well as its distance to the alveolar crest (Fig. 1h-k) measured as a vertical line in the upper second molar region (Elian et al., 2005; Güncü et al., 2011; Khojastehpour et al., 2016). This PSAAC was identified as a well-defined, corticated, circular hypodensity or C-shaped curve of the lateral sinus wall and registered as *non-detected vs present* (including the intraosseous, below the membrane, or on the outer cortex presentations).

- With the purpose of analyzing the infraorbital region, the greater diameter of IOF in the three orthogonal planes, the vertical distance from the IOF to the AC (Bahşi et al., 2019a; Dagistan et al., 2017; Nanayakkara et al., 2016) (Fig. 2a-c), as well as the presence/absence of the canalis sinuosus (von Arx et al., 2013) (Csin, Fig. 2b and c) and of the AIOF (Ali et al., 2018) (Fig. 2d-f) in the anterior wall of MS were also included in the analysis.
- The morphometric evaluation of the GPC and the GPF included the measurement of the length of the GPC in the sagittal plane from the central point of the pterygopalatine fossa (PPF, superior aspect) to the central point of the GPF (inferior aspect) following established criteria (Tomaszewska et al., 2015) with modifications. The length of GPC was obtained in millimeters, considering the sum of the length of two lines intersecting in the center of the canal (Fig. 3a). Furthermore, the maximum anteroposterior diameter of the GPC in the axial plane and its distance in relation to the posterior nasal spine (PNS), the NPC, and the pterygoid hamulus (Bahşi et al., 2019b; Rapado-González et al., 2015) were measured with the sagittal palatal plane positioned through the center of the supero-inferior dimension of the hard palate (Fig. 3b). Also, for each GPF, several observations were made using axial or coronal reconstructions: *(1)* perpendicular distance from the medial wall of GPF to the midline maxillary suture (MMS, Fig. 3c) (Bahşi et al., 2019b, Ikuta et al., 2013); *(2)* perpendicular distance from the center of GPF opening to the AC (Fig. 3c); *(3)* the angle between the horizontal plane of the palatine bone and the vertical axis of the GPC measured in the coronal view (Fig. 3d); *(4)* the localization of the GPF with respect to the posterior margin of the palatine bone

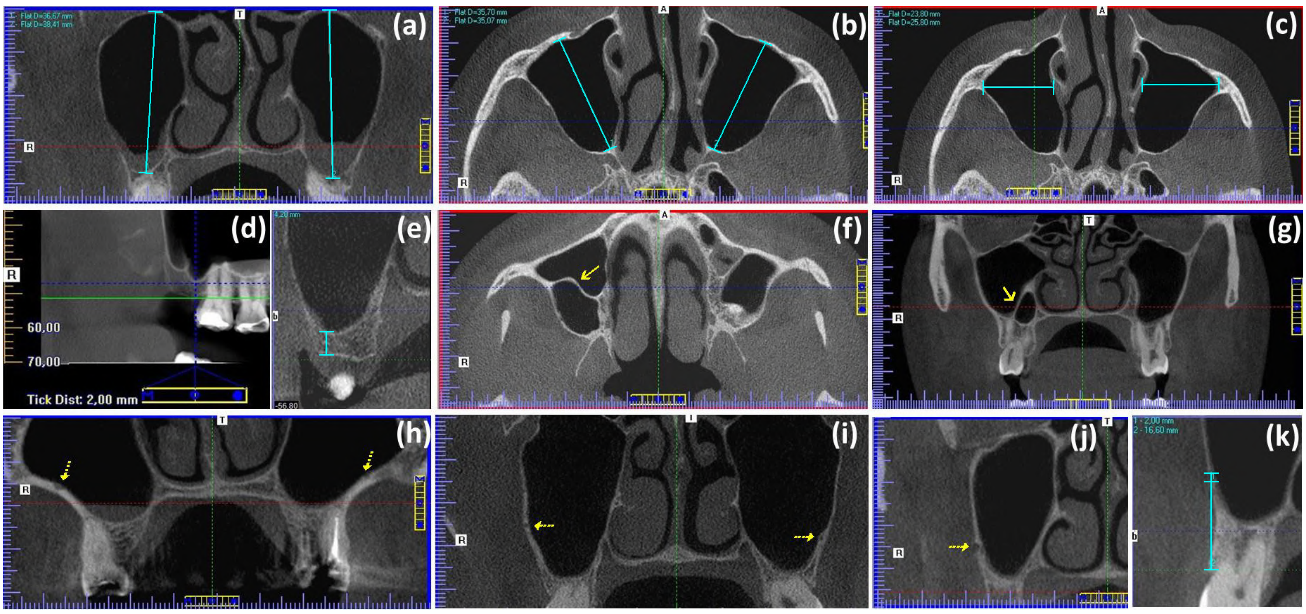

Fig. 1.- Representative CBCT scans of MS and accompanying anatomical structures. Images (a) to (e) illustrate the method of measurement (green lines) of some variables as follows: (**a**) maximum craniocaudal (height), (**b**) maximum anteroposterior (depth), and (**c**) maximum transversal (width); (**d** and **e**) minimum perpendicular distance from the sinus floor to the alveolar crest. (**f**) Axial and (**g**) coronal views demonstrating the presence of antral septa (solid arrows). Images (h) to (k) depict the anatomical location of the PSAA canal as detected through coronal sections (dotted arrows): (**h**) below the membrane, (**i**) intraosseous, and (**j**) on the outer cortex. (**i**) Measurement of the diameter of and the distance from the PSAA canal to the alveolar crest (green lines).

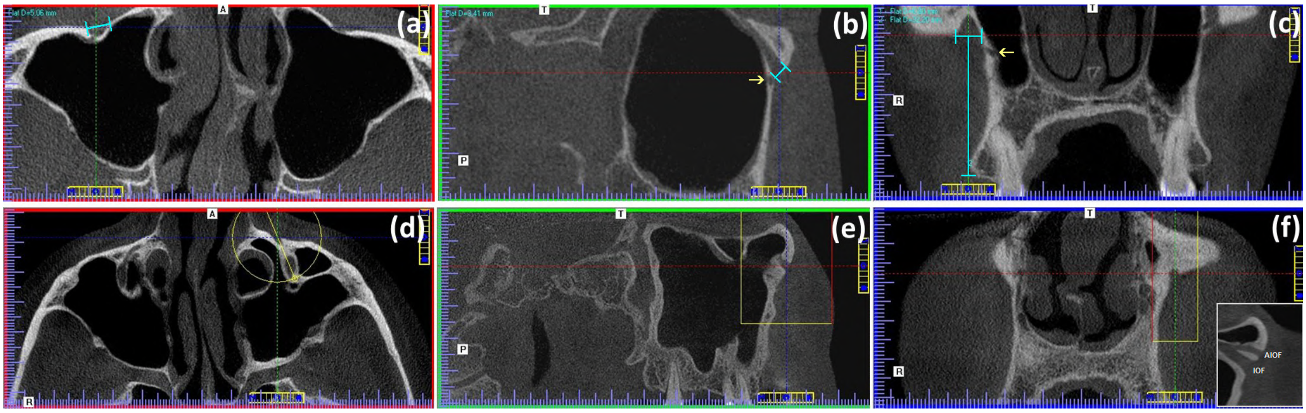

Fig. 2.- CBCT scans of the infraorbital region showing: (**a**) the greater transverse (axial) diameter of IOF, (**b**) the greater sagittal diameter of IOF and the CSin (solid arrow) within the anterior wall of the MS, and (**c**) the greater coronal diameter of IOF, the CSin (solid arrow), and the vertical distance to the crest of the alveolar bone from the mid-point of the IOF. The lower row shows the (**d**) axial, (**e**) sagittal, and (**f**) coronal sections used to view additional cut planes in order to explore the canal leading to the AIOF (inset).

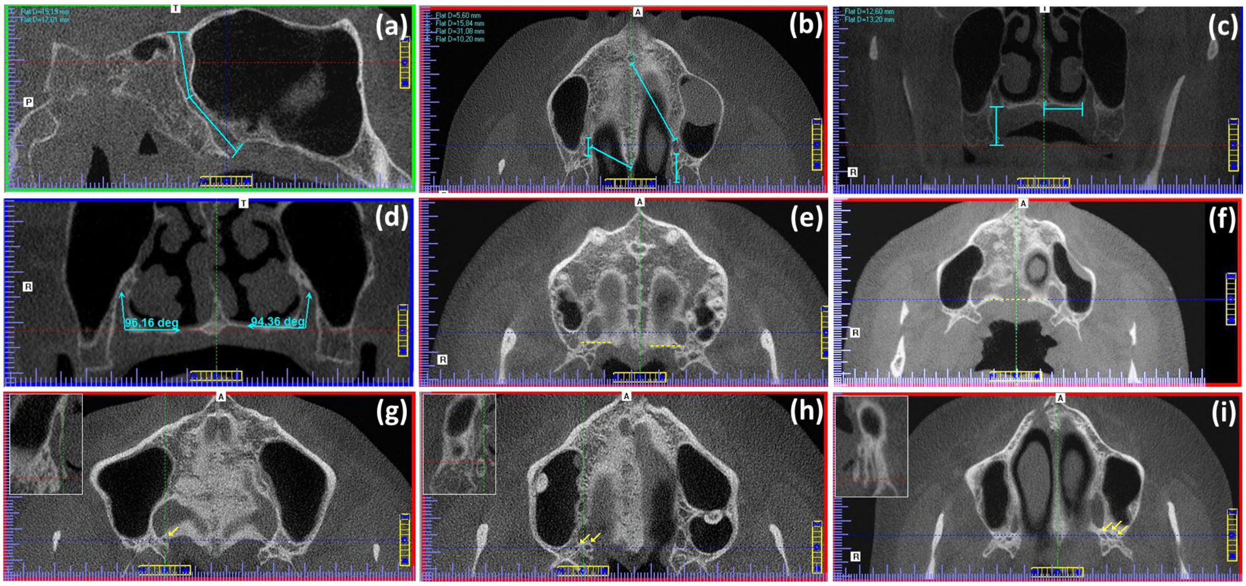

Fig. 3.- Landmarks selected to determine the position and dimensions of the GPC and the GPF in different tomographic planes. The green lines illustrate the path by which the measurements were obtained: (**a**) length of GPC in the sagittal plane; (**b**) maximum anteroposterior diameter of the GPC in the axial plane and its distance regarding the posterior nasal spine, NPC, and the pterygoid hamulus; (**c**) distance between the medial wall of GPF and the MMS and distance from the center of GPF to the alveolar crest; (**d**) angle between the horizontal plane of the palatine bone and the vertical axis of the GPC; localization anterior (**e**) and on the same line (**f**) of the GPF with reference to a tangent line to the posterior margin of the palatine bone (dashed yellow lines); (**g-i**) axial sections showing one, two, and three openings of LPF (solid yellow arrows), respectively (insets: coronal views used to determine the trajectory of the corresponding lesser palatine canals).

(i.e., *anterior vs on the same line*, Fig. 3e and f); and *(5)* the number of the lesser palatine foramina (LPF, i.e., *one vs two or more*, Fig. 3g-i) (Bahşi et al., 2019b; Gibelli et al., 2017).

- Several anatomical landmarks were assessed on the maxillary midline. In the sagittal plane, the shape of NPC was classified according to earlier descriptions (Bahşi et al., 2019c; Hakbilen and Magat, 2018; Jayasinghe et al., 2020) in several groups including *hourglass- shaped*, *cone-shaped*, *funnel-shaped*, *cylindrical*, *banana-shaped,* and *branched* (Fig. 4a-f). In addition, the form of NPC was classified in the coronal plane in three groups: *Y-shaped*, *single canal*, and *double canal* (Fig. 4g-i), whereas in the axial plane (Fig. 4o and p), the shape (i.e., *round-*, *oval-*, *triangle-*, *heart-*, or *kidney-shaped*) and number of openings (i.e., *one vs two or more*) of NPC at the mid-level, nasopalatine foramen (NPF), and incisive foramen (IF) were examined according to defined criteria

(Bahşi et al., 2019c). Alternatively, some quantitative parameters were calculated on the maxillary midline, including the anteroposterior diameters of NPF and IF, the length of NPC (Fig. 4q), measured as the distance between the midpoints of NPF and IF (Bahşi et al., 2019c, Bornstein et al., 2011; Hakbilen and Magat, 2018), the minimum anterosuperior buccal bone thickness (Fig. 4r), and the NPC angle (Fig. 4s) located anteriorly among the axis of NPC and the palatal plane (Bahşi et al., 2019c). Furthermore, MPS maturation was evaluated on the central axial view of the palate and categorized in stages A to E (Fig. 5 a-e) using validated data (Angelieri et al., 2013).

- All incidental findings defined as unexpected bone abnormalities with potential clinical significance (Price et al., 2012) such as torus palatinus (Fig. 5f), palatal/buccal exostoses (Figs. 5g and h), and idiopathic osteosclerosis (Fig. 5i), were documented for both posterior maxillary segments and the anterior maxilla/upper middle line. Conversely, findings such as dental caries, periapical/periodontal conditions, root remnants, altered tooth morphology, supernumerary teeth, and eruption disturbances were ruled out of the study.

Statistical methods

Data processing was completed in standard statistical software (SPSS, v.27.0, IBM, Armonk, NY). Several steps were carried out during the analytic process. Initially, the intra-observer variability was determined through double assessments for each parameter conducted simultaneously by the same examiners using 20 DICOM files chosen following a simple random sampling procedure. For comparisons, the reliability between the two series of data was assessed by using the Cohen's kappa (κ) or the weighted kappa (κ_w) statistics for categorical variables and the intraclass correlation coefficient (ICC) for quantitative variables. The interval between tests 1 and 2 was 12 months.

Bivariate analyses were performed to detect differences in morphological and dimensional variables regarding independent variables. For quantitative variables, the mode of distribution of the data was analyzed using the Kolmogorov-Smirnov test. Because the data were normally distributed, they were analyzed using the independent samples *t*-test. Homoscedasticity was confirmed

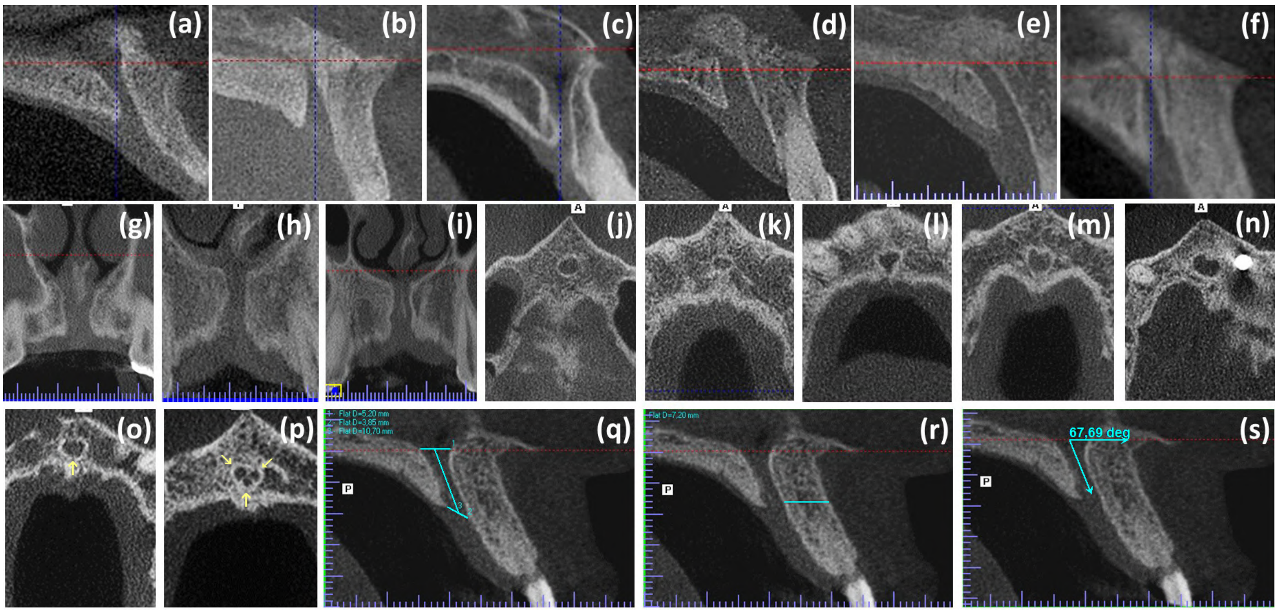

Fig. 4.- CBCT images showing morphological and dimensional evaluations of different anatomical landmarks assessed on the maxillary midline. The morphological variations of NPC were classified in the sagittal plane as: (**a**) hourglass-shaped, (**b**) cone-shaped, (**c**) funnel-shaped, (**d**) cylindrical, (**e**) banana-shaped, and (**f**) branched. In the coronal plane, the configuration of NPC was categorized as: (**g**) Y-shaped, (**h**) single canal, and (**i**) double canal. In the axial plane the shapes of NPF, IF or NPC were classified at each level as: (**j**) round-shaped, (**k**) oval-shaped, (**l**) triangle-shaped; (**m**) heart-shaped, or (**n**) kidney-shaped, whereas the number of openings was stratified as having (**o**) one and (**p**) two or more openings (solid yellow arrows). Measurements of anatomical structures in sagittal sections included (**q**) the length of the NPC and the diameters of IF and NPF, (**r**) the minimum anterosuperior buccal bone thickness, and (**s**) the NPC angle.

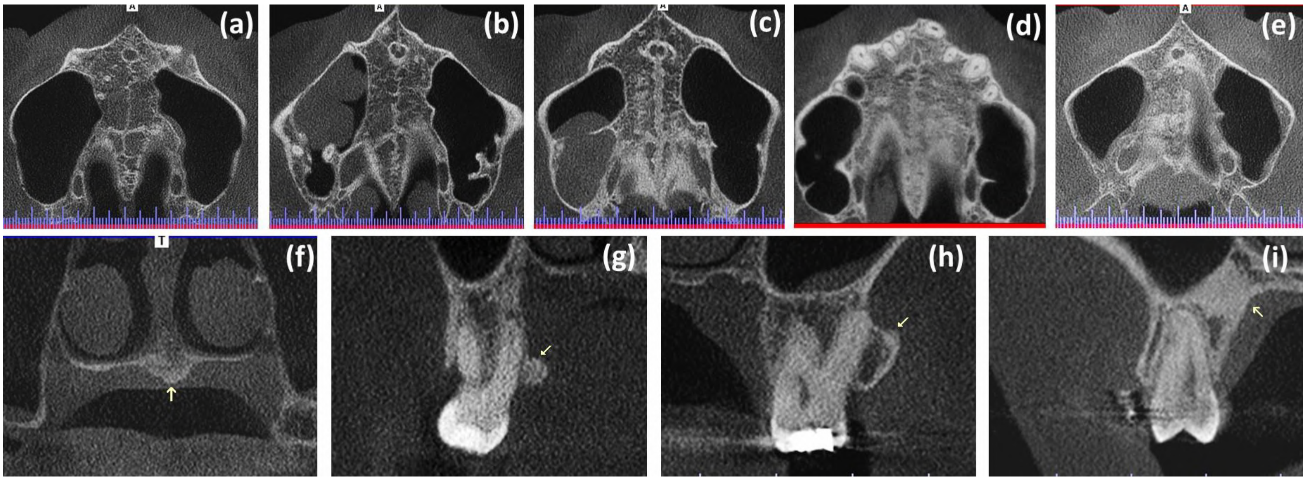

Fig. 5.- CBCT images showing maturation stages of the midpalatal suture (upper row) and some incidental findings of the maxillary region (lower row). (**a**) Stage A of maturation of the midpalatal suture seen as a unique high-density line at the midline. (**b**) Stage B of maturation identified as a scalloped high-density line in some areas and, in other areas, as two parallel, scalloped, high-density lines close to each other and separated by small low-density spaces. (**c**) Stage C of maturation visualized as two parallel, scalloped, and high-density lines separated in some areas by small low-density spaces. (**d**) Stage D of maturation visualized as two scalloped, high-density lines on the maxillary portion of the palate but not observed on the palatine bone. (**e**) Stage E of maturation in which the midpalatal suture cannot be recognized. The lower row shows magnified coronal views demonstrating the presence of (**f**) a torus palatinus in the midline of the palate (solid yellow arrow), (**g**) a palatal exostosis of the maxillary alveolar process (solid yellow arrow), (**h**) a buccal exostosis of the maxillary alveolar process (solid yellow arrow), and (**i**) the tomographic appearance of an apical idiopathic osteosclerosis (solid yellow arrow).

using Levene's test for equality of variances. Furthermore, Pearson's chi-square test (χ^2) was used to compare categorical variables.

Finally, univariate and multivariate binary logistic regression analyses were applied to confirm the association of significant candidate variables with the sex adjusting for independent confounding variables with a level of significance of P <0.20 identified in the bivariate analyses. With this purpose, all continuous data included in the regression models were dichotomized according to the optimal cut-offs points obtained from receiver operating characteristic (ROC) curve analysis. Positive associations occurred when the odds ratio (OR) was >1 and the confidence interval (CI) did not show a value of 1 on any of the constructs. In addition, the Hosmer-Lemeshow statistic was used to assess the goodness of fit of the regression models. Statistical significance was assumed at a value of P <0.05.

RESULTS

Sample characteristics and reproducibility analysis

The study included 208 DICOM files acquired from 83 males with an age range from 18 to 76 years (mean 47.02 ± 15.87) and 125 females with an age range from 18 to 86 years (mean 52.36 ± 15.57). Based on the ROC curve, for all comparisons the optimal cut-off point of the age was estimated in 50.5 years. For each DICOM file, irrespective of the sex, age, side, or alveolar process status, a total of 40 anatomical variables were gathered and analyzed. It was noteworthy that 242 (58.20%) out of 416 posterior maxillary segments were categorized as non-atrophic, 134 (32.20%) as partially atrophic, and 40 (9.60%) as atrophic. Likewise, the anterior maxillary alveolar process status was classified as non-atrophic in 140 (67.30%) out of 208 cases, partially atrophic in 49 (23.60%) cases, and atrophic in 19 (9.10%) cases. Overall, in the reproducibility analysis, the variability between the two series of data obtained by the same examiners was distributed around either the mean or the observed values, without trends towards over- or under-estimation, so that the study results did not show important differences for intra-observer reliability for any of the quantitative or for categorical parameters tested. Thus, the reliability values varied between 0.866 and 1.000, being significantly excellent (P <0.001; ICC, Cohen's κ, and κ_w tests) for all of the variables.

Bivariate comparisons of demographic and tomographic characteristics of the sample

Tables 1 and 2 display the between-group comparisons of the posterior maxillary region- or of the anterior maxilla/upper middle line-related variables regarding to the sex distribution. From Table 1 is apparent that while no significant differences (all P >0.05, χ^2 or unpaired t tests) were detected between sex categories with respect to the minimum distance from the sinus floor to the AC; presence of antral septa; detection, diameter, and distance to the AC of the PSAAC; detection of Csin or AIOF; angle among the horizontal plane of PB and the GPC; localization of the GPF regarding to the posterior margin of the PB; number of the LPF; nor to incidental findings; those data regarding the maximum height, depth, and width of MS; axial, sagittal, and coronal dimensions of IOF; distance from the IOF to the AC; length of GPC in the sagittal plane; anteroposterior diameter of the GPC in the axial plane; distance from the GPC to the PNS, NPC, and to pterygoid hamulus; as well as distance of GPF to the MMS and to AC were significantly greater (all P <0.05, unpaired t-test) in the male group in comparison with the female group. Conversely, both the age and the posterior alveolar process status fulfilled the condition to be deemed as independent confounding variables for the association among sex categories and the variations of maxillary anatomical structures, as they attained P- values <0.20 (χ^2 or unpaired t tests) in the bivariate tests. Otherwise, only the mean values of the length of NPC at sagittal plane, the minimum anterior-superior buccal bone thickness, and the diameter of IF were significantly higher in the male group (P <0.01, unpaired t-test) when compared with the female group (Table 2), whereas the age and the anterior maxillary alveolar process status also had a confounding influence on the results (P <0.20, χ^2 or unpaired t tests). Additionally, in order to identify further sources of variability, all morphological and morphometric data were evaluated by comparing with age, maxillary sides, and alveolar process status when indicated. As a result, no significant differences (all P-values >0.05, χ^2 or unpaired t tests, data not shown) could be established for any parameter of the posterior segments with respect to age and maxillary sides. On the contrary, those cases with atrophic/partially atrophic posterior alveolar processes showed significantly lesser distances from the sinus floor or from lower border of the PSAAC to the AC and a greater proportion of the GPF were located on the same line of the posterior margin of the PB (P-values <0.05, data not shown). In the same way, data of the anterior maxilla/upper middle line showed significantly decreased mean values (P-values <0.01, unpaired t test, data not shown) for both the length of NPC at sagittal plane and the minimum anterior-superior buccal bone thickness in cases with age >50.5 years and atrophic/partially atrophic alveolar process status. Moreover, cases aged >50.5 years had a significantly greater proportion (P <0.001, χ^2 test, data not shown) of stage E of maturation of the MPS. Hence, these findings confirmed the confounding effect of the age and of the alveolar process status on the outcomes.

Outcomes from univariate and multivariate binary logistic regression models

The outcomes from univariate and multivariate models for the association of those variables that yielded significant differences in the bivariate analyses of both posterior maxillary region and anterior maxilla/upper middle line with the sex of the individuals, are presented in Tables 3 and 4, respectively. In general, the Hosmer-Lemeshow goodness-of-fit test values fluctuated from 0.206 to 0.994, indicating that the models were adequately adjusted. Regarding posterior maxillary region-related variables, it can be seen from Table 3, that the OR was significantly increased (P <0.05, Wald's test) for male group in cases with MS height >35.65 mm, MS depth >35.44 mm, MS width >26.65 mm, diameter of IOF in the axial plane >4.15 mm, diameter of IOF in the sagittal plane >3.67 mm, diameter of IOF in the coronal plane >3.71 mm, distance from the mid-point of the IOF to the AC >29.72 mm, length of GPC in the sagittal plane >35.60 mm, anteroposterior diameter of the GPC in the axial plane >5.55 mm, distance from the GPC to the PNS >15.78 mm, distance from the GPC to the NPC >31.94 mm, distance from the GPC to the pterygoid hamulus >9.25 mm, distance from the medial wall of GPF

Table 1. Bivariate comparisons of posterior maxillary region-related variables regarding to the sex distribution.

Parameter		Sex category[a] Male (n = 166)	Female (n = 250)	P-value
Age (years)[b]		47.15 ± 15.96	52.36 ± 15.44	0.001[e]
Posterior alveolar process status[c]	Non-atrophic	90 (54.20)	152 (60.80)	0.183[f]
	Atrophic/partially atrophic	76 (45.80)	98 (39.20)	
Maximum MS height (mm)[b]		39.23 ± 4.90	34.48 ± 4.23	<0.001[e]
Maximum MS depth (mm)[b]		37.35 ± 3.74	34.45 ± 3.22	<0.001[e]
Maximum MS width (mm)[b]		27.97 ± 5.08	25.80 ± 4.20	<0.001[e]
Minimum distance from the sinus floor to the AC (mm)[b]		6.25 ± 3.68	6.34 ± 3.01	0.762[e]
Antral septa[c]	Present	75 (45.20)	98 (39.20)	0.226[f]
	Absent	91 (54.80)	152 (60.80)	
Detection of PSAAC[c]	Present[d]	125 (75.30)	189 (75.60)	0.945[f]
	Non-detected	41 (24.70)	61 (24.40)	
Diameter of PSAAC (mm)[b]		1.37 ± 0.55	1.26 ± 0.44	0.060[e]
Distance among lower border of the PSAAC to the AC (mm)[b]		16.16 ± 3.76	15.90 ± 3.67	0.549[e]
Greater diameter of IOF in the axial plane (mm)[b]		4.50 ± 1.07	4.12 ± 0.92	<0.001[e]
Greater diameter of IOF in the sagittal plane (mm)[b]		3.99 ± 0.91	3.51 ± 0.86	<0.001[e]
Greater diameter of IOF in the coronal plane (mm)[b]		3.96 ± 0.81	3.59 ± 0.72	<0.001[e]
Distance from the mid-point of the IOF to the AC (mm)[b]		31.29 ± 3.29	29.69 ± 2.76	<0.001[e]
Detection of Csin[c]	Present	152 (91.60)	214 (85.60)	0.067[f]
	Absent	14 (8.40)	36 (14.40)	
AIOF[c]	Present	34 (20.50)	34 (13.60)	0.063[f]
	Absent	132 (79.50)	216 (86.40)	
Length of GPC in the sagittal plane (mm)[b]		37.58 ± 3.05	34.97 ± 3.01	<0.001[e]
Anteroposterior diameter of the GPC in the axial plane (mm)[b]		6.34 ± 1.57	5.27 ± 1.22	0.003[e]
Distance from the GPC to the PNS (mm)[b]		16.44 ± 1.29	15.33 ± 1.71	<0.001[e]
Distance from the GPC to the NPC (mm)[b]		33.11 ± 3.37	31.81 ± 3.14	<0.001[e]
Distance from the GPC to the pterygoid hamulus (mm)[b]		9.69 ± 1.68	9.00 ± 1.69	0.001[e]
Distance from the medial wall of GPF to the MMS (mm)[b]		13.87 ± 1.45	13.53 ± 1.45	0.020[e]
Distance from the center of GPF to the AC (mm)[b]		11.18 ± 2.36	9.31 ± 2.33	<0.001[e]
Angle among the horizontal plane of PB and the GPC (degrees)[b]		93.27 ± 7.76	94.41 ± 9.08	0.172[e]
Localization of the GPF regarding to the posterior margin of the PB[c]	Anterior	121 (72.90)	179 (71.60)	0.774[f]
	On the same line	45 (27.10)	71 (24.80)	
Number of the LPF[c]	One	90 (54.20)	159 (63.60)	0.056[f]
	Two or more	76 (45.80)	91 (36.40)	
Incidental findings[c]	Absent	155 (93.40)	232 (92.80)	0.242[f]
	Palatal/buccal exostoses	11 (6.60)	14 (5.60)	
	Idiopathic osteosclerosis	--	4 (1.60)	

Abbreviations: MS, maxillary sinus; AC, alveolar crest; PSAAC, posterior superior alveolar artery canal; IOF, infraorbital foramen; Csin, canalis sinuosus; AIOF, accessory infraorbital foramen; GPC, greater palatine canal; PNS, posterior nasal spine; NPC, nasopalatine canal; GPF, greater palatine foramen; MMS, midline maxillary suture; PB, palatine bone; LPF, lesser palatine foramina
[a]Data based on the sum of right- and left-maxillary posterior sides
[b]Values are given as mean ± SD
[c]Values given as n (%) of cases within each parameter according to the sex category
[d]Including intraosseous (n = 217), below the sinus membrane (n = 81), and on the outer cortex (n = 16) locations
[e]Two-sided unpaired t-test
[f]Two-sided Pearson's chi-square test (χ^2)

Table 2. Bivariate comparisons of anterior maxilla/upper middle line-related variables regarding to the sex distribution.

Parameter		Sex category: Male (n = 83)	Sex category: Female (n = 125)	P-value
Age (years)[a]		47.02 ± 15.87	52.36 ± 15.57	0.015[c]
Anterior maxillary alveolar process status[b]	Non-atrophic	51 (61.40)	89 (71.20)	0.142[d]
	Atrophic/partially atrophic	32 (38.60)	36 (28.80)	
Sagittal morphology of NPC[b]	Hourglass-shaped	22 (26.50)	27 (21.60)	0.421[d]
	Cone-shaped	10 (12.00)	11 (8.80)	
	Funnel-shaped	15 (18.10)	22 (17.60)	
	Banana-shaped	14 (16.90)	24 (19.20)	
	Cylindrical	16 (19.30)	37 (29.60)	
	Branched	6 (7.20)	4 (3.20)	
Coronal morphology of NPC[b]	Y-shaped	29 (34.90)	40 (32.00)	0.491[d]
	Single canal	48 (57.80)	80 (64.00)	
	Double canal	6 (7.20)	5 (4.00)	
Axial mid-level morphology of NPC[b]	Round-shaped	36 (43.40)	45 (36.00)	0.302[d]
	Oval-shaped	15 (18.10)	29 (23.20)	
	Triangle-shaped	8 (9.60)	5 (4.00)	
	Heart-shaped	17 (20.50)	31 (24.80)	
	kidney-shaped	7 (8.40)	15 (12.00)	
Number of NPC at mid-level of axial plane[b]	One canal	65 (78.30)	104 (83.20)	0.377[d]
	Two or more canals	18 (21.70)	21 (16.80)	
Length of NPC at sagittal plane[a]		13.04 ± 3.02	10.93 ± 2.42	<0.001[c]
NPC angle at sagittal plane[a]		69.06 ± 8.57	67.11 ± 9.26	0.123[c]
Minimum anterior-superior buccal bone thickness[a]		7.22 ± 1.51	6.03 ± 1.71	0.001[c]
Diameter of IF[a]		4.08 ± 0.92	3.48 ± 0.96	0.001[c]
Axial morphology of IF[b]	Round-shaped	29 (34.90)	43 (34.40)	0.098[d]
	Oval-shaped	13 (15.70)	9 (7.20)	
	Triangle-shaped	18 (21.70)	24 (19.20)	
	Heart-shaped	18 (21.70)	45 (36.00)	
	kidney-shaped	5 (6.00)	4 (3.20)	
Number of IF at axial plane[b]	One opening	78 (94.00)	120 (96.00)	0.504[d]
	Two or more openings	5 (6.00)	5 (4.00)	
Diameter of NPF[a]		3.67 ± 1.82	3.41 ± 1.63	0.296[c]
Axial morphology of NPF[b]	Round-shaped	28 (33.70)	39 (31.20)	0.403[d]
	Oval-shaped	28 (33.70)	30 (24.00)	
	Triangle-shaped	4 (4.80)	6 (4.80)	
	Heart-shaped	7 (8.40)	17 (13.60)	
	kidney-shaped	16 (19.30)	33 (26.40)	
Number of NPF at axial plane[b]	One opening	46 (55.40)	85 (68.00)	0.066[d]
	Two or more openings	37 (44.60)	40 (32.00)	
MPS maturation[b]	Stage A	3 (3.60)	--	0.259[d]
	Stage B	5 (6.00)	11 (8.80)	
	Stage C	12 (14.50)	16 (12.80)	
	Stage D	17 (20.50)	24 (19.20)	
	Stage E	46 (55.40)	74 (59.20)	
Incidental findings[b]	Absent	78 (94.00)	107 (85.60)	0.059[d]
	Torus palatinus	5 (6.00)	18 (14.40)	

Abbreviations: NPC, nasopalatine canal; IF, incisive foramen; NPF, nasopalatine foramen; MPS, midpalatal suture
[a]Values are given as mean ± SD
[b]Values given as n (%) of cases within each parameter according to the sex category
[c]Two-sided unpaired t-test
[d]Two-sided Pearson's chi-square test (χ^2)

Table 3. Univariate/multivariate binary logistic regression analyses for association of significant posterior maxillary region-related variables with the sex trait adjusting for age and alveolar process status.

Parameters		Cases[a]		Univariate analysis		Multivariate binary logistic regression analysis		Calibration[d]
		Male (n = 166)	Female (n = 250)	Unadjusted OR (95% CI)[b]	P-value[c]	Adjusted OR (95% CI)[b]	P-value[c]	
MS height	≤35.65 mm	36 (21.70)	155 (62.00)	Referent	<0.001		<0.001	0.206
	>35.65 mm	130 (78.30)	95 (38.00)	5.89 (3.76 – 9.23)		5.94 (3.77 – 9.35)		
MS depth	≤35.44 mm	45 (27.10)	145 (58.00)	Referent	<0.001		<0.001	0.786
	>35.44 mm	121 (72.90)	105 (42.00)	3.71 (2.43 – 5.68)		3.82 (2.48 – 5.87)		
MS width	≤26.65 mm	60 (36.10)	141 (56.40)	Referent	<0.001		<0.001	0.590
	>26.65 mm	106 (63.90)	109 (43.60)	2.29 (1.53 -3.42)		2.28 (1.52 – 3-43)		
Diameter of IOF in the axial plane	≤4.15 mm	66 (39.80)	138 (55.20)	Referent	0.002		0.004	0.881
	>4.15 mm	100 (60.20)	112 (44.80)	1.87 (1.25 – 2.78)		1.80 (1.21 – 2.70)		
Diameter of IOF in the sagittal plane	≤3.67 mm	59 (35.50)	140 (56.00)	Referent	<0.001		<0.001	0.280
	>3.67 mm	107 (64.50)	110 (44.00)	2.31 (1.54 – 3.46)		2.30 (1.53 – 3.46)		
Diameter of IOF in the coronal plane	≤3.71 mm	63 (38.00)	146 (58.40)	Referent	<0.001		<0.001	0.929
	>3.71 mm	103 (62.00)	104 (41.60)	2.30 (1.54 – 3.43)		2.19 (1.46 – 3.28)		
Distance from the mid-point of the IOF to the AC	≤29.72 mm	63 (38.00)	126 (50.40)	Referent	0.013		0.013	0.837
	>29.72 mm	103 (62.00)	124 (49.60)	1.66 (1.11 – 2.48)		1.67 (1.11 – 2.50)		
Length of GPC in the sagittal plane	≤35.60 mm	45 (27.10)	140 (56.00)	Referent	<0.001		<0.001	0.440
	>35.60 mm	121 (72.90)	110 (44.00)	3.42 (2.24 – 5.23)		3.41 (2.22 – 5.22)		
Anteroposterior diameter of the GPC in the axial plane	≤5.55 mm	50 (30.10)	153 (61.20)	Referent	<0.001		<0.001	0.414
	>5.55 mm	116 (69.90)	97 (38.80)	3.66 (2.41 – 5.56)		3.74 (2.44 – 5.72)		
Distance from the GPC to the PNS	≤15.78 mm	49 (29.50)	154 (61.60)	Referent	<0.001		<0.001	0.839
	>15.78 mm	117 (70.50)	96 (38.40)	3.83 (2.52 – 5.83)		4.06 (2.65 – 6.24)		
Distance from the GPC to the NPC	≤31.94 mm	66 (39.80)	128 (51.20)	Referent	0.022		0.015	0.696
	>31.94 mm	100 (60.20)	122 (48.80)	1.59 (1.07 – 2.37)		1.65 (1.10 – 2.47)		
Distance from the GPC to the pterygoid hamulus	≤9.25 mm	64 (38.60)	136 (54.40)	Referent	0.002		0.005	0.994
	>9.25 mm	102 (61.40)	114 (45.60)	1.90 (1.28 – 2.84)		1.79 (1.19 – 2.69)		
Distance from the medial wall of GPF to the MMS	≤14.98 mm	121 (72.90)	207 (82.80)	Referent	0.016		0.012	0.950
	>14.98 mm	45 (27.10)	43 (17.20)	1.79 (1.11 – 2.88)		1.85 (1.15 – 3.00)		
Distance from the center of GPF to the AC	≤9.25 mm	45 (27.10)	151 (60.40)	Referent	<0.001		<0.001	0.791
	>9.25 mm	121 (72.90)	99 (39.60)	4.10 (2.68 – 6.28)		4.10 (2.67 – 629)		

Abbreviations: MS, maxillary sinus; IOF, infraorbital foramen; AC, alveolar crest; GPC, greater palatine canal; PNS, posterior nasal spine; NPC, nasopalatine canal; GPF, greater palatine foramen; MMS, midline maxillary suture.
[a]Values are given as n (%) of males and females within each dichotomized parameter according ROC curve analysis. [b]Odds ratio (95% confidence interval). [c]Wald test. [d]Hosmer & Lemeshow goodness-of-fit test.

Table 4. Univariate/multivariate binary logistic regression analyses for association of significant anterior maxilla/upper middle line-related variables with the sex trait adjusting for age and alveolar process status.

Parameters		Cases[a]		Univariate analysis		Multivariate binary logistic regression analysis		Calibration[d]
		Male (n = 83)	Female (n = 125)	Unadjusted OR (95% CI)[b]	P-value[c]	Adjusted OR (95% CI)[b]	P-value[c]	
Length of NPC at sagittal plane	≤11.57 mm	24 (28.90)	77 (61.60)	Referent	<0.001		<0.001	0.981
	>11.57 mm	59 (71.10)	48 (38.40)	3.94 (2.17 – 7.16)		4.89 (2.55 – 9.36)		
Minimum anterior-superior buccal bone thickness	≤6.57 mm	23 (27.70)	76 (60.80)	Referent	<0.001		<0.001	0.803
	>6.57 mm	60 (72.30)	49 (39.20)	4.05 (2.22 – 7.37)		4.86 (2.53 – 9.34)		
Diameter of IF	≤3.60 mm	27 (32.50)	80 (64.00)	Referent	<0.001		<0.001	0.561
	>3.60 mm	56 (67.50)	45 (36.00)	3.69 (2.05 – 6.63)		4.11 (2.23 – 7.57)		

Abbreviations: NPC, nasopalatine canal; IF, incisive foramen
[a]Values are given as n (%) of males and females within each dichotomized parameter according ROC curve analysis. [b]Odds ratio (95% confidence interval). [c]Wald test. [d]Hosmer & Lemeshow goodness-of-fit test.

to the MMS >14.98 mm, and distance from the center of GPF to the AC >9.25 mm. It was further striking that, regarding anterior maxilla/upper middle line-related variables (Table 4), the OR was also significantly increased for male group in cases with a length of NPC at sagittal plane >11.57 mm, minimum anterior-superior buccal bone thickness >6.57 mm, and a diameter of IF >3.60 mm. After adjusting for the effects of confounders, all these candidate variables remained strong and independently associated with the male sex (P <0.05).

DISCUSSION

Detailed study of the maxillary anatomical structures has been helpful in diverse fields, including oral and maxillofacial surgery, otorhinolaryngology, ophthalmology, plastic surgery, head and neck surgery, as well as in forensic and anthropological practices (Ali et al., 2018; Paknahad et al., 2017). As can be appreciated from the references provided, there are many dry-skull- and CBCT-based studies in which anatomical variations of the MS, infraorbital region, hard palate, anterior maxillary region, and their related anatomical structures have been examined separately, but the information has been not only fragmentary, but also the results have been controversial. At the knowledge of the authors, this is the first study, using CBCT scans, that reports comprehensively data concerning the strength/independence of dimensional differences and morphological variations of diverse maxillary structures based on sex comparisons, and taking into account synchronously the modifying effect of the age and alveolar process status on the measurements and observations performed in the sample. Alternatively, this study demonstrated that CBCT imaging is a reliable method for the assessment of morphological and morphometric features of various reference points related with the maxillary bone, as the intra-observer reproducibility values were significantly excellent for the evaluated data in all multiplanar reconstructions. The clinical relevance of the accurate knowledge about the occurrence, exact location, and dimensions of these structures lies in its implication in numerous surgical procedures, including the surgical removal of impacted or supernumerary teeth, or also in orthognathic, implant, periodontal, endodontic, or sinus surgery (Ali et al., 2018; Manzanera et al., 2018; Martins-Júnior et al., 2017; von Arx et al., 2013) among many others, as the inattention of these anatomical variations may lead to surgical failures and/or complications.

It has been acknowledged that male and female cranial structures differ, which is referred as sexual dimorphism (Thornhill and Gangestad, 2006), and that this phenomenon is as great as in other parts of the body (Baughan and Demirjian, 1978).

Considering that estrogen levels limit the growth of facial bones, while testosterone, along with growth hormones, enhance it (Thornhill and Gangestad, 2006), it would be possible to argue that a high ratio of testosterone-to-estrogen might affect the facial growth (Bardin and Catterall, 1981). In agreeance with the former, in this study, the dimensions of the right and left MS were significantly greater in males when compared with those of females. This finding is consistent with those of previous studies (Farias et al., 2019; Kanthem et al., 2015; Paknahad et al., 2017; Sahlstrand-Johnson et al., 2011; Uthman et al., 2011), but differs from other (Genç et al., 2018) in which no sexual dimorphism was identified in relation to these parameters. Moreover, like in this study, some researchers have found no significant differences between the two sides (Farias et al., 2019; Sahlstrand-Johnson et al., 2011), whereas others have documented statistical differences between the right and left MS both in males and females (Uthman et al., 2011). Despite former discrepancies, all resulting data from the MS measurements appear to correspond well with those disclosed by others (Farias et al., 2019; Genç et al., 2018; Kanthem et al., 2015; Paknahad et al., 2017; Sahlstrand-Johnson et al., 2011; Uthman et al., 2011). Overall, these results are especially important considering that both the number and total duration of respiratory infections have been linked negatively with male, but positively with female sex (Thornhill and Gangestad, 2006). Moreover, large national surveys from North America have reported that chronic rhinosinusitis is approximately twice as common in females as in males (Ference et al., 2015). In contrast, the distance from the floor of the sinus to the AC appears not to be influenced by sexual dimorphism or the side of the maxillary segment, but rather by the atrophic/partially atrophic condition of the alveolar crest, which is in line with studies that have shown that the reduced vertical dimension in the posterior maxilla of edentulous individuals is linked to the ridge resorption and the MS pneumatization (Canger and Celenk, 2012; Farina et al., 2011).

Other sinus-related structures analyzed, for which divergent outcomes have been published, were the antral septa and the PSAAC. It has been proposed that, etiologically, antral septa might represent partly congenital abnormalities (primary septa) derived from the developing maxilla or partly acquired abnormalities (secondary septa) related to the irregular atrophy of the posterior maxillary alveolar process (Hungerbühler et el. 2019; Talo Yildirim et al., 2017). In this study, regardless of the origin, a high prevalence of sinus septa, with no significant differences according to sex, age, side, or alveolar process status was detected in the scans, which concurs with some studies (Genç et al., 2018; Talo Yildirim et al., 2017), which have suggested that there is a wide variation in the prevalence of sinus septa, irrespective of the demographic characteristics of the individuals or the degree of alveolar atrophy. On the other hand, the differences in the studies related to the PSAAC are very wide. In the present study, the PSAAC was large enough to be identified by CBCT scans in more than three quarters of the cases, being the intraosseous presentation the most frequently observed (69.11%), followed by the presentation below the sinus membrane (25.80%), and on the outer cortex (5.09%), which is relatively in accordance with the frequencies reported in some studies (Elian et al., 2005; Güncü et al., 2011). Even so, the comparison of detection rates per sex, sides, age category, or alveolar process status did not throw significant differences. Although, these results coincide, at least partially, with those of an earlier study (Genç et al., 2018), andalso differs from others which have reported significantly greater detection rates in females (Güncü et al., 2011) and older adults (Khojastehpour et al., 2016). Moreover, whereas it has been proposed that the diameter and the distance from the artery to the AC are greater in males compared to females (Genç et al., 2018; Güncü et al., 2011; Khojastehpour et al., 2016), the present results failed to show such differences. Notwithstanding, it was noteworthy that this distance was significantly less in cases with atrophic/partially atrophic alveolar process, as has also been described by others (Tehranchi et al., 2017; Velasco-Torres et al., 2016) who postulates that, since variations in the level of the alveolar process depend on the absence of teeth, the height of the residual alveolar crest might be considered as an utmost factor in determining the approximate position of the PSAAC.

Another issue of discussion concerns the sexual dimorphism in the characteristics and morphometric aspects of the infraorbital region, since although it is difficult to compare the results presented herein with other experimental data due to differences in the landmarks used, in consonance with other observations (Bahşi et al., 2019a), this study confirmed, at least in part, that not only the axial, sagittal, and coronal dimensions of IOF, but also the distance from the IOF to the AC, are significantly greater in the male group with no side-related differences. Nevertheless, some authors have failed to identify statistical differences according to sex, though several morphometric parameters have shown higher values in males than in females and significant differences between the left and right sides (Dagistan et al., 2017). Two other important structures evaluated in this region were the Csin and AIOF. With regard to Csin, an important but little-known structure that has a singular tortuous pathway within the anterior wall of the MS below the orbital margin (von Arx et al., 2013), although no significant sex-related differences could be detected, the high detection rate in this study was remarkable and confirms that it should be regarded as a common reference landmark and not an anatomical anomaly of the superior alveolar nerve (Wanzeler et al., 2015). Conversely, the detection rate of the AIOF in the present study, albeit low and showing no significant sex-related differences, was practically analogous to various reported data (Ali et al., 2018; Martins- Júnior et al., 2017), but also dissimilar from that described in other studies (Dagistan et al., 2017; Nanayakkara et al., 2016; Polo et al., 2019) performed on adult dry skulls or CBCT evaluations. In fact, on the basis of its detection frequency some authors believe that the occurrence of AIOF might have a genetic basis (Polo et al., 2019).

The current study also analyzed a series of parameters useful to characterize the GPC in this adult sample. Accordingly, seven specific measurements were significantly higher in the male group, including the length of GPC in the sagittal plane, the anteroposterior diameter of the GPC in the axial plane, the distance from the GPC to the PNS, NPC, and to pterygoid hamulus, as well as the distance of GPF to the MMS and to AC. Although there is great variability in the measurements obtained by other authors, the results obtained in this work indicated a close concordance with the published data (Aoun et al., 2015; Bahşi et al., 2019b; Gibelli et al., 2017, Ikuta et al., 2013; Rapado-González et al., 2015; Tomaszewska et al., 2015). Assuming that age, side, or alveolar process status had no statistical influence on the measurements, all significant sex-related differences detected in various measurements can be also accounted by sexual dimorphism and are consistent with reports of male-female differences of the craniofacial complex (Aoun et al., 2015; Baughan and Demirjian, 1978; Gibelli et al., 2017, Görürgöz and Öztaş, 2022; Tomaszewska et al., 2015). However, discordant data have been also reported regarding these dimorphic traits (Bahşi et al., 2019b; Ikuta et al., 2013; Rapado-González et al., 2015). Another outstanding issue of the herein results was that, in absence of age-, side-, or sex-related differences, a significant greater proportion of GPF located on line with the posterior margin of the PB were observed in cases with atrophic/partially atrophic alveolar process. Although little information is available about this relationship, this finding might be in agreement with a study which suggests that the anteroposterior position of GPF does not depend upon the sex and side (Gibelli et al., 2017); instead, it might actually be related to the decreased alveolar ridge dimensions in maxillary posterior segments of edentulous and partially edentulous individuals (Farina et al., 2011). A further point of agreement between this work and prior investigations (Bahşi et al., 2019b; Gibelli et al., 2017) refers to the lack of significant differences in terms of sex, age, side, and alveolar process status for the number of LPF and for the angle among the horizontal plane of PB and the GPC. Nonetheless, due to the inconstant reported frequency of LPF, but also because the reference points used in this and other works differ from each other, more data would require for determining the variability of this anatomic trait.

The outcome analysis for the anterior maxilla/ upper middle line showed differences only for some variables. In terms of sex, the present results were similar to other researches that found significantly greater measures for the length of NPC (Bornstein et al., 2011; Görürgöz and Öztaş, 2022; Hakbilen and Magat, 2018; Khojastepour et al., 2017; Rai et al., 2021), anterior- superior buccal bone thickness (Bornstein et al., 2011; Hakbilen and Magat, 2018; Khojastepour et al., 2017), and diameter of IF (Bahşi et al., 2019c; Görürgöz and Öztaş, 2022; Khojastepour et al., 2017; Rai et al., 2021) in the male group. Nevertheless, dissenting data have also been reported (Bahşi et al., 2019c; Hakbilen and Magat, 2018). Although the exact reason for differences between men and women is not fully clear, it might be argued that these variations constitute a reflection of hormone-dependent sexually dimorphic traits. At the same time, and in agreement with data that suggest that the NPC is not a static structure but shows dimensional changes liaised with parameters such as aging and tooth loss (Hakbilen and Magat, 2018; Mardinger et al., 2008), the values presented herein for the length of NPC and the buccal bone thickness were significantly smaller in cases with age >50.5 years or atrophic/partially atrophic alveolar process, so that these measurements might related to bone remodeling and increased structural loss observed with age progression (Hakbilen and Magat, 2018). It is important to highlight that the current results might parallel, at least partially, those described by other studies (Bahşi et al., 2019c; Görürgöz and Öztaş, 2022; Hakbilen and Magat, 2018; Jayasinghe et al., 2020), which found that the age, sex, or alveolar process status had no significant effects on the number of nasal/buccal openings, angulation, or shapes of the NPC. In this sense, it has been concluded that the morphology of the NPC is highly variable and different populations show diverse traits/shapes (Görürgöz and Öztaş, 2022; Jayasinghe et al., 2020). Another investigated subject was the maturation of the MPS, in which regardless of the sex or alveolar process status, stage E was found to be significantly more frequent in cases aged >50.5 years. Whereas there is no available information pertaining to the maturation of facial sutures in adulthood, this finding concurs with evidence that stage E increases in prevalence with age (Angelieri et al., 2017). Inasmuch as the continuous progress of skeletal maturation can lead to the obliteration of the MPS (Reis et al., 2020), the age of the individuals may be a practical alternative to predict some MPS stages (Angelieri et al., 2015). The last topic evaluated in this work included the detection of incidental findings on both sides of the posterior maxillary region and on the anterior maxilla/upper middle line. The results showed a low frequency of these alterations, the most common being torus palatinus (11.10%), followed by palatal/buccal exostoses (6.00%), and just a small number of cases of idiopathic osteosclerosis (1.00%). Considering that no significant differences were detectable between the proportions observed according to sex, age, side, or alveolar process status, these detection rates were close similar to those already reported for maxillary CBCT scans (Lopes et al., 2017; Price et al., 2012). Despite the low detection frequency, since these abnormalities can arise anywhere regardless of the sex, age group or alveolar process status, its recognition emphasizes the need to fully examine the volume of the CBCT study to detect the presence of hidden disturbances that may require intervention or monitoring (Price et al., 2012).

It is important to point here that the differences observed between the studies may be attributable to several factors related with the variation in anthropometric characteristics of the sample population, ethnic variability of anatomical structures (Ali et al., 2018; Bahşi et al., 2019c; Gibelli et al., 2017; Görürgöz and Öztaş, 2022; Hakbilen and Magat, 2018; Manzanera et al., 2018; Tomaszewska et al., 2015), age groups analyzed (Hakbilen and Magat, 2018; Talo Yildirim et al., 2017), alongside some features related with the methodological heterogeneity, among these, sample size (Hakbilen and Magat, 2018; Jayasinghe et al., 2020), type of image examination (Khojastehpour et al., 2016; Talo Yildirim et al., 2017), measurement techniques, and different anatomical landmarks (Görürgöz and Öztaş, 2022; Jayasinghe et al., 2020; Velasco-Torres et al., 2016). Despite of aforesaid, it has been accepted that although the collected information can vary according to different populations, the outcomes concerning the possible influence of the sex on each parameter are almost unanimously concordant, when studies are performed according to the same anatomical landmarks (Gibelli et al., 2019). Adding to the former findings, in the present study a total of 14 covariates related to the maxillary posterior region and three covariates related to the maxillary anterior/upper midline were strongly and independently associated with the male sex even after adjusting for age and alveolar process status. This finding is important mainly because, in addition to the fact that these variables may be usefulness for defining safe surgical areas during the planning of different maxillofacial surgical approaches, taking altogether, the CBCT measurements might constitute useful features for sexing of skeletal remains in the forensic or anthropology context when other methods of identification have been inconclusive (Kanthem et al., 2015; Uthman et al., 2011). Hence, additional studies with different statistical approaches using discriminant analyses to investigate different populations are essential to confirm and validate the results obtained in the present study.

As a final point, two main limitations were identified in this study. First, CBCT assessments were performed in a Colombian population that possesses a complex ethnic structure of individuals of different ethnic origins. This fact may preclude the generalizability of the study outcomes to other ethnic groups with different maxillary morphological features. Second, although overall the increased values of 17 covariates were strongly and independently associated with the male sex, other parameters, including the chewing function, extent of tooth loss, and the period of wearing prosthesis might have an important effect on the reported data. Even so, since to transfer the results to clinically relevant conditions, the findings must be strong and constant across different comparisons, adhering to the outcomes presented, it appears that, regardless of dental and prosthetic features, all of these covariates are robustly linked to the male sex.

CONCLUSION

Based on the current data, it would possible to conclude that the maxillary bone can present several morphological variations, as well as dimensional differences that may be strongly liaised to sex but are independent of age, side, and the state of the alveolar process of the population observed. Even so, both aging and alveolar process status should be considered when applying the anatomical variation data to the needs of the particular case.

ACKNOWLEDGEMENTS

This study has been supported by the Technical Research Council of the Faculty of Dentistry of University of Antioquia (CIFO-Code 2021-40871). Special thanks to RADEX 3D Specialized Radiology Center, Medellín, Colombia for providing CBCT scans.

REFERENCES

ALI IK, SANSARE K, KARJODKAR FR, SALVE P (2018) Cone beam computed tomography assessment of accessory infraorbital foramen and determination of infraorbital foramen position. *J Craniofac Surg,* 29(2): e124-e126.

ANGELIERI F, CEVIDANES LH, FRANCHI L, GONÇALVES JR, BENAVIDES E, MCNAMARA JA JR (2013) Midpalatal suture maturation: classification method for individual assessment before rapid maxillary expansion. *Am J Orthod Dentofacial Orthop,* 144(5): 759-769.

ANGELIERI F, FRANCHI L, CEVIDANES LH, MCNAMARA JA JR (2015) Diagnostic performance of skeletal maturity for the assessment of midpalatal suture maturation. *Am J Orthod Dentofacial Orthop,* 148(6): 1010-1016.

ANGELIERI F, FRANCHI L, CEVIDANES LHS, GONÇALVES JR, NIERI M, WOLFORD LM, MCNAMARA JA JR (2017) Cone beam computed tomography evaluation of midpalatal suture maturation in adults. *Int J Oral Maxillofac Surg,* 46(12): 1557-1561.

AOUN G, NASSEH I, SOKHN S, SAADEH M (2015) Analysis of the greater palatine foramen in a Lebanese population using cone-beam computed tomography technology. *J Int Soc Prev Community Dent,* 5 (Suppl 2): S82-S88.

BAHŞI I, ORHAN M, KERVANCIOĞLU P, YALÇIN ED (2019a) Morphometric evaluation and surgical implications of the infraorbital groove, canal and foramen on cone-beam computed tomography and a review of literature. *Folia Morphol (Warsz),* 78(2): 331- 343.

BAHŞI İ, ORHAN M, KERVANCIOĞLU P, YALÇIN ED (2019b) Morphometric evaluation and clinical implications of the greater palatine foramen, greater palatine canal and pterygopalatine fossa on CBCT images and review of literature. *Surg Radiol Anat*, 41(5): 551-567.

BAHŞI I, ORHAN M, KERVANCIOĞLU P, YALÇIN ED, AKTAN AM (2019c) Anatomical evaluation of nasopalatine canal on cone beam computed tomography images. *Folia Morphol (Warsz)*, 78(1): 153-162.

BARDIN CW, CATTERALL JF (1981) Testosterone: a major determinant of extragenital sexual dimorphism. *Science*, 211(4488): 1285-1294.

BAUGHAN B, DEMIRJIAN A (1978) Sexual dimorphism in the growth of the cranium. *Am J Phys Anthropol,* 49 (3): 383-390.

BORNSTEIN MM, BALSIGER R, SENDI P, VON ARX T (2011) Morphology of the nasopalatine canal and dental implant surgery: a radiographic analysis of 100 consecutive patients using limited cone-beam computed tomography. *Clin Oral Implants Res*, 22(3): 295-301.

CANGER EM, CELENK P (2012) Radiographic evaluation of alveolar ridge heights of dentate and edentulous patients. *Gerodontology*, 29(1): 17-23.

DAGISTAN S, MILO□LU Ö, ALTUN O, UMAR EK (2017) Retrospective morphometric analysis of the infraorbital foramen with cone beam computed tomography. *Niger J Clin Pract*, 20(9): 1053-1064.

ELIAN N, WALLACE S, CHO SC, JALBOUT ZN, FROUM S (2005) Distribution of the maxillary artery as it relates to sinus floor augmentation. *Int J Oral Maxillofac Implants*, 20(5): 784-787.

FARIAS GOMES A, DE OLIVEIRA GAMBA T, YAMASAKI MC, GROPPO FC, HAITER NETO F, POSSOBON RF (2019) Development and validation of a formula based on maxillary sinus measurements as a tool for sex estimation: a cone beam computed tomography study. *Int J Legal Med*, 133(4): 1241-1249.

FARINA R, PRAMSTRALLER M, FRANCESCHETTI G, PRAMSTRALLER C, TROMBELLI L (2011) Alveolar ridge dimensions in maxillary posterior sextants: a retrospective comparative study of dentate and edentulous sites using computerized tomography data. *Clin Oral Implants Res*, 22(10): 1138-1144.

FERENCE EH, TAN BK, HULSE KE, CHANDRA RK, SMITH SB, KERN RC, CONLEY DB, SMITH SS (2015) Commentary on gender differences in prevalence, treatment, and quality of life of patients with chronic rhinosinusitis. *Allergy Rhinol (Providence)*, 6(2):82-88.

GENÇ T, DURUEL O, KUTLU HB, DURSUN E, KARABULUT E, TÖZÜM TF (2018) valuation of anatomical structures and variations in the maxilla and the mandible before dental implant treatment. *Dent Med Probl*, 55(3): 233-240.

GIBELLI D, BORLANDO A, DOLCI C, PUCCIARELLI V, CATTANEO C, SFORZA C (2017) Anatomical characteristics of greater palatine foramen: a novel point of view. *Surg Radiol Anat*, 39(12): 1359-1368.

GIBELLI D, BORLANDO A, BARNI L, SARTORI P, CAPPELLA A, PUCCIARELLI V, CATTANEO C, SFORZA C (2019) Anatomy of infraorbital foramen: influence of sex, side, and cranium size. *J Craniofac Surg*, 30(4): 1284-1288.

GÖRÜRGÖZ C, ÖZTAŞ B (2021) Anatomic characteristics and dimensions of the nasopalatine canal: a radiographic study using cone-beam computed tomography. *Folia Morphol (Warsz)*, 80(4): 923-934.

GÜNCÜ GN, YILDIRIM YD, WANG HL, TÖZÜM TF (2011) Location of posterior superior alveolar artery and evaluation of maxillary sinus anatomy with computerized tomography: a clinical study. *Clin Oral Implants Res*, 22(10): 1164-1167.

HAKBILEN S, MAGAT G (2018) Evaluation of anatomical and morphological characteristics of the nasopalatine canal in a Turkish population by cone beam computed tomography. *Folia Morphol (Warsz)*, 77(3): 527-535.

HUNGERBÜHLER A, ROSTETTER C, LÜBBERS HT, RÜCKER M, STADLINGER B (2019) Anatomical characteristics of maxillary sinus septa visualized by cone beam computed tomography. *Int J Oral Maxillofac Surg*, 48(3): 382-387.

IKUTA CR, CARDOSO CL, FERREIRA-JÚNIOR O, LAURIS JR, SOUZA PH, RUBIRA-BULLEN IR (2013) Position of the greater palatine foramen: an anatomical study through cone beam computed tomography images. *Surg Radiol Anat*, 35(9): 837-842.

JAYASINGHE RM, HETTIARACHCHI PVKS, FONSEKA MCN, NANAYAKKARA D, JAYASIGHE RD (2020) Morphometric analysis of nasopalatine foramen in Sri Lankan population using CBCT. *J Oral Biol Craniofac Res*, 10(2): 238-240.

KANTHEM RK, GUTTIKONDA VR, YELURI S, KUMARI G (2015) Sex determination using maxillary sinus. *J Forensic Dent Sci*, 7(2): 163-167.

KHOJASTEHPOUR L, DEHBOZORGI M, TABRIZI R, ESFANDNIA S (2016) Evaluating the anatomical location of the posterior superior alveolar artery in cone beam computed tomography images. *Int J Oral Maxillofac Surg*, 45(3): 354-358.

KHOJASTEPOUR L, HAGHNEGAHDAR A, KESHTKAR M (2017) Morphology and dimensions of nasopalatine canal: a radiographic analysis using cone beam computed tomography. *J Dent (Shiraz)*, 18(4): 244-250.

LOPES IA, TUCUNDUVA RM, HANDEM RH, CAPELOZZA AL (2017) Study of the frequency and location of incidental findings of the maxillofacial region in different fields of view in CBCT scans. *Dentomaxillofac Radiol*, 46(1): 20160215.

MANZANERA E, LLORCA P, MANZANERA D, GARCÍA-SANZ V, SADA V, PAREDES-GALLARDO V (2018) Anatomical study of the maxillary tuberosity using cone beam computed tomography. *Oral Radiol*, 34(1): 56-65.

MARDINGER O, NAMANI-SADAN N, CHAUSHU G, SCHWARTZ-ARAD D (2008) Morphologic changes of the nasopalatine canal related to dental implantation: a radiologic study in different degrees of absorbed maxillae. *J Periodontol*, 79(9): 1659-1662.

MARTINS-JÚNIOR PA, RODRIGUES CP, DE MARIA ML, NOGUEIRA LM, SILVA JH, SILVA MR (2017) Analysis of anatomical characteristics and morphometric aspects of infraorbital and accessory infraorbital foramina. *J Craniofac Surg*, 28(2): 528-533.

NANAYAKKARA D, PEIRIS R, MANNAPPERUMA N, VADYSINGHE A (2016) Morphometric analysis of the infraorbital foramen: the clinical relevance. *Anat Res Int,* 2016: 7917343.

PAKNAHAD M, SHAHIDI S, ZAREI Z (2017) Sexual dimorphism of maxillary sinus dimensions using cone-beam computed tomography. *J Forensic Sci*, 62(2): 395-398.

POLO CL, ABDELKARIM AZ, VON ARX T, LOZANOFF S (2019) The morphology of the infraorbital nerve and foramen in the presence of an accessory infraorbital foramen. *J Craniofac Surg*, 30(1): 244-253.

PRICE JB, THAW KL, TYNDALL DA, LUDLOW JB, PADILLA RJ (2012) Incidental findings from cone beam computed tomography of the maxillofacial region: a descriptive retrospective study. *Clin Oral Implants Res*, 23(11): 1261-1268.

RAI S, MISRA D, MISRA A, KHATRI M, KIDWAI S, BISLA S, JAIN P (2021) Significance of morphometric and anatomic variations of nasopalatine canal on cone-beam computed tomography in anterior functional zone - a retrospective study. *Ann Maxillofac Surg*, 11(1): 108-114.

RAPADO-GONZÁLEZ O, SUÁREZ-QUINTANILLA JA, OTERO-CEPEDA XL, FERNÁNDEZ-ALONSO A, SUÁREZ-CUNQUEIRO MM (2015) Morphometric study of the greater palatine canal: cone-beam computed tomography. *Surg Radiol Anat*, 37(10): 1217-1224.

REIS LG, RIBEIRO RA, VITRAL RWF, REIS HN, DEVITO KL (2020) Classification of the midpalatal suture maturation in individuals older than 15 years: a cone beam computed tomographic study. *Surg Radiol Anat*, 42(9): 1043-1049.

SAHLSTRAND-JOHNSON P, JANNERT M, STRÖMBECK A, ABUL-KASIM K (2011) Computed tomography measurements of different dimensions of maxillary and frontal sinuses. *BMC Med Imaging*, 11: 8.

TALO YILDIRIM T, GÜNCÜ GN, COLAK M, NARES S, TÖZÜM TF (2017) Evaluation of maxillary sinus septa: a retrospective clinical study with cone beam computerized tomography (CBCT). *Eur Rev Med Pharmacol Sci*, 21(23): 5306-5314.

TEHRANCHI M, TALEGHANI F, SHAHAB S, NOURI A (2017) Prevalence and location of the posterior superior alveolar artery using cone-beam computed tomography. *Imaging Sci Dent*, 47(1): 39-44.

THORNHILL R, GANGESTAD SW (2006) Facial sexual dimorphism, developmental stability, and susceptibility to disease in men and women. *Evol Hum Behav*, 27(2): 131-144.

TOMASZEWSKA IM, KMIOTEK EK, PENA IZ, ŚREDNIAWA M, CZYŻOWSKA K, CHRZAN R, NOWAKOWSKI M, WALOCHA JA (2015) Computed tomography morphometric analysis of the greater palatine canal: a study of 1,500 head CT scans and a systematic review of literature. *Anat Sci Int,* 90(4): 287-297.

UTHMAN AT, AL-RAWI NH, AL-NAAIMI AS, AL-TIMIMI JF (2011) Evaluation of maxillary sinus dimensions in gender determination using helical CT scanning. *J Forensic Sci*, 56(2): 403-408.

VELASCO-TORRES M, PADIAL-MOLINA M, ALARCÓN JA, O´VALLE F, CATENA A, GALINDO-MORENO P (2016) Maxillary sinus dimensions with respect to the posterior superior alveolar artery decrease with tooth loss. *Implant Dent*, 25(4): 464-470.

VON ARX T, LOZANOFF S, SENDI P, BORNSTEIN MM (2013) Assessment of bone channels other than the nasopalatine canal in the anterior maxilla using limited cone beam computed tomography. *Surg Radiol Anat*, 35(9):783-790.

WANZELER AM, MARINHO CG, ALVES JUNIOR SM, MANZI FR, TUJI FM (2015) Anatomical study of the canalis sinuosus in 100 cone beam computed tomography examinations. *Oral Maxillofac Surg*, 19(1):49-53.

Parahiatal hernia: A rare type of hernia and the answer to an anatomical challenge

Fátima Senra Lorenzana[1], Asunción Acosta Mérida[2], Noman Zafar[1], Alberto Martínez Isla[3]

[1] Emergency Surgery Unit, General Surgery Department, Northwick Park Hospital, London North West University Healthcare Trust

[2] Unidad de Cirugía Esofagogástrica, Departamento de Cirugía General, Hospital Universitario de Gran Canaria Doctor Negrín

[3] Upper GI Surgical Unit, General Surgery Department, Northwick Park Hospital, London North West University Healthcare Trust, Honorary Clinical Senior Lecturer Imperial College London

SUMMARY

Parahiatal hernias are rare. They are difficult to diagnose preoperatively, as the clinical symptoms may be similar to hiatal and paraoesophageal hernias. Here, we report two cases of parahiatal hernia that were preoperatively diagnosed and successfully repaired laparoscopically; using the particular anatomic characteristics of this hernia, we also review the controversial oesophageal hiatal anatomy, as the surgical community often refers to the left bundle of the right crus as the left crus. There is no consensus on the indication or surgical technique to repair them.

The first case is a 59-year-old woman with non-specific abdominal symptoms, in whom the preoperative gastroscopy and computed tomography (CT) raised the suspicion for parahiatal hernia. The second case is a 68-year-old woman who presented to the emergency department with abdominal distention and nausea, but no vomiting. Preoperative CT raised the suspicion of an incarcerated parahiatal hernia. Both patients underwent laparoscopic repair of the parahiatal hernia and a Toupet fundoplication. They had an uneventful postoperative course. After more than 4 years of follow-up, they are both asymptomatic. Parahiatal hernias are a rare form of diaphragmatic hernia that occur through a diaphragmatic defect lateral to an anatomically normal oesophageal hiatus, with herniation of contents between the left portion of the right crus and the left crus. Up to five different anatomical variations have been described. The knowledge of these anatomical variations has an impact on the type of surgical repair that will need to be performed if a parahiatal hernia is found.

Key words: Parahiatal hernia – Left crus – Oesophageal hiatus – Gastroesophageal reflux

INTRODUCTION

Parahiatal hernia (PH) is a rare form of diaphragmatic hernia that occurs from muscular defects separate from the oesophageal hiatus and the foramina of Morgagni (Demmy et al., 1994; Scheidler et al., 2002; Palanivelu et al., 2008; Ohtsuka et al., 2012; Lew and Wong, 2013; Takemura et al., 2013; Akiyama et al., 2017; Staerkle et al.,

Corresponding author:
Alberto Martínez Isla. General Surgery Department, Northwick Park Hospital, Watford Road, Harrow, HA1 3UJ London, United Kingdom. E-mail: a.isla@imperial.ac.uk

Submitted: April 26, 2023. **Accepted:** June 16, 2023

https://doi.org/10.52083/YJGE5299

2018; Preda et al., 2019; Li et al., 2020). The anatomical studies of the oesophageal hiatus reported by Collis et al. in 1954 demonstrated that there is a large right crus and a smaller left crus which takes no part in the formation of the oesophageal hiatus (Collis et al., 1954). PH result from the herniation of intraabdominal contents between the left portion of the right crus and the left crus lateral to, but distinct from, an intact oesophageal hiatus (Koh et al., 2016; Li et al., 2020). PH are often misdiagnosed as paraoesophageal hernias (POH), as they may have similar radiological findings (Koh et al., 2016).

Although the symptoms of PH are similar to POH, the herniation through a parahiatal defect is generally associated with a high risk of developing perforation and strangulation of the involved organs, which can be life-threatening (Li et al., 2020). There is no consensus regarding the diagnosis and treatment of PH (Li et al., 2020) .

It is common in surgical practice to call the "left crus" the bundle of muscles situated medially to the oesophagus, when in actuality both medial and lateral muscles are part of the right crus. The importance of this anatomical variation lies on the higher risk of complications associated to PH, advocating for an early repair, and on the different surgical approach required for PH with no reflux symptoms in comparison to those that do have acid reflux symptoms and POH.

The aim of this paper is to present two cases of PH treated in our unit and also to review the anatomy of the oesophageal hiatus, clarifying which is the true left crus, and highlighting the importance of its anatomical knowledge when performing a surgical repair of a PH.

CLINICAL CASES

The first case is a 59-year-old woman, with no remarkable past medical history and no previous abdominal surgeries, who presented with dyspepsia, nausea, vomiting and abdominal pain. An oesophago-gastro-duodenoscopy (OGD) was performed, showing a patulous oesophagogastric junction (OGJ) and a herniation of the fundus in a parahiatal fashion with the OGJ at the correct position (36cm from incisor) (Fig. 1A). The CT scan

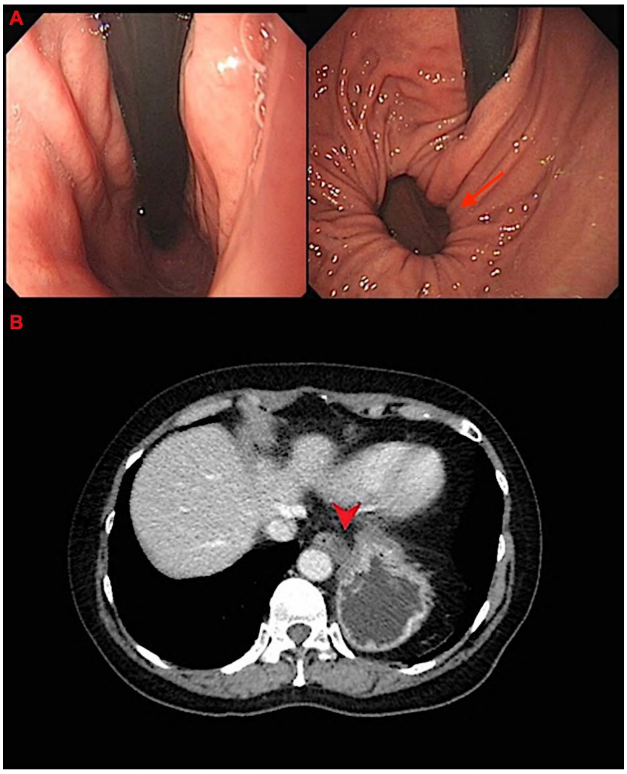

Fig. 1.- Preoperative study case 1. **A:** gastroscopy (arrow: herniation in parahiatal fashion). **B:** CT scan (arrowhead: parahiatal defect).

revealed a left PH (Fig. 1B) with a clear bundle of muscle between the oesophagus and the herniated stomach (Fig. 1B, arrow). The patient subsequently underwent elective surgery.

The second case is a 68-year-old woman, with no other comorbidities, who presented to the emergency department with a short history of abdominal pain, distention and nausea, but no vomiting. She underwent a CT abdomen pelvis that suggested an incarcerated PH (Fig. 2). Decision was made to take her for emergency surgery.

In the first case, a PH between the left portion of the right crus and the left crus was identified intraoperatively (Fig. 3. 1: right portion right crus; 2: left portion right crus; 3: left crus; O: oesophagus; PH: parahiatal hernia). A laparoscopic tension-free parahiatal-defect repair, reinforced with a biological mesh and a Toupet fundoplication, was performed.

In the second case, an incarcerated PH was identified. A laparoscopic Toupet fundoplication was also performed, together with a primary repair of the parahiatal defect and closure of the hiatus. A 28Fr chest drain inserted transabdominally through one of the laparoscopic ports was left in the left chest. It was removed on post-operative day 3.

The post-operative course was uneventful in both patients, being both able to tolerate a soft diet upon discharge. More than four years after surgery they both were asymptomatic. Both patients were followed up with post-operative barium swallow, with no evidence of gastroesophageal reflux or hernia recurrence.

DISCUSSION

PH is a rare form of diaphragmatic hernia. They are distinctly different from POH, such that they occur through a diaphragmatic defect lateral to an anatomically normal oesophageal hiatus (Rodefeld and Soper, 1998; Scheidler et al., 2002; Lew and Wong, 2013; Takemura et al., 2013; Preda et al., 2019) . The hiatus is structurally normal and both crura are intact (Rodefeld and Soper, 1998). Their exact incidence is unknown, being estimated in 0.2-0.35% from different case series (Scheidler et al., 2002; Palanivelu et al., 2008; Koh et al., 2016; Akiyama et al., 2017; Staerkle et al., 2018; Preda et al., 2019; Li et al., 2020). In our series, the incidence is of 0.23% (2 out of 850 fundoplications for hiatus hernia and gastroesophageal reflux). They are characterized by the presence of a separate extrahiatal diaphragmatic defect between the left portion of the right crus and the left crus with an intact oesophageal hiatus (Koh et al., 2016; Lew and Wong, 2013; Akiyama et al., 2017) (Fig. 4).

They can be classified based on their aetiology (primary or secondary), complications (complicated and uncomplicated), and association with the OGJ (normal OGJ or displaced OGJ) (Palanivelu et al., 2008; Lew and Wong, 2013). Congenital or primary PH develop as a result of a failure of the embryonic pleuroperitoneal canal to obliterate during embryogenesis, resulting in a persistent pneumoenteric recess that is located immediately to the left of the oesophageal hiatus (Demmy et al., 1994; Rodefeld and Soper, 1998; Palanivelu et al., 2008; Ohtsuka et al., 2012; Lew and Wong, 2013; Takemura et al., 2013; Li et al., 2020). Although these hernias may arise from both sides of the pneumoenteric recess, they are usually found

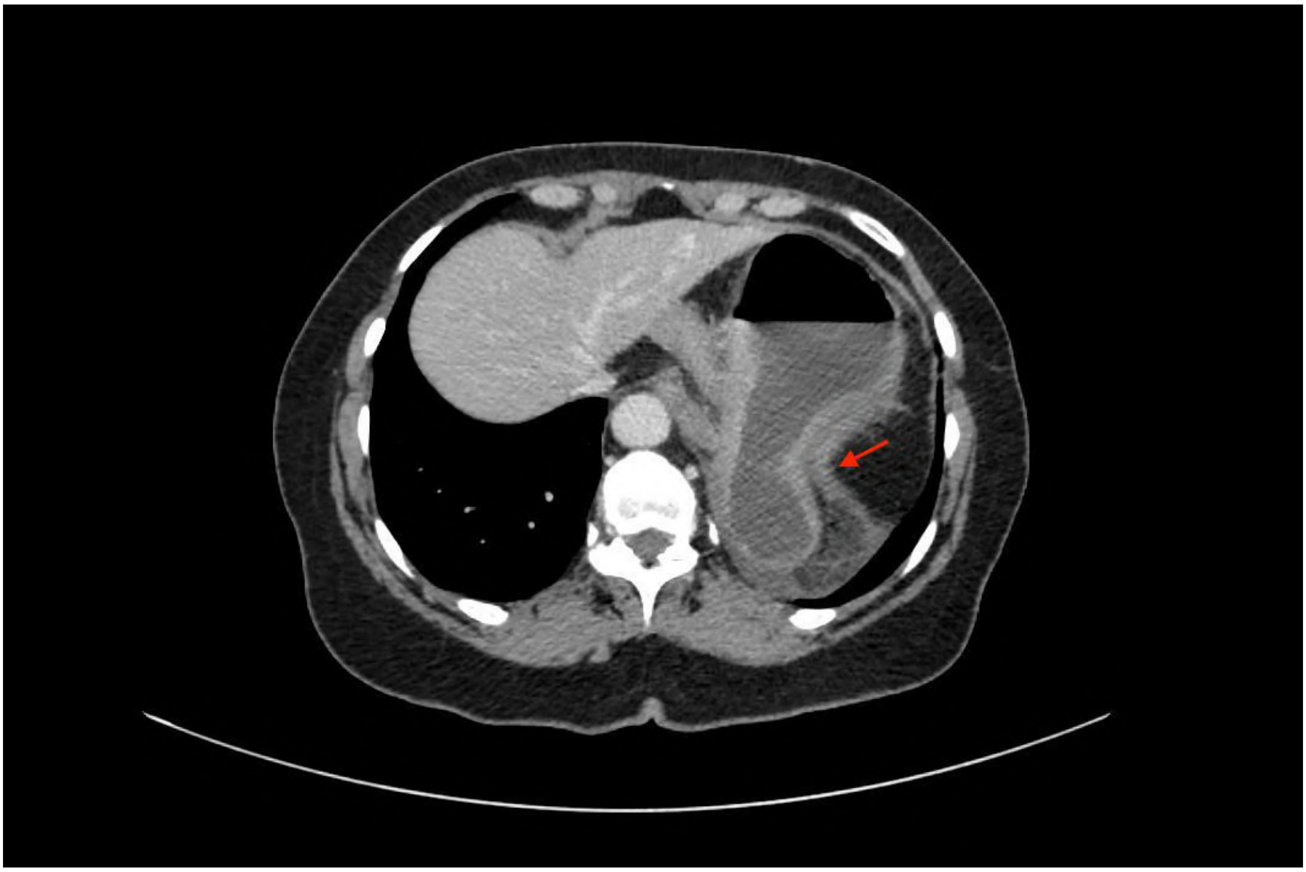

Fig. 2.- Preoperative CT scan case 2 showing incarcerated parahiatal hernia (arrow).

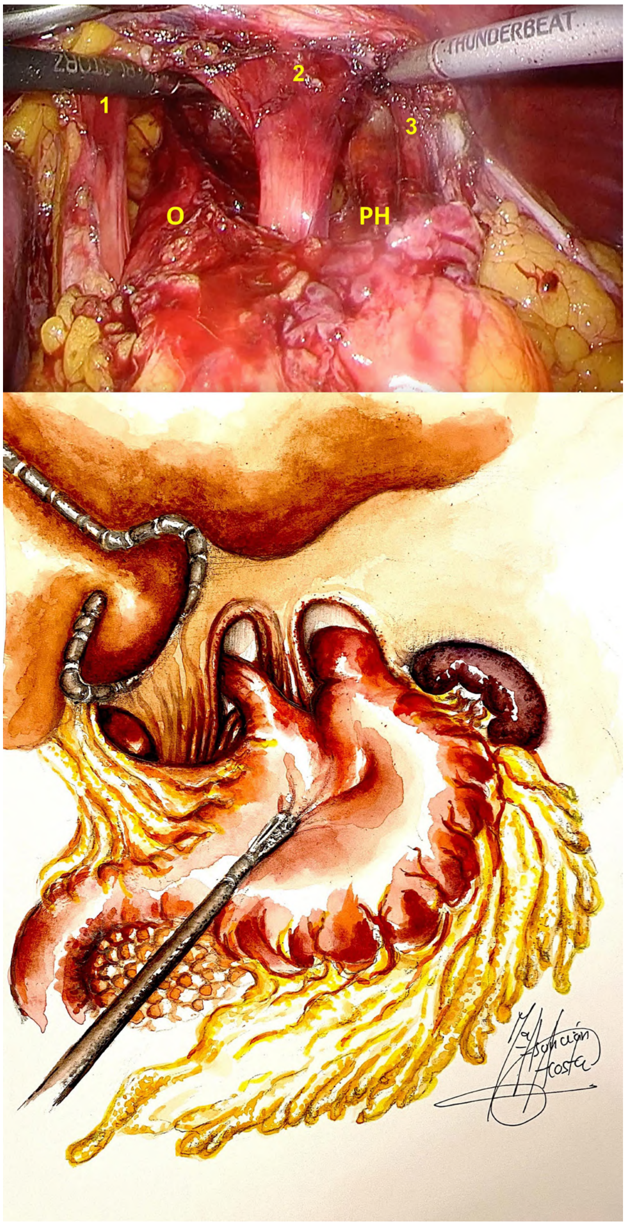

Fig. 3.- Intraoperative findings in case 1 showing the oesophageal hiatus (O) and the parahiatal defect (PH), in comparison to drawing of intraoperative appearance of parahiatal hernias. 1: right portion of the right crus. 2: left portion of the right crus. 3: left crus.

on the left side, possibly due to the presence of the liver on the right side (Takemura et al., 2013; Koh et al., 2016). Acquired or secondary PH can be a result of traumatic injury to the diaphragm or iatrogenic injury from previous surgery in the left upper quadrant of the abdomen (Lew and Wong, 2013). Secondary PH are known to occur after oesophagectomy or cardiomyotomy, probably due to excessive manipulation of the crura or incision on the diaphragm, or while dissecting the GOJ (Palanivelu et al., 2008). The content of the sac is most often the gastric fundus, prone to volvulation (Palanivelu et al., 2008).

Unlike the mechanism of POH, which occur as the stretching of the phreno-oesophageal membrane, there are no morphological changes of the phreno-oesophageal membrane in PH (Li et al., 2020).

The fibres of the right crus arise from the main tendon and in varying degree from the median arcuate ligament (Collis et al., 1954). Some of these fibres may arise from this latter ligament to the left of the midline, but in all cases they can readily be separated from the left crural fibres (Collis et al., 1954). There is no decussation of muscle fibres in front or behind the oesophageal orifice, but varying degrees of muscle overlap are a constant feature (Collis et al., 1954). The fibres on the left part of the right crus, which often arise from the median arcuate ligament, pass upwards above the fibres already mentioned to reach the left side of the hiatus. This produces an effect of a double-breasted coat, more or less well marked from case to case. In the standard type, the median arcuate ligament is always present, although in many cases it is poorly developed (36%) (Collis et al., 1954).

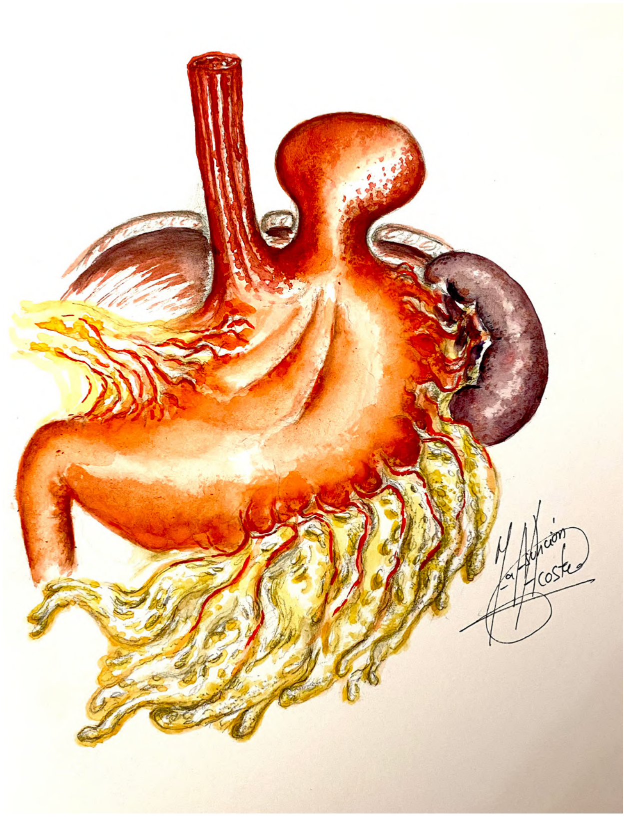

Fig. 4.- Drawing of anatomical appearance of parahiatal hernias.

John Leigh Collis, an English thoracic surgeon, et al. described in 1954 the different anatomical variations of the crura of the diaphragm based on cadaveric anatomical studies (Collis et al., 1954). Up to five different variations of the anatomy of the hiatus were described (Fig. 5). In most cases the left part of the right crus is medial to the oesophagus, and during the hiatal hernia repair the two portions of the right crus are the muscles included in the repair. This is often mistaken in surgical practice, quoting the suturing of the right pillar to the left pillar.

In the type one or standard type of muscular arrangements at the oesophageal hiatus, the muscle quality is good, with a good overlap of the fibres from the right across to the left. The fibres pass inferiorly to the similar band passing from the left to the right. A good median arcuate is present. The fibres of the left crus take no part in the boundaries of the oesophageal orifice (Collis et al., 1954).

Type two is a weak variety of the standard type. The muscle is quite good, but the overlap of fibres between the two parts of the right crus is poorly developed. No median arcuate ligament is present (Collis et al., 1954).

In the type-three variant, a shift to the left is described. A strong median arcuate ligament is present, and many fibres destined for the right of the oesophageal orifice arise from this ligament to the left of the mid-line. The left crus is independent from these fibres and plays no part in forming the oesophageal orifice (Collis et al., 1954).

The type-four variant is characterized by the absence of the median arcuate ligament. The band of fibres on the right side of the oesophagus arises wholly from the left crus and crosses underneath, in scissor fashion; a corresponding band from the right crus going to the left of the oesophageal orifice (Collis et al., 1954).

In the last variant (type five), a complete shift to the left is observed. It is the most uncommon variant (2%). The left crus supplies all muscle fibres taking part in the formation of the oesophageal orifice. The overlapping fibres pass in the same direction as with a standard type diaphragm. This would be reversed in a congenital transposition (Collis et al., 1954).

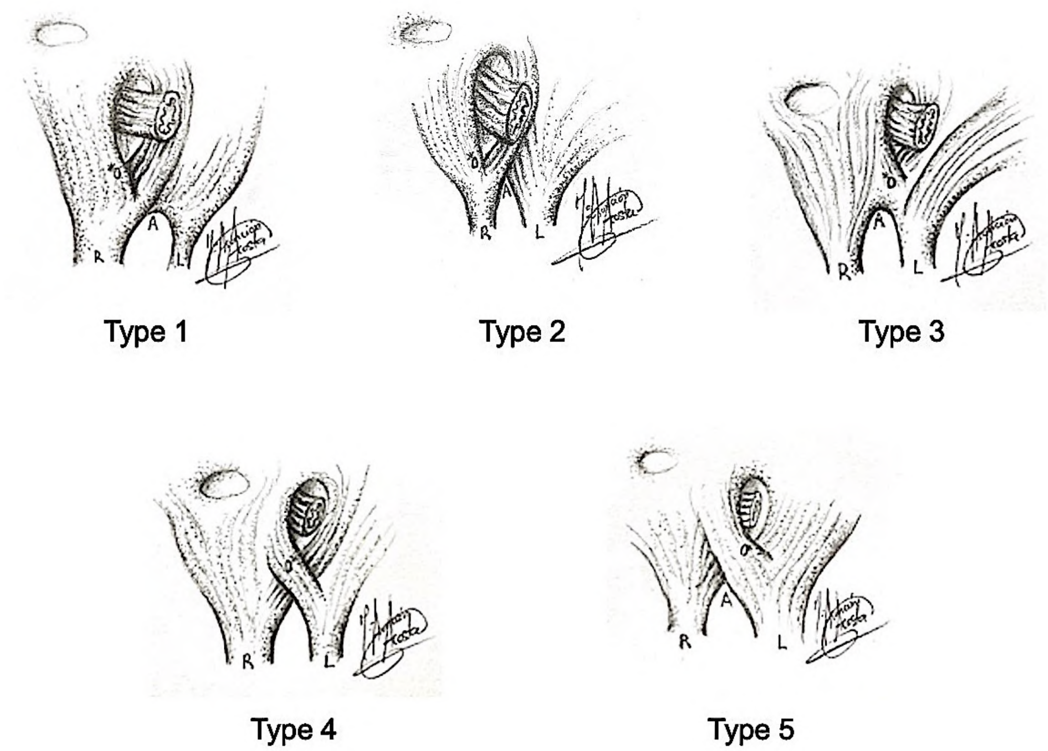

Fig. 5.- Anatomical variations of the oesophageal hiatus depending on the disposition and insertions of the diaphragmatic crura. R: right crus. L: left crus. O*: oesophageal hiatus. A: Aortic hiatus.

Unlike in our cases, it is difficult to diagnose a PH preoperatively (Ohtsuka et al., 2012; Akiyama et al., 2017). Most PH are diagnosed intraoperatively, during the repair of preoperatively presumed hiatal or POH (Lew and Wong, 2013). Clinically, it is difficult to differentiate between a parahiatal and a hiatal or paraoesphageal hernia, as they can present with epigastric pain, nausea, vomiting, heartburn and post-prandial bloating (Scheidler et al., 2002; Lew and Wong, 2013; Akiyama et al., 2017; Staerkle et al., 2018). Radiologically, if the crural musculature between the hiatus and the hernia orifice can be identified on an abdominal computed tomography (CT), as in our cases, it might aid in the diagnosis of PH (Akiyama et al., 2017). Preoperative studies in suspected PH should be the same as for hiatal or POH, including appropriate history looking for gastroesophageal reflux symptoms, preoperative OGD, and pH studies and manometry if indicated.

The detailed knowledge of the hiatal anatomy is crucial given the complications associated to PH and the type of hiatal repair required. Because of a high risk of perforation, incarceration and strangulation of involved organs, when preoperatively identified, surgery is always indicated to correct the parahiatal defect (Scheidler et al., 2002; Lew and Wong, 2013; Staerkle et al., 2018). Intraoperatively, in cases where a PH is suspected, focused dissection should be performed at the left crus; the right crus should be left alone, as unnecessary dissection might disrupt an otherwise normal hiatus (Koh et al., 2016). Fundoplication is also typically not required unless the patient has symptomatic reflux or there is a hiatal defect (Koh et al., 2016; Staerkle et al., 2018; Preda et al., 2019). In our cases, we associated a fundoplication to the parahiatal defect repair, as a hiatal defect was seen intraoperatively in both cases. In the first case, the fundoplication was also indicated for the gastroesophageal reflux symptoms that the patient presented preoperatively. Moreover, extensive hiatal dissection with the subsequent destruction of the natural antireflux mechanism, required to achieve the parahiatal defect repair, is also an indication for associating an antireflux procedure. Deep anatomical knowledge is fundamental for appropriate choice of surgical repair. The differentiation between the oesophageal hiatus, formed by the two portions of the right crus, and the parahiatal space found between the left and the right crus, can be referred by surgeons as a challenge, as the hiatal anatomy is not clearly described in most surgical papers that refer to this type of condition: usually the left portion of the right crus is referred as the "left crus", which is anatomically incorrect. This misunderstanding of the hiatal anatomy may lead to suboptimal surgical repairs. An incorrect repair of the hiatus may lead to long-term post-operative complications, such as recurrence of the hernia, gastroesophageal reflux and all its complications, as well as stricturing of the hiatus with dysphagia that may require endoscopic dilatation, re-do of the hiatal repair, or even oesophagectomy in cases with severe strictures resistant to less invasive treatments.

The repair of these hernias can be performed through an open or a laparoscopic approach. Laparoscopic repair provides many benefits, including better visualization of the operative field, faster recovery and shorter hospital stay, and can be performed safely by laparoscopic surgeons familiar with the repair of paraoesophageal and hiatal hernias (Lew and Wong, 2013). The surgical principle of tension-free repair should be also applied to PH. This can be done either by primary repair, with a prosthetic mesh, or both (Lew and Wong, 2013). In circumstances where large defect size and fibrosis prevent tension-free primary repair, the use of a composite mesh can provide effective repair of the hernia with good outcome (Lew and Wong, 2013). As seen in our patients, the few cases published to date had no post-operative complications; recurrence in the long term after surgery was not reported.

CONCLUSIONS

PH are an uncommon type of diaphragmatic hernia. These hernias arise between the left portion of the right crus and the left crus, existing up to five different types of configurations of the hiatal anatomy. And the two bundles of muscle that are repaired during antireflux surgery in most cases belong to the right crus. Preoperative diagnosis is challenging, given the similarity with hiatal hernias in imaging and symptoms. Surgical repair of these diaphragmatic defects is advocated in all cases, given the high risk of complications; and deep knowledge of the anatomy of the hiatus is fundamental to perform an appropriate repair with or without an anti-reflux procedure, depending on the intraoperative findings and the patient's preoperative symptoms. An anti-reflux procedure should be performed if there are any reflux symptoms, if there is a hiatal defect, or after an extensive mobilization of the oesophagogastric junction. This can be done by an open or a laparoscopic approach, with or without mesh reinforcement of the repair.

REFERENCES

AKIYAMA Y, IWAYA T, ENDO F, CHIBA T, TAKAHARA T, OTSUKA K, NITTA H, KOEDA K, MIZUNO M, KIMURA Y, SASAKI A (2017) Laparoscopic repair of parahiatal hernia after esophagectomy: a case report. *Surg Case Rep,* 3(1): 3-7.

COLLIS JL, KELLY TD, WILEY AM (1954) Anatomy of the crura of the diaphragm and the surgery of hiatus hernia. *Thorax*, 9(3): 175-189.

DEMMY TL, BOLEY TM, CURTIS JJ (1994) Strangulated parahiatal hernia: Not just another paraesophageal hernia. *Ann Thorac Surg*, 58(1): 226-227.

KOH YX, ONG LWL, LEE J, WONG ASY (2016) Para-oesophageal and parahiatal hernias in an Asian acute care tertiary hospital: An underappreciated surgical condition. *Singapore Med J*, 57(12): 669-675.

LEW PS, WONG ASY (2013) Laparoscopic mesh repair of parahiatal hernia: a case report. *Asian J Endosc Surg*, 6(3): 231-233.

LI J, GUO C, SHAO X, CHENG T, WANG Y (2020) Another type of diaphragmatic hernia to remember: parahiatal hernia. *ANZ J Surg*, 90(11): 2180-2186.

OHTSUKA H, IMAMURA K, ADACHI K (2012) An unusual diaphragmatic hernia. *Gastroenterology*, 142(7): 1420, 1623.

PALANIVELU C, RANGARAJAN M, JATEGAONKAR PA, PARTHASARATHI R, BALU K (2008) Laparoscopic repair of parahiatal hernias with mesh: A retrospective study. *Hernia*, 12(5): 521-525.

PREDA SD, PĂTRAŞCU S, UNGUREANU BS, CRISTIAN D, BINTINTAN V, NICA CM, CALU V, STRÂMBU V, SAPALIDIS K, SURLIN VM (2019) Primary parahiatal hernias: A case report and review of the literature. *World J Clin Cases*, 7(23): 4020-4028.

RODEFELD MD, SOPER NJ (1998) Parahiatal hernia with volvulus and incarceration: laparoscopic repair of a rare defect. *J Gastrointest Surg*, 2(2): 193-197.

SCHEIDLER MG, KEENAN RJ, MALEY RH, WIECHMANN RJ, FOWLER D, LANDRENEAU RJ (2002) "True" parahiatal hernia: A rare entity radiologic presentation and clinical management. *Ann Thorac Surg*, 73(2): 416-419.

STAERKLE RF, SKIPWORTH RJE, LEIBMAN S, SMITH GS (2018) Emergency laparoscopic mesh repair of parahiatal hernia. *ANZ J Surg*, 88(6): E564-E565.

TAKEMURA M, MAYUMI K, IKEBE T, HAMANO G (2013) Laparoscopic repair of secondary parahiatal hernia with incarceration of the stomach: A case report. *J Med Case Rep*, 7(1): 1.

Absence of musculocutaneous nerve associated with the presence of an accessory head of the biceps brachii muscle: report of a bilateral case and its clinical implications

Emilio Farfán[1,2], Felipe Araya[1], Manuel Barroilhet[1], Francisco Cornejo[1], Agustín Gutiérrez[1], Matías Vergara[1], Oscar Inzunza[1,2], Natalia Sánchez[1], Jaritza Tramolao[1], Verónica Inostroza[1]

[1] *Departamento de Anatomía, Escuela de Medicina, Pontificia Universidad Católica de Chile, Chile*

[2] *Morpho-Clinical Research Lab, Escuela de Medicina, Pontificia Universidad Católica de Chile, Santiago, Chile*

SUMMARY

The anatomical variants of the biceps brachii muscle (BBM) are frequent, mostly unilaterally than bilaterally, and are associated with supernumerary muscle bellies, the total absence of the muscle or one of its heads, and variations in the points of origin and insertion. In the same way, the variants of the musculocutaneous nerve (MCN) can include alterations in its course, number of branches, or anatomical relations, whereas its absence is considered an atypical variation. The aim of this work was to report the absence of musculocutaneous nerve associated with the presence of one accessory head of the biceps brachii muscle. Dissection of a female cadaver, fixed in 10% buffered formaldehyde, which did not present previous surgeries in the studied area was performed. Variations were noted in both upper limbs related to accessory muscle bellies and change in innervation. Anatomical relations of muscles and nerves were determined by following proximal to distal ends, relation, vascularization, and innervation pattern. The absence of MCN associated with the presence of one accessory head of the BBM were found bilaterally. These anatomical variations are atypical. Clinically, these variations can produce compressive symptoms that could generate confusing diagnostics and conduce to unnecessary procedures on the arm, inducing iatrogenic actions.

Key words: Musculocutaneous nerve – Absence – Biceps brachii muscle – Accessory head

INTRODUCTION

The biceps brachii muscle (BBM) is in the anterior brachial region, comprised of two heads originated in the scapula. The short head (BBsh) originates in the vertex of the coracoid process, and the long head (BBlh) in the supraglenoid tubercle; the two form the mass of the muscle whose distal tendon is inserted in the radial tuberosity. The heads of the BBM receive innervation from the musculocutaneous nerve (MCN) and vascularization from the brachial vessels (Standring, 2016).

Corresponding author:
Dr. Verónica Inostroza. Departamento de Anatomía, Escuela de Medicina, Pontificia Universidad Católica de Chile, Santiago de Chile, Av. Libertador Bernardo O'Higgins #340. Phone: +56223542189. E-mail: vfinostr@uc.cl

Submitted: May 17, 2023. **Accepted:** June 16, 2023

https://doi.org/10.52083/ZLOH6744

The anatomical variations of this muscle can include accessory heads, total absence of the muscle or one of its heads, complete separation from the muscle belly, variations in the points of origin, and insertion or fusion with neighboring muscles (Testut, 1884; Tubbs et al., 2016).

On the other hand, the MCN originates from the lateral fascicle (C5-C6) of the brachial plexus, typically at the axillary level, where it is located laterally to the median nerve and axillary artery. It is directed inferiorly and laterally, perforating the coracobrachialis muscle, which it crosses to access the anterior compartment of the arm. In the arm, it passes between the BBM and the brachialis muscle, emerging at the level of the cubital fossa, deep to the cephalic vein, where it continues as the lateral antebrachial cutaneous nerve (Standring, 2016). In its course, it emits muscle branches for the coracobrachialis, BBM, and brachialis and an articular branch for the elbow joint capsule. In addition, it can emit communicating branches for the median, ulnar, radial, and medial brachial cutaneous nerves (Rouvière and Delmas, 2005). The MCN can vary in its course, number of branches, or anatomical relations (Gümüsburun and Adigüzel, 2000; Farfán et al., 2020), whereas its absence is considered an atypical variation (Kaur et al., 2014).

In the initial stages of limb development, a homogeneous somatic mesoderm-derived mesenchyme without the presence of nerve fibers is observed; later, at the base of the limb bud, the ventral primary rami of spinal nerves branch to the distal end (Keibel and Mall, 1912). Tosney and Landmesser (1985) demonstrate that the location and morphology of the growth cones of the motor neurons innervating the muscle primordia of the limbs are determined by the connective tissue cues where they develop (Tosney and Landmesser, 1985). Similarly, the somatic mesodermal-derived connective tissue is an important source of molecular signals for limb muscle pattern development (Chevallier et al., 1977; Kardon et al., 2003).

The aim of this work was to report the absence of musculocutaneous nerve associated with the presence of one accessory head of the biceps brachii muscle in an adult woman.

CASE REPORT

A case is described of the bilateral presentation of a nerve variation associated with a muscle variation, observed during the dissection of upper limbs in a cadaver, female, Caucasian, aged 87 years at the time of death, fixed in 10% formaldehyde buffer and conserved in a cold chamber at 4ºC. The cadaver had no prior surgeries in the studied area, and the cause of death was cardiorespiratory arrest.

Muscle variants

The right BBM presented a flat, thin accessory head, which originated on the anterior side of the distal third of the humeral diaphysis, near the insertion of the coracobrachialis muscle; from there, the fascicle joined the distal tendon of the BBM. Its irrigation came from fine brachial vessels, and its innervation from a branch originating from the lateral antebrachial cutaneous nerve. Separating the accessory head of the BBM, there is a muscle partition where the vessels and nerves travel (Fig. 1A, Table 1). The left BBM presented a spindle-shaped accessory head, which originated in the proximal third of the humeral diaphysis, between the insertion point of the coracobrachialis muscle and the origin of the brachial muscle (Fig. 1B, Table 1); from there, the fascicle joined the distal tendon of the BBM. Its irrigation came from fine brachial vessels, and its innervation from a branch originating from the lateral antebrachial cutaneous nerve. On the plane that separates the accessory head of the BBM, there is a muscle partition where the vessels and nerves travel (Fig. 1A, Table 1).

Nerve variants

In the upper right limb, the absence of the MCN was noted, originating that the muscle branch for the coracobrachialis muscle came from the lateral fascicle of the brachial plexus. The muscle branches for the BBlh, BBsh, and the brachial muscle came from the median nerve, as well as the lateral antebrachial cutaneous nerve. The muscle branch for the accessory head of the BBM originated jointly with this last nerve (Figs. 1A and 2A). In the upper left limb, the absence of the MCN is noted; in this case, the coracobrachialis mus-

Table 1. Accessory muscle belly measurements

	Right	Left
Overall length (mm)	133.66	163.59
Muscle belly length (mm)	80.61	104.74
Distal tendon length (mm)	58.05	58.85
Transverse muscle belly diameter (mm)	9.08	15.43
Anteroposterior muscle belly diameter (mm)	2.23	7.97

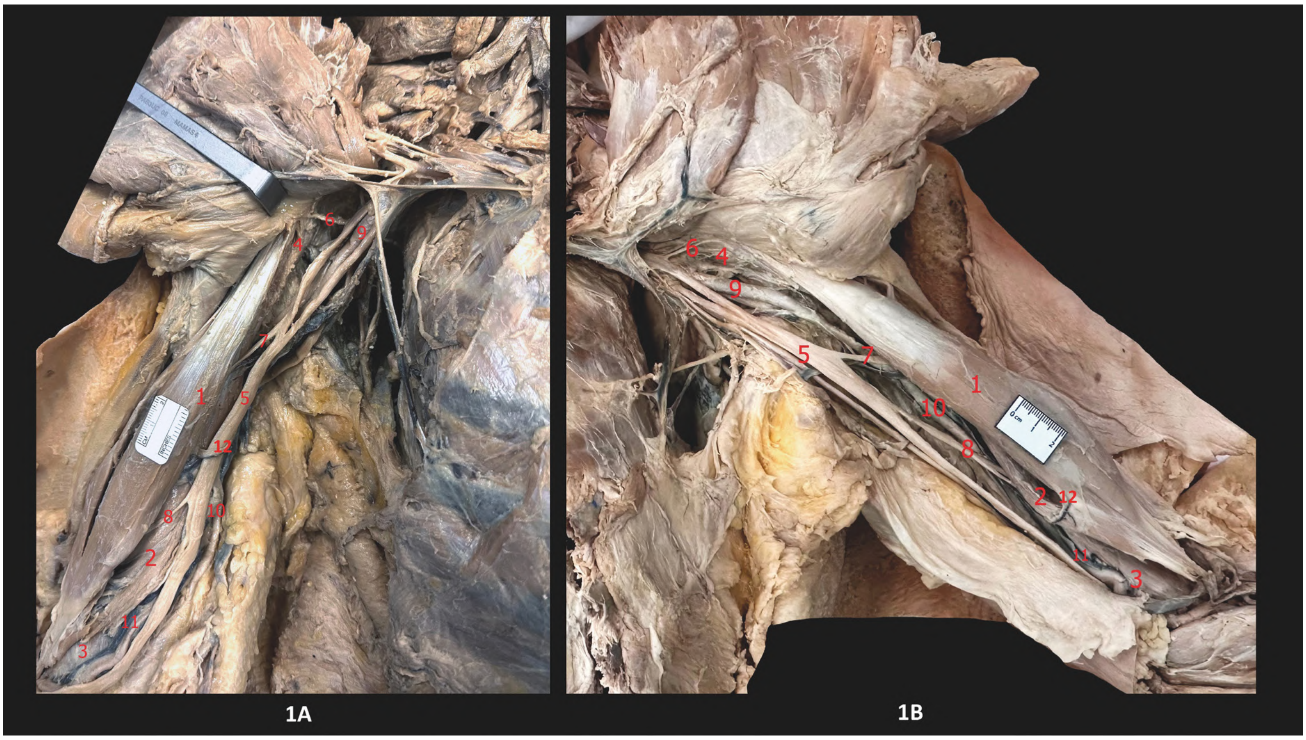

Fig. 1.- Dissection of the nerve variant. In "**A**" the right arm and in "**B**" the left side, showing the BBM with the accessory head. 1. Biceps brachii muscle (BBM); 2. Accessory head of the biceps brachii muscle; 3. Brachialis muscle; 4. Coracobrachialis muscle (covered by fascia); 5. Median nerve; 6. Muscular branch to the coracobrachialis muscle; 7. Muscular branch to the biceps brachii muscle; 8. Lateral antebrachial cutaneous nerve; 9. Axillary artery; 10. Brachial artery; 11. Brachial artery and vein; 12. Muscular branch of the brachial vessels.

cle received two muscle branches that originated from the lateral fascicle of the brachial plexus. The muscle branches for the BBlh, BBsh, and the brachial muscle came from the median nerve, as well as the lateral antebrachial cutaneous nerve. The muscle branch for the accessory head of the BBM originated jointly with this last nerve (Figs. 1B and 2B).

DISCUSSION

The evidence shows that the presence of one or more supernumerary muscle bellies is the most common variation of the BBM. In contrast, the total absence of the MCN and a complete takeover by the median nerve of the innervation of the coracobrachialis, biceps brachii, and the brachialis muscles is an unusual variation of the brachial plexus (Prasada Rao and Chaudhary, 2001). A meta-analysis that included 78 articles and 10,603 upper limbs reported that accessory heads have a prevalence of 9.6% in the BBM, being the presence of one accessory head the most frequent (8.4%). Nevertheless, the presentation of bilateral accessory heads, as reported in this study, is atypical (Lee et al., 2011). In fact, in a sample of 175 cadavers (350 arms), 15.4% of accessory humeral heads in the BBM were found, with 12.6% corresponding to unilateral and 2.8% to bilateral cases (Rodríguez-Niedenführ et al., 2003). In the case of the MCN absence, according to a systemat-

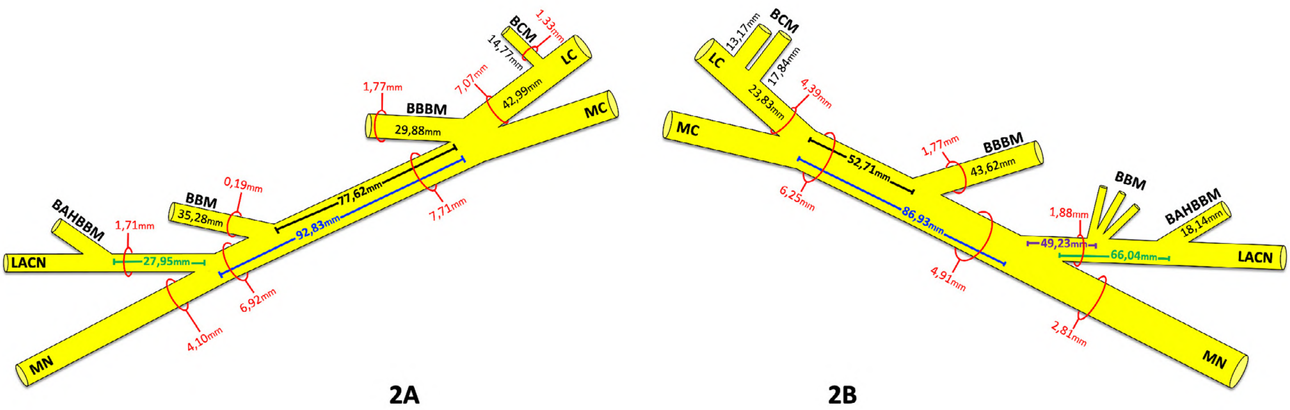

Fig. 2.- Scheme of the nerve distribution in the arm, in "**A**" the right side and in "**B**" the left side. On both sides: LC. Lateral cord of brachial plexus; MC. Medial cord of brachial plexus; MN. Median nerve; LACN. Lateral antebrachial cutaneous nerve; BCM. Branch to coracobrachialis muscle; BBBM. Branch to biceps brachii muscle; BBM. Branch to brachialis muscle; BAHBBM. Branch to accessory head of the biceps brachii muscle. The red circles indicate the transverse diameter of the nerve structures. The black bar within the median nerve indicates the distance from the formation of the median nerve to the origin of the first nerve branch. The blue bar within the median nerve indicates the distance from the formation of the median nerve to the origin of the second nerve branch. The purple and green bars within the second nerve branch indicate the distance between the origin of the second nerve branch and its terminal branches. The nerve branching is not symmetrical.

ic review and meta-analysis, the prevalence varies from 1.66% to 13% (Hunter and Zdilla, 2021; Choi et al., 2002).

A more comprehensive study about variations of the biceps brachii muscle was published by Rodriguez-Niedenführ et al. (2003): they generate a classification of accessory heads of the BBM. Using the place of origin and location of the accessory belly as criteria, they describe three types: superior humeral heads that represent 1.5%, inferomedial humeral heads corresponding to 9%, and inferolateral humeral heads corresponding to 0.3% (Rodríguez- Niedenführ et al., 2003). More recent classifications propose four types of accessory heads for the BBM with different subtypes (Szewczyk et al., 2022). Type I has two heads (64%); this subdivides into type IA with a single muscle belly and type IB with two muscle bellies. Type II has three heads (26%), classified as four subtypes: type IIA originates from the middle part of the humeral axis; type IIB originates in the coracoid process together with the short head; type IIC originates in the tendon of the pectoralis major muscle, and type IID originates in the glenohumeral joint capsule. Type III (6%) is characterized as presenting four heads, and type IV (4%) has five heads. In our report, both accessory bellies originate in the lower half of the humerus and were located medially to the BBM. In this sense, the accessory heads found correspond to the inferomedial humeral head type described by Rodríguez-Niedenführ et al. (2003), and to type IIA described by Szewczyk et al. (2022). Regarding MCN, it is classified by the communications between the musculocutaneous and median nerves, depending on whether the communicating branch arose from the MCN before (type I) or after (type II) it pierced the coracobrachialis muscle, and type III when the MCN did not pierce the coracobrachialis muscle (Venieratos and Anagnostopoulou, 1998). In that sense, the variation found here it is similar to type III; however, instead of having a communicating branch, the MCN is fused with the median nerve.

The presence of accessory heads of the BBM has been often associated with variations of the MCN (Wang et al., 2011; Yamamoto et al., 2018), describing alterations that include either change in its course, total absence or communications of the MCN with the median nerve in presence of the accessory heads of the BBM (Mehta, 2009; Lee et al., 2014; Tubbs et al., 2016). For example, cases of accessory heads associated with the presence of two MCN, one proximal that was adjusted to the normal course and ended after innervating the coracobrachialis muscles and BBM, and another distal MCN that emerged from the median nerve in the lower part of the arm, innervating the BBM and brachial muscles to end as a lateral antebrachial cutaneous nerve (Abu-Hijleh, 2005). In the same way, bilateral accessory heads of the BBM associated with course variations and branching patterns of the MCN have been reported. In that case, a third accessory head originated from the deep fascia of the brachial muscle on both arms. On the right side, the MCN did not perforate to the coracobrachialis muscle; however, it was also innervating the muscles of the anterior compartment of the arm. In contrast, on the left side, the MCN had the usual course (Saluja et al., 2017). This case appears similar to what is reported bilaterally here.

The origin of this variation comes from embryonic development. Long-standing experimental data indicate that in the limb bud, the branching of the motor rami of brachial and lumbar plexuses depends entirely on the segregation of mesenchymal-derived structures (Keibel and Mall, 1912). Between the fourth and seventh weeks of development, the muscular precursor cells derived from the dorsolateral region of cervical myotomes migrate to the upper limb bud. The cues coming from the connective tissue are relevant for the differentiation of the cleavage pattern of the ventral and dorsal limb compartment and for the distribution of motor neurons that will innervate it (Tosney and Landmesser, 1985). Then, the limb bud mesenchyme is penetrated by the ventral primary branches of the spinal nerves located in front of the upper limb bud, being necessary for muscle development. In particular, BBsh originates from a common muscular precursor with the brachial and coracobrachialis muscles, whereas BBlh originates from an independent precursor (Murillo-González et al., 2018). Pioneering work by W. H. Lewis in seven-week human embryos traced the composition of the brachial plexus branches (Lewis, 1902). In the developing brachial plexus, the median nerve emerges as a combination of ventral segmental branches, from which the MCN originates. In agreement with that, the variation reported here would have been generated by a defect in the separation of the median nerve and the MCN, altering the course of the MCN and, therefore, the contact between the upper limb bud and its developing nerves. This could modify the typical cone growth sequence, explaining the innervation of the anterior compartment arm muscles (Mehta, 2009; Pacholczak et al., 2011).

In practical terms, the accessory heads in the BBM produce greater force in forearm flexion. However, a supernumerary muscle belly can also cause neurovascular compression of the median nerve, the MCN, or the brachial artery, which can produce neurological and vascular alterations, making it clinically relevant. In this regard, when the patient is resistant to treatment, it would be necessary a careful evaluation of the arm anterior compartment looking for possible muscle variations (Enix et al., 2021). This is more relevant in the Asian population, where the prevalence of accessory heads in the BBM reaches 35%, unlike the non-Asian population where it has been reported at 25% (Techataweewan et al., 2016).

Finally, the presence of a supernumerary head could affect the course and branching of the MCN (Kosugi et al., 1992), therefore, it is advisable to take into account the anatomical variations of the MCN when faced with findings of this type muscle variation.

CONCLUSION

The absence of MCN associated with the presence of one accessory head of the BBM is atypical. Even in that case, it is clinically relevant because it can generate compressive symptoms that could confuse the specialist performing the diagnostic evaluation, and also the one conducting the procedures on the arm, inducing iatrogenic actions. For this reason, it is recommended that specialists in the area (surgeons and traumatologists) be aware of this type of variation.

ACKNOWLEDGEMENTS

The authors sincerely thank those who donated their bodies to science so that anatomical research and teaching could be performed. Results from such research can potentially increase scientific knowledge and can improve patient care. Therefore, these donors and their families deserve our highest respect.

ETHICS APPROVAL AND CONSENT FOR PUBLICATION

The body was obtained through the Donation Program of the Faculty of Medicine at the Pontifical Catholic University of Chile (PUC), which complies fully with the World Medical Association's Declaration of Helsinki and national legal and ethical requirements. Consequently, the study was approved by the MED-UC Scientific Ethics Committee of the Pontifical Catholic University of Chile (No: 220304004).

REFERENCES

ABU-HIJLEH MF (2005) Three-headed biceps brachii muscle associated with duplicated musculocutaneous nerve. *Clin Anat,* 18(5): 376-379.

CHEVALLIER A, KIENY M, MAUGER A (1977) Limb-somite relationship: origin of the limb musculature. *J Embryol Exp Morphol*, 41: 245-258.

CHOI D, RODRÍGUEZ-NIEDENFÜHR M, VÁZQUEZ T, PARKIN I, SAÑUDO JR (2002) Patterns of connections between the musculocutaneous and median nerves in the axilla and arm. *Clin Anat*, 15(1): 11-17.

ENIX D, SCALI F, SUDKAMP K, KEATING R (2021) Supernumerary head of the biceps brachii muscle: An anatomic variant with clinical implications. *J Chiropr Med*, 20(1): 37-42.

FARFÁN E, ECHEVERRÍA M, INOSTROZA V, SCHNEEBERGER D, INZUNZA O (2020) Positional anomaly between the brachial plexus and the scalene muscles, concomitant with an anomalous path of the musculocutaneous nerve. Case report and clinical implication. *Int J Morphol,* 38(4): 845-852.

GÜMÜSBURUN E, ADIGÜZEL E (2000) A variation of the brachial plexus characterized by the absence of the musculocutaneous nerve: a case report. *Surg Radiol Anat,* 22(1): 63-65.

HUNTER D, ZDILLA M (2021) The absent musculocutaneous nerve: A systematic review. *Transl Res Anat*, 22: 100092.

KARDON G, HARFE BD, TABIN CJ (2003) A Tcf4-positive mesodermal population provides a prepattern for vertebrate limb muscle patterning. *Dev Cell*, 5(6): 937-944.

KAUR P, KUMAR R, JAIN A (2014) Variations in innervation of muscles in anterior compartment of arm-a cadaveric study. *J Clin Diagnostic Res,* 8(5): AC01-AC03.

KEIBEL F, MALL F (1912) *Manual of human embryology*. Lippincott Company, Philadelphia and London. pp 116-128.

KOSUGI K, SHIBATA S, YAMASHITA H (1992) Supernumerary head of biceps brachii and branching pattern of the musculocutaneus nerve in Japanese. *Surg Radiol Anat,* 14(2): 175-185.

LEE SE, JUNG C, AHN KY, NAM KI (2011) Bilateral asymmetric supernumerary heads of biceps brachii. *Anat Cell Biol*, 44(3): 238-240.

LEE SH, JEON JY, YOON SP (2014) A combined variation of the musculocutaneous nerve associated with a supernumerary head of the biceps brachii muscle. *Folia Morphol*, 73(3): 366-369.

LEWIS WH (1902) The development of the arm in man. *Am J Anat,* 1: 145-183.

MEHTA V, YADAV Y, ARORA J, KUMAR H, SURI RK, RATH G (2009) Clinico-embryological perspective of a rare accessory brachial muscle with possible musculocutaneous nerve compression. *Morphologie: Bull Assoc Anat*, 93(300): 27-29.

MURILLO-GONZÁLEZ J, DE LA CUADRA-BLANCO C, ARRÁEZ-AYBAR LA, HERRERA-LARA ME, MINUESA-ASENSIO A, MÉRIDA-VELASCO JR (2018) Development of the long head of the biceps brachial tendon: A possible explanation of the anatomical variations. *Ann Anat*, 218: 243-249.

PACHOLCZAK R, KLIMEK-PIOTROWSKA W, WALOCHA JA (2011) Absence of the musculocutaneous nerve associated with a supernumerary head of biceps brachii: a case report. *Surg Radiol Anat*, 33(6): 551-554.

PRASADA RAO, CHAUDHARY SC (2001) Absence of musculocutaneous nerve: two case reports. *Clin Anat,* 14(1): 31-35.

RODRÍGUEZ-NIEDENFÜHR M, VÁZQUEZ T, CHOI D, PARKIN I, SAÑUDO JR (2003) Supernumerary humeral heads of the biceps brachii muscle revisited. *Clin Anat,* 16(3): 197-203.

ROUVIÈRE H, DELMAS A (2005) *Anatomía humana descriptiva, topográfica y funcional. Tomo 3. Miembros.* 11th ed. Elsevier Masson, Barcelona, pp 196-198.

SALUJA S, DAS SS, KUMAR D, GOSWAMI P (2017) Bilateral three-headed biceps brachii muscle and its clinical implications. *Int J Appl Basic Med*, 7(4): 266-268.

STANDRING S (2016) *Gray's Anatomy. The anatomical basis of clinical practice.* 41th ed. Elsevier, UK, pp 824-825.

SZEWCZYK B, SANUDO JR, PODGÓRSKI M, ZIELINSKA N, PIRES MB, ARAGONÉS P, OLEWNIK Ł (2022) A proposal for a new classification of the supernumerary heads of the biceps brachii muscle. *Biomed Res Int,* 2022: 1510363.

TECHATAWEEWAN N, TOOMSAN Y, MANEENIN C, TUNGSRITHONG N, TAYLES N (2016) Supernumerary heads to biceps brachii muscle and Asian population history. *Homo*, 67(6): 484-491.

TESTUT L (1884) *Les anomalies musculaires chez l´homme, expliquées par l´anatomie comparée: leur importance en anthropologie.* Vol. 3. G. Masson Editeur, Paris, pp 371-395.

TOSNEY KW, LANDMESSER LT (1985) Growth cone morphology and trajectory in the lumbosacral region of the chick embryo. *J Neurosci*, 5(9): 2345-2358.

TUBBS RS, SHOJA MM, LOUKAS M (2016) *Bergman's comprehensive encyclopedia of human anatomic variation.* 1st ed. Wiley Blackwell, New Jersey, pp 293-294.

VENIERATOS D, ANAGNOSTOPOULOU S (1998) Classification of communications between the musculocutaneous and median nerves. *Clin Anat,* 11: 327-331.

WANG P, HSIEN YL, HO WY, LIU CC, HSIAO TH (2011) A rare case of multiple neuromuscular variations in the axilla and arm. *Kaohsiung J Med Sci*, 27(3): 121-124.

YAMAMOTO M, KOJYO U, YANAGISAWA N, MITOMO K, TAKAYAMA T, SAKIYAMA K, ABE S (2018) Morphology and relationships of the biceps brachii and brachialis with the musculocutaneous nerve. *Surg Radiol Anat,* 40(3): 303-311.

Effectiveness of mind mapping as compared to didactic lectures for teaching anatomy among first-year medical students - A randomized control study

Sunil Mathew[1], Stephen Dayal[2], Nachiket Shankar[3]

[1] Department of Anatomy, Saveetha Medical College and Hospital, Chennai, Tamil Nadu, India

[2] Department of Anatomy, St. John's Medical College, Bangalore, Karnataka, India

[3] Department of Anatomy and Medical Education, St. John's Medical College, Bangalore, Karnataka, India

SUMMARY

Several methods have been suggested to encourage greater student participation during lectures. Mind mapping is a learning tool that uses pictorial representations of concepts and their relationships. The objectives of this study were to compare the knowledge acquisition in anatomy and perceptions between didactic lectures and mind mapping among first year students at a medical college in India. First year undergraduate medical students (n=60 in one batch and n=149 in the next batch) were randomly divided into two groups which received either the mind-mapping intervention or a didactic lecture. Eight topics were covered in such a manner. After each topic, the groups crossed over and received the alternate intervention. Each intervention was followed by a ten-item single-best-response multiple-choice knowledge test. The perceptions of students were obtained using a questionnaire which had both quantitative and qualitative components. The data were summarized using means and standard deviations. Group differences were estimated using the independent sample T test. The mean scores on the multiple-choice-questions (MCQ) test were significantly higher after mind-mapping compared to didactic lectures in seven out of eight sessions. The perceptions of the students about mind mapping were largely positive, especially in relation to integration and interest. One drawback mentioned about the mind-mapping method was that it was relatively time-consuming. Mind mapping resulted in significantly greater knowledge acquisition as compared to didactic lectures, and was well received by the students. It has the potential to be used more widely in anatomy education.

Key words: Mind mapping – Didactic lectures – Medical students – Anatomy

INTRODUCTION

The first-year curriculum for undergraduate students in medical colleges in India includes the subjects of anatomy, physiology, and bio-

Corresponding author:
Nachiket Shankar, Professor. Department of Anatomy and Medical Education St. John's Medical College, Sarjapur Road, Bangalore – 560034 Karnataka, India. E-mail: nachiket.s@stjohns.in

Submitted: March 14, 2023. **Accepted:** May 26, 2023

https://doi.org/10.52083/NQMT1904

chemistry. Nearly half of the curricular time is devoted to anatomy (RGUHS, 2019). A wide variety of teaching and learning methods are employed for anatomy instruction, which includes 220 hours devoted to lectures (RGUHS, 2019). The challenges faced by students while learning anatomy include difficulties in the visualization of structures, the vast and often abstract nature of the information and the limited time available (Cheung et al., 2021a). Additionally, the approaches and resources utilized by students to learn anatomy are likely to influence the acquisition of the desired learning outcomes (Cheung et al., 2021b; Patera, 2021). There have been many attempts to modernize the teaching and learning of anatomy to make it more clinically relevant and participatory while simultaneously adapting to a decrease in the available time due to an ever-expanding curriculum (Ahmad et al., 2021; Bay and Ling, 2007; Johnson et al., 2012; Miller et al., 2002; Sugand et al., 2010).

Didactic lectures have been part of anatomy education in medical schools for many years (Sugand et al., 2010). Lectures have the potential for an efficient and effective method to convey information to students (Luscombe and Montgomery, 2016). A major drawback of the didactic lecture is its tendency to become a passive and monotonous monologue (Najmi, 1999). Several guidelines and strategies have been proposed to improve the learning outcomes from lectures (Leonardi, 2007; Regula, 2020; Richardson, 2008; Zakrajsek, 2018). Previous studies have shown that well-conducted lectures have a positive impact on student perceptions and knowledge gain (Demir et al., 2017; Reed et al., 2008; Zinski et al., 2017). There have been many attempts to transform potentially boring and content-heavy didactic lectures into active learning sessions by introducing meaningful activities during the lecture (Chimmalgi, 2019; Morton and Colbert-Getz, 2017; Shankar and Roopa, 2009).

Mind maps are pictorial representations of concepts and their relationships (D'Antoni et al., 2010). Buzan formally defined mind maps and introduced them to the world in the 1970s' (Buzan, 2018). The three essential features of a mind map are a central image, thick branches radiating from the central image and a single keyword or image placed on each branch (Buzan, 2018). Secondary and tertiary branches can then be added as the mind map develops (Buzan, 2018). Mind maps differ from concept maps in being more visual and less complex (Eppler, 2006). The utility of mapping techniques has been explained using the constructivist learning theory. Learners must initially use their pre-existing knowledge and sequentially build on it as they construct mind maps. Linkages between different images and keywords help to create integration networks within the brain for better retrieval and application of information. This enables deep learning as opposed to superficial rote learning (Pudelko et al., 2012). Mind maps have been used to facilitate learning in diverse settings (Amrita et al., 2017; Budd, 2004; Edwards and Cooper, 2010; Farrand et al., 2002; Kalyanasundaram et al., 2017; Merchie and Van Keer, 2012; Samsudin and Irwanto, 2021; Tungprapa, 2015). A meta-analysis of 52 studies conducted in 2014 suggests that the use of mind mapping improves academic achievement (Zhao, 2014). Mind maps have also shown to be helpful in teaching and learning anatomy (Abdolahi et al., 2011; Deshatty and Mokashi, 2013; Ghanbari et al., 2010; Ren and Jiang, 2019; Teli et al., 2020).

Traditional lectures are usually didactic, reinforcing the passive learning patterns to which students are used. There is a pressing need to transform the traditional lecture setting from a passive into a more active one. In the present study, mind mapping was introduced in the lecture setting to try and make learning more active and effective. It was hypothesized that the use of mind maps in lecture settings would improve knowledge acquisition compared to traditional lectures. The research objectives of the study were the following: 1) to compare the scores on an immediate post-session multiple-choice-question (MCQ) test obtained by 1st-year undergraduate medical students taught anatomy by traditional lectures or mind mapping; 2) to assess the perceptions of these students about the mind mapping method of learning and the traditional lecture.

MATERIAL AND METHODS

Study design and population

Approval from the institutional ethics committee was obtained prior to the study. All students who enrolled for the undergraduate medical course in the years 2015 and 2016 were included in the study. The number of students in the batches of 2015-16 and 2016-17 were 60 and 149 respectively. A universal sampling strategy was employed. Written informed consent to participate in the study was taken from the students.

This was a randomized-control cross-over study (Fig. 1). The students of each batch were randomized into two groups using an online random number generator. One of the investigators (SM) conducted all the mind-mapping sessions, while another investigator (SD) took all the didactic lectures. The lectures were selected based on the mutual convenience of the investigators. To ensure standardization of the content, the specific learning objectives of each session were defined in advance. Students allotted to the mind-map group (MMG) were taken to a classroom and administered the intervention by SM, which will be described in more detail later. Concurrently, the students in the didactic lecture group (DLG) were taken to another classroom and taught using a didactic lecture by SD. The groups crossed over after each session (Fig. 1). A total of eight topics were thus covered (Fig. 1). All the sessions were of a duration of one hour. The sessions were scheduled to ensure that there was at least a two-week gap between successive sessions.

The interventions

The schedule for the anatomy classes was made available to the students at least two weeks in advance. The dissections of the relevant regions were completed prior to the interventions to enable better comprehension. There were no specific instructions provided to the students regarding prior preparation before either intervention.

An introductory session on mind maps was taken by an SM for the entire batch of students before the actual intervention. During this session, the students were introduced to the concept of mind maps and to guidelines for their creation. These guidelines included those related to style, clarity, keywords, and visual elements (Fig. 2). For the mind-mapping session, the students were divided into groups of six. The students in each group were made to sit around in a circle. The mind-mapping session for the MMG started with

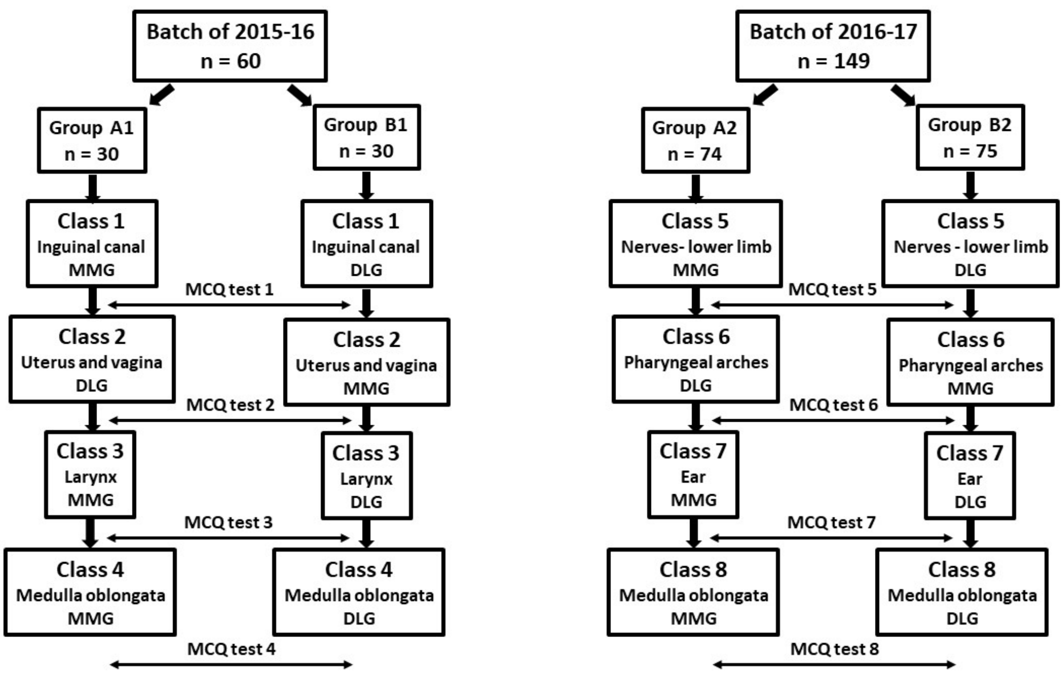

Fig. 1.- A schematic representation of the study design.

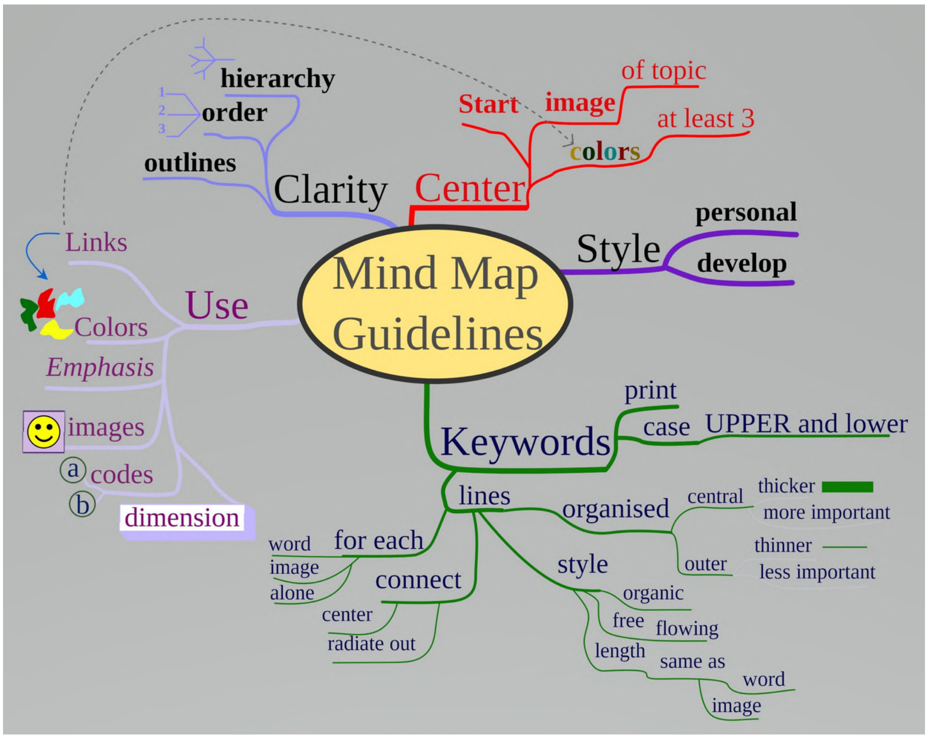

Fig. 2.- The mind map that was used as an example to demonstrate the guidelines for their creation (from Nicoguaro, CC BY-SA 3.0 <https://creativecommons.org/licenses/by-sa/3.0).

listing of the specific learning objectives for the topic by the teacher. It is important to note that the teacher did not explain the topic during the mind-mapping session. As mind map is a visual tool that encourages creative thinking and collaboration among students; we wanted to give the students the opportunity to explore the topic on their own. Each group was then asked to create mind maps on chart paper that was provided to them (Fig. 3). The students were free to refer to available resources such as textbooks and online resources. This exercise was conducted for half an hour. The next 20 minutes were spent discussing the mind maps and clarifying any doubts that the students had. The teacher's input on the topic was restricted to clarifying any doubts that the students had during the time allotted for discussion of the mind maps. The session ended with the administration of a 10-item MCQ test as described below.

The DLG simultaneously received a one-hour didactic lecture session on the same topic, followed by the administration of the MCQ test. The didactic lecture was taken using PowerPoint slides and a blackboard. The specific learning objectives were explicitly stated at the beginning of the didactic lectures as well. As an example, the specific learning objectives for the class on the major nerves of the lower limb are mentioned below.

Describe the femoral, obturator, sciatic, tibial, and common peroneal nerves under the following headings:

Origin

Root value

Course with important relations

Distribution with important branches

Termination

Applied aspects

The outcomes

At the end of each session, students in both groups were administered a 10-item MCQ test. Each item was of the single-best response type and contained four options. The MCQs' were based on the defined specific learning objectives for each session. The test items contained both factual and application-based questions. The first author created the MCQs based on best-practice guidelines, following which they were scrutinized by the other authors for any technical flaws or errors before administration to the students (Boland et

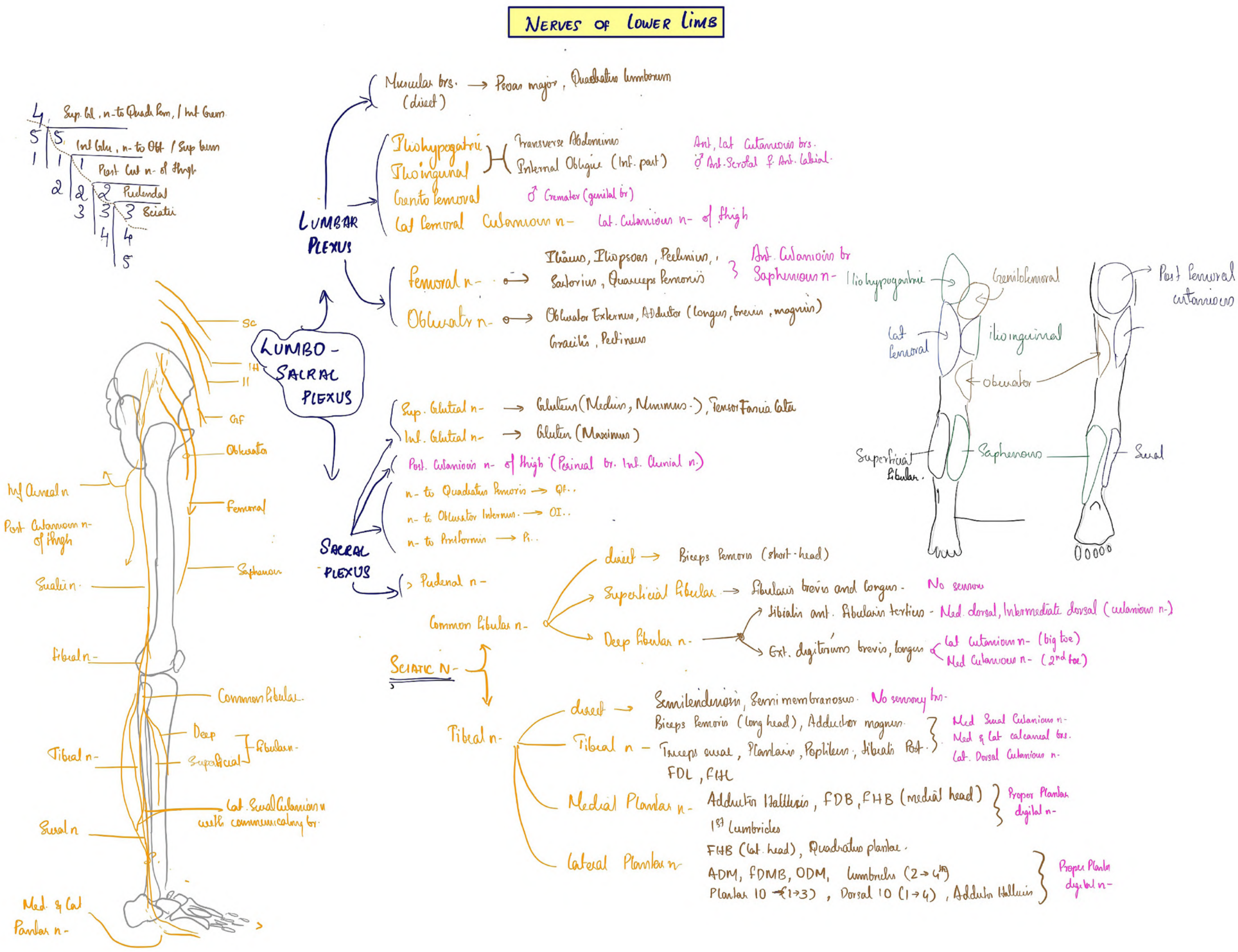

Fig. 3.- An example of a mind-map developed by a group of students for the class on the nerves of the lower limb.

al., 2010). The perceptions of the students about mind-mapping compared to traditional lectures were obtained using a questionnaire designed for the purpose (Table 2). The questionnaire contained 10 statements and two open-ended questions. The statements had to be responded to using a five-point Likert scale with higher scores indicating more favorable perceptions towards mind-mapping. The open-ended questions in the questionnaire were “What were the aspects of the mind mapping sessions that you enjoyed or benefitted from?” and “What were the aspects of the mind mapping sessions that you did not enjoy or benefit from?”.

Statistical analysis

The mean and standard deviation of the test scores and questionnaire item scores were calculated. Group differences were estimated using the independent sample T test. A P value of less than 0.05 was considered statistically significant. Version 16 of SPSS was used for statistical analysis. A thematic analysis was performed on responses to the open-ended questions in the questionnaire.

RESULTS

Table 1 shows the mean scores obtained by the two groups for the eight sessions. The mean scores obtained by the MMG were higher for all the eight sessions and significantly so for seven sessions. The responses to the statements in the perception questionnaire are summarized in Table 2. The mean scores for the items in the questionnaire suggest that students were overall positive about the role of mind mapping in facilitating learning as compared to lectures. The students felt that mind-mapping sessions were more interesting and helped them better integrate content. However, they were more equivocal about the perceived role of mind mapping in learning concepts and aiding exam preparation.

Table 1. Comparison of the mean MCQ test scores between the two groups.

CLASS OF 2015-16	MMG[a]	DLG[b]	P value
Lecture 1	n = 30 8.50 ± 0.95	n = 30 8.03 ± 0.9	0.07
Lecture 2	n = 27 8.60 ± 0.62	n = 30 8.04 ± 0.94	0.01*
Lecture 3	n = 29 8.68 ± 0.06	n = 30 7.86 ± 0.73	0.001*
Lecture 4	n = 29 8.72 ± 0.59	n = 29 8.06 ± 0.7	0.001*
CLASS OF 2016- 17	**MMG[a]**	**DLG[b]**	**P value**
Lecture 5	n = 71 8.23 ± 1.24	n = 71 7.75 ± 1.05	0.01*
Lecture 6	n = 70 8.43 ± 1.17	n = 71 7.97 ± 0.91	0.01*
Lecture 7	n = 72 8.24 ± 1.00	n = 72 7.86 ± 0.88	0.02*
Lecture 8	n = 70 8.19 ± 1.11	n = 72 7.83 ± 0.86	0.04*

n is the number of students who were present for each class; aMMG – mind-map group; bDLG – didactic lecture group; * indicates those results that were significant (P<0.05)

Table 2. Mean item scores on the perception questionnaire (n = 170).*

Sl. No.	Item	Mean ± SD
1.	Mind mapping helps me to recall facts better than lectures	3.29 ± 0.2
2.	Mind mapping helps in learning concepts better than traditional lectures	3.12 ± 0.1
3.	Mind mapping is more interesting than lectures	3.6 ± 0.9
4.	Mind mapping helps me to integrate information better than a lecture	3.6 ± 0.7
5.	Mind mapping helps me to prepare for the exams better than lectures	3.04 ± 0.1
6.	Mind mapping helps me to retain information longer than lectures	3.4 ± 0.1
7.	Mind mapping helps me to apply the information that I learn better than lectures	3.3 ± 0.1
8.	The mind mapping session can replace lectures	3.5 ± 1.2
9.	Mind mapping should continue for future batches	3.4 ± 1.1
10.	I would be willing to participate in more mind-mapping sessions	3.3 ± 1.0

*Likert scale: 1 - Strongly disagree; 2 - Disagree; 3 - Not sure; 4 - Agree; 5 - Strongly Agree

The responses to the open-ended questions revealed that students enjoyed the creativity and visual elements required in constructing mind maps. They also mentioned that mind maps helped to classify and consolidate information in a manner which helped them retain it and facilitate future revision. The other aspects appreciated by the students were the interactive nature and novelty of the mind map sessions. The most important drawback of the mind map sessions perceived by the students was the limited time that was available. Some of them felt that creating mind maps was complicated and therefore required more help from the teacher. The need for prior preparation before a mind map session was stated as one of its disadvantages. Inadequate coverage of topics during mind-mapping sessions was another concern of the students.

DISCUSSION

The results of the present study suggest that the creation of mind maps by students is at least as effective as didactic lectures for achieving learning outcomes in anatomy. Previous studies have shown that incorporating mind mapping as a study strategy improves learning (Amrita et al., 2017; D'Antoni AV et al., 2010; Deshatty and Mokashi, 2013; Farrand et al., 2002; Kalyanasundaram et al., 2017; Ying et al., 2017) Mind maps have also been successfully used to reinforce learning (Ashakiran et al., 2012). The use of mind maps by teachers during a lecture to present content appears to facilitate learning (Abdolahi et al., 2011; Duffy et al., 2015; Ghanbari et al., 2010; Johnson, 2014; Teli et al., 2020). In the current study, students in the MMG had to actively construct mind maps in the classroom as part of the intervention. A study in which students had to draw maps along with the teacher during histology lecture classes showed a significant improvement in the examination results as compared to the previous years (Kotzé and Mole, 2015). This method could be added to the ever-growing list active learning methods that can be used in the classroom to facilitate learning. This is especially pertinent in the Indian context where a competency-based curriculum has been introduced for undergraduate medical education in 2019 (Medical Council of India, 2019). One of the endeavors of this curriculum is to replace didactic teaching methods with active learning methods.

The positive perceptions of the students about mind mapping in this study are similar to other studies (Amrita et al., 2017; Ashakiran et al., 2012; Deshatty and Mokashi, 2013; Kalyanasundaram et al., 2017; Ren and Jiang, 2019; Teli et al., 2020). An important insight gained from this study is that adequate time needs to be given to students if mind maps are used in a lecture setting. This aspect has been also mentioned in previous studies where mapping has been used as a learning strategy (Pudelko et al., 2012). It is likely that the perception of inadequate coverage was because students were accustomed to attending didactic lectures in which the teacher acted as a knowledge provider. On the other hand, the mind map intervention in this study involved a more active, non-linear approach to learning which might have given rise to this perception (Petersen et al., 2020). The need for prior preparation was probably felt more acutely by the MMG, as this would have facilitated more meaningful group discussions and improvement in the quality of mind maps. However, this was not the case in the didactic lecture, where the content was provided by the teacher. A previous study has shown that learner engagement is positively associated with prior knowledge (Dong et al., 2020).

The present study provides a potential for the use of mind maps in the classroom. The perceptions of the students in this study suggests that meticulous planning is required to ensure that the maximum benefit is obtained from the use of mind maps in lecture settings. This includes the prior training of students, adequate content related preparation for the class, clear learning objectives, attention to logistic details such as grouping, access to material for map creation and provision of feedback. The time constraints involved in mind mapping may to a large extent be overcome if these measures are taken.

Concept maps have also been successfully used to improve learning in anatomy (Anand and Singel, 2017; Nicoara et al., 2020). A recent study in high-school children suggests that mind maps may be more effective than concept maps in a classroom setting (Samsudin and Irwanto, 2021). Mind maps are more visual, simpler to construct and allow greater room for creativity as compared to concept maps (Davies, 2011; Eppler, 2006). This perhaps makes them more suitable than concept maps for use in contexts like the present study. There may be several reasons why the MMG obtained significantly better test scores for seven out of the eight sessions. Mind maps are thought to assist in the integration of information and thereby promote deep learning (Davies, 2011). Visual representations of information are often easier to comprehend than text or audio (Davies, 2011). This is likely to be even more relevant for a subject like anatomy, which requires learners to visualize structures and morphological changes. The creation of mind maps requires active participation of students, thereby enhancing learning as compared to more passive methods like lectures (Davies, 2011; Pudelko et al., 2012). It has been suggested that the instructional design processes that accompany mapping interventions like working in groups and provision of feedback could be responsible for the positive learning outcomes rather than the mapping process itself (Pudelko et al., 2012). It should be emphasized that teachers who intend to use mind maps need to understand the metacognitive principles that underlie their creation.

This study has some limitations. The quality of the lecturers and facilitators may have influenced the outcome. The study was not teacher-randomized, as there were very few faculty members with sufficient expertise in mind-mapping techniques to conduct sessions for the MMG. In the MMG, students were divided into small groups to create mind maps. This may have had an influence on the test results rather than the creation of mind maps per se. Although the interval between two consecutive sessions was at least two weeks, it is possible that students in the MMG utilized mind maps during subsequent didactic lecture sessions and thereby contributed to a carryover effect. The topics selected for the intervention were based on mutual convenience of the two faculty members who administered the interventions (SM and SD). It was therefore difficult to standardize the difficulty levels of the topics. This may have also influenced the results.

CONCLUSIONS

The results of the present study suggest that the creation of mind maps by students is at least as effective as didactic lectures for achieving learning outcomes in anatomy. There is a need for rigorous clarification studies to understand the extent to which different aspects of mind mapping contribute to learning. More justification studies comparing mind maps and other mapping methods such as concept mapping are also needed. The use of software in the creation of digital mind maps and their role vis-à-vis conventionally drawn mind maps warrants further study as well.

ACKNOWLEDGMENTS

The authors wish to thank the students who participated in this study.

REFERENCES

ABDOLAHI M, JAVADNIA F, BAYAT PD, GHORBANI R., GHANBARI A, GHODOOSI, B (2011) Mind map teaching of gross anatomy is sex dependent. *Int J Morphol*, 29(1): 41-44.

AHMAD K, KHALEEQ T, HANIF U, AHMAD N (2021) Addressing the failures of undergraduate anatomy education: Dissecting the issue and innovating a solution. *Ann Med Surg,* 61: 81-84.

AMRITA RS, KRISHNA P, RISHMITHA R., MEGAN F (2017) Effect of mind-maps among medical students. *South-East Asian J Med Educ,* 11(2): 45-46.

ANAND MK, SINGEL TC (2017) Learning with concept maps versus classical lecture and demonstration methods in regards to gross anatomy of knee joint: A comparison. *Indian J Anat,* 6(1): 41-48.

ASHAKIRAN S, MURTHY NK, DEEPTHI R, PRABHAVATHI K, GANESH G (2012) Reinforcing learning of vitamins by mind maps. *J Res Med Educ Ethics,* 2(3): 194-199.

BAY BH, LING EA (2007) Teaching of anatomy in the new millennium. *Singapore Med J*, 48(3): 182-183.

BOLAND RJ, LESTER NA, WILLIAMS E (2010) Writing multiple-choice questions. *Acad Psychiatry,* 34(4): 310-316.

BUDD JW (2004) Mind maps as classroom exercises. *J Econ Educ,* 35(1): 35–46.

BUZAN T (2018) *Mind map mastery*. Watkins, London.

CHEUNG CC, BRIDGES SM, TIPOE GL (2021a) Why is anatomy difficult to learn? The implications for undergraduate medical curricula. *Anat Sci Educ,* 14(6): 752-763.

CHEUNG CC, YANG J, TIPOE GL (2021b) Multifactorial learning challenges in anatomy: What is the niche in current research? *Anat Sci Educ,* 14(6): 856-858.

CHIMMALGI M (2019) Interactive lecture in the dissection hall: Transforming passive lecture into a dynamic learning experience. *Anat Sci Educ,* 12(2): 191-199.

D'ANTONI AV, ZIPP GP, OLSON VG, CAHILL TF (2010) Does the mind map learning strategy facilitate information retrieval and critical thinking in medical students. *BMC Med Educ,* 10: 1-11.

DAVIES M (2011) Concept mapping, mind mapping and argument mapping: what are the differences and do they matter? *High Educ,* 62(3): 279-301.

DEMIR EA, TUTUK O, DOGAN H, EGELI D, TUMER C (2017) Lecture attendance improves success in medical physiology. *Adv Physiol Educ,* 41(4): 599-603.

DESHATTY DD, MOKASHI V (2013) Mind map as a learning tool in anatomy. *Int J Anat Res,* 1(2): 100-103.

DI LEONARDI BC (2007) Tips for facilitating learning: The lecture deserves some respect. *J Contin Educ Nurs,* 38(4): 154-161.

DONG A, JONG MS, KING RB (2020) How does prior knowledge influence learning engagement? The mediating roles of cognitive load and help-seeking. *Front Psychol,* 11: 591203.

DUFFY RM, GUERANDEL A, CASEY P, MALONE K, KELLY BD (2015) Experiences of using Prezi in psychiatry teaching. *Acad Psychiatry,* 39(6): 615-619.

EDWARDS S, COOPER N (2010) Mind mapping as a teaching resource. *Clin Teach*, 7: 236-239.

EPPLER MJ (2006) A comparison between concept maps, mind maps, conceptual diagrams, and visual metaphors as complementary tools for knowledge construction and sharing. *Inf Vis*, 5(3): 202-210.

FARRAND P, HUSSAIN F, HENNESSY E (2002) The efficacy of the 'mind map' study technique. *Med Educ,* 36: 426-431.

GHANBARI A, JAVADNIA F, ABDOLAHI M (2010) Teaching of gross anatomy for students of medicine by mind map-based PowerPoint slides. *Med Teach,* 32(3): 272.

JOHNSON EO, CHARCHANTI AV, TROUPIS TG (2012) Modernization of an anatomy class: From conceptualization to implementation. A case for integrated multimodal-multidisciplinary teaching. *Anat Sci Educ,* 5(6): 354-366.

JOHNSON LR (2014) Using mind maps to teach medical students. *Med Educ,* 48(11): 1124-1125.

KALYANASUNDARAM M, ABRAHAM S, RAMACHANDRAN D, JAYASEELAN V, BAZROY J, SINGH Z, PURTY A (2017) Effectiveness of mind mapping technique in information retrieval among medical college students in Puducherry - A pilot study. *Indian J Community Med*, 42(1): 19-23.

KOTZÉ SH, MOLE CG (2015) Making large class basic histology lectures more interactive: The use of draw-along mapping techniques and associated educational activities. *Anat Sci Educ,* 8(5): 463-470.

LUSCOMBE C, MONTGOMERY J (2016) Exploring medical student learning in the large group teaching environment: Examining current practice to inform curricular development. *BMC Med Educ,* 16(1): 1-9.

MEDICAL COUNCIL OF INDIA (2019) *Regulations on graduate medical education (amendment)*.

MERCHIE E, VAN KEER H (2012) Spontaneous mind map use and learning from texts: The role of instruction and student characteristics. *Procedia - Soc Behav Sci,* 69: 1387-1394.

MILLER SA, PERROTTI W, SILVERTHORN DU, DALLEY AF, RAREY KE (2002) From college to clinic: Reasoning over memorization is key for understanding anatomy. *Anat Rec,* 269(2): 69-80.

MORTON DA, COLBERT-GETZ JM (2017) Measuring the impact of the flipped anatomy classroom: The importance of categorizing an assessment by Bloom's taxonomy. *Anat Sci Educ,* 10(2): 170-175.

NAJMI RS (1999) Lecture as a mode of instruction in undergraduate medical education. *J Pak Med Assoc,* 49(2): 30-33.

NICOARA SM, SZAMOSKOZI SE, MITREA DA, LEUCUTA DC (2020) Concept mapping, an effective tool for long-term memorization of anatomy - a quasi-experimental research carried out among 1st year general medicine students. *Eur J Investig Heal Psychol Educ,* 10(1): 530-543.

PATERA E (2021) Is there a correlation between how medical students study and prepare for anatomy and the reasons why they find anatomy difficult? *Anat Sci Educ,* 14(6): 853-855.

PETERSEN CI, BAEPLER P, BEITZ A, CHING P, GORMAN KS, NEUDAUER CL, ROZAITIS W, WALKER J D, WINGERT D (2020) The tyranny of content: "Content Coverage" as a barrier to evidence-based teaching approaches and ways to overcome it. *CBE Life Sci Educ.*19(2):ar17.

PUDELKO B, YOUNG M, VINCENT-LAMARRE P, CHARLIN B (2012) Mapping as a learning strategy in health professions education: A critical analysis. *Med Educ,* 46(12): 1215-1225.

REED DN, LITTMAN TA, ANDERSON CI, DIRANI GR, GAUVIN JM, APELGREN KN, SLOMSKI CA (2008) What is an hour-lecture worth? *Am J Surg,* 195(3): 379-381.

REGULA J (2020) How to prepare educational lecture: EAGEN 50 years of experience. *Dig Dis,* 38(2): 100-103.

REN Y, JIANG X (2019) A mind map teaching mode for sports anatomy based on 3D body. *Int J Emerg Technol Learn,* 14(10): 4-17.

RGUHS (2019) *Revised ordinance governing MBBS degree course and curriculum of phase I subjects - November 2019*.

RICHARDSON D (2008) Don't dump the didactic lecture; fix it. *Adv Physiol Educ,* 32(1): 23-24.

SAMSUDIN A, IRWANTO I (2021) Which is more effective, a mind map or a concept map learning strategy? *Cakrawala Pendidik,* 40(2): 520-531.

SHANKAR N, ROOPA R (2009) Evaluation of a modified team-based learning method for teaching general embryology to 1st year medical graduate students. *Indian J Med Sci*, 63(1): 4-12.

SUGAND K, ABRAHAMS P, KHURANA A (2010) The anatomy of anatomy: A review for its modernization. *Anat Sci Educ,* 3(2): 83-93.

TELI C, KATE N, KADLIMATTI HS (2020) Comparison of mind mapping and didactic instructional method in learning neuroanatomy for first MBBS students. *Indian J Clin Anat Physiol,* 7(2): 243-246.

TUNGPRAPA T (2015) Effect of using the electronic mind map in the educational research methodology course for master-degree students in the faculty of education. *Int J Inf Educ Technol*, 5(11): 803-807.

YING G, JIANPING X, HAIYUN L, XIA L, JIANYU Y, QUN X, JIANYUN Y (2017) Using mind maps to improve medical student performance in a pharmacology course at Kunming Medical University. *J Coll Physicians Surg Pakistan,* 27(7): 404-408.

ZAKRAJSEK T (2018) Reframing the lecture versus active learning debate: Suggestions for a new way forward. *Educ Heal Prof,* 1: 1-3.

ZHAO G (2014) The effect of mind mapping on teaching and learning: A meta-analysis. *Stand J Educ Res Essay,* 2(1): 17-31.

ZINSKI A, BLACKWELL KTCPW, BELUE FM, BROOKS WS (2017) Is lecture dead? A preliminary study of medical students' evaluation of teaching methods in the preclinical curriculum. *Int J Med Educ,* 8: 326-333.

Macroscopic study of the collection of human fetuses from Granada University

Kevin Doello[1,3,4], Cristina Mesas[2,3,4], Francisco Quiñonero[2,3,4], Gloria Perazzoli[2,3,4], Consolación Melguizo[2,3,4], Miguel Guirao[2], Jose Prados[2,3,4]

[1] *Medical Oncology Service, Virgen de las Nieves Hospital, 18014 Granada, Spain*

[2] *Department of Anatomy and Embryology, University of Granada, Granada 18071, Spain*

[3] *Institute of Biopathology and Regenerative Medicine (IBIMER), Biomedical Research Center (CIBM), Granada 18100, Spain*

[4] *Instituto Biosanitario de Granada, (ibs.GRANADA), SAS-Universidad de Granada, Granada 18012, Spain*

SUMMARY

The anatomical collections of fetuses are a valuable element of study and research in universities. At the University of Granada, the Department of Human Anatomy and Embryology has a collection of 283 fetuses. The purpose of this article has been to carry out an exhaustive study on these fetuses to present data related to the malformations they presented. Regarding the results, it is worth noting the presence of a higher frequency of aborted fetuses between 4.5 and 6 months of development and the presence of macroscopically evident malformations in 56% of them. In conclusion, this study assesses the usefulness for teaching and research of this anatomical material and the results provide data of interest on fetal development and the etiology of spontaneous abortions.

Key words: Fetuses – Abortions – Malformations – Anatomical collections

INTRODUCTION

Fetal development is a complex process that could be divided into three periods (trimesters), each with distinct developmental milestones. During the first trimester, the fertilized egg undergoes rapid cell division and differentiation, leading to the formation of the major organs and systems of the body. By the end of the first trimester, the fetus is about 3 inches long and weighs around 1 ounce. In the second and third trimesters, the fetus undergoes further growth and development. The skeleton begins to harden, and the nervous system becomes more advanced. During the third trimester, the fetus gains the most weight and continues to develop its organ systems. By the time of birth, the average fetus is about 20 inches long and weighs around 7.5 pounds. Fetal development is a critical period that lays the foundation for a person's health and well-being throughout their life (Blencowe et al., 2012; Filippi et al., 2023; O'Rahilly and Müller, 2010).

To study fetal development, anatomical collections of human fetuses have been created in many medical schools and faculties around the world. These collections provide invaluable resources for researchers, educators, and medical professionals who seek to better understand human development and improve patient care. The value of

Corresponding author:
José Prados. Institute of Biopathology and Regenerative Medicine (IBIMER), Biomedical Research Centre (CIBM), University of Granada, Spain. Phone: +34-958249322; Fax: +34-958246296. E-mail: jcprados@ugr.es

Submitted: May 25, 2023. **Accepted:** June 12, 2023

https://doi.org/10.52083/NFXY2293

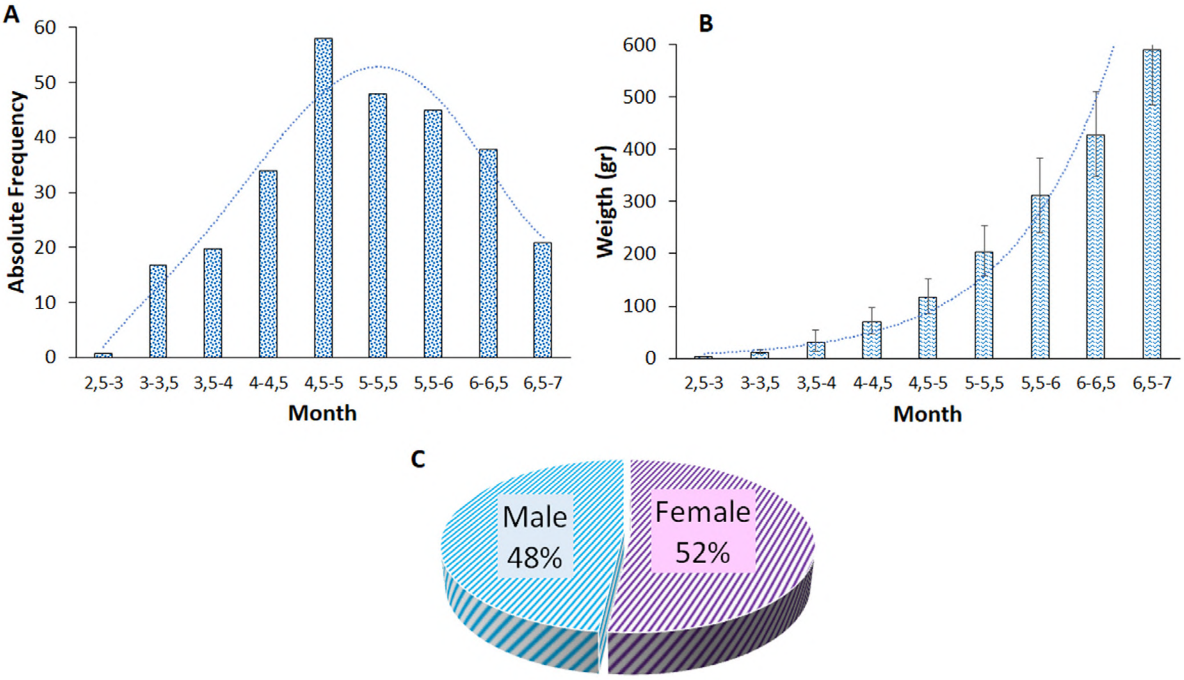

Fig. 1.- Abortive fetuses of the Granada University. **A**. Distribution of abortive fetuses by week of gestation. **B.** Evolution of weight (gr) in abortive fetuses by week of gestation. **C.** Sex distribution in abortive fetuses by week of gestation.

fetal anatomical collections lies in their ability to provide a comprehensive view of human development, from the early embryonic stages to full-term fetuses. By examining these specimens, researchers and educators can identify the normal and abnormal features of fetal anatomy and understand the complex interactions that occur during development. Additionally, these collections serve as a valuable resource for training future medical professionals, allowing them to gain hands-on experience in human anatomy and pathology (Knoeff, 2015; Kosenko et al., 2022). Among the most rep-

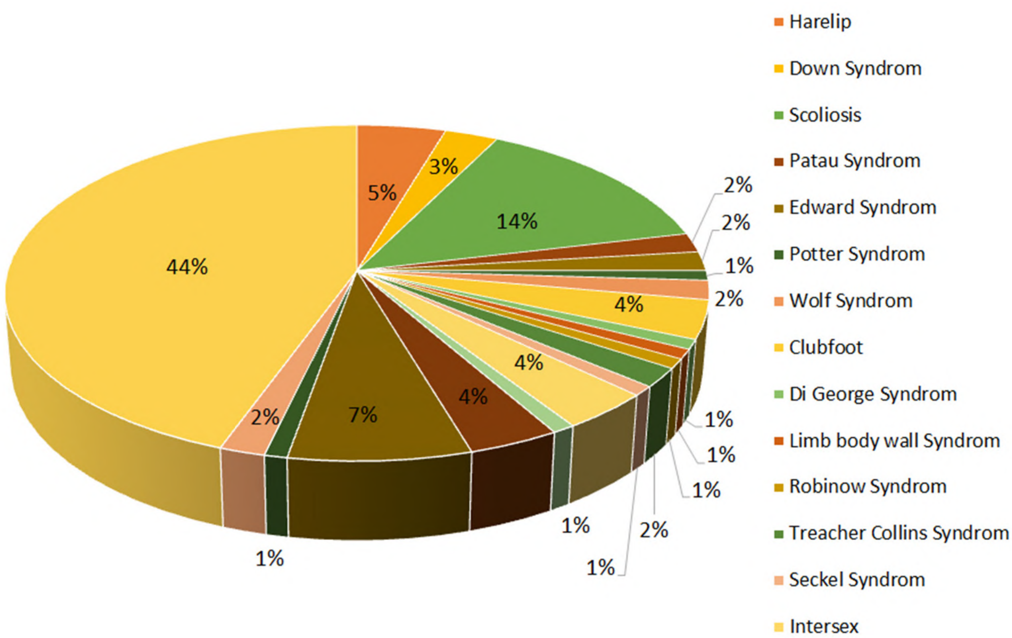

Fig. 2.- Description of the malformation in the collection of fetuses from the University of Granada.

resentative collections are the Carnegie Collection (Carnegie Institution) of Washington, which includes more than 15,000 specimens from early embryos to term fetuses, and the Kyoto Collection, which contains more than 6,000 specimens and is known for its extensive documentation of abnormal fetuses (Brown, 1987; Spradling, 1997; Tanaka et al., 2020; Yamaguchi and Yamada, 2018).

Our main was to carry out a descriptive study of the collection of human fetuses from the Department of Anatomy and Embryology of the Granada University.

MATERIALS AND METHODS

Human Fetuses (n=283) from the collection of the Department of Human Anatomy and Embryology of the University of Granada were classified by weight at the time of acquisition, apex-coccyx (CV) distance, and apex-tail distance. From the VC distance we determine the approximate gestational age. Likewise, the existence of malformative macroscopic features was analyzed. With all these data, a descriptive statistical study was carried out. This research has been approved by the ethics committee of the Faculty of Medicine of Granada (3440/CEIH/2023).

RESULTS

Regarding the distribution of abortive fetuses, it should be noted that their highest frequency was concentrated between 4.5 and 6 months of gestation (18 and 24 weeks), decreasing slowly and following an inverse gamma distribution (Fig. 1A). Weight, as expected, evolved exponentially with increasing gestational age (Fig. 1 B). Slightly more female (52%) than male fetuses were observed, although these differences were likely due to sample-specific variability (Fig. 1C). According to the detected malformations, the most frequent was to find fetuses with hypertelorism and micrognathia not associated with any specific syndrome and scoliosis. Malformations compatible with some chromosomal syndromes and other congenital malformations such as Down syndrome, Patau, Edwards, Wolf, Potter, Di George, Robinow, Treacher-Collins syndrome or intersex anomalies were detected. A large proportion of fetuses (44%) did not present clear macroscopic malformations (Figs. 2 and 3).

Fig. 3.- Examples of congenital malformations found in the collection of human fetuses from the University of Granada. **A**. Wolf-Hirschorn syndrome (head in Greek helmet). **B**. Patau syndrome (cleft lip, genital malformations, short sternum). **C**. Potter syndrome (periorbital edema, mycorgnathia, and low-set malformed ears). **D**. VACTERL (anal atresia and genital malformations). **E**. Down syndrome (broad nasal root, hypertelorism, and macroglossia). **F**. Robinow syndrome (achondroplasic cranial changes, hypertelorism, and characteristic nose). **G**. Scoliosis. **H**. Anophthalmia. **I**. Edwards syndrome (rocking chair feet, hypertelosimus, retrognathia, and auricular malformations). **J**. Limb body Wall syndrome (scoliosis and gastroschisis). **K**. Dolichocephaly. **L**. Treacher Collins syndrome (characteristic fascia with large oral cleft).

DISCUSSION

The most frequent malformations found in human fetuses aborted between 3 and 6 months of development include central nervous system defects, such as anencephaly and hydrocephalus, and chromosomal abnormalities, such as Down syndrome. Other malformations found in fetuses at this stage include heart defects, skeletal abnormalities, and gastrointestinal defects (Naeye, 1983; Roets et al., 2023). In our collection, the most frequently malformations were fetuses with characteristics of hypertelorism and micrognathia not attributable to specific syndromes and scoliosis. In addition, to a lesser extent, fetuses with anomalies such as Down syndrome, Patau, Edwards, Wolf, Potter, Di George, Robinow, Treacher-Collins syndrome, or intersex anomalies were observed. Mora-Alferez et al., (2016) in a study on abortive human fetuses and chromosomal malformations, indicated that the most frequent chromosomal anomalies in spontaneously aborted fetuses were trisomies 16, 22 and 9. These are anomalies mostly in internal organs and without clear distinctive macroscopic features. Thus, they probably correspond to fetuses that have been classified as hypertelorism and micrognathia without a clear syndromic correspondence. In addition, these malformations have been determined in fetuses older than six months, so it would be very likely to find younger fetuses with the chromosomal alterations described by Mora-Alferez et al., (2016). However, this study was very difficult at the macroscopic level with fetuses under six months.

On the other hand, no human fetuses younger than 3 months were found in our collection, probably because abortions at this stage are usually spontaneous and the embryos are extracted undetectable or by curettage. Almost 70% of spontaneous abortions occur before 8 weeks of gestation (Alves and Rapp, 2023). In our case, the human fetuses showed a curious distribution as spontaneous fetal abortions increased towards week 18, being higher between weeks 18 and 24. Interestingly, they followed an inverse gamma distribution. This distribution is similar to that described in infectious disease susceptibility, suggesting the infection as the cause of the abortion at this stage. In addition, 56% of the fetuses also had signs of malformations that would make them more susceptible to these infectious factors. It is known that infections can occur at any stage of fetal development, but the highest incidence occurs at the first and second trimesters. During this period, the fetus is particularly susceptible to infection due to the immaturity of its immune system and the high rate of cell division and differentiation (Kollmann et al., 2017; Limperopoulos et al., 2002; Marbán-Castro et al., 2021; Plourde and Bloch, 2016). Several factors can increase the risk of infections, including maternal age, maternal immune status, and exposure to environmental pathogens. Maternal infections, such as urinary tract infections, can also increase this risk. In addition, certain lifestyle factors, such as smoking and alcohol consumption, may also increase the risk of infections (Pascoal et al., 2023; Wiegersma et al., 2023). In addition, malformed human fetuses are at increased risk of developing infections due to their weakened immune systems and compromised barrier function. Studies have shown that fetuses with malformations have a higher incidence of infections such as cytomegalovirus, rubella, toxoplasmosis, and syphilis. Furthermore, human fetuses with chromosomal abnormalities are also at increased risk of infections, as their immune systems are not fully developed (Fitzpatrick et al., 2022; Marbán-Castro et al., 2021; Wang et al., 2019).

CONCLUSION

In conclusion, this study highlights the interest of human fetus material for teaching and research purposes, and provides new data regarding fetal development and the etiology of abortions in the fetal stage, highlighting the absolute frequency per week, the possible etiologies, and the presence of macroscopic malformative anomalies in 56% of them.

ACKNOWLEDGEMENTS

The authors sincerely thank those who donated their bodies to science so that anatomical research and teaching could be performed. Results from such research can potentially increase scientific knowledge and can improve patient care. Therefore, these donors and their families deserve our highest respect.

REFERENCES

ALVES C, RAPP A (2023) Spontaneous Abortion. In: *StatPearls*. Treasure Island (FL): StatPearls Publishing. http://www.ncbi.nlm.nih.gov/books/NBK560521/

BLENCOWE H, COUSENS S, OESTERGAARD MZ, CHOU D, MOLLER AB, NARWAL R, ADLER A, VERA C, SAY L, LAWN JE (2012) National, regional, and worldwide estimates of preterm birth rates in the year 2010 with time trends since 1990 for selected countries: A systematic analysis and implications. *Lancet*, 379(9832): 2162-2172.

BROWN DD (1987) The Department of Embryology of the Carnegie Institution of Washington. *Bioessays*, 6(2): 92-96.

FILIPPI L, SCARAMUZZO RT, PASCARELLA F, PINI A, MORGANTI R, CAMMALLERI M, BAGNOLI P, CIANTELLI M (2023) Fetal oxygenation in the last weeks of pregnancy evaluated through the umbilical cord blood gas analysis. *Front Pediatr*, 11: 1140021.

FITZPATRICK D, HOLMES NE, HUI L (2022) A systematic review of maternal TORCH serology as a screen for suspected fetal infection. *Prenat Diagn*, 42(1): 87-96.

KNOEFF R (2015) Touching anatomy: On the handling of preparations in the anatomical cabinets of Frederik Ruysch (1638-1731). *Stud Hist Philos Biol Biomed Sci*, 49: 32-44.

KOLLMANN TR, KAMPMANN B, MAZMANIAN SK, MARCHANT A, LEVY O (2017) Protecting the Newborn and Young Infant from Infectious Diseases: Lessons from Immune Ontogeny. *Immunity*, 46(3): 350-363.

KOSENKO O, STEINICKE C, KIELSTEIN H, STEGER F (2022) Fetal development in anatomical preparations of Ruysch and the Meckels in comparison. *Int J Environ Res Public Health*, 19(22): 14896.

LIMPEROPOULOS C, MAJNEMER A, SHEVELL MI, ROHLICEK C, ROSENBLATT B, TCHERVENKOV C, DARWISH HZ (2002) Predictors of developmental disabilities after open heart surgery in young children with congenital heart defects. *J Pediatr*, 141(1): 51-58.

MARBÁN-CASTRO E, GONCÉ A, FUMADÓ V, ROMERO-ACEVEDO L, BARDAJÍ A (2021) Zika virus infection in pregnant women and their children: A review. *Eur J Obstet Gynecol*, 265: 162-168.

MORA-ALFEREZ AP, PAREDES D, RODRÍGUEZ O, QUISPE E, CHAVESTA F, DE ZIGHELBOIM EK, DE MICHELENA M (2016) Anomalías cromosómicas en abortos espontáneos. *Rev Per Ginecol Obstet*, 62(2): 141-151.

NAEYE RL (1983) Maternal age, obstetric complications, and the outcome of pregnancy. *Obstet Gynecol*, 61(2): 210-216.

O'RAHILLY R, MÜLLER F (2010) Developmental stages in human embryos: Revised and new measurements. *Cells Tissues Organs*, 192(2): 73-84.

PASCOAL LB, CARELLOS EVM, TARABAI BHM, VIEIRA CC, REZENDE LG, SALGADO BSF, DE CASTRO ROMANELLI RM (2023) Maternal and perinatal risk factors associated with congenital syphilis. *Trop Med Int Health,* 28(6): 442-453.

PLOURDE AR, BLOCH EM (2016) A literature review of Zika Virus. *Emerg Infect Dis*, 22(7): 1185-1192.

ROETS E, BEERNAERT K, CHAMBAERE K, DELIENS L, VAN BERKEL K, DE CATTE L, VANHAESEBROUCK S, ROELENS K, DOMBRECHT L (2023) Pregnancy termination at viable stage in daily clinical practice: A nationwide mortality follow-back study in Flanders, Belgium. *Prenat Diagn,* 43(6):781-791.

SPRADLING AC (1997) The Carnegie Institution of Washington, Department of Embryology. *Mol Med,* 3(7): 417-419.

TANAKA S, SAKAMOTO R, KANAHASHI T, YAMADA S, IMAI H, YONEYAMA A, TAKAKUWA T (2020) Shoulder girdle formation and positioning during embryonic and early fetal human development. *PloS One*, 15(9): e0238225.

WANG Y, LI S, MA N, ZHANG Q, WANG H, CUI J AND WANG S (2019) The association of ToRCH infection and congenital malformations: A prospective study in China. *Eur J Obstet Gynecol,* 240: 336-340.

WIEGERSMA AM, BOOTS A, LANGENDAM MW, LIMPENS J, SHENKIN SD, KOROSI A, ROSEBOOM TJ, DE ROOIJ SR (2023) Do prenatal factors shape the risk for dementia?: A systematic review of the epidemiological evidence for the prenatal origins of dementia. *Soc Psychiatry Psychiatr Epidemiol,* doi: 10.1007/s00127-023-02471-7.

YAMAGUCHI Y, YAMADA S (2018) The Kyoto collection of human embryos and fetuses: History and recent advancements in modern methods. *Cells Tissues Organs*, 205(5-6): 314-319.

Academic benefits of using cadaveric material in health sciences education: Report of an experience

Emilio Farfán[1,2], Oscar Inzunza[1,2]

[1] Departamento de Anatomía, Escuela de Medicina, Pontificia Universidad Católica de Chile, Santiago, Chile
[2] Morpho-Clinical Research Lab, Escuela de Medicina, Pontificia Universidad Católica de Chile, Santiago, Chile

SUMMARY

The use of cadaveric material to study anatomy has been curbed by the requirements for its maintenance and use and by the anatomical contents in medical curricula, negatively affecting students. This study aimed to demonstrate the reported benefits of using cadaveric material in teaching anatomy. The benefits were categorized into 3 groups: audiovisual resources, teaching, and institutional cooperation and research. 1) Audiovisual resources: 2234 photographs, 256 videos, 16 websites, 28 anatomical replicas using 3D printing, the Laminario Anatómico, and a gymkhana online simulator. Students were surveyed about their perception and use of these resources. Their responses indicate they are considered useful tools for teaching and learning. 2) Teaching: all the practical activities with cadaveric material are comprehensively undertaken in different formats every year. 15 undergraduate programs have prosection activities, 9 graduate degree programs and 4 post-graduate qualification programs have prosection and dissection activities, and 22 graduate degree programs have cadaveric surgical training. 3) Institutional cooperation and research: 2 doctoral theses, 1 master's thesis, and 37 publications. The use of cadaveric material is a contribution that strengthens all aspects of academia in the development of both instructors and institutions.

Key words: Cadaveric material – Academic benefits – Teaching – Anatomy

INTRODUCTION

It is accepted that the use of cadaveric material for teaching anatomy is the only opportunity to empirically confirm the location of the organs and body systems (Inzunza, 2008; Sañudo et al., 2021), despite the fact that three-dimensional (3D) visualization technologies and anatomical replicas are gaining ground due to their ever-increasing realism (Hackett and Proctor, 2016; Yammine and Violato, 2016; Kausar et al., 2020). It is known that multidimensional learning activities that relate cadaveric anatomy to living anatomy ensure the participation and enthusiasm of the learner (Pather, 2015; Abdel et al., 2017; Sadeesh et al., 2021). Although this methodology is old, it confronts the student with visual keys that are

Corresponding author:
Dr. Emilio Farfán Cabello. Departamento de Anatomía, Escuela de Medicina, Pontificia Universidad Católica de Chile, Santiago de Chile, Av. Libertador Bernardo O'Higgins #340. Phone: +56223542189. E-mail: efarfanc@uc.cl

Submitted: February 20, 2023. **Accepted:** June 16, 2023

https://doi.org/10.52083/XYGX8978

highly relevant to learning these subjects (Guillot et al., 2007; Dissabandara et al., 2015). However, the use of cadaveric material for teaching in this discipline has been reduced in the curricula, essentially due to time limitations, instructors' training, and the resources needed to teach with corpses, which has decreased the overall level of applied anatomical knowledge in the youngest generations (Leung et al., 2006; Standring, 2009; Estai and Bunt, 2016). This puts the transmission of fundamental knowledge, values, and competences at risk (Rehkämper, 2016; Chipamaunga and Prozesky, 2019). This is worrying: the data show that students in those medical schools that discontinued anatomical work with cadaveric material have been seriously hindered in their clinical abilities and skills (Rizzolo and Stewart, 2006; Stephens et al., 2021). Coincidently, malpractice suits have steadily increased over time (Li et al., 2018).

There are 24 recognized medical schools in Chile with a minimum program duration of 6 years and a maximum of 7. The minimum number of semesters with anatomy courses is 2, with a maximum of 4. Tiznado-Matzner et al. (2019) collected data on 12 anatomy laboratories in Chilean universities, of which just three claimed to have human cadaveric specimens to fully engage with in practical activities. This exposes the difficulties that institutions have in accessing cadaveric material, which implies investments in infrastructure and training of instructors and technicians in using cadaveric preparations for morphological study (Gnanakumar et al., 2018; Singal, 2022). It is understood that the lack of this material poses a disadvantage in accessing knowledge founded on anatomical reality (Farfán et al., 2021). In addition, it must be recognized that there has been a progressive reduction in experts in morphological sciences.

This study aimed to expand on the reported academic benefits of using cadaveric material for audiovisual resources, teaching, and institutional cooperation and research.

MATERIALS AND METHODS

A descriptive study was conducted during the year 2022. All the resources and activities developed from using cadaveric material were organized to analyze the anatomical subjects, separating them into three categories: 1. Audiovisual resources: all the audiovisual resources made from cadaveric material were compiled; 2. Teaching: all undergraduate and postgraduate training programs were organized, and the type of teaching they received was described; 3. Institutional cooperation and research: the publications and institutional affiliations created from cadaveric material were compiled.

Additionally, to know the opinion and ascertain the extent to which the audiovisual resources gen-

Table 1. Audiovisual resources produced from cadaveric material.

Category	Photos	Videos	Websites	Laminario Anatómico	Gymkhana Simulator	3D Printing
Head	235	52	1	18	1	1
Central Nervous System	50	12	1	14	1	0
Neck	50	23	1	12	1	2
Thorax	272	52	1	13	1	7
Abdomen	153	37	1	16	1	9
Pelvis	61	22	1	11	1	5
Back	50	7	1	23	1	0
Upper Limb	80	27	1	8	1	2
Lower Limb	90	24	1	8	1	2
Descriptive Anatomy	1043	0	7	55	7	0
Sectional Anatomy	150	0	0	79	0	0
Total	**2234**	**256**	**16**	**257**	**16**	**28**

erated are used, in addition to student preferences and their opportunities to access this material (Table 1), at the end of the second semester of 2021, an online survey in Likert format was sent (Google Forms; Google LLC, Mountain View, California, USA) to all the undergraduate Medical, Dentistry, and Physiotherapy students in the Department of Anatomy at the Pontificia Universidad Católica de Chile who used all these resources. The survey included 16 selection questions about the use of audiovisual resources. 284 first- and second-year students responded, 55% men and 45% women, whose average age was 18 years, and represented 73% of the population, obtaining a homogeneous response rate among the different courses.

The authors confirm that every effort was made to comply with all local and international ethical guidelines and laws concerning the use of human cadaveric donors in anatomical research. After authorization from the appropriate ethics review board, 30 bodies were obtained through the donation program in the Pontificia Universidad Católica de Chile (PUC) Faculty of Medicine. This donation program fully complies with the World Medical Association's Declaration of Helsinki and national legal and ethical requirements, was approved by the CEC (Comité Ético Científico) MED-UC of the Pontificia Universidad Católica de Chile (No: 190115002).

Data and statistical analysis

The data collected were organized in Microsoft® Excel tables for MacOS (v.16.43, Microsoft® Corporation) and then exported to GraphPad Prism 9.0 for MacOS (v9.1.0. GraphPad Software, La Jolla, California USA) to generate descriptive statistics.

RESULTS

Audiovisual resources

Photographs: A registry of 2234 photos of dissections carried out on cadaveric preparations (Fig. 1A); 3D printing replicas: 28 replicas of cross sections digitized and printed using 3D technology (Fig. 1B); Websites: 16 websites with original

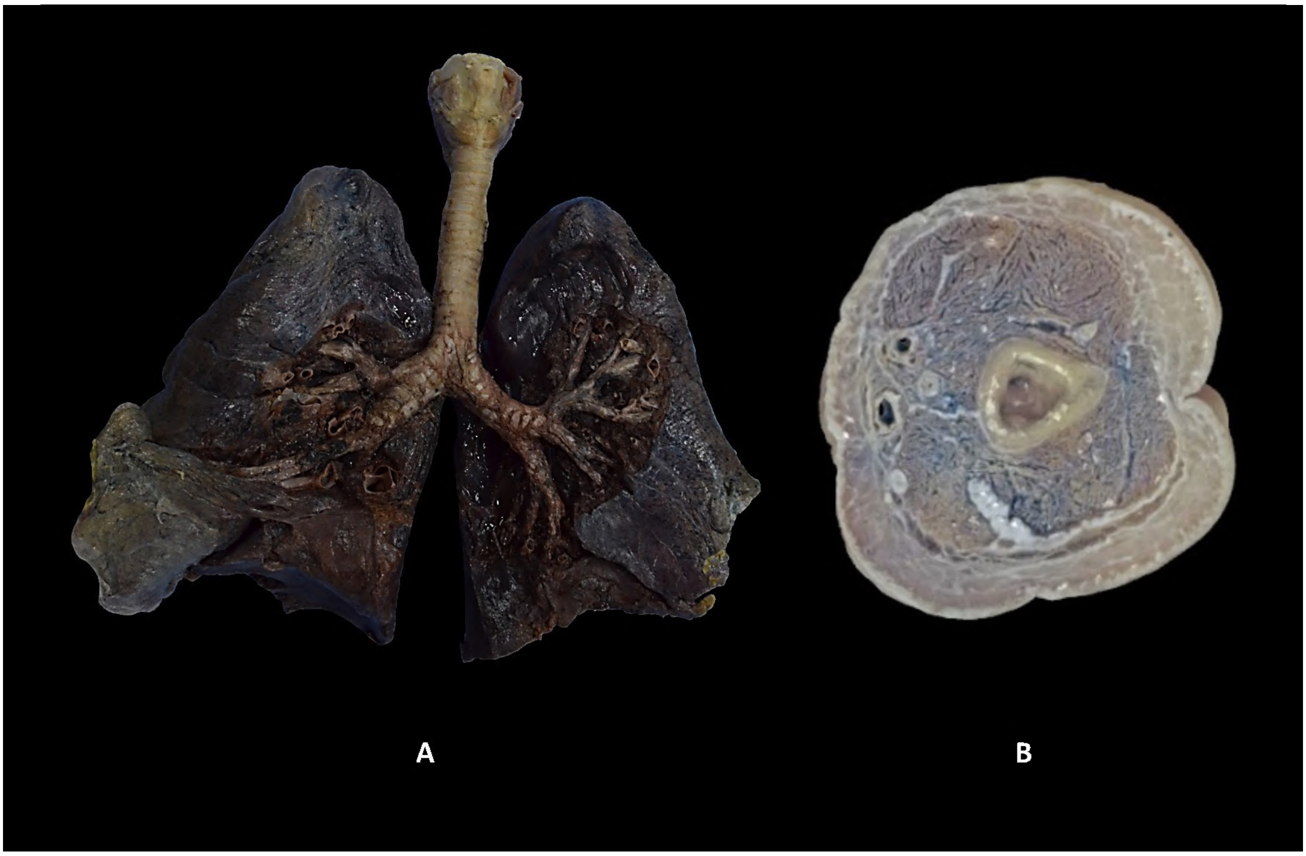

Fig. 1.- A. Photograph of lower airway dissection. **B.** Anatomical replica printed with 3D technology of an arm.

texts on anatomical contents supported by photos; Laminario Anatómico, an interactive photographic web atlas for the recognition of anatomical structures in cadaveric images and videos, with sections on descriptive anatomy, topographic anatomy, sectional anatomy. These sections include all systems and regions of the human body and can be retrieved from anywhere and on any device with internet access. (Fig. 2A); Videos: A registry of 256 videos with explanations on anatomical content using cadaveric preparations, an average of 4 minutes each (Fig. 2B); Gymkhana online simulator, a software that can simulate practical assessments conducted in the anatomy building, which has 16 different content simulations; in it, students can perform evaluations of descriptive anatomy, topographic anatomy, embryology, and histology. In addition, students can configure the number of questions and the duration of each station, being able to practice freely without the pressure of an evaluation (Fig. 3, Table 1). All these resources were generated from cadaveric material and are free and open access.

Undergraduate student survey

The survey results indicated that 98.5% of the undergraduates use a computer, 70.3% a tablet, and 60.5% a smartphone as a study tool. Concerning Internet access, 87.1% have mobile Internet on their study device; however, 87.6% use Wi-Fi when studying.

In relation to the audiovisual resources generated by the authors' department, 79.9% said they use the Laminario Anatómico for daily study, and 97.9% use it to prepare for theoretical and practical evaluations (gymkhanas).

Concerning the use of anatomy videos recorded in the anatomy building, 68.7% of the students surveyed indicated that they use them for daily study, 68.3% at least once a week, 83.7% review them to prepare for theoretical examinations and gymkhanas, and 94% consider this tool to be a contribution to their learning. Regarding the gymkhana online simulator, 74.7% of students confirmed they use it for examination preparation.

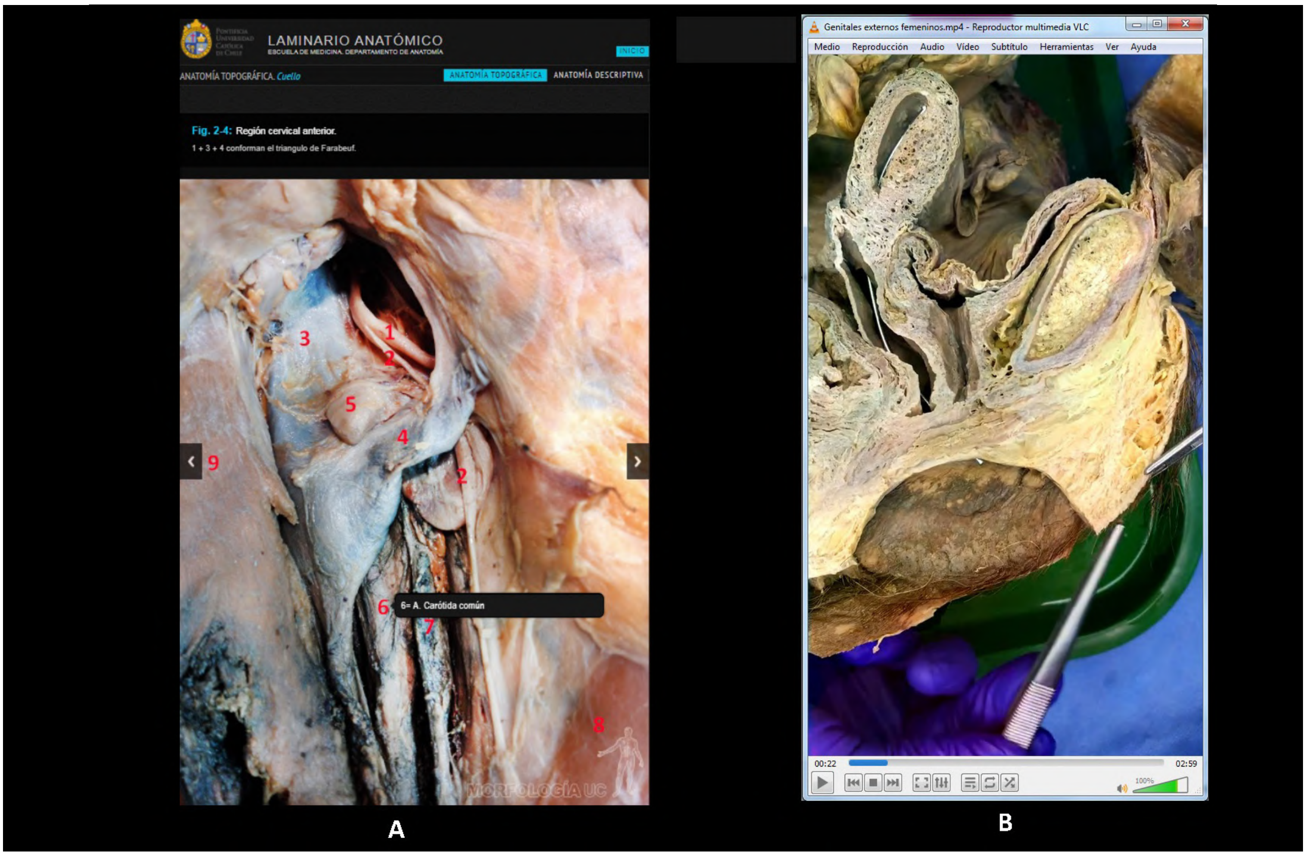

Fig. 2.- **A.** Image from the "Laminario Anatómico". The black box indicates the name of the structure labeled when clicking on the number 6. **B.** Screenshot of an explanatory video on anatomical content recorded in the anatomy building.

Table 2. Teaching using cadaveric material in undergraduate and graduate degree studies.

N°	Undergraduate programs	Course code	Graduate degree programs	Course code
1	Medicine I	MED-111A	Orthopedics	No code
2	Medicine II	MED-212A	General surgery I	No code
3	Medicine III	MED-213A	General surgery II	No code
4	Dentistry I	MED-101o	Otorhinolaryngology	No code
5	Dentistry II	MED-102o	Oncological surgery	No code
6	Dentistry III	MED-201o	Maxillofacial surgery	No code
7	Kinesiology I	MEK-101A	Orthodontics	No code
8	Kinesiology II	KIN-102A	Oral Radiology	No code
9	Speech Therapy I	MEF-101A	Master in Medical Physics	MAF3000
10	Speech Therapy II	FON-102A		
11	Teaching Physical Education I	MEP-101A		
12	Teaching Physical Education II	MEP-201A		
13	Occupation Therapy	MET-201A		
14	Nursing	MEB-103F		
15	Nutrition	MEN-101A		

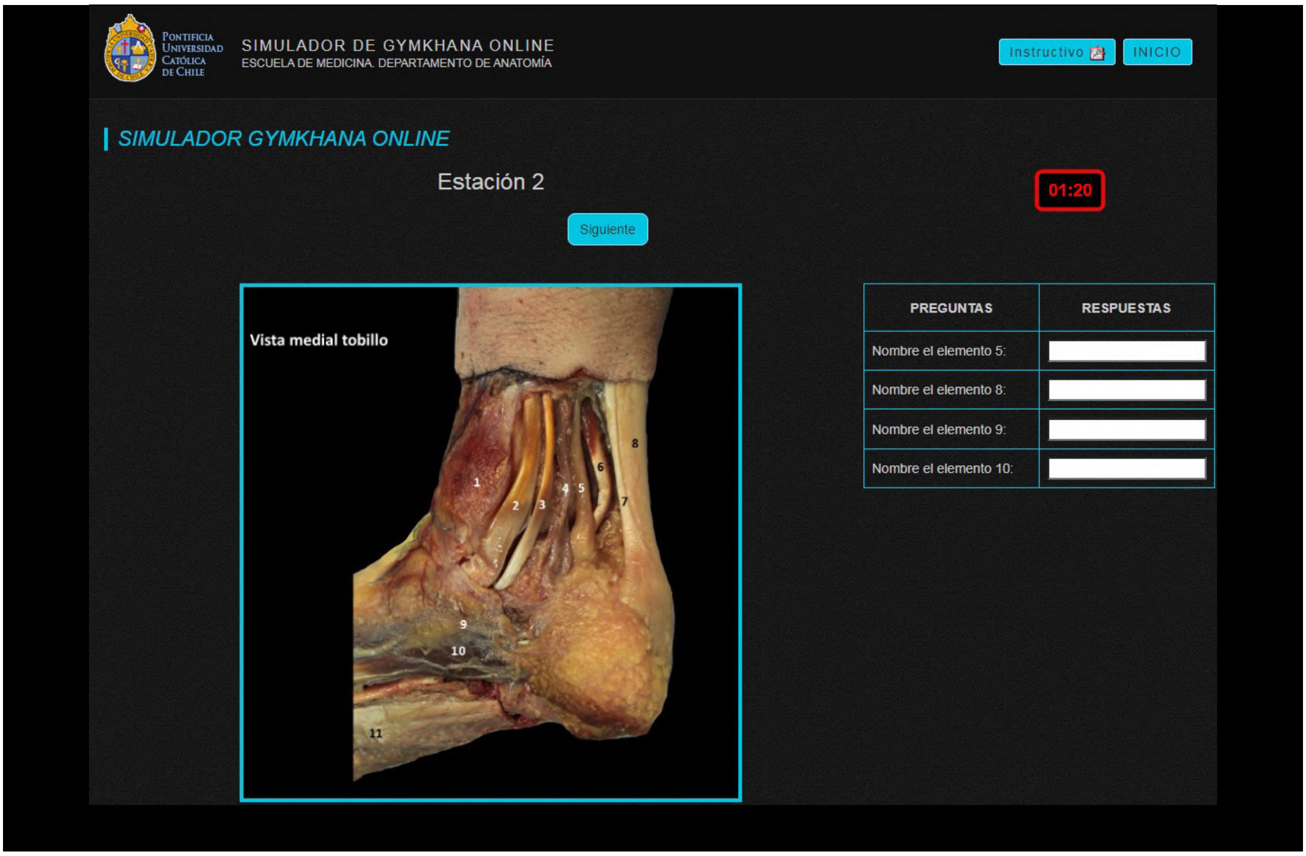

Fig. 3.- Photograph of the "Gymkhana Online Simulator". The light blue box shows the image about which questions are asked, the calypso blue box the questions and blank spaces to answer, and the red box is the time remaining to change to the following image.

Teaching anatomy

There are 15 undergraduate programs structured on 5, 10, and 15 credits (5 credits = 64 hours of instruction). In these courses, prosection activities are carried out in the anatomy building (Table 2). Graduate degree teaching for 8 medical specialty programs and 1 master's program structure is based on 5 credits; these activities include prosection and dissection. Post-graduate

Table 3. Teaching using cadaveric material in graduate qualification programs.

N°	Graduate qualification programs	Course code	Surgical training	Course code	Type of surgical approach
1	Diploma in Human Anatomy	DAH	Hip prosthesis	No code	Manual
2	Diploma in Head and Neck Anatomy	DACYC	Knee prosthesis	No code	ROSA robot
3	Diploma in Neuroanatomy	MEDNAH	Ankle prosthesis	No code	Manual
4	Diploma in Histology and Embryology	MEDDHEA	Hallux valgus correction	No code	Manual
5			Shoulder prosthesis	No code	Manual
6			Elbow prosthesis	No code	Manual
7			Hand tendon repair	No code	Manual
8			Cochlear implant	No code	Manual
9			Blepharoplasty	No code	Manual
10			Scoliosis correction	No code	Manual
11			Spinal osteosynthesis	No code	Manual
12			Skin flaps	No code	Manual
13			Nasal septum correction	No code	Manual
14			Prostatectomy	No code	HUGO robot
15			Nephrectomy	No code	HUGO robot
16			Bariatric surgery	No code	HUGO robot
17			Penile prosthesis	No code	Manual
18			Organ procurement	No code	Manual
19			Canthotomy	No code	Manual
20			Entropion	No code	Manual
21			Ectropion	No code	Manual
22			Abdominal hernias	No code	Laparoscopy

qualification teaching for 4 diploma programs is structured into 20 credits; these activities include prosection and dissection. 22 structured surgical training programs carry out cadaveric surgical simulation training (Table 3). All programs are offered in one academic year, and the courses have been repeated every year since 2021.

Institutional cooperation and research

The Department of Anatomy has made cadaveric material available for 2 doctoral theses and 1 master's thesis (Table 4). In relation to scientific article output, 37 papers have been published on cadaveric dissections in 18 years (Table 4).

Table 4. Institutional cooperation and Research.

Institutional cooperation	Dissections
Doctoral Thesis 1	30
Doctoral Thesis 2	8
Master's thesis 1	6
Anatomy Publications	**N°**
Cadaveric dissections	37

DISCUSSION

The audiovisual resources produced from cadaveric material have been very well received by the students, who have skills *per se* in using technologies (Farfán et al., 2016). This is demonstrated in the survey responses, which indicate a positive answer on using such tools, which also affects student performance, i.e., the "Laminario Anatómico". Since the implementation of this resource, the results of the gymkhanas have yielded an increase in performance, e.g., in gymkhana 4 of the MEK-101A course in 2014, the average score was 39 out of 56 total points. By contrast, in 2015, the average was 37 out of 56. However, the average score on gymkhana 4 in 2016 (when the Laminario Anatómico was implemented) was 41 out of

56; the following year, it was 42 out of 56. On the other hand, the direct benefit of producing these resources is an economic saving, given that all the resources mentioned here were created based on projects that made their funding possible, which is “a zero cost” for the department and simultaneously an achievement for the instructor, which has benefit to their academic career. For example, a virtual dissection table is over US$ 80,000, a cost that is not reasonable for any institution and far beyond the cost of developing all the audiovisual resources generated in the authors’ department from cadaveric material. Further, for the students, cadaveric material work remains the preferred means of learning anatomy (Johnson et al., 2013; Viswasom and Jobby, 2017; Mustafa et al., 2021).

Given the authors’ successful experience as a teaching team, they consider the integration between technology and the resources generated using cadaveric material fundamental (Casado et al., 2012; Paech et al., 2018; Bork et al., 2021; Nakai et al., 2022), and it has become one of the pillars that supports their teaching-departmental development. These resources stand in support of the demands that the current education system must consistently satisfy the rise in new teaching methods equipped with greater flexibility and the ability to generate student-centered learning, which can be also seen in other experiences regarding the development of applications that combine the use of cadaveric material and technology (McMenamin et al., 2014; Moro et al., 2014; Dua et al., 2021). Additionally, within the scope of institutional cooperation, the Internet resources produced from cadaveric material are free to access, so students and instructors from other universities can also use them; however, the impact on other universities has not been measured. This is not a minor point, since these tools were widely used during the Covid-19 pandemic due to the impossibility of attending anatomy buildings, which has been commented on in recent publications (Bauler et al., 2021; Babacan and Dogru Yuvarlakbas, 2022).

In relation to teaching, the authors’ anatomy department offers differentiated courses on morphological sciences for the various programs in the faculty of medicine and the different graduate degree programs. The undergraduate programs mentioned in Table 2 include more than 1200 students per year, taught by instructors corresponding to the equivalent of 11 full working days, who perform prosection activities in the laboratories. On the other hand, the graduate degree programs mentioned in Tables 2 and 3 include approximately 200 students annually, who, through prosection, dissection, and surgical training activities can verify the theoretical contents from the source, developing, in addition, basic surgical skills and a suitable three-dimensional conceptualization of the human body. This is highly relevant, since there is consensus among researchers that training with corpses is important for surgeons to understand the anatomical approaches, which increases their knowledge, surgical confidence, and skills, underscoring that dissection contributes significantly to the work of prosection (Hazan et al., 2018; Kobayashi and Nudeshima, 2018; Torres et al., 2018; Sañudo et al., 2021). These findings provide evidence of the role of dissection in learning and the application of practical anatomical knowledge (Thompson and Marshall, 2020; Huynh et al., 2021), surfacing as the first preference of those who study anatomy, and it enables greater knowledge acquisition (Zibis et al., 2021). The benefits of cadaveric anatomy training reflect the real evolution of medicine and its learning (Jansen et al., 2014), and it suggests that dissection be re-established as the primary method of anatomy education to guarantee safe medical practice (Ghosh, 2017; Onigbinde et al., 2021). The evidence and international experiences justify incorporating cadaveric anatomy training in the curricula of medical specialties (Memon, 2018; Dee et al., 2021).

An interesting point to consider is that laboratory work with small groups is effective in the education of human anatomy, especially when the use of samples is varied, combining preparations, plastinated bodies, corpses, body parts, and methods (Chan and Ganguly, 2008; Fu et al., 2022), a material that over the years the authors have managed to produce and are periodically renewed. The practical activities and the structured practical assessments (gymkhanas), carried out on cadaveric preparations, essentially demand lived experiences in the activities in the anatomy building, being placed above the greater or lesser skill or experience the student has in terms of their school of origin and the initial cultural capital they possess (Inzunza et al., 2017).

With respect to research and institutional collaboration, history shows that by the end of the 19th century, due to the scant supply of morphological training in Chile, it was customary to send young doctors to Europe for graduate training (Cárdenas, 2020). Currently, there are graduate degree offerings in Chile, both master's and doctoral programs in morphological sciences, diploma programs, and continuing education courses. However, the paucity of cadaveric material needed to achieve a representative sample of the population is making researchers in the 21st century repeat the behaviors of the 19th century, having to leave to seek cadaveric material for their research in other institutions, an area in which the authors have been able to collaborate by receiving researchers from external graduate degree programs in their department.

Participation in medical gross anatomy increases students' visual-spatial ability (Lufler et al., 2012; Vorstenbosch et al., 2013); therefore, it is reasonable to think that moving forward, anatomy learning should still be cadaveric-based coupled with complementary technological innovations (Chang Chan et al., 2019; Uruthiralingam and Rea, 2020; Cheung et al., 2021; Iwanaga et al., 2021; Abu Bakar et al., 2022).

Finally, it is only fair to point out that none of these teaching contributions and results would be possible without the invaluable generosity of those who joined the Body Donation for Science and Teaching Program. These people disinterestedly donated their bodies to continue serving life after their death. It is hoped that, with the generation of these academic benefits, the authors will be honoring their donors' wishes.

This study has significant limitations. It is in the context of the national reality of Chile, which is a limitation because there are countries where there is no lack of cadaveric material for the teaching of human anatomy. Therefore, it is possible that some researchers do not identify with the problem.

CONCLUSIONS

The use of cadaveric material is a contribution that strengthens all aspects of academia, teacher training, student learning, and the positioning of institutions: 1) for the management of teaching material, it facilitates the development and production of new resources, avoiding unreasonable costs; furthermore, the generation of these resources is an opportunity to create basic clinical projects that can access competitive funds; 2) for teaching, it represents the best chance to verify the studied theoretical contents empirically, as well as develop surgical skills and abilities; 3) for morphological research and institutional collaboration, it is the generation of new instances of teamwork within the university and with other universities, producing robust research projects that culminate in the publication of results in indexed journals with an impact factor.

University authorities must know and understand these benefits when deciding to use cadaveric material in their institutions. With these results, we hope to encourage them to develop body donation programs for science.

ACKNOWLEDGMENTS

The authors thank the people who generously donate their bodies to science, contributing to developing new professionals.

ETHICS APPROVAL AND CONSENT TO PARTICIPATE

The body was obtained through the Faculty of Medicine donation program at the Pontificia Universidad Católica de Chile (PUC), which complies fully with the World Medical Association's Declaration of Helsinki and national legal and ethical requirements. Consequently, the program was approved by the MED-UC Scientific Ethics Committee of the Pontificia Universidad Católica de Chile (No: 190115002).

REFERENCES

ABU BAKAR YI, HASSAN A, YUSOFF MSB, KASIM F, ABDUL MANAN SULONG H, HADIE SNH (2022) A scoping review of effective teaching strategies in surface anatomy. *Anat Sci Educ,* 15(1): 166-177.

ABDEL EM, KHALIL MK (2017) Measuring medical students' motivation to learning anatomy by cadaveric dissection. *Anat Sci Educ,* 10(4): 363-371.

BABACAN S, DOGRU YUVARLAKBAS S (2022) Digitalization in education during the COVID- 19 pandemic: emergency distance anatomy education. *Surg Radiol Anat,* 44(1): 55-60.

BAULER LD, LESCIOTTO KM, LACKEY-CORNELISON W (2021) Factors impacting the rapid transition of anatomy curricula to an online environment in response to Covid-19. *Anat Sci Educ,* 15(2): 221-232.

BORK F, LEHNER A, ECK U, NAVAB N, WASCHKE J, KUGELMANN D (2021) The effectiveness of collaborative augmented reality in gross anatomy teaching: A quantitative and qualitative pilot study. *Anat Sci Educ,* 14(5): 590-604.

CÁRDENAS VJ (2020) Historia de la anatomía en Chile. Parte II. El alma mater. *Int J Morphol.* 38(4): 1074-1089.

CASADO MI, CASTAÑO G, ARRÁEZ-AYBAR LA (2012) Audiovisual material as educational innovation strategy to reduce anxiety response in students of human anatomy. *Adv Health Sci Educ Theory Pract.* 17(3): 431-440.

CHAN LK, GANGULY PK (2008) Evaluation of small-group teaching in human gross anatomy in a Caribbean medical school. *Anat Sci Educ,* 1(1): 19-22.

CHANG CHAN AY, CATE OT, CUSTERS E, LEEUWEN M, BLEYS R (2019) Approaches of anatomy teaching for seriously resource-deprived countries: A literature review. *Educ Health (Abingdon),* 32(2): 62-74.

CHEUNG CC, BRIDGES S M, TIPOE GL (2021) Why is anatomy difficult to learn? The implications for undergraduate medical curricula. *Anat Sci Educ,* 14(6): 752-763.

CHIPAMAUNGA S, PROZESKY D (2019) How students experience integration and perceive development of the ability to integrate learning. *Adv Health Sci Educ Theory Pract,* 24(1): 65-84.

DEE EC, ALTY IG, AGOLIA JP, TORRES-QUINONES C, VAN HOUTEN T, STEARNS DA, LILLEHEI CW, SHAMBERGER RC (2021) A surgical view of anatomy: perspectives from students and instructors. *Anat Sci Educ,* 14(1): 110-116.

DISSABANDARA LO, NIRTHANAN SN, KHOO TK, TEDMAN R (2015) Role of cadaveric dissections in modern medical curricula: a study on student perceptions. *Anat Cell Biol,* 48(3): 205-212.

DUA A, COPPOLA KM, MULHERON GW, TROUPE D, LEBEAU R (2021) Development of a novel peer-sharing application to supplement learning from cadaveric dissection. *Anat Sci Educ,* 14(4): 491-504.

ESTAI M, BUNT S (2016) Best teaching practices in anatomy education: A critical review. *Ann Anat,* 208: 151-157.

FARFÁN E, CÁRDENAS J, ESPINOSA-NAVARRO O, LIZANA PA, PACHECO J, SALINAS P, RIVEROS A, VILLARROEL M (2021) Profile of morphology teachers in Chilean universities. *Int J Morphol,* 39(6): 1615-1624.

FARFÁN E, SCHNEEBERGER D, BESA J, SALGADO G, INZUNZA O (2016) Web al servicio de la anatomía: Relato de una experiencia docente. *Int J Morphol,* 34(1): 136-142.

FU X, WU X, LIU D, ZHANG C, XIE H, WANG Y, XIAO L (2022) Practice and exploration of the “student-centered” multielement fusion teaching mode in human anatomy. *Surg Radiol Anat,* 44(1): 15-23.

GNANAKUMAR S, KOSTUSIAK M, BUDOHOSKI KP, BARONE D, PIZZUTI V, KIROLLOS R, SANTARIUS T, TRIVEDI R (2018) Effectiveness of cadaveric simulation in neurosurgical training: A review of the literature. *World Neurosurg,* 118: 88-96.

GHOSH SK (2017) Cadaveric dissection as an educational tool for anatomical sciences in the 21st century. *Anat Sci Educ,* 10(3): 286-299.

GUILLOT A, CHAMPELY S, BATIER C, THIRIET P, COLLET C (2007) Relationship between spatial abilities, mental rotation and functional anatomy learning. *Adv Health Sci Educ Theory Pract,* 12(4): 491-507.

HACKETT M, PROCTOR M (2016) Three-dimensional display technologies for anatomical education: A literature review. *J Sci Educ Technol,* 25: 641-654.

HAZAN E, TORBECK R, CONNOLLY D, WANG JV, GRIFFIN T, KELLER M, TRUFANT J (2018) Cadaveric simulation for improving surgical training in dermatology. *Dermatol Online J,* 24(6): 13030/qt5cq2n3vp.

HUYNH N, BURGESS A, WING L, MELLIS C (2021) Anatomy by whole body dissection as an elective: Student outcomes. *J Surg Educ,* 78(2): 492-501.

INZUNZA O (2008) Competencias generales en medicina, rol de la anatomía. *Int J Morphol,* 26(2): 243-246.

INZUNZA O, SCHNEEBERGER D, SALGADO G, CANTIN M (2017) Actividades prácticas en anatomía: Factor nivelador de los contrastes de origen entre los alumnos de medicina. *Int J Morphol,* 35(2): 494-499.

IWANAGA J, LOUKAS M, DUMONT AS, TUBBS RS (2021) A review of anatomy education during and after the COVID-19 pandemic: Revisiting traditional and modern methods to achieve future innovation. *Clin Anat,* 34(1): 108-114.

JANSEN S, COWIE M, LINEHAN J, HAMDORF JM (2014) Fresh frozen cadaver workshops for advanced vascular surgical training. *ANZ J Surg,* 84(11): 877-880.

JOHNSON IP, PALMER E, BURTON J, BROCKHOUSE M (2013) Online learning resources in anatomy: What do students think? *Clin Anat,* 26(5): 556-563.

LEUNG KK, LU KS, HUANG TS, HSIEH BS (2006) Anatomy instruction in medical schools: connecting the past and the future. *Adv Health Sci Educ Theory Pract,* 11(2): 209-215.

LUFLER RS, ZUMWALT AC, ROMNEY CA, HOAGLAND TM (2012) Effect of visual-spatial ability on medical students’ performance in a gross anatomy course. *Anat Sci Educ,* 5(1): 3-9.

KAUSAR T, CHANDIO S, QUDDUS I, QURESHI GS, BALOCH ZH, PARIO A (2020) Effectiveness of teaching with visualisation table in comparison to traditional lecture in anatomy department, Jinnah Sindh Medical University. *J Coll Physicians Surg Pak,* 30(10): 1074-1077.

LI Y, GAO D, LIANG W, QIU L, LIU X, ZHANG L, DENG Z (2018) A comparison of malpractice lawsuits mediated and judged in court in China. *J Forensic Leg Med,* 54: 109-113.

MCMENAMIN PG, QUAYLE MR, MCHENRY CR, ADAMS JW (2014) The production of anatomical teaching resources using three-dimensional (3D) printing technology. *Anat Sci Educ,* 7(6): 479-486.

MEMON I (2018) Cadaver dissection is obsolete in medical training! A misinterpreted notion. *Med Princ Pract,* 27(3): 201-210.

MORO C, ŠTROMBERGA Z, RAIKOS A, STIRLING A (2017) The effectiveness of virtual and augmented reality in health sciences and medical anatomy. *Anat Sci Educ,* 10(6): 549-559.

MUSTAFA AG, TAHA NR, ZAQOUT S, AHMED MS (2021) Teaching Musculoskeletal Module using dissection videos: feedback from medical students. *BMC Med Educ,* 21(1): 604.

KOBAYASHI E, NUDESHIMA J (2018) Current state of surgical training using cadavers in Japan compared with Western countries. *Surg Today,* 48(9): 891-893.

NAKAI K, TERADA S, TAKAHARA A, HAGE D, TUBBS RS, IWANAGA J (2022) Anatomy education for medical students in a virtual reality workspace: A pilot study. *Clin Anat,* 35(1): 40-44.

ONIGBINDE OA, CHIA T, OYENIRAN OI, AJAGBE AO (2021) The place of cadaveric dissection in post-COVID-19 anatomy education. *Morphologie,* 105(351): 259-266.

PAECH D, KLOPRIES K, DOLL S, NAWROTZKI R, SCHLEMMER HP, GIESEL FL, KUNER T (2018) Contrast-enhanced cadaver-specific computed tomography in gross anatomy teaching. *Eur Radiol,* 28(7): 2838-2844.

PATHER N (2015) Teaching anatomy: prosections and disections. In: Chan L, Pawlina W (eds). *Teaching Anatomy*. Springer Cham, Heidelberg New York Dordrecht London, pp 213-221.

REHKÄMPER G (2016) Human dissection in medical education: More than just anatomy. *GMS J Med Educ,* 33(5): Doc68.

RIZZOLO LJ, STEWART WB (2006) Should we continue teaching anatomy by dissection when ...? *Anat Rec B New Anat,* 289(6): 215-218.

SADEESH T, PRABAVATHY G, GANAPATHY A (2021) Evaluation of undergraduate medical students' preference to human anatomy practical assessment methodology: a comparison between online and traditional methods. *Surg Radiol Anat,* 43(4): 531-535.

SAÑUDO J, TALARICO E, DUPARC F, VÁZQUEZ T, VALDERRAMA F, MOMPEO B, MIRAPEIX R, ELIZONDO-OMAÑA R, LARKIN T, MCHANWELL S, MARANILLO E, MORIGGL B, KONSCHAKE M (2021a) Practical pregraduate teaching in Human Anatomy: A review. *Eur J Anat,* 25(S1): 81-90.

SAÑUDO J, VÁZQUEZ T, TALARICO E, DUPARC F, PAULSEN F, MACCHI V, FEIGL G, ELIZONDO-OMAÑA R, DE CARO R, ARAGONÉS P, MCHANWELL S, MORIGGL B, KONSCHAKE M (2021b) Practical postgraduate teaching in Human Anatomy: A review. *Eur J Anat,* 25(S1): 91-99.

SINGAL A (2022) Transforming anatomy education: then and now. *Anat Sci Int,* 97(2): 230-231.

STANDRING S (2009) New focus on anatomy for surgical trainees. *ANZ J Surg,* 79(3): 114-117.

STEPHENS GC, REES CE, LAZARUS MD (2021) Exploring the impact of education on preclinical medical students' tolerance of uncertainty: a qualitative longitudinal study. *Adv Health Sci Educ Theory Pract,* 26(1): 53-77.

THOMPSON AR, MARSHALL AM (2020) Participation in dissection affects student performance on gross anatomy practical and written examinations: Results of a four-year comparative study. *Anat Sci Educ,* 13(1): 30-36.

TIZNADO-MATZNER G, BUCAREY-ARRIAGADA S, ARAVENA PC (2019) Recorrido por la realidad de los laboratorios de anatomía humana de 12 Universidades Chilenas. *Int J Morphol,* 37(1): 17-21.

TORRES K, DENISOW-PIETRZYK M, PIETRZYK Ł, MACIEJEWSKI R, TORRES A (2018) Does simulation-based training facilitate the integration of human anatomy with surgery? A report of a novel surgical anatomy course. *Folia Morphol (Warsz),* 77(2): 279-285.

URUTHIRALINGAM U, REA PM (2020) Augmented and virtual reality in anatomical education - a systematic review. *Adv Exp Med Biol,* 1235: 89-101.

YAMMINE K, VIOLATO C (2016) The effectiveness of physical models in teaching anatomy: a meta-analysis of comparative studies. *Adv Health Sci Educ Theory Pract,* 21(4): 883-895.

VISWASOM AA, JOBBY A (2017) Effectiveness of video demonstration over conventional methods in teaching osteology in anatomy. *J Clin Diagn Res,* 11(2): JC09-JC11.

VORSTENBOSCH MA, KLAASSEN TP, DONDERS AR, KOOLOOS JG, BOLHUIS SM, LAAN RF (2013) Learning anatomy enhances spatial ability. *Anat Sci Educ,* 6(4): 257-262.

ZIBIS A, MITROUSIAS V, VARITIMIDIS S, RAOULIS V, FYLLOS A, ARVANITIS D (2021) Musculoskeletal anatomy: evaluation and comparison of common teaching and learning modalities. *Sci Rep,* 11(1): 1517.

Author Index to Volume 27, 2023

T

U

V

W

Y

Z

European Journal of Anatomy